

Development and Characterization of Polyurea-based Thermoset Resins

Vom Fachbereich für Maschinenbau und Verfahrenstechnik
der Technischen Universität Kaiserslautern
zur Erlangung des akademischen Grades

Doktor-Ingenieur (Dr.-Ing.)
genehmigte Dissertation

von

Dipl.- Chem. Núria Castellà

aus Badalona (Spanien)

Tag der mündlichen Prüfung: 19 Januar 2009

Prüfungsvorsitzender: Prof. Dipl.-Ing. Dr. techn. habil. H.-J. Bart
1. Berichterstatter: Prof. Dr.-Ing. habil. Dr. h.c. J. Karger-Kocsis
2. Berichterstatter: Prof. Dr.-Ing. P. L. Geiss

ACKNOWLEDGEMENTS

The present work was accomplished between October 2006 and January 2009 at the Institute for composite Materials (Institut für Verbundwerkstoffe GmbH, IVW) of the Technical University of Kaiserslautern, Germany.

First of all I would like express my gratitude to my Ph.D. supervisor, Prof. Dr.-Ing. habil. Dr.h.c. József Karger-Kocsis, for giving me the opportunity to work in his group. It was a great pleasure and honour for me to be under your tutoring. With me, I took a pinch of your never-ending knowledge but most important you will be always a point of reference not only in my professional but also in my personal life for your goodness, honesty and humility.

Thanks as well to Prof. P. L. Geiß to accept being the co-referent of this PhD thesis and Prof. Dipl.-Ing. Dr. techn. habil. H.-J. Bart to preside over the examination committee.

I am deeply indebted to my dear colleague and friend Dr. Sergiy Grishchuk, whose inestimable support, willingness to help and deep knowledge made this work possible and for providing every day a stimulating and pleasant environment in which to learn and work.

I would also like to thank Mikhail Unik for his valuable task in 3P/EP hybrids, as well as the student assistants Marta Embil, Yasmina Fernández, Manoel de la Fuente, Esther Rivas and Nacho Flores whose help speed up the investigations. Further I would like to thank the colleagues of the Institute for the pleasant work atmosphere, especially Pia Eichert, Heidi Plocharzik, Hermann Giertzsch, Stefan Schmitt, and Ralf Schimmele for their kind help in the experiments.

I am especially grateful to my dear good friends Lada Gyurova, Christina Baltá, Angela Cabrero, Pablo Carballeira, Jenny Wilber and Lucía Fontán among many others for their constant encouragement and for the nice time spend together during the arduous task of writing.

I wish to thank my entire family, especially my sister and my brothers, my in-laws, my nephews and nieces, my aunts and uncles, my cousins for their love and care. A special thank to my boyfriend Christoph Riedel for the courage and love that he has given me during the whole process.

Lastly, and most importantly, I wish to thank my parents, Jaume Castellà and Teresa Maymó. They bore me, raised me, taught me, supported me and loved me. With my deepest gratitude I dedicate them this thesis (A vosaltres estimats pares).

Table of Contents

Acknowledgements.....	I
Table of contents.....	III
Abstract/ Kurzfassung.....	VI
List of Abbreviations and symbols	IX
1. Introduction.....	1
2. Background.....	5
2.1. 3P Chemistry.....	5
2.2. 3P Uses and challenges.....	19
3. Objectives.....	23
4. Experimental.....	26
4.1. Materials.....	26
4.1.1. Waterglass.....	26
4.1.2. Polyisocyanates.....	26
4.1.3. Phosphates.....	27
4.1.4. Vinylester Resins.....	27
4.1.5. Epoxy Resins.....	28
4.1.6. Melamine Formaldehyde Resin.....	28
4.2. Sample Preparation.....	29
4.2.1. 3P Resin.....	29
4.2.2. 3P/ Hybrid Resin	29
4.2.2.1. Vinylester Resin	29
4.2.2.2. Epoxy Resin.....	30
4.2.2.3. Melamine Formaldehyde Resin.....	30
4.2.3. 2P/ Hybrid Resin.....	31
4.2.3.1. Vinylester Resin.....	31
4.2.3.2. Epoxy Resin.....	31
4.2.3.3. Melamine Formaldehyde Resin.....	31
4.3. Morphology.....	32
4.3.1. Scanning Electron Microscope.....	32
4.3.2. Atomic Force Microscope.....	33

4.4. Mechanical Characterisation	34
4.4.1. Fracture Mechanics	34
4.4.2. Flexural Test	36
4.4.3. Dynamic Mechanical Thermal Analysis	36
4.5. Analytical/Thermal Characterisation	38
4.5.1. Attenuated Total Reflectance Infrared Spectroscopy	38
4.5.2. Differential Scanning Calorimetry	40
4.5.3. Rheology	41
4.5.4. Thermogravimetric Analysis	43
4.5.5. Flammability test	44
5. Results and Discussion	46
5.1. 3P Resin	46
5.1.1. Kinetics	46
5.1.2. Rheology	50
5.1.3. Morphology	51
5.1.4. Mechanical Properties	55
5.1.5. Thermal Properties	59
5.2. 3P/ Hybrid Resin	63
5.2.1. Vinylester Resin	63
5.2.1.1. Rheology	63
5.2.1.2. Morphology	63
5.2.1.3. Mechanical Properties	66
5.2.1.4. Thermal Properties	69
5.2.2. Epoxy Resin	71
5.2.2.1. Rheology	71
5.2.2.2. Morphology	72
5.2.2.3. Mechanical Properties	74
5.2.2.4. Thermal Properties	77
5.2.3. Melamine Formaldehyde Resin	80
5.2.3.1. Rheology	80
5.2.3.2. Morphology	80
5.2.3.3. Mechanical Properties	82
5.2.3.4. Thermal Properties	85

5.3. 2P/Hybrid Resin	89
5.3.1. Vinylester Resin	89
5.3.1.1. Rheology	89
5.3.1.2. Morphology	90
5.3.1.3. Mechanical Properties	93
5.3.1.4. Thermal Properties	96
5.3.2. Epoxy Resin	100
5.3.2.1. Rheology	100
5.3.2.2. Morphology	101
5.3.2.3. Mechanical Properties	103
5.3.2.4. Thermal Properties	106
5.3.3. Melamine Formaldehyde Resin	109
5.3.3.1. Rheology	109
5.3.3.2. Morphology	109
5.3.3.3. Mechanical Properties	112
5.3.3.4. Thermal Properties	114
6. Summary and Outlook	118
7. Appendix	126
8. Literature	129
List of Publications	142
Curriculum vitae	144

ABSTRACT

Proprietary polyurea based thermosets (3P resins) were produced from polymeric methylene diphenylisocyanate (PMDI) and water glass (WG) using a phosphate emulsifier. Polyisocyanates when combined with WG in presence of suitable emulsifier result in very versatile products. WG acts in the resulting polyurea through a special sol-gel route as a cheap precursor of the silicate (xerogel) filler produced in-situ. The particle size and its distribution of the silicate are coarse and very broad, respectively, which impart the mechanical properties of the 3P systems negatively.

The research strategy was to achieve initially a fine water in oil type (W/O = WG/PMDI) emulsion by “hybridising” the polyisocyanate with suitable thermosetting resins (such as vinyl ester (VE), melamine/formaldehyde (MF) or epoxy resin (EP)). As the presently used phosphate emulsifiers may leak into the environment, the research work was directed to find such “reactive” emulsifiers which can be chemically built in into the final polyurea-based thermosets. The progressive elimination of the organic phosphate, following the European Community Regulation on chemicals and their safe use (REACH), was studied and alternative emulsifiers for the PMDI/WG systems were found. The new hybrid systems in which the role of the phosphate emulsifier has been overtaken by suitable resins (VE, EP) or additives (MF) are designed 2P resins. Further, the cure behaviour (DSC, ATR-IR), chemorheology (plate/plate rheometer), morphology (SEM, AFM) and mechanical properties (flexure, fracture mechanics) have been studied accordingly. The property upgrade targeted not only the mechanical performances but also thermal and flame resistance. Therefore, emphasis was made to improve the thermal and fire resistance (e.g. TGA, UL-94 flammability test) of the in-situ filled hybrid resins.

Improvements on the fracture mechanical properties as well as in the flexural properties of the novel 3P and 2P hybrids were obtained. This was accompanied in most of the cases by a pronounced reduction of the polysilicate particle size as well as by a finer dispersion. Further the complex reaction kinetics of the reference 3P was studied, and some of the main reactions taking place during the curing process were established. The pot life of the hybrid resins was, in most of the cases, prolonged, which facilitates the posterior processing of such resins. The thermal

resistance of the hybrid resins was also enhanced for all the novel hybrids. However, the hybridization strategy (mostly with EP and VE) did not have satisfactory results when taking into account the fire resistance. Efforts will be made in the future to overcome this problem. Finally it was confirmed that the elimination of the organic phosphate emulsifier was feasible, obtaining the so called 2P hybrids. Those, in many cases, showed improved fracture mechanical, flexural and thermal resistance properties as well as a finer and more homogeneous morphology.

The novel hybrid resins of unusual characteristics (e.g. curing under wet conditions and even in water) are promising matrix materials for composites in various application fields such as infrastructure (rehabilitation of sewers), building and construction (refilling), transportation (coating of vessels, pipes of improved chemical resistance)...

KURZFASSUNG

Polyurea-basierte Harze, abgekürzt als 3P und kommerzialisiert durch Polinvent GmbH, (Budapest, Hungary), sind aus polymeren Methyldiphenylisocyanat (PMDI) und Wasserglass (WG) zusammen mit einem Phosphat-Emulgator hergestellt. Polyisocyanate, falls sie mit Wasserglas gemischt werden, bzw. reagieren, liefern in Anwesenheit von geeigneten Katalysatoren sehr vielseitige Produkte. Das WG wirkt dabei über einen speziellen Sol-Gel Weg als ein preiswerter Präkursor des Silikatfüllstoffs (Xerogel), welches in-situ in der resultierenden Polyurea Matrix erzeugt wird. Die Größe und die Verteilung der Silikatpartikel sind üblicherweise zu grob bzw. zu breit und beeinflussen dadurch die mechanischen Eigenschaften negativ.

Der Schwerpunkt der Forschungsarbeiten war die Herstellung und Optimierung feiner Wasser-im-Öl Typ (W/O = WG/PMDI+Modifikatorharz) Emulsionen. Dies wurde durch die Kombination von Polyisocyanaten mit geeigneten duroplastischen Harzen (wie Vinylester (VE), Epoxid (EP) oder Melamin/Formaldehyd (MF)) erreicht. Da der bisher ausschließlich angewendete Phosphat-Emulgator aus der Polyureamatrix in die Umwelt diffundiert, wurde im Rahmen der Forschungsarbeiten die Suche auf Emulgatoren für die WG/PMDI Systemen gerichtet, die in die endgültige Polyurea-

basierte Harze chemisch eingebaut werden können. Die progressive Substitution von Phosphaten lieferte neue Hybridsysteme, abgekürzt als 2P Harze, wobei die Emulgatorfunktion des Phosphats durch die oben aufgelisteten duroplastischen Harze übernommen wurde. Die Vernetzung (DSC, ATR-IR), Chemorheologie (Platte/Platte Rheometer), Morphologie (REM, AFM) und die mechanischen Eigenschaften (Biegebelastung, Bruchmechanik) der resultierenden in-situ silikatgefüllten Hybridharze wurden untersucht und die Vor- und Nachteile dargelegt. Eine weitere Aufgabe der Forschungsarbeit bestand darin, die Temperaturbeständigkeit und die Flammwidrigkeit der neuen Hybridsysteme zu verbessern (TGA, bzw. UL-94 Flammpbarkeitsstest).

Durch die „Hybridisierungsstrategie“ konnten die mechanischen Eigenschaften (Bruchzähigkeit, Biegesteifigkeit) der neuen 3P und 2P verbessert werden. Diese Steigerungen waren in meisten Fällen mit einer deutlichen Abnahme der Polysilikat Partikelgröße und einer engen Partikelgrößenverteilung verbunden. Des Weiteren wurde die komplexe Reaktionskinetik vom 3P Referenz-Harz untersucht und die wichtigsten Reaktionen des Aushärtungsprozesses wurden nachgewiesen. Durch Anwendung von VE, EP und MF Harzen wurde die Topfzeit der resultierenden Harzen verlängert und dadurch die spätere Verarbeitung erleichtert. Die Temperaturbeständigkeit der neuen 3P und 2P Hybridsystemen wurde deutlich erhöht. Andererseits wurde besonders bei Verwendung von VE und EP Harzen die Flammwidrigkeit durch die Hybridisierung negativ beeinflusst. Durch die Entwicklung der sogenannten 2P Hybridharze wurde nachgewiesen dass der Phosphat-Emulgator vollkommen ersetzt werden kann. Die meisten der neuartigen Hybridsysteme haben verbesserte bruchmechanische Eigenschaften, erhöhte Biegesteifigkeit und Temperaturbeständigkeit. Dies wurde durch die Entstehung einer feiner Polysilikatdispersion bzw. eines Konetzwerkes erklärt.

Die neuen Hybridsysteme mit ungewöhnlichen Eigenschaften (z.B. Aushärtung bei nassen Bedingungen, oder sogar unter Wasser) sind aussichtsreiche Matrices für Verbundwerkstoffe in verschiedenen Anwendungsgebieten wie zum Beispiel, Infrastruktur (Abflussrohrsanierung), Bauausführung (Baugrubenbewehrung), Transportwesen (Gefäßbeschichtungen, chemikalienbeständige Röhren) usw.

LIST OF ABBREVIATIONS AND SYMBOLS

Abbreviations

3PB	3-Point-Bending Test
3P	(Polyurea - Polysilicate - Phosphate) resin
2P	(Polyurea - Polysilicate) resin
AFM	Atomic Force Microscope
ASTM	American Society for Testing Materials
ATR-IR	Attenuated Total Reflection Infrared Spectrometer
BA	Bisphenol-A
CT	Compact Tension Specimen
DMTA	Dynamic Mechanical Thermal Analysis
DPO	Diphenyl Octyl Phosphate
DSC	Differential Scanning Calorimetry
DTG	Differential Thermogravimetry
EEW	Epoxy Equivalent Weight
EP	Epoxy resin
FTIR	Fourier Transformed Infrared Spectroscopy
IPN	Interpenetrating Polymer Network
ISO	International Organization for Standardization
MF	Melamine Formaldehyde resin
PMDI	Polymeric 4,4'-diphenylmethane Diisocyanate
REACH	Registration, Evaluation, Authorisation and Restriction of Chemical Substances
RT	Room Temperature
SEM	Scanning Electron Microscope
S _N 2	Bimolecular Nucleophilic Substitution
TCP	Tricresyl Phosphate
TEOS	Tetraethoxysilane
TGA	Thermogravimetric Analysis
TMOS	Tetramethoxysilane
UV	Ultraviolet Light

VE	Vinylester resin
VE1	Vinylester resin (29 wt.-% styrene content)
VE2	Vinylester resin (33 wt.-% styrene content)
VE3	Vinylester resin (45 wt.-% styrene content)
VEUH	Vinylester-urethane resin
VOC	Volatile Organic Compounds
WG	Waterglass
W/O	Water-in-Oil Emulsion

Symbols

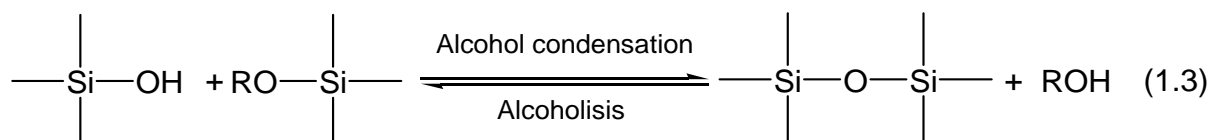
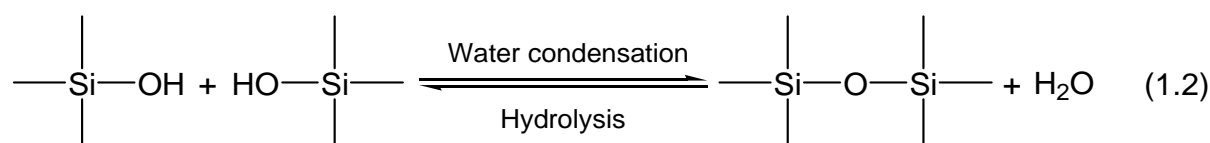
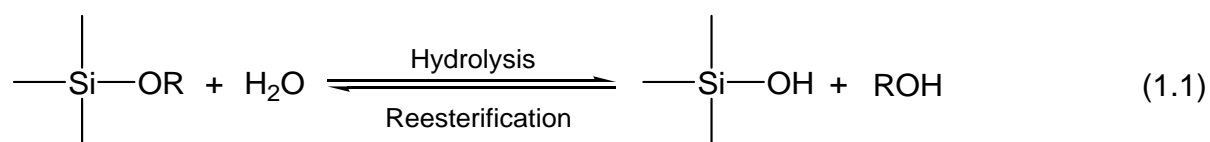
K_c [MPa.m ^{1/2}]	Fracture toughness
G_c [kJ.m ²]	Fracture energy
f	Form factor
ϕ	Calibration factor
ε	Strain
σ	Stress
ε_F	Flexural strain
σ_F	Flexural stress
γ	Shear strain
τ	Shear stress
E_B [MPa]	Modulus of elasticity under bending
E [MPa]	Modulus of elasticity
E^* [MPa]	Complex modulus of elasticity
E' [MPa]	Storage modulus
E'' [MPa]	Loss modulus
G [Pa]	Shear Modulus
G^* [Pa]	Complex dynamic modulus
G' [Pa]	Storage modulus
G'' [Pa]	Loss modulus
$\tan \delta$	Mechanical loss factor
T_g [°C]	Glass transition temperature
T_{trans} [°C]	Transition temperature

T_{gel} [°C]	Gel temperature
$T_{5\%}$ [°C]	Temperature at 5% mass loss
d_n [μm]	Number average particle diameter
d_w [μm]	Weight average particle diameter
s	Standard deviation

1. INTRODUCTION

Nowadays, the research interest for organic-inorganic hybrid materials is fuelled mostly by possible improvements in the mechanical properties and fire resistance [1]. The studied resins, designated 3P resins (from polyisocyanate, phosphate, polysilicate) and marketed by Polinvent Ltd (Budapest, Hungary), belong to the organic-inorganic materials, as they are based on a polyurea organic matrix with in-situ produced inorganic polysilicate particles. There are numerous ways to produce organic-inorganic systems. Nevertheless, the related methods can be grouped whether the inorganic framework is incorporated in preformed stage (fillers and reinforcements) or, in the case of the present study, is produced in situ in the organic (polymer) phase.

The in situ techniques are usually variants of the sol-gel chemistry. Sol-gel chemistry is an area of material science that dates back to the mid-1800s. "Sol-gel" denotes a process by which largely inorganic polymers are synthesized. A "sol" is a dispersion of colloidal particles and a "gel" is an interconnected polymeric network formed by assembly of the sol. The sol-gel process, as the name implies, involves the evolution of inorganic networks through the formation of a colloidal suspension (sol) and gelation of the sol to form a network in a continuous liquid phase (gel) (Fig.1.1) [2-5]. The precursors for synthesizing these colloids consist of a metal or metalloid element surrounded by various active ligands. Alkoxides are most popular because these groups easily hydrolyze and the silicate framework forms in the subsequent polycondensation process (c.f. Eq. 1-3).



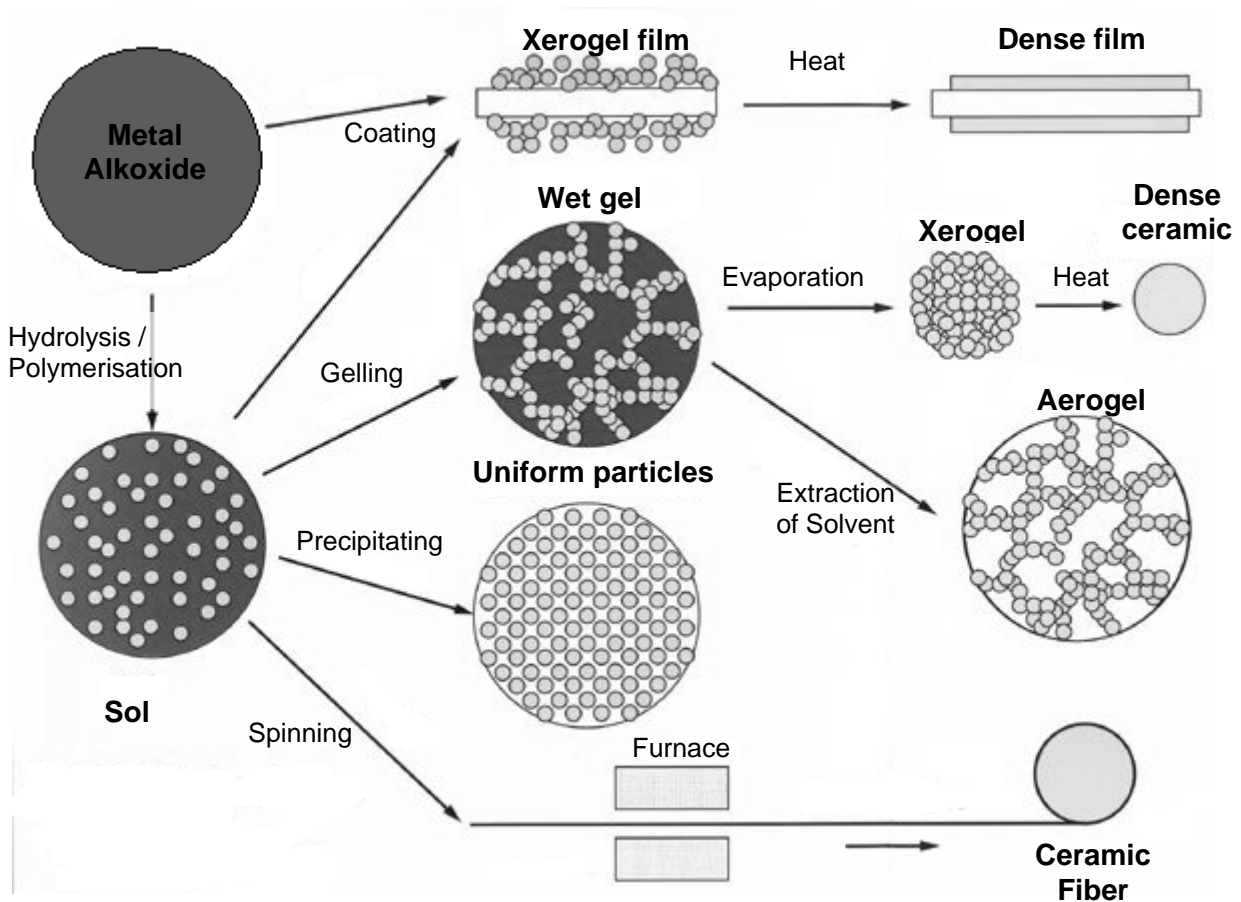


Fig.1.1 - Sol-gel technologies and their products.

The most widely used alkoxides are the alkoxysilanes, such as tetramethoxysilane (TMOS) and tetraethoxysilane (TEOS). However, other alkoxides such as aluminates, titanates and borates are also commonly used in the sol gel process. Albeit by this way nanoscaled filler dispersion can be achieved, it is not yet widely used in the practice due to the high price of organosilane compounds. As a consequence, there is a great demand for cheap silicate precursor alternatives which can replace the organosilanes. Therefore, water glass (WG) is a potential and promising candidate for this task. Although WG has been already used in the ancient Egypt, its versatile properties broaden the application fields even today. The aqueous WG solutions are usually characterized by their density and mass (or molar) ratio of $\text{SiO}_2/\text{Me}_2\text{O}$ (called modulus) where Me_2O stays for the alkali oxide (usually Na_2O or K_2O) and they are strongly alkaline. A special property of WG is that it “hardens” physically by water evaporation, as well as chemically by various reactions. The “hardening” or “silicification” process may be induced by atmospheric CO_2 (see later in section Background). The silica gel formed is a hydrogel, more exactly a

hydro/xerogel depending on its actual water content. This silicification process takes place when dispersing WG in polyisocyanates yielding high reactive water-in-oil type (W/O) emulsion. The use of polyisocyanates with a functionality higher than two yields crosslinked polyurea based systems. Recall that WG contains two “active” components, viz. water (towards polyisocyanates) and alkalisilicates (silicification). The above mentioned polyurea formation can hardly be controlled and the CO₂ by-product may cause undesired foaming. [6-7]

Emulsions, such as WG/PMDI, are unstable and thus do not form spontaneously. Over time, they tend to revert to the stable state of oil separated from water. In a W/O emulsion water droplets (from WG) are contained in a continuous oil solvent (polyisocyanate) stabilized by an emulsifier. Emulsifiers are a type of surfactants, or tensides, which lower the interfacial tension between two liquids, increasing the stability of the emulsions, so that once formed, does not change significantly over time (Fig.1.2). Emulsifiers are usually organic compounds that are amphiphilic, meaning they content both hydrophobic groups (“tails”) and hydrophilic groups (“heads”). Therefore, emulsions are soluble in both organic solvents and water [8-9]. The selected emulsifiers for the 3P systems tricresyl phosphate and diphenyl-2-ethylhexyl phosphate, are responsible for controlling and stabilizing the W/O emulsion and slowing down the reaction of the polyurea formation. In the final crosslinked product it works as plasticizer. Recall that the silicate particle size is controlled by that one of the initial W/O emulsion and that the emulsifier effect should be accompanied with a size reduction of silicate particles in the crosslinked resin. This should have some favourable effect on the mechanical performance.

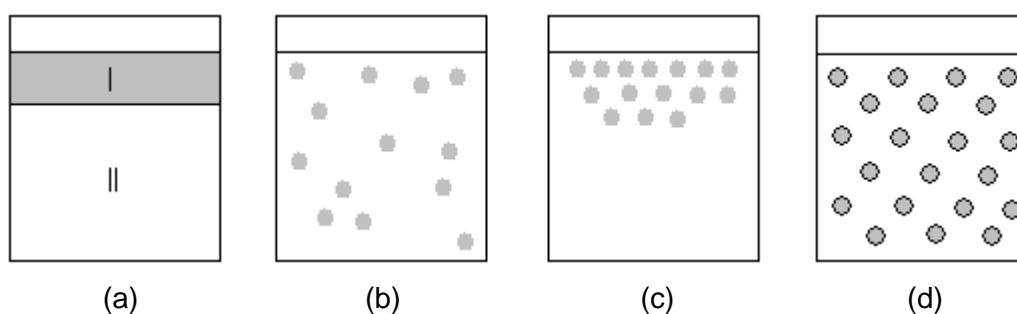


Fig.1.2 - (a) Two immiscible liquids, not emulsified; (b) an emulsion of phase I dispersed in phase II; (c) the unstable emulsion reverts progressively into its initial components; (d) the surfactant (emulsifier) positions itself on the interface between phase I and phase II, stabilizing the emulsion.

The research interest is focused, also to find alternative emulsifiers of reactive nature for the PMDI/WG systems to replace the organic phosphates. 'Reactive' means that the selected emulsifiers should be chemically built in the final cross-linked structure in order to avoid their "leakage". Note that this occurs in the case of the presently used organic phosphates, which slowly diffuse out of the matrix to the environment, and represent potential pollutants. On that account efforts were made to obtain novel types of 3P resins without phosphate, denoted 2P (polyisocyanate and polysilicate). One of our main strategies was to hybridize the organic matrix with other resins in order to improve the properties of the 3P resins. Three different resins were chosen for their promising features; vinyl ester resin, epoxy resin and melamine formaldehyde resin. The fundamental premises to choose these resins were their stability in a strong alkaline medium (provided by WG) and the possibility to build them chemically in the resulting polyurea matrix. First of all, 3P hybrid systems of VE, EP and MF were produced and their mechanical and thermal properties were tested. Once it was asserted that the hybridization of the 3P systems with the different resins was feasible, attempts were made to obtain the same hybrid systems in absence of the organic phosphate emulsifier. This strategy resulted in the so called 2P hybrids. The possible emulsifying effect, control and stabilization of the W/O emulsion of the selected resins, were checked as well as the slowing down of the reaction of polyurea formation ("pot life" of the related resin allowing its processing) [10-12].

2. BACKGROUND

2.1. 3P Chemistry

The chemistry of the 3P resins involves basically the reaction between a polymeric methylene diphenylisocyanate (PMDI) and water glass (WG). WG was dispersed in the polymeric methylene diphenylisocyanate resulting in a water-in-oil type emulsion (W/O). In order to stabilize the emulsion various phosphates (tricresyl phosphate and diphenyl-2-ethylhexyl phosphate), which are also good flame retardant agents, are used. Note that these phosphates act as emulsifiers for the WG in PMDI mixture. The latter is basically a water-in-oil type (W/O) emulsion. The role of the emulsifier is to slow down some chemical reaction occurring between the WG and PMDI, as it will be discussed later. The phosphate remains dispersed in the cured 3P system and will be leached by time. As this process is hazardous for the environment, efforts were made to either reduce the phosphate content or replace it. Moreover attention was paid on how to fix chemically the phosphate replacing compounds in the final polyurea-based system.

Water glass:

When melting sodium carbonate and silicon dioxide, an anhydrous, amorphous water glass and carbon dioxide are formed. Sodium silicates are traditionally classified according to the acid which they are derived as orthosilicate Na_4SiO_4 ($2\text{Na}_2\text{O}\cdot\text{SiO}_2$); metasilicate Na_2SiO_3 ($\text{Na}_2\text{O}\cdot\text{SiO}_2$); disilicate $\text{Na}_2\text{Si}_2\text{O}_5$ ($\text{Na}_2\text{O}\cdot 2\text{SiO}_2$); tetrasilicate $\text{Na}_2\text{Si}_4\text{O}_9$ ($\text{Na}_2\text{O}\cdot 4\text{SiO}_2$).

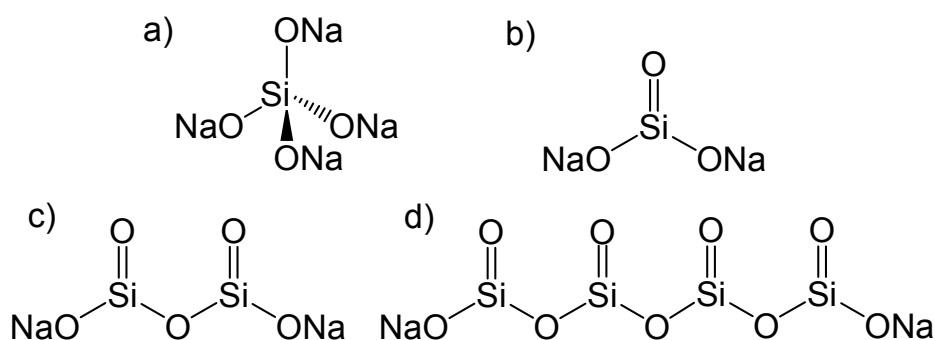
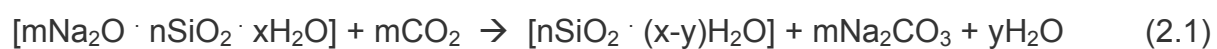


Fig. 2.1.1 - a) orthosilicate; b) metasilicate; c) disilicate; d) tetrasilicate.

Sodium silicate is stable in neutral and alkaline solutions. On the contrary, in acidic solutions the silicate reacts to form silicic acid, which when heated forms silica gel. Water glass has the property to “harden” physically by water evaporation or chemically by various reactions. The “silicification” process induced by atmospheric CO₂ is the hardening reaction that also takes place when WG is mixed with isocyanates, whereas the isocyanate undergoes a reaction producing carbon dioxide [13]. In WG the initial equilibrium reaction is shifted towards the formation of polysilicic acid as NaOH is neutralized by CO₂. The reaction ends up with the dehydration of polysilicic acid to form an in-situ polysilicate framework [14].



Water glass

Silica gel

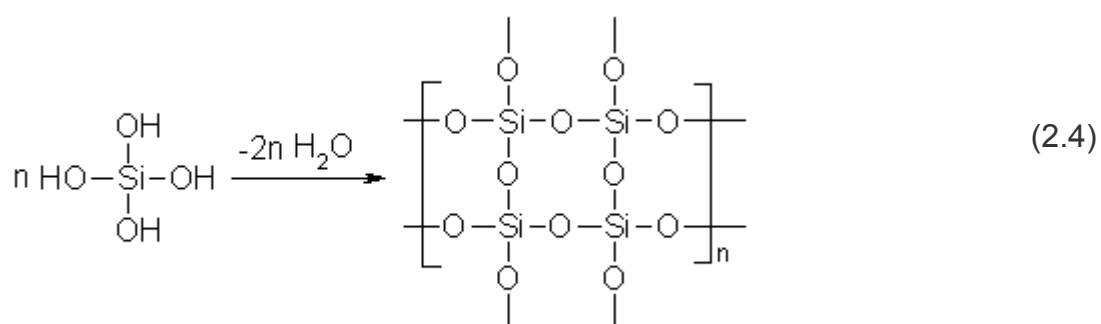
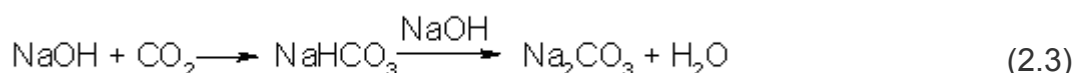
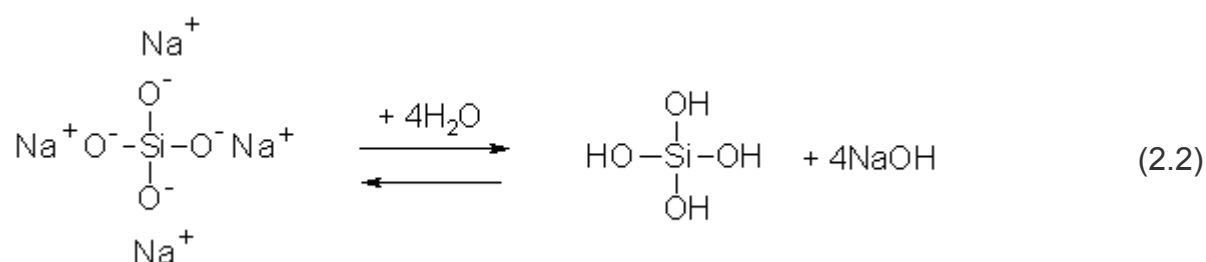


Fig 2.1.2 – (2.1) Global equation of the silicification process; (2.2) equilibrium equation of the aqueous sodium silicate; (2.3) neutralization of the NaOH formed in the previous reaction; (2.4) dehydration of the silicic acid to form silica hydro/xerogel.

The silica gel formed is a xerogel, more accurately a hydro/xerogel depending on the actual constitutional water content [15-17].

Isocyanates:

Isocyanates are high reactive organic compounds. Their high reactivity is provided by the electronic structure. Having a look at the “resonance structures” of the isocyanate one can clearly see that the electron density is much smaller at the carbon atom since this is bonded to two strong electron-withdrawing atoms such as oxygen and nitrogen (cf. Fig.2.1.3). Therefore isocyanate reactions occur preferably through addition to the C=N double bond by a nucleophile containing an active hydrogen atom. The reactivity of the isocyanate functional group will be increased or decreased whether R is an electron-withdrawing group or an electron-donating group. Electron-withdrawing groups increase the isocyanate reactivity because they reduce even more the electron density on the carbon rendering it more reactive. For that reason aromatic isocyanates are more reactive than the aliphatic ones. Steric hindrance can also reduce the reactivity of the isocyanate [18-22].

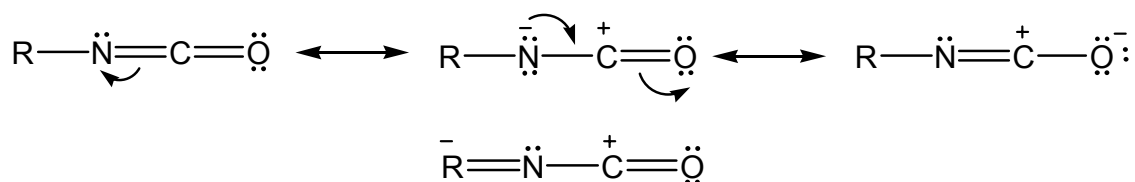


Fig. 2.1.3 - Three possible resonance structures for the isocyanate group, where R can be an electron withdrawing group or an electron donating group. The fourth structure is only possible if the group R is able to support a negative charge such as aromatic groups are.

Isocyanates can undergo a vast range of reactions with compounds that possess active hydrogen bonded to a nucleophilic centre as well as self addition reactions. Next some of these reactions will be briefly explained.

Isocyanate reaction with water (Fig.2.1.4): The nucleophilic oxygen atom of a water molecule attacks the isocyanate carbonyl to yield an unstable molecule of carbamic acid that decomposes forming carbon dioxide as by product and an amine which reacts rapidly with a second isocyanate molecule to form urea.

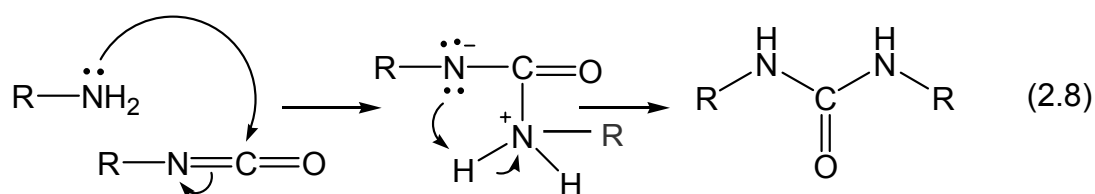
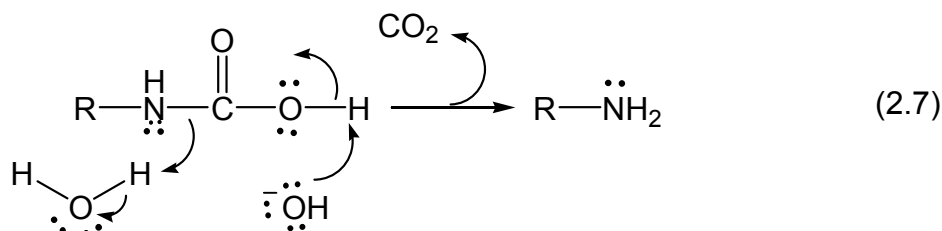
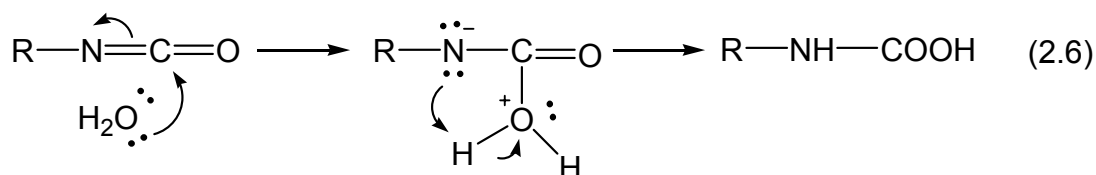
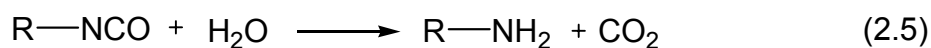


Fig. 2.1.4 - (2.5) Global equation; (2.6) nucleophilic addition of a molecule of water to the isocyanate carbonyl and the corresponding protonation-deprotonation reactions yielding a molecule of carbamic acid; (2.7) decomposition of the unstable carbamic acid formed; (2.8) reaction between the amine formed and a new isocyanate molecule, formation of urea.

Isocyanate reaction with amines (Fig.2.1.5): Nucleophilic addition of the amine group to the isocyanate electrophilic carbonyl to yield a molecule of urea (cf. Fig.2.1.4 2.8 for the reaction mechanism). It is a very fast and exothermic reaction which does not require any catalysation. Aromatic amines react slower than aliphatic amines; the aromatic ring is an electron withdrawing group that reduces the nucleophilic character of the amine. On the contrary, aliphatic chains are electron donating groups which increase the nucleophilicity and thus the reactivity with isocyanates.

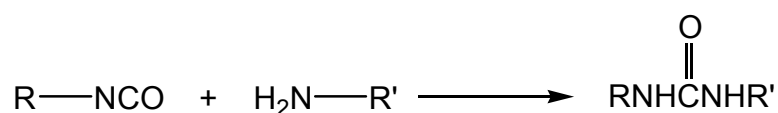


Fig. 2.1.5 - Reaction between isocyanates and amines to form urea.

Isocyanate reaction with alcohols (Fig.2.1.6): The polyaddition reaction between an isocyanate and an alcohol yields a molecule of urethane. The reactivity between these two groups is moderate and requires basic catalysation.

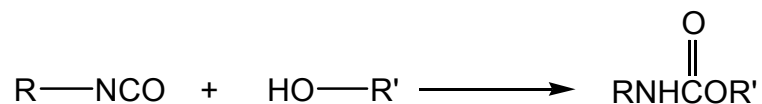


Fig. 2.1.6 - Reaction between isocyanates and alcohols to form urethane.

Isocyanate reaction with carboxylic acids (Fig.2.1.7): The reaction between an isocyanate and a carboxylic acid forms an amide and carbon dioxide as a by-product.

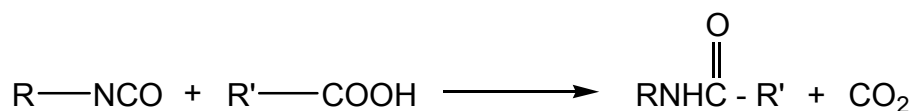


Fig. 2.1.7 - Reaction between isocyanates and carboxylic acids to form amides and CO₂.

Isocyanate reaction with ureas (Fig.2.1.8): When the active hydrogen of a urea group reacts with isocyanate a biuret group develops. Even though the reactivity of the ureas is lower than the primary reactant, amine, they are still capable of nucleophilic attack at the isocyanate under more rigorous reaction conditions. Biuret are normally formed at temperatures between 100°C and 150°C. This reaction is usually involved in the crosslinking of polyurethane.

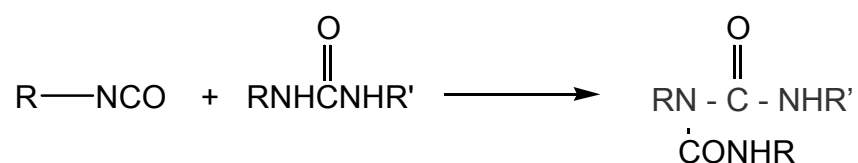


Fig. 2.1.8 - Reaction between isocyanates and ureas to form biuret groups.

Isocyanate reaction with urethanes (Fig.2.1.9): As with the reaction with urea when the active hydrogen of a urethane group reacts with isocyanate an allophanate group is formed. This reaction, as well as the former reaction with urea, is reversible and occurs at temperatures between 120°C and 150°C, and when not catalyzed, it is rather slow.

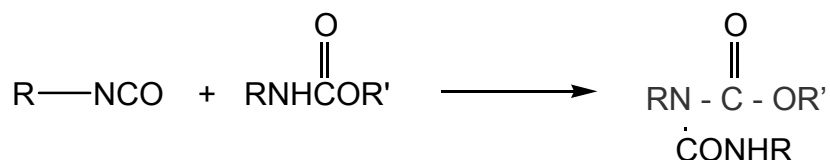


Fig. 2.1.9 - Reaction between isocyanates and urethanes to form allophanate groups.

Isocyanates can also react with themselves to form dimers, trimers, polymers carbodiimides and uretoneimines at high temperatures and in the presence of certain catalysators.

Dimerization (Fig.2.1.10): When two molecules of isocyanate react with each other they form a dimer, a four member heterocyclic ring, which is not very stable since the strain of the four member ring is very high.

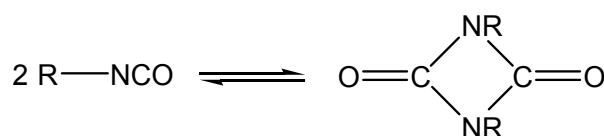


Fig. 2.1.10 - Dimerization reaction of isocyanates to form uretdiones.

Trimerization (Fig.2.1.11): Three molecules of isocyanate can trimerize to form a six member ring molecule of isocyanurate. The trimerization reaction of the isocyanates is favoured at temperatures below 120°C.

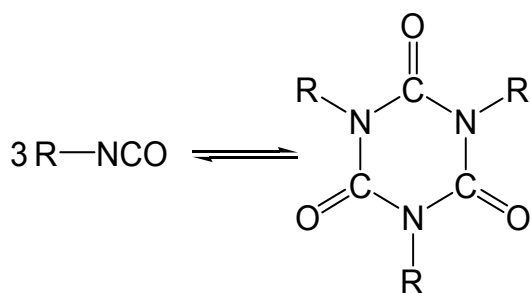


Fig. 2.1.11 - Trimerization reaction of isocyanates to form isocyanurates.

Carbodiimide formation (Fig. 2.1.12): Another important reaction between an isocyanate and itself is the formation of carbodiimides, which is a condensation reaction that can only take place at high temperature without catalyst. However, with

a suitable catalyst, it can occur at room temperature. If the functionality of the isocyanates is more than one, polycarbodiimides will be produced.

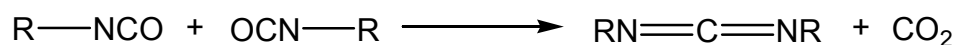


Fig. 2.1.12 – Reaction of two molecules of isocyanate forming a molecule of carbodiimide and CO_2 as side product.

Uretonimine formation (Fig. 2.1.13): The carbodiimide formed in the previous reaction can further react reversibly with an isocyanate group to form uretonimine.

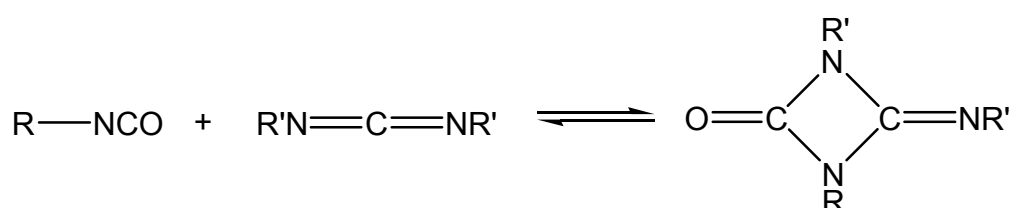


Fig. 2.1.13 – Reaction between isocyanate and carbodiimide to form uretonimine.

The reactivity of the $-\text{NCO}$ group depends on its structure and is different for every hydrogen containing nucleophilic compounds. Next the reactivities of $-\text{NCO}$ with other groups are listed, from the most reactive primary aliphatic amine ($\sim 10^5 \text{ L}\cdot\text{mol}^{-1}\cdot\text{s}^{-1}$ relative reaction rate) to the less reactive amide ($\sim 0.1 \text{ L}\cdot\text{mol}^{-1}\cdot\text{s}^{-1}$ relative reaction rate):

Primary aliphatic amine > secondary aliphatic amine > primary aromatic amine > primary hydroxyl \approx water > carboxylic acid > secondary hydroxyl > ureas > tertiary hydroxyl > urethane > amide.

Reaction in 3P resins:

WG reacts with isocyanate to form at the end polyurea in a polyaddition type reaction. The strong alkali media provided by WG facilitates the nucleophilic addition of the hydroxide ions to the electrophilic carbonyl of the isocyanate. The first reaction is followed by the deprotonation of the acid hydrogen and the protonation of the nitrogen yielding a high unstable carbamic acid that decomposes giving the corresponding amine and carbon dioxide [23-27].

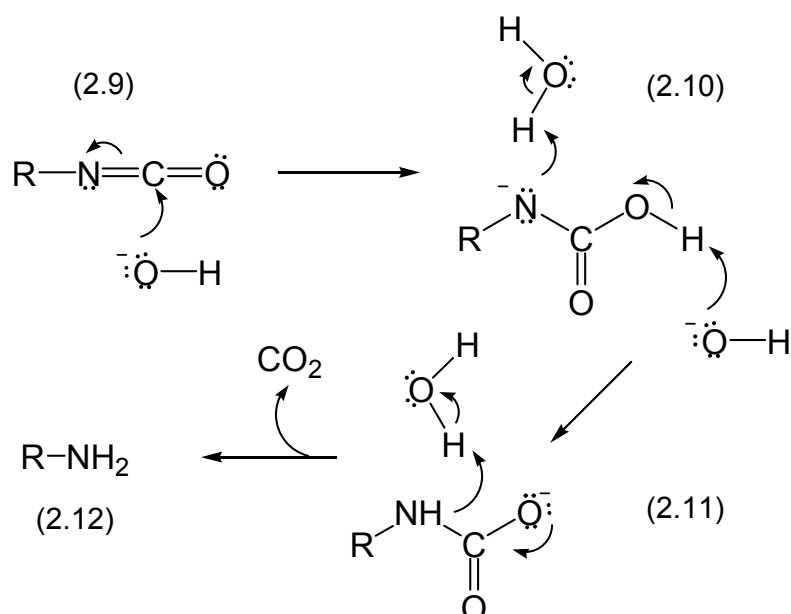


Fig. 2.1.14 – (2.9) nucleophilic addition of the hydroxide to the isocyanate;
 (2.10) Protonation-deprotonation reactions; (2.11) Decomposition of the carbamic acid;
 (2.12) formation of the amine.

The amine formed reacts rapidly with other isocyanate molecules again by nucleophilic addition to yield the final polyurea. The whole reaction is very fast and exotherm. Therefore the use of a suitable emulsifier was required to control the development of the $-\text{NH}_2$ and thus the polyurea/polyisocyanurate side reaction.

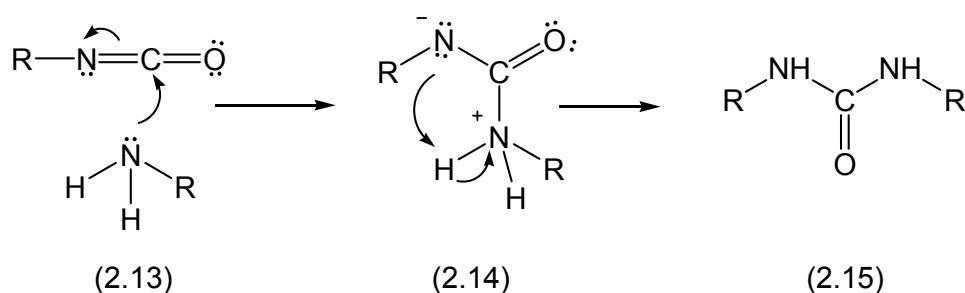


Fig. 2.1.15 - (2.13) nucleophilic addition of the amine to the isocyanate electrophilic carbonyl;
 (2.14) protonation-deprotonation reactions; (2.15) formation of urea.

3P - Vinylester Hybrid Resins

Vinylester resins (VE; Fig.2.1.16) are produced by the esterification of an epoxy resin with an unsaturated monocarboxylic acid. VEs provide outstanding chemical resistance (also alkali-resistant, which is prerequisite to combine it with WG) and are quite polar, which make them compatible with PMDI.

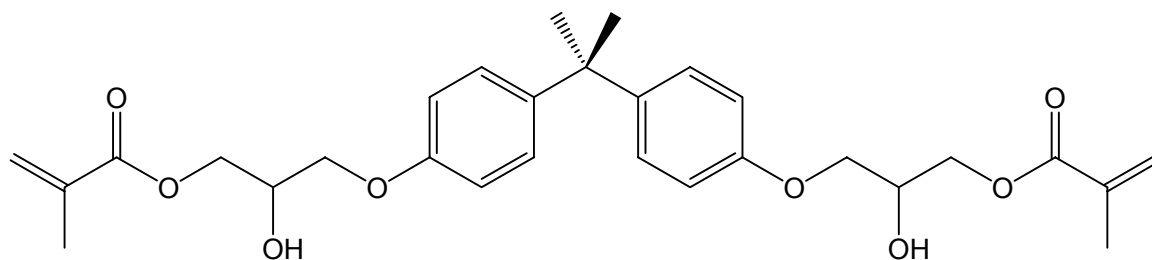


Fig. 2.1.16 – Chemical structure of vinyl ester based on bisphenol A.

The terminal insaturation of the VE can react to give crosslinking either by homopolymerization of the VE with itself or by copolymerization with unsaturated monomers (reactive diluents), such as styrene. Styrene, being a reactive diluent, crosslinks via free radical polymerization with VE, using for example benzoyl peroxide as initiator (cf. Fig. 2.1.17).

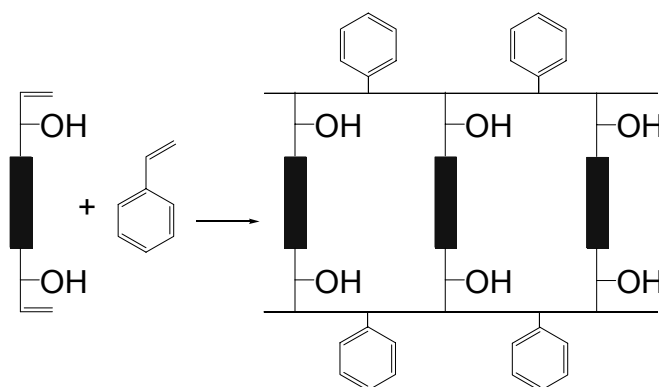


Fig. 2.1.17 – Scheme of the crosslinked structure of vinyl ester and styrene.

The secondary free hydroxyl groups of the VE are capable to react with polyisocyanates to form a urethane modified vinyl ester resin (cf. Fig. 2.1.18) [20-22, 28-31].

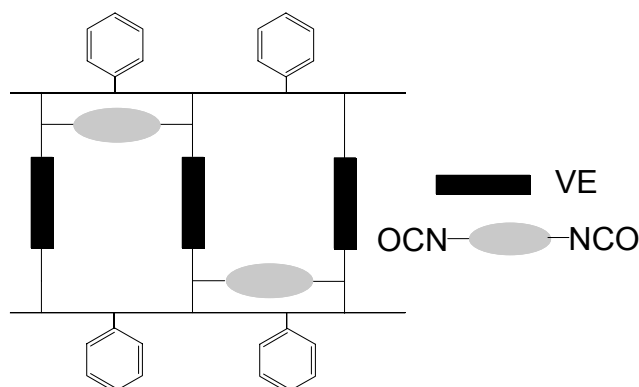


Fig. 2.1.18 – Scheme of the crosslinked structure of vinyl ester-styrene in presence of polyisocyanate.

Reactions in 3P - Epoxide Hybrid Resins

Most common epoxy resins (Fig.2.1.19) are produced by a reaction between epichlorohydrin and bisphenol A. The chemistry of epoxies allows obtaining resins with versatile properties. In general, epoxies are known for their excellent adhesion, chemical and heat resistance, good-to-excellent mechanical properties and very good electrical insulating properties.

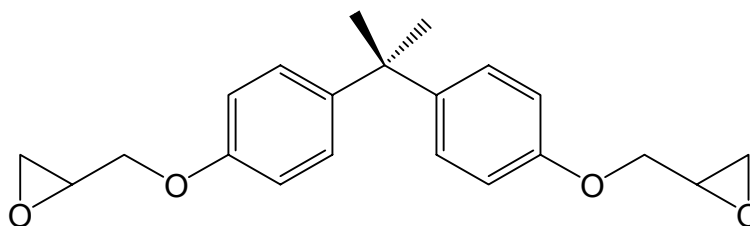


Fig. 2.1.19 – Chemical structure of bisphenol A based epoxy resin.

The chemistry of epoxies is mainly based on the nucleophilic addition to one of their electrophilic carbons forming the epoxy ring with the consequent ring opening. The nucleophilic addition to an epoxide can be base or acid catalyzed. Besides, epoxy rings are especially reactive due to the three member ring. This ring is under a great strain, including torsional strain.

Under acidic conditions, first an oxonium ion is formed. The ring opening takes place when a nucleophile attacks the electrophilic carbon. For substituted epoxies, the ring opening is regioselective forming the most stable carbocation, which is normally the most substituted carbon. However, not very high molecular weight compounds are thus obtainable.

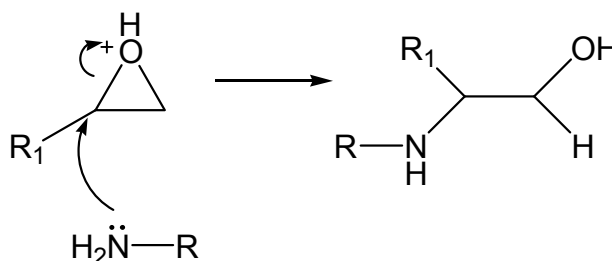


Fig. 2.1.20 – Nucleophilic addition to an epoxide under acid conditions.

Under basic conditions, the ring opening is also regioselective since the nucleophile tends to attack the less hindered carbon, in accordance with standard S_N2 nucleophilic addition reaction process (cf. Fig.2.1.21).

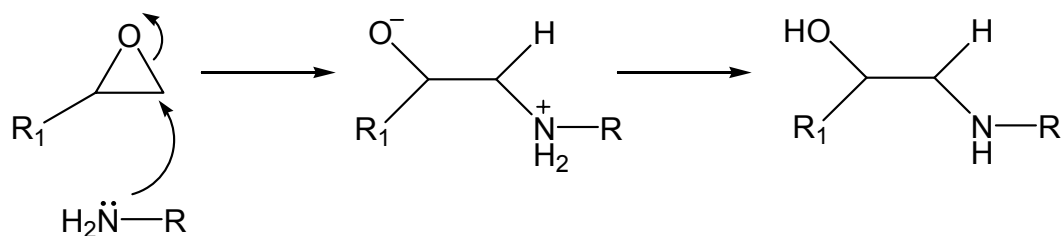


Fig. 2.1.21 – Nucleophilic addition to an epoxide in basic conditions.

In the 3P systems the amine obtained from the reaction between isocyanate and hydroxide from WG (Fig.2.1.14) can undergo a nucleophilic attack to the less substituted carbon of the epoxide (note that the reaction medium is a strong alkali) causing the epoxide ring opening. As a result an alcohol group is formed (Fig.2.1.21) which can react with other isocyanate molecules, as described before for the secondary hydroxyls of vinyl ester (cf. Fig.2.1.18), to form a urethane crosslink (Fig.2.1.22).

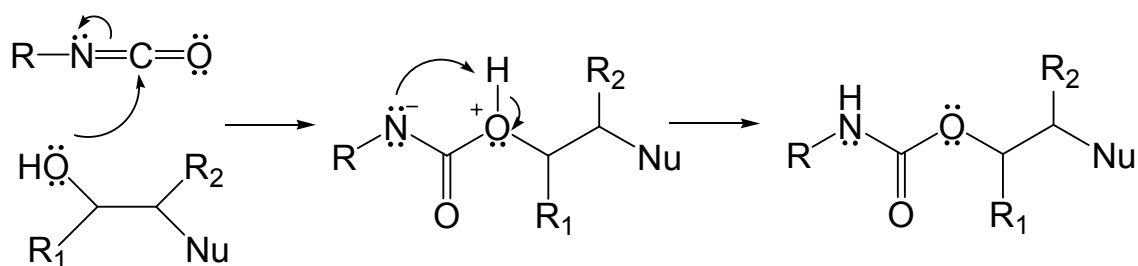


Fig. 2.1.22- Urethane linkage formed from the reaction between the hydroxyl of the formed alcohol and an isocyanate molecule.

Hydroxide anions, from the basic reaction media WG, can as well give a nucleophilic addition to the epoxide ring yielding a diol group, which can once more react with isocyanate molecules obtaining further urethane modified epoxy resin. This nucleophilic addition reaction is quite improbable, since it is less favoured than the reaction where amines are the nucleophiles.

The epoxide group can also react with isocyanate to form oxazolidone linkage as shown in Fig 2.1.23. Oxazolidone is a saturated, five-member heterocyclic group. This cyclic structure is very stiff which imparts rigidity and excellent thermal properties to the polymer. This reaction occurs only at high temperatures i.e. above 180°C or with basic catalysation. Thus the formation of oxazolidone can be controlled by proper selection of temperature and/or catalyst.

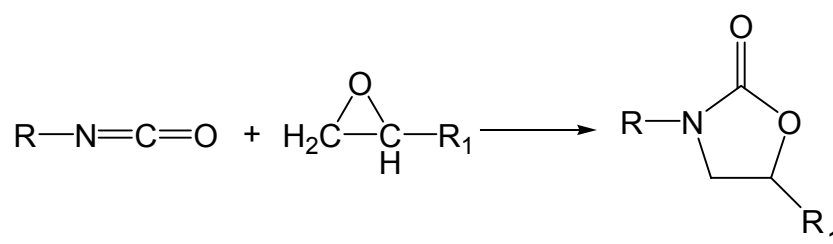


Fig. 2.1.23 – Formation of an oxazolidone, a stable five member heterocyclic ring.

When isocyanates are heated at temperatures below 120°C trimerization to form isocyanurates is favoured. When isocyanates react with epoxies (especially in presence of amines in the temperature range of 70-150°C) the formation of oxazolidones is also started (Fig 2.1.24) [20-22, 32-40].

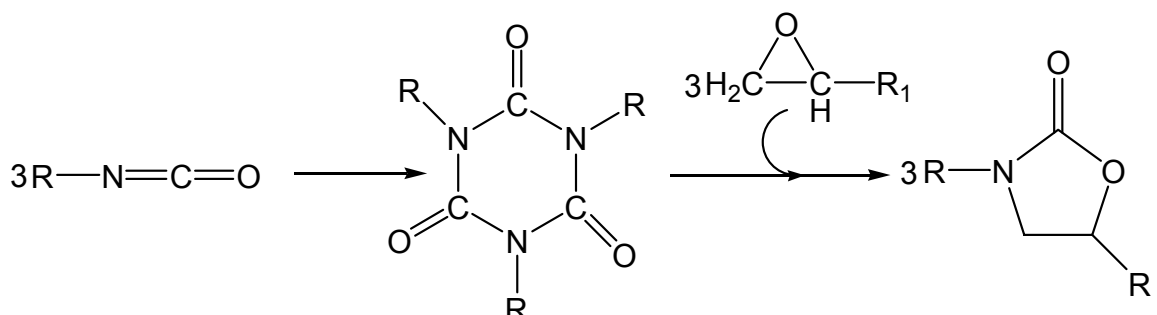


Fig. 2.1.24 – Trimerization of isocyanate to form a molecule of isocyanurate and the posterior reaction with epoxide yielding a molecule of oxazolidone.

Reactions in 3P - Melamine Formaldehyde (MF) Hybrid Resins

Melamine formaldehyde (MF) resins belong to the amino resin family and are widely used, among others, in surface coating systems. To synthesize it, the melamine molecule is reacted with formaldehyde under neutral or slightly alkaline conditions, in a manner analogous to those of urea. A major difference is that, in the initial nucleophilic addition to formaldehyde, each amino group of the melamine may form a dimethylol derivative (Fig 2.1.25). Melamine reacts with maximum six molecules of

formaldehyde per molecule, so nine different methylolmelamines are formed from mono- to hexamethylolmelamine.

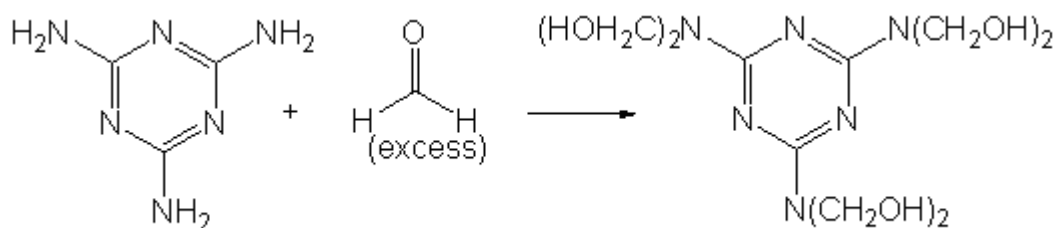


Fig. 2.1.25 – Reaction between melamine and formaldehyde to form melamine formaldehyde in its methylated form hexa(methylol)melamine.

MF cures with the application of heat or an acid catalyst. Two types of condensation reactions are possible: the reaction of an amino group with a methylol group to form a methylene linkage (Fig. 2.1.26) and the mutual condensation of pairs of methylol groups to give methylene ether linkages (Fig. 2.1.27).

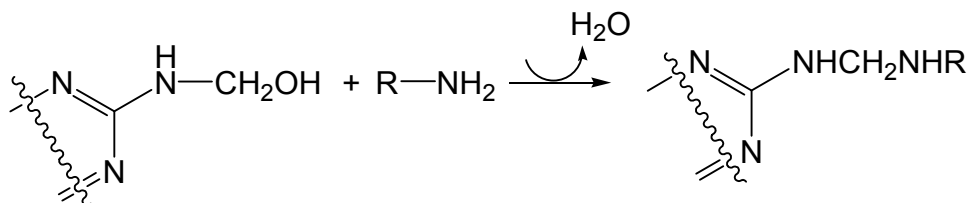


Fig. 2.1.26 – Condensation reaction between melamine formaldehyde and amine yielding a methylene linkage.

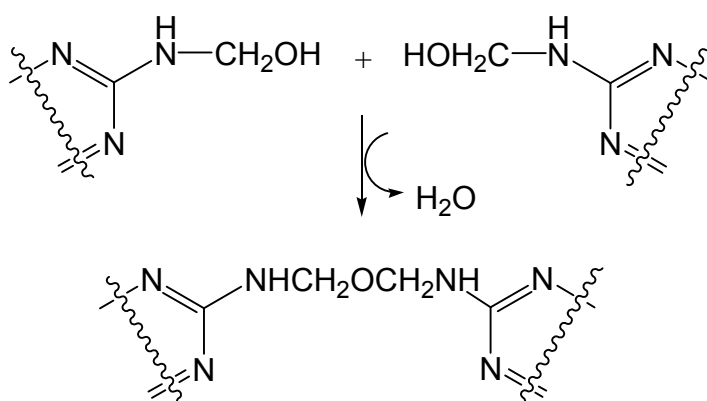


Fig. 2.1.27 – Condensation reaction between two molecules of melamine formaldehyde obtaining an ether linkage.

It is generally believed that the first reaction leading to a methylene crosslinking site is favoured by low pH, by relatively low formaldehyde to melamine (F/M) ratios and by relatively high temperatures during final cure; whilst the second reaction involving the ether linkage is believed to be favoured by high pH and high F/M. It is known that higher curing temperatures improve the acid (corrosion) resistance. This fact is often attributed to conversion of methylene ether to methylene bridges (Fig. 2.1.28), which are far more resistant to hydrolysis than the ether linkage, labile in acidic conditions. Therefore, MF is a good crosslinking agent for diverse polymers containing carboxyl, hydroxyl groups, amines and isocyanates, as well as with polymers containing -CH- and -NH- reactive site groups.

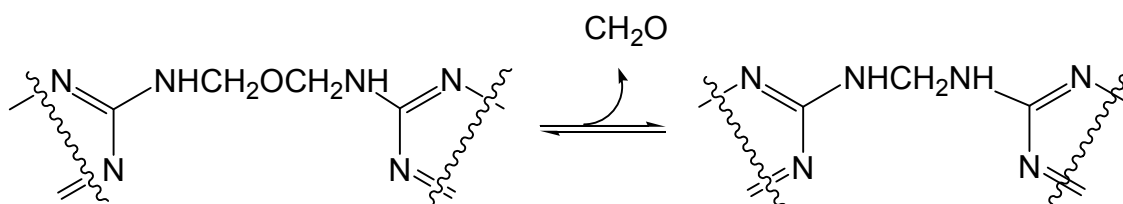


Fig. 2.1.28 – Conversion of methylene ether to methylene bridges.

In the 3P resin chemistry, when MF is dispersed in isocyanate, the hydroxyls from the methylolated melamine react with isocyanates to produce urethane crosslinking sites between polyurea and MF (Fig. 2.1.29).



Fig. 2.1.29 – Reaction between melamine formaldehyde and isocyanate.

Among other possible but less probable reactions count the reaction between the amines, formed thanks to the reaction of isocyanates with water glass (c.f. Fig 2.1.14), with the hydroxyls of the methylolated melamine, as previously explained. However, this reaction is practically inexistent since first, the majority of the amine formed will react with isocyanates to form the polyurea matrix and second, the MF crosslinking speed is practically zero at room temperature while it increases exponentially with temperatures above 100°C. Therefore, the crosslinking with

amines ensues mainly during the curing of the resin, at which point most or all the amine formed in the reaction shown in Fig. 2.1.14 is consumed [20-22, 41-56].

2.2. Uses of 3P resins

The 3P resin is basically a polyurea-based system. Therefore its applications are closely related with those of polyurea (c.f. Fig. 2.1). Polyurea belongs to the family of synthetic polymers obtained from di- or polyisocyanates and di- or polyamines. The condensation reaction is similar to the one of polyurethane although polyurethanes and polyureas show different mechanical and chemical properties. Polyureas can be classified into two groups whether they are aliphatic or aromatic. Aromatic polyureas are often of lower cost than aliphatic ones but they are less resistant to UV radiation, over a period of time colour changes as well as superficial oxidation can occur and they are also more rigid due to the aromatic rings.

Properties and characteristics

Polyurea systems cure quickly. Because of their rapid gel time, moisture does not affect their set up or curing. This is advantageous when using polyurea in wet zones or with high humidity. Polyurea has excellent abrasion resistance, which is important in foot traffic areas. Polyureas also have high heat resistance and are able to resist to thermal shocks. They can be formulated to show high flexibility and high impact / toughness and still have excellent heat distortion resistance. Systems with high temperature stability can withstand working temperatures up to 120°C and intermittent temperatures up to 180°C. Their application range is from -30°C to 150°C.

Polyurea systems are also resistant to many chemicals such as acetic acid, diesel fuel, 2-methylbutane, water, NaCl/water, ammonium hydroxide, sodium hydroxide, potassium hydroxide, sulfuric acid, hydrochloric acid, phosphoric acid without showing any changes in its properties. On the other hand polyurea swells in methanol and toluene [57].

One of the most important advantages of polyureas is that they are 100% solid materials. They contain no volatile organic compounds (VOC), which make them environmentally friendly, and they release no vapours, fumes or chemicals during or after application.

Building and construction

Polyureas are suitable for sealing of metal building seams and fasteners; protection of spray polyurethane foam roofing from hail, birds, traffic and ice build-up; coat expanded rigid polystyrene panels providing physical, chemical and weather protection; lining of steel, masonry or wooden tanks, silos, pipes and flumes; as well as building foundations and other sub-grade applications (piers, pylons), marine applications buoys, moorings; roofing, walls made of concrete, wood, masonry, geotextiles; suitable for automobile roadways, parking garages and pedestrian walkway surfaces, skid and slip resistant. Polyurea coatings and linings are increasingly used to protect steel pipes from corrosion, especially for pipes that are insulated with polyurethane foam. It has been demonstrated its ability to last longer than paint and maintenance services and costs are reduced. They are also used to protect the inside surface of water and sewer pipes in infrastructure rehabilitation work.

Infrastructure

Polyurea is a very fast set material, which makes it ideal for use in line striping and pavement marking. It can be returned to service for traffic and pedestrian use in only a few minutes after application. It is much more durable than paint and typically lasts much longer between maintenance cycles. Polyurea flooring systems are most popular for their rapid turnaround installation capabilities. Other benefits with polyurea flooring systems are their duration for use in areas of high traffic. They are used in clean/dirty rooms as a waterproofing and protective coating from daily pressure cleaning operations. Polyurea can be formulated to be flexible and resilient allowing the flooring system to protect objects that may fall on them. The ability of polyureas to outlast paint and fight off corrosion is a major reason these systems are being

specified for bridge deck and structure. The most common applications of polyurea are coatings on bridges put over steel and concrete. Spray application to a geotextile fabric to form a seamless monolithic membrane for ponds, canals and reservoirs, containment of spills, stops the escape of effluents and other fluids and liquids. Polyureas are also recommended for lining large diameter pipes, manholes, clear wells and process tanks for potable and non-potable water, basins, lift stations and reserve fire water tanks, and to prevent losses of contained water. Polyureas are used for the containment of petroleum products at the drilling site or storage tank farm by lining the berms; it encapsulates asbestos, regulated medical waste and other less than environmentally friendly fluids and materials; it may be used to repair or replace existing containment of vessels liners.

Transport

Lining of rail freight cars to provide abrasion resistance, improve sanitation and reduced friction for a more complete discharge or emptying of material; lining of cargo holds on ships to provide abrasion resistance, ease of sanitation and cleaning; mining industry; abrasion resistant surfaces for snow plows, salt and sand spreaders, dump trucks, sanitation trucks and dumpsters; lining of hot asphalt dump trucks - applied over open-cell flexible foam to seal the surface and provide a good wear surface; provides tough, abrasion, chemical and corrosion-resistant liner for truck beds and under carriages, wheel and fender wells, trailers, stock trailers, etc... Polyureas are commonly used to line liquid containment railcars for their waterproofing and chemical resistance benefits. Hopper style rail cars have benefited from the strength of polyurea and its ability to resist abrasion and load release. These cars often carry coal, sand, and other abrasive materials. Polyurea can be applied quickly and it will last longer than many other conventional systems when properly applied.

Others

Polyurea is used extensively in the water and wastewater industries and are ideal liners for most water tanks, including salt water. Polyurea can withstand most chemical gases produced at waste treatment facilities. Several polyurea systems are

available for potable water; meat and dairy processing plants, butcher shop floors and walls; stock feeding barns; veterinary hospital and clinic examination and treatment floors; kennel floors may have a compressible foam applied underneath the coating for animal comfort; Zoo environments; waste processing plants, etc... Polyurea coatings protect steel tanks from corrosion, chemicals, and other natural weather and jobsite elements. With proper surface preparation, substrate condition, formulation choice, primers, and installation procedures, polyurea goes on fast and stays on long. Polyureas are great for extending the life of older tanks and can offer limited structural characteristics as well. These systems can be applied during primary construction or in a retrofit environment. With their fast application advantages and ability to adhere to properly prepared substrates, polyureas are ideal for new storage tank primary lining and rehabilitation projects. They provide a stable surface for decorative items such as artificial landscapes, stage props, art objects, etc. Polyureas are also suitable in production of plastic articles by spraying into open (one side) moulds; patios, driveways, garage and basement floors; sealing and corrosion protection of sewer access covers [58-67].

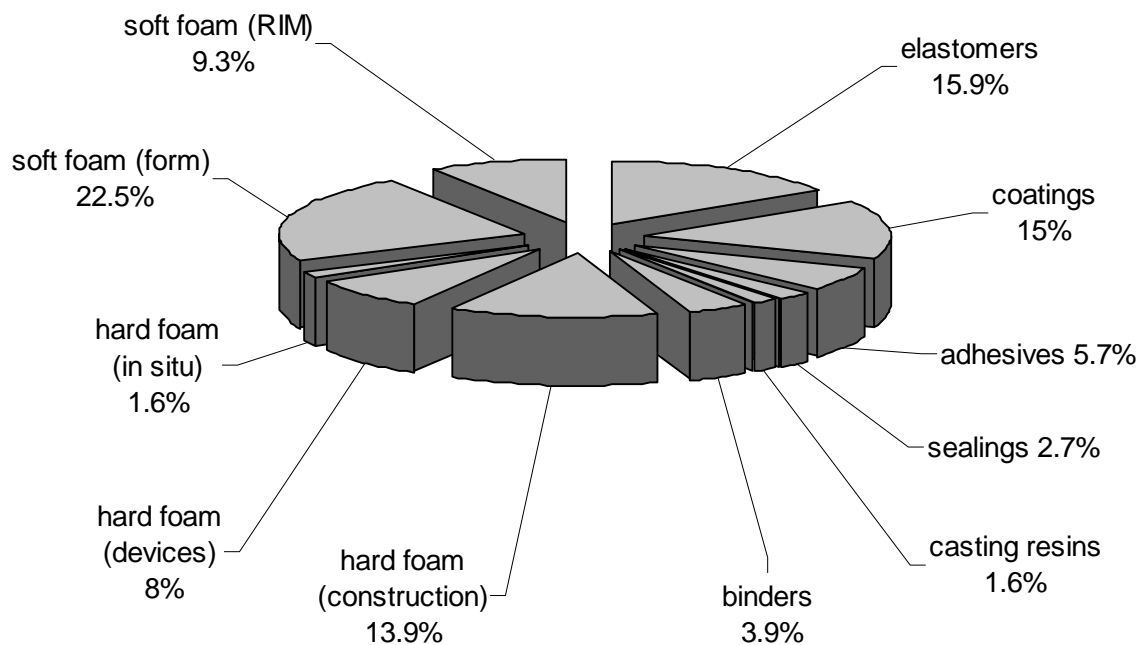


Fig. 2.1 – Main applications of polyurea.

3. OBJECTIVES

The present work was aimed at developing novel thermosetting polyurea hybrid resins with in-situ produced silicate filler from WG. A further aim was to improve their properties, not only mechanical but also thermal and fire resistance properties, compared to the state-of-art 3P resins.

Similarly to thermoplastics, the dispersion-type morphology strongly affects the toughness response also of thermosetting resins. The role of the modifier particles produced either by phase segregation during curing or incorporated in performed shape, is to relieve the triaxial stress state in the crack tip upon loading. Just after that, however, the matrix deformability will be the key toughness controlling parameter [68]. Therefore, in order to enhance the mechanical properties, efforts were made to reduce the mean particle size of the inorganic phase, make their distribution narrower and more homogeneous throughout the polyurea matrix. It means, to obtain a finer water-in-oil emulsion (W/O = waterglass/polyisocyanate) compared to the present 3P resins. This research direction is driven by the finding of Kiefer et al. [69] on the example of epoxy resins the authors demonstrated that a fine dispersion of holes (pores) with small particle size (in micrometres range) is as efficient from the viewpoint of strength and toughness as a similar fine dispersion of spherical fillers. Moreover, attempts were made to improve the bonding between the organic matrix (polyurea) and the inorganic phase (polysilicate). Besides the dispersion type morphology, improved mechanical properties can be achieved by increasing the crosslinking degree, which is associated to higher T_g and stiffness. One of our main strategies to reach the above mentioned goals was the hybridization with other suitable resins. Suitable resins were chosen, among other reasons, based on their negligible or low reactivity with WG; their non-interference with polyurea formation in presence of WG; and their stability in strong alkali media such the one provided by WG. Besides, the generation of hybrid resins of interpenetrating network (IPN) structures was considered as a promising tool to improve the property profile of the present 3P resins. The resins chosen for hybridization, resins are the following:

Vinylester resin (VE)

VE resin was selected as “co-agent” for the PMDI/WG system, considering the commercial success of unsaturated polyester and vinylester “hybrid resin” with polyisocyanates. Note that VE crosslinks via free radical induced copolymerization with styrene and therefore does not compete with the polyurea formation. On the other hand, the secondary -OH groups of VE may react with the isocyanate groups of polyisocyanate yielding a more tightly crosslinked network structure. The outcome of this reaction, along with further approaches to improve the toughness of the so-called vinylester–urethane hybrids (VEUH), was already subjects of investigations. Furthermore, VEs are known as chemically resistant and thus able to withstand strong alkali media such as WG. Moreover, VE itself may act as an additional emulsifier for the dispersion of WG (W/O emulsion) and thus may also influence the WG-induced reactions. So, VE is expected to reduce the mean particle size of the in-situ formed polysilicate phase and to form a conetwork with the polyisocyanate/polyurea through urethane formation [29, 70].

Epoxy resin (EP)

The selection of EP resins, as a possible hybridization component of the 3P hybrid resins, was due to their outstanding mechanical properties and chemical resistance to the alkali media provided by the WG. Moreover, EP may act as well as an additional emulsifier for the dispersion of WG (W/O emulsion). Likewise to VE resins, the hybridization of the 3P resins with EP is expected to result in a reduction of the mean particle size of the polysilicate particles and to form a conetwork with the polyisocyanate/polyurea. Further, EP resins are known for their excellent adhesion, thermal resistance, very good electrical insulating properties, apart from resistance to moisture and low shrinkage [69-70].

Melamine formaldehyde (MF)

MF resin was chosen when looking for alternative emulsifiers of reactive nature for the PMDI/WG systems. ‘Reactive’ means that the related emulsifiers should be chemically built in the final crosslinked structure. Water free MF resins are resistant to strong alkalis and via its methylol ($-\text{CH}_2\text{OH}$) groups reactive towards the $-\text{NCO}$ groups of the polyisocyanate. We were interested to check whether MF can replace phosphate and thus overtake the role of an ‘active emulsifier’. A further target with

the incorporation of MF was to improve the mechanical and thermal properties of the corresponding hybrid resins [71-72].

Following the European Community Regulation on chemicals and their safe use REACH (Registration, Evaluation, Authorisation and Restriction of Chemical substances) (EC 1907/2006) [73], which calls for the progressive substitution of the most dangerous chemicals when suitable alternatives have been identified, additional reactive emulsifiers for the isocyanate/waterglass systems were checked. Our intention was to replace the present organic phosphate emulsifiers being environmental contaminant (since they “leak” as not chemically built in). These new emulsifiers should prolong the pot life of the hybrid systems as well as enhance or maintain their properties. Therefore the 3P resins (from polyisocyanate, phosphate, polysilicate) and their hybrids were substituted by the novel 2P hybrid resins (from polyisocyanate, polysilicate), which were synthesised and characterised.

Further, attempts were made to clarify the structure of the hybrid systems as well as to shed light on the complex kinetics of their chemical reaction pathways.

4. EXPERIMENTAL

4.1. MATERIALS

4.1.1. Waterglass

The silicate source was provided by two different types of Waterglass (WG) with very similar properties. Waterglass Inosil Na-5120 (sodium silicate type) was donated by ASAG Umwelttechnik (Neukirchen-Vluyn, Deutschland). This WG had a “modulus”, i.e. $\text{SiO}_2/\text{Na}_2\text{O} = 2.02 \pm 0.02$ and viscosity: 600 ± 100 mPa·s. Waterglass Betol 3P (Woellner Silikat GmbH, Ludwigshafen, Deutschland) is a sodium silicate aqueous solution, which viscosity, 600 ± 100 mPa·s and „modulus“ $\text{SiO}_2/\text{Na}_2\text{O} = 2.0 \pm 0.05$ are similar to the former. Depicted in Fig. 4.1.1 one can observe the characteristic structure of silica crystals (a) and the one of sodium silicate glass (b).

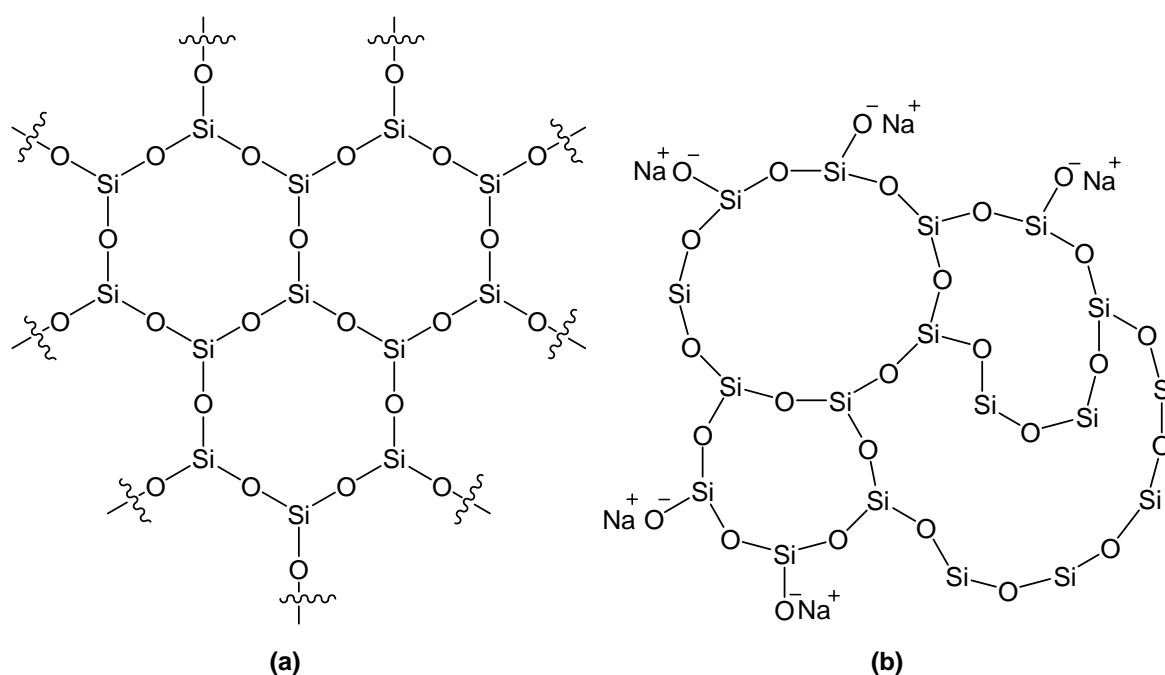


Fig. 4.1.1 - (a) Structure of crystallised silica SiO_2 and (b) structure of sodium silicate glass $x\text{SiO}_2 \cdot y\text{Na}_2\text{O}$.

4.1.2. Polyisocyanates

As polyisocyanate “source” 4,4'-diphenylmethane diisocyanate (MDI) (c.f. Fig. 4.1.2) and a mixture of its higher functionality prepolymers (PMDI) was used. Ongronat[®] CR-30-60 was purchased from Borsodchem Rt (Kazincbarcika, Hungary) and showed the following characteristics: -NCO content 30-31.5 wt. %, viscosity: 520-680 mPa·s, acidity max. 0.05 wt.% and a density of 1.23 g/ml.

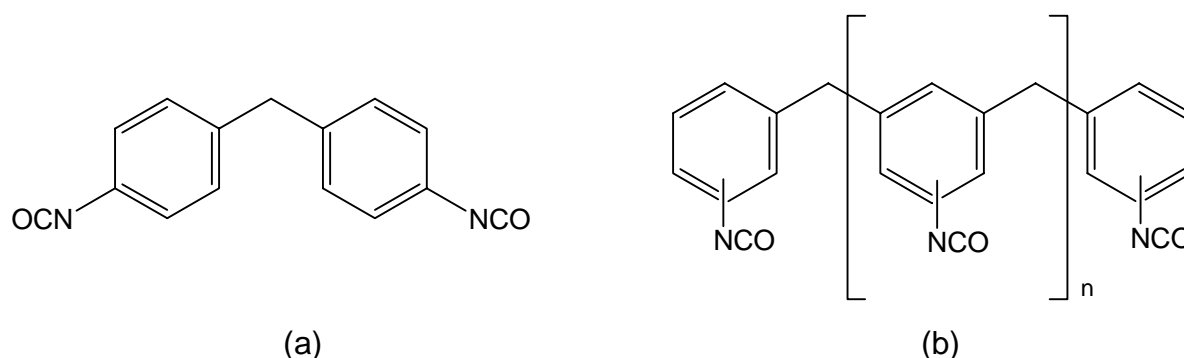


Fig. 4.1.2 - (a) Chemical structure of MDI and (b) chemical structure of PMDI.

4.1.3. Phosphates

For the PMDI/WG system two different emulsifiers were used (c.f. Fig. 4.1.3): tricresylphosphate (TCP) (Disflamoll TCP, Lanxess Deutschland GmbH, Leverkusen, Germany) with an 8.4 wt.% of phosphorous content, 1.18 g/ml density at 20°C and 69 mPa·s viscosity at 20°C and diphenyl-2-ethylhexyl phosphate (DPO) (Lanxess Deutschland GmbH, Leverkusen, Germany) with an 8.6 wt.% of phosphorous content, 1.086 g/ml density at 20°C and 22 mPa·s viscosity at 20°C .

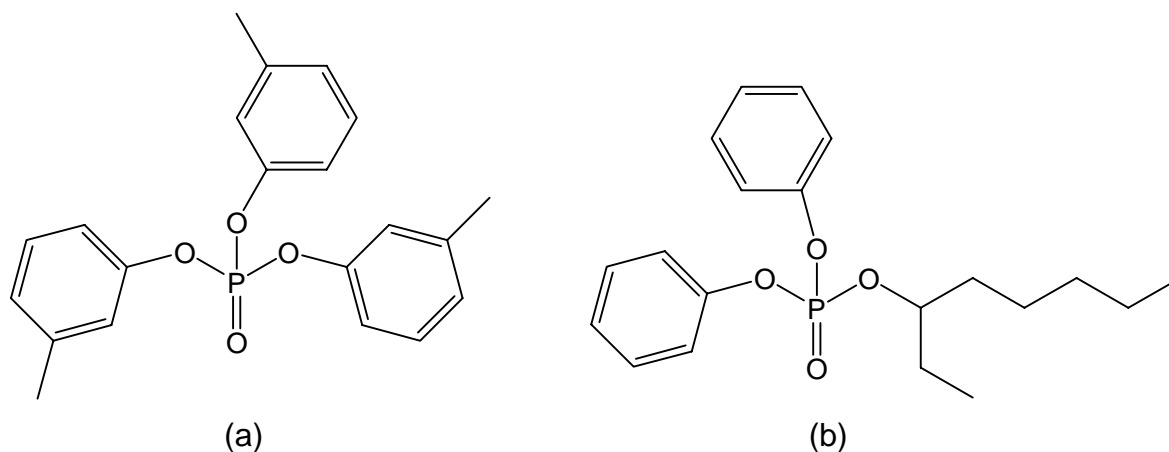


Fig. 4.1.3 - (a) Chemical structure of TCP and (b) chemical structure of DPO.

4.1.4. Vinylester resins

To hybridize the base 3P resin three different vinylester (VE) types were used. Daron XP-45-A2, a vinylester based on bisphenol-A (BA, c.f. Fig. 4.1.4) (DSM Composite Resins AG, Schaffhausen, Switzerland) with a density of 1.080 g/ml; viscosity of 175-225 mPa·s and styrene content of approx. 12-28%; Derakane 411-350 epoxy

vinylester resin based on BA donated by Ashland Deutschland GmbH, Krefeld, Germany showed the following characteristics: density 1.046 g/ml; viscosity 350 mPa·s and styrene content of 45% and Derakane 441-400 epoxy Vinylester resin based on BA, also donated by Ashland Deutschland GmbH, Krefeld, Germany, with lower styrene content with a density of 1.070 g/ml; viscosity 430 mPa·s and styrene content of 33%.

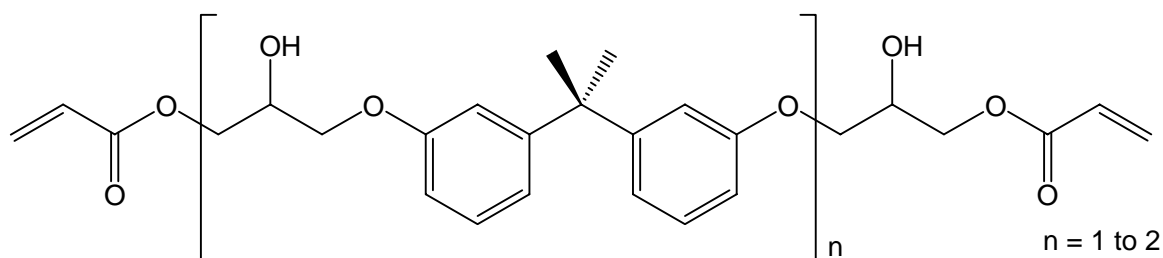


Fig. 4.1.4 - (a) Chemical structure of an epoxy vinyl ester based on BA.

4.1.5. Epoxy resins

Epoxy resin (EP, c.f. Fig. 4.1.5) D.E.R.331 (Dow Deutschland, Schwalbach, Germany) based on bisphenol A and epichlorohydrin was used to study further hybridizations of the 3P base resin. The characteristics of this EP are 22.4 - 23.6% of epoxide; EEW = 189 g/eq; viscosity 11-14 Pa·s and density 1.16 g/ml.

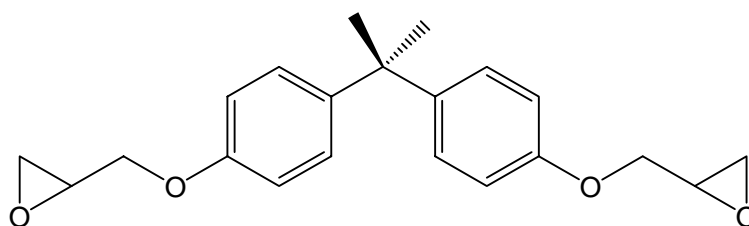


Fig. 4.1.5 - (a) Structure of an epoxy resin based in bisphenol-A.

4.1.6. Melamine formaldehyde resin

Melamine formaldehyde resin (MF) (HIPE®ESIN MF 100C) was purchased from Agrolinz Melamine International Italia S.r.l (Castellanza, Italy). This MF was a white powder of ~0.6 kg/dm³ bulk density and with less than 2.0 wt.% of volatile content. MF owes outstanding properties such as clarity, stability to heat, light, chemicals,

abrasion and fire resistance. It is soluble at room temperature in water and water/alcohol mixtures (c.f. Fig. 4.1.6).

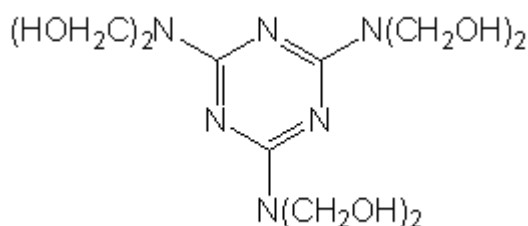


Fig. 4.1.6 - (a) Structure of methylolated melamine formaldehyde.

4.2. SAMPLE PREPARATION

4.2.1. 3P Resin

To prepare the unmodified 3P resin samples the corresponding emulsifier and the PMDI were first homogenized and afterwards WG was dispersed to obtain a stable W/O emulsion. The resin was degassed in vacuum to remove the air bubbles. The component ratio is as follows: 42 wt.% PMDI; 40 wt.% WG and 18 wt.% phosphate. In order to determine the possible property modifications three different mixing and curing regimes were performed. The chosen mixing regimes were the following: 1 min at 800 rpm; 1 min at 2000 rpm and 3 min at 2000 rpm. The influence of the mixer type was also studied; therefore the final WG dispersion of the same resin was carried out either with a propeller mixer or with a cogged-wheel mixer. The final 3P resin was cured according to the following schemes: (a) room temperature (RT) for 7 days; (b) RT for 20h and 80°C for 4h; (c) RT for 20h and 100°C for 4h (d) RT for 20h and 140°C for 4h.

4.2.2. 3P/ Hybrid Resins

4.2.2.1. Vinylester Resin (VE)

The synthesis of the 3P/VE hybrid resins was performed by first homogenising TCP and PMDI for 3 min at 1400 rpm and degassing the mixture. Next the VE was dispersed in WG for 5min at 2000 rpm with a cogged-wheel mixer and the resulting mixture was as well degassed in order to facilitate the final degassing, afterwards

dibenzoyl peroxide, 1,5 wt.% amount of VE, was dissolved. Finally the two components, PMDI/TCP and WG/VE were mixed for 1 min at 800rpm and the air bubbles were removed under vacuum. The curing conditions were 20h at room temperature and 4h at 100°C. Three different 3P/VE resins were synthesized with varying 3P/VE ratio, viz.; 25/75, 50/50 and 75/25 wt.%. For comparison purposes the corresponding 3P and 3P/VE resins, having 3P/VE ratios of 100/0 and 0/100 wt.%, respectively, were also prepared.

4.2.2.2. Epoxy Resin (EP)

To prepare the 3P/EP hybrid resins the PMDI, the emulsifier DPO and the EP were first homogenized and degassed prior to dispersing the WG with a cogged-wheel mixer. Three different dispersing regimes with different mixing times and same mixing speed were performed: 3 min at 2000rpm; 2 min at 2000rpm and 1,5 min at 2000rpm. The final mixture was degassed under vacuum. The 3P/EP ratio was varied from 85/15, 80/20, 75/25 to 65/35 wt.%. Other 3P/EP ratios were not prepared due to the high viscosity of the EP resin. The samples were cured 20h at room temperature and thereafter 4h at 100°C, in order to remove the water from the matrix, the samples were “dried” finally 24h at 125°C.

4.2.2.3. Melamine formaldehyde resin (MF)

The 3P/MF resins were prepared first by homogenising the TCP and the PMDI for 1 min at 1400 rpm. Subsequently MF was dispersed in the PMDI/TCP mixture for 1 min at 800 rpm with a cogged-wheel mixer and degassed under vacuum. WG was added and dispersed in the final system for 1 min at 800 rpm with a cogged-wheel mixer. Some samples were prepared with NH₄Cl (0,2 wt.% of the total MF content), used as an initiator for the MF crosslinking, to prove the influence of the latter in the final properties of the hybrid system. For comparison purposes varying 3P/MF ratios were prepared, viz.; 15 wt.%, 10 wt.%, 5 wt.%, 2.5 wt.%, 1 wt.%, 0.5 wt.% MF in terms of total resin content.

4.2.1. 2P/ Hybrid Resins

4.2.3.2. Vinylester Resin (VE)

To prepare the 2P/VE/MF hybrid resins first the dibenzoyl peroxide (1.5 wt.% of the VE content) was dissolved in the VE and in a separate beaker the MF was dispersed with a cogged-wheel mixer for 1 min at 2000 rpm in the PMDI and degassed. Subsequently the VE and the MF/PMDI were mixed with each other for 1 min at 800 rpm. Finally the WG was dispersed in the mixture for 1 min at 800 rpm and the final resin was degassed under vacuum. To cure the 2P/VE/MF resins the samples were kept 20h at RT and 4h at 100°C. Six different series with increasing MF content were synthesised 0.5 wt.%; 1 wt.%; 2.5 wt.%; 5 wt.%; 10 wt.% and 15 wt.% of the total 2P resin content. The 2P-MF/VE ratio was kept constant 1:1 to simplify the study. When studying the 3P/VE hybrid resins, the 3P/VE 50/50 (1:1) possessed good mechanical properties combined with the narrowest and finest dispersion of the inorganic phase. Therefore the ratio 2P-MF/VE 1:1 was chosen.

4.2.3.3. Epoxy resin (EP)

The preparation of the 2P/EP hybrid resins was carried out by homogenising the PMDI and the EP for 1 min at 2000 rpm and dispersing the WG with a cogged-wheel mixer during 1 min at 1500 rpm. The final mixture was degassed in vacuum and cured 20h at RT and 4h at 100°C. Finally the samples were dried for 24h at 125°C in order to eliminate the matrix-linked water.

4.2.3.4. Melamine formaldehyde resin (MF)

The 2P/MF hybrid resins were produced as follows: different amounts of MF (0.5 wt.%; 1 wt.%; 2.5 wt.%; 5 wt.%; 10 wt.% and 15 wt.% of the total sample weight) were dispersed in PMDI with a cogged-wheel mixer for 1 min at 2000 rpm and then the air bubbles were removed under vacuum. Afterwards WG was added and dispersed for 1 min at 800 rpm. The resulting mixture was degassed in vacuum. The curing regime was 20h at RT and 4h at 100°C.

4.3. MORPHOLOGY CHARACTERIZATION

4.3.1 Scanning Electron Microscope

The scanning electron microscopy (SEM) is a method for high-resolution imaging of surfaces. The SEM uses electrons to create the image by focusing a high energy beam of electrons onto the surface of the sample and detecting signals from the interaction of the incident electrons with the sample's surface. These incident electrons, also referred to as primary electrons, dislodge electrons from the specimen itself. The dislodged electrons, also known as secondary electrons, are attracted and collected by a detector, and then translated into a signal. To produce the SEM image, the electron beam is swept across the area being inspected, producing many such signals. These signals are then amplified, analyzed, and translated into images of the topography being inspected [74].

An SEM (JSM 5400 device of Jeol, Tokyo, Japan) was used to determine the failure mode, the mean particle size and size distribution of the silicate phase on fracture surfaces of CT specimens. As the 3P resin and its hybrids were non-conductive the surface was coated with an Au–Pd alloy before SEM investigation. SEM pictures of minimum three showing more than 100 particles were taken into consideration when determining the particle size distribution. The latter was quantified by the mean number d_n (Eq.4.1) and weight average d_w particle diameter (Eq. 4.2) respectively. Some polished surfaces were ‘mapped’ for phosphor in order to locate the position of the emulsifier. Mapping occurred in SEM by means of a wavelength dispersive X-ray spectrometer (WDX-3PC rom Microspec, Fremont, CA, USA). For this test the surface of the specimens was coated by carbon.

$$d_n = \frac{\sum D_i \cdot N_i}{\sum N_i} \quad (4.1)$$

$$d_w = \frac{\sum D_i \cdot N_i^2}{\sum D_i \cdot N_i} \quad (4.2)$$

Where N_i is number of particles with diameter D_i

4.3.2 Atomic Force Microscope

The atomic force microscope (AFM) is a very high-resolution (in nanometre range) type of scanning probe microscope. In atomic force microscopy (AFM), a probe consisting of a sharp tip located near the end of a cantilever beam is raster scanned across the sample surface using piezoelectric scanners (Fig.4.3.2). Changes in the tip-sample interaction are often monitored using an optical lever detection system, in which a laser beam is reflected from the cantilever onto a position-sensitive photodiode (Fig. 4.3.1). During scanning, a particular operating parameter is maintained at a constant level, and images are generated through a feedback loop between the optical detection system and the piezoelectric scanners. Three imaging modes, contact mode, non-contact mode, and intermittent contact or tapping mode, can be used to produce topographic images of sample surfaces [75-79].

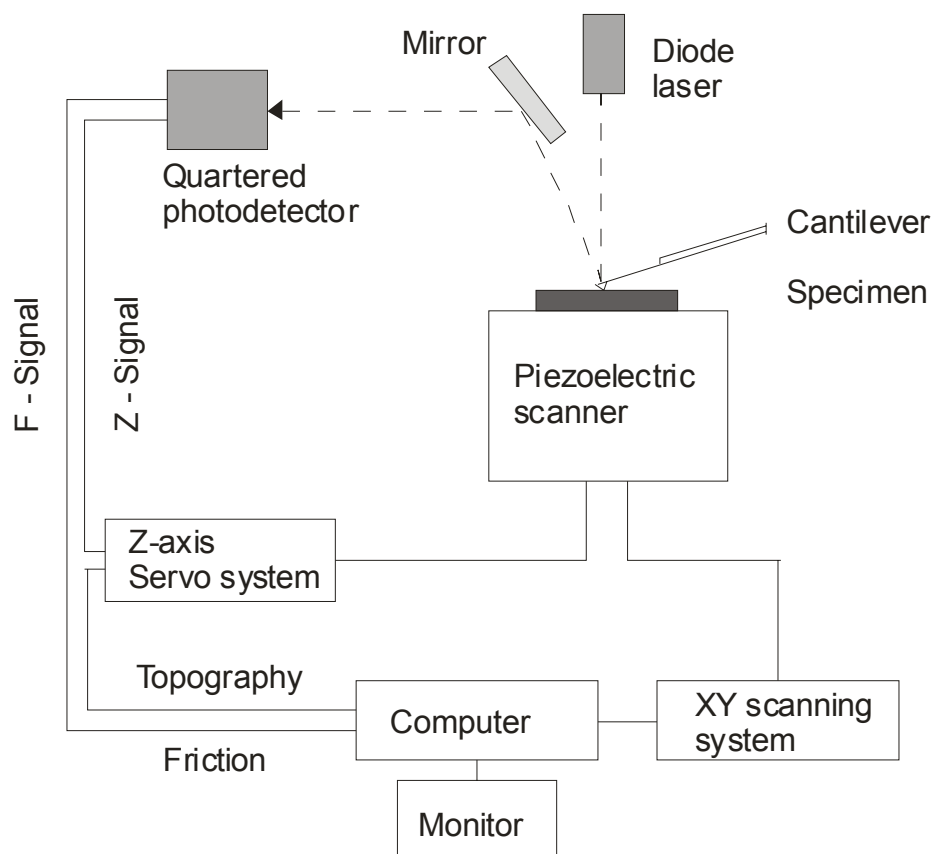


Fig. 4.3.1 - Scheme of the working principle of an AFM.

To obtain further information on the morphology of some systems atomic force microscopic (AFM) studies were carried out. Polished surfaces of the specimens were eroded by Ar^+ ion bombardment. This occurred in a secondary neutrals mass

spectrometer (SNMS, INA3 of Leybold, Cologne, Germany) working at 500 eV energy under normal incidence. The overall ion dose ($1.9 \times 10^{18} \text{ Ar}^+/\text{cm}^2$) resulted in a surface roughening of ca. 200 nm. The surface profile was scanned by AFM (Veeco/Digital Instruments, Mannheim, Germany) in tapping mode and the related amplitude- and height-contrast images captured.

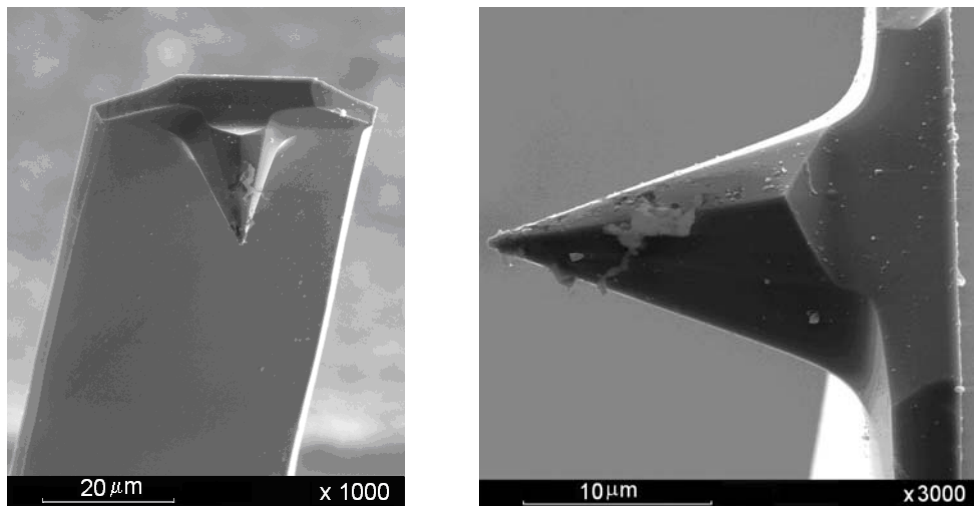


Fig. 4.3.2 - Images of the cantilever (left) and the cantilever's tip (right) of an AFM.

4.4. Mechanical Characterisation

4.4.1 Fracture Mechanics

The fracture toughness (K_{Ic}) and fracture energy (G_c) were measured according to ISO 13586-1 standard. The tests were done with a Zwick universal testing machine type 1445 (Ulm, Germany) at room temperature with a crosshead speed of $v = 1 \text{ mm/min}$. The CT specimens (dimension: $35 \times 35 \times 3 \text{ mm}^3$; length x width x thickness) were notched before loading by sawing. The sawn notch of the CT specimens was sharpened by a razor blade. The razor blade, fixed in a rig, was positioned in the notch root before hitting the fixing rig with a hammer. This yielded the desired sharp crack (c.f. Fig. 4.4.1).

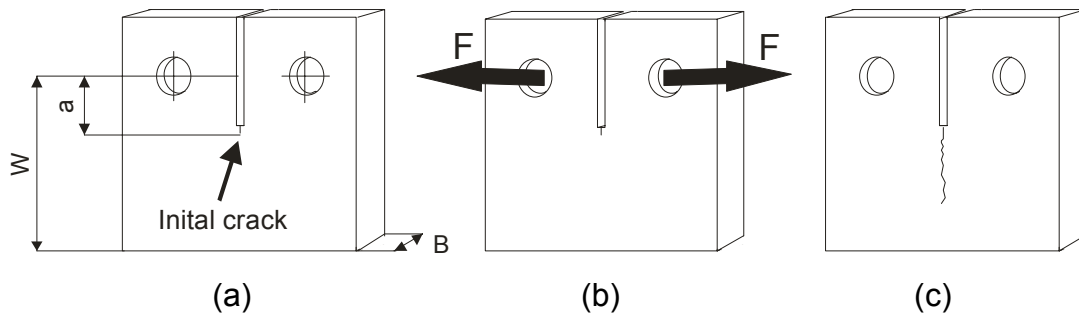


Fig. 4.4.1 - (a) CT specimen with the initial notch performed with a razor blade, (b) direction of the applied stress and (c) resulting specimen after the test.

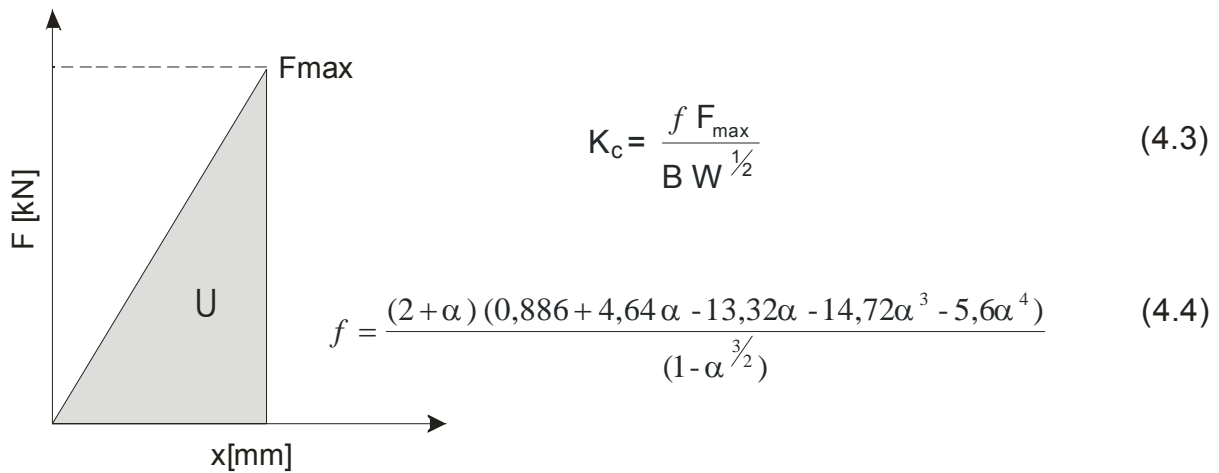


Fig. 4.4.2 – Force-displacement curve, where F is the load applied, x is the load line displacement, U is the energy and F_{max} is the maximum force endured by a sample.

$$\alpha = \frac{a}{W} \quad (4.5)$$

The equation 4.3 allows us to calculate the fracture toughness (K_c), where f is the form factor (c.f. eq. 4.4), F_{max} is the maximum force endured by a sample; B is the thickness of the sample and W is the length of the lever arm. The parameter α can be calculated using Eq. 4.5, where a is the crack length.

The fracture energy G_c is calculated by Eq. 4.6, where U is the energy obtained from the force-displacement curve and f is an energy calibration factor given by Eq. 4.7 [80-82].

$$G_c = \frac{U}{B W \phi} \quad (4.6)$$

$$\phi = \frac{(1,9118 + 19,118\alpha - 2,5122\alpha^2 + 23,226\alpha^3 + 20,54\alpha^4)(1 - \alpha)}{(19,118 - 5,0244\alpha - 69,67\alpha^2 - 82,16\alpha^3)(1 - \alpha) + 2(1,9118\alpha - 2,5122\alpha^2 - 23,226\alpha^3 + 20,54\alpha^4)}$$

(4.7)

4.4.2 Flexural Test

The three-point-bending flexural test provides values for the modulus of elasticity in bending E_B , flexural stress σ_f , flexural strain ε_f and the flexural stress-strain response of the material. The stiffness of materials when subject to bending is of great importance for their use in engineering and structural applications [83-84].

The flexural properties, viz. modulus and strength of the resins, were determined on rectangular specimens ($60 \times 10 \times 3 \text{ mm}^3$; length \times width \times thickness) at room temperature according to EN 63. The span length of the specimens was 50 mm and their loading occurred with $v = 1 \text{ mm/min}$ deformation rate.

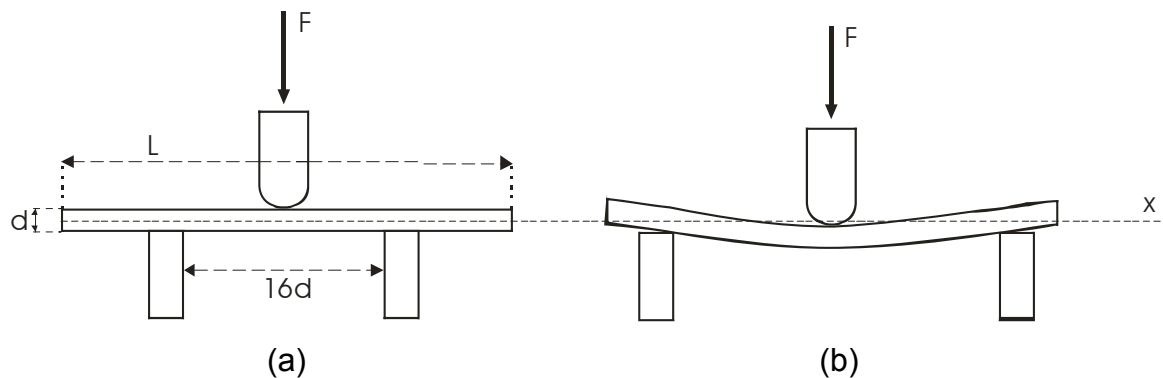


Fig. 4.4.3 - (a) typical 3-point-bending flexural test configuration; (b) deformation experimented by a specimen under an applied stress.

4.4.3 Dynamic Mechanical Thermal Analysis (DMTA)

In order to get information on the phase structure and thermodynamical properties dynamic mechanical thermal analysis (DMTA) was performed. The DMTA spectra informs us about the change in the complex modulus E^* , its constituents (storage and loss modulus E' and E'' respectively) and the mechanical loss factor $\tan \delta$ as a function of temperature T . The related information covers also the relaxation transitions (onset, intensity, etc.), which are not detectable by other methods. In a

dynamic mechanical thermal analysis the specimen is deformed sinusoidally (strain, ε) and the sinusoidally varying responding force (stress, σ) is measured (c.f. Fig 4.4.4). Since the material is not completely elastic the stress resulting from the strain will not be in phase. The shift between stress and strain is denoted δ .

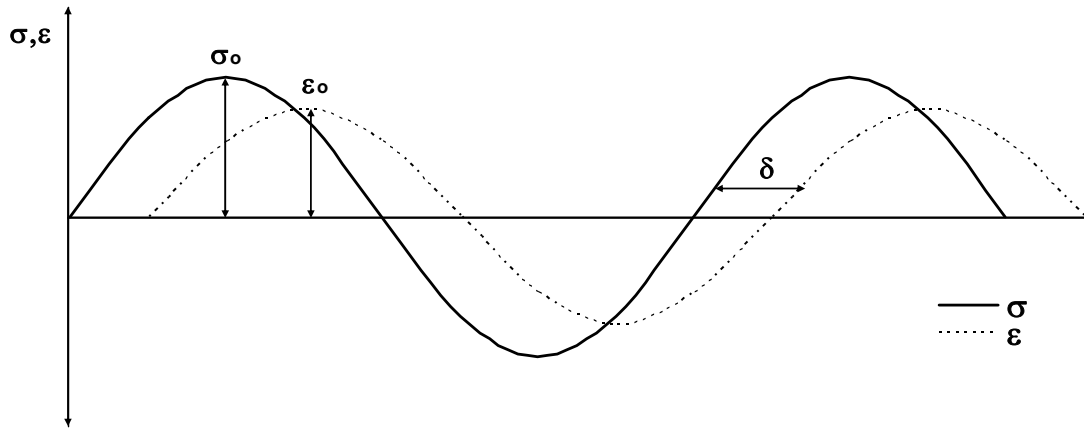


Fig. 4.4.4 – Depiction of the stress (σ_0) and strain (ε_0) curves of a DMTA test.

$$\varepsilon = \varepsilon_0 \sin(\omega t) \quad (4.8)$$

$$\sigma = \sigma_0 \sin(\omega t + \delta) = \sigma_0 \sin(\omega t) + \sigma_0 \cos(\omega t) \sin(\delta) \quad (4.9)$$

Therefore stress can be expressed in two terms, the first one describes the in phase stress and the second one describes a curve shifted 90 degrees out of phase (eq. 4.9). The two separate terms are defined as elastic or storage modulus E' and viscous or loss modulus E'' . The storage modulus E' represents the energy absorbed by a material after every deformation cycle and reverted to the system as recovery energy and the loss modulus E'' represents the mechanical losses due to non-elastic effects. The ratio between stress and strain is the complex modulus E^* , which is a complex number as it contains both real and imaginary components:

$$\sigma/\varepsilon = E^* = \sigma_0/\varepsilon_0 e^{i\delta} = \sigma_0/\varepsilon_0 [\cos(\delta) + i \sin(\delta)] = E' + iE'' \quad (4.10)$$

The greater the loss modulus E'' in comparison to the storage modulus E' the more mechanical loss is generated in the material. Losses are often referred to as damping. A good measure for the damping performance is the loss tangent [17, 84-88]:

$$\tan (\delta) = E''/E' \quad (4.11)$$

The DMTA were taken on rectangular specimens (60 x 10 x 3 mm, length x width x thickness) in three point bending configuration (span length: 50 mm) at 1 Hz using a DMA Q8000 of TA Instruments (New Castle, DE, USA). Tests were performed under amplitude control using sinusoidal oscillation and under dynamic conditions in the interval $T = +25^{\circ}\text{C} \dots +250^{\circ}\text{C}$ at a heating rate of $1^{\circ}\text{C min}^{-1}$.

4.5 ANALYTICAL/THERMAL CHARACTERISATION

4.5.1 Attenuated Total Reflectance Infrared Spectroscopy (ATR-IR)

Infrared (IR) spectroscopy is a spectroscopic technique that uses infrared photons to induce vibrational excitation of covalently bonded atoms and groups. A molecule with N atoms has $3N$ degrees of freedom. Thereof, 3 degrees of freedom are translational, 3 rotational degrees of freedom for a non-linear and 2 for a linear molecule. We thus have $3N-6$ vibrational degrees of freedom for a non-linear and $3N-5$ for a linear molecule. These vibrations are bonding types (number equals the number of chemical bonds), bending types (change of bonding angles), torsional vibrations, out-of-plane vibrations, and others. When the frequency of a specific vibration is equal to the frequency of the IR radiation directed on the molecule, the molecule absorbs the radiation. Infrared spectrometers permit to obtain absorption spectra of compounds that are unique reflection of their molecular structure [90-91].

Attenuated total reflectance infrared (ATR-IR) spectroscopy is one of the few available tools to measure the changes that occur in a totally internally reflected infrared beam when the beam comes into contact with a sample. The technique was developed by N.J. Harrick in the 1960's. Attenuated total reflectance (ATR) spectroscopy utilizes the phenomenon of total internal reflection. In ATR-IR, the IR light passes through the optically denser material and reflects at the surface of the sample (c.f. Fig 4.5.1.). According to Maxwell's theory, when the propagation of light takes place through an optically thin, non-absorbing medium, it forms a standing wave perpendicular to the total reflecting surface. If the sample absorbs a fraction of this radiation, the propagating wave interacts with the sample and its energy or frequency becomes attenuated, giving rise to a reflection spectrum, very similar to

the absorption spectra. In other words, in order to determine the chemical composition of a surface, it can be done using the ATR accessory in the IR spectrophotometer. The infrared radiation is reflected from the surface of the sample, and the resultant spectrum reveals the functional groups present on the surface. For the technique to be successful, the following two requirements must be met:

→ The sample must be in direct contact with the ATR crystal, because the incident wave only extends beyond the crystal $0.5\ \mu\text{m} - 5\ \mu\text{m}$.

→ The refractive index of the crystal must be significantly greater than that of the sample or else internal reflectance will not occur since the light will be transmitted rather than internally reflected in the crystal [92-93].

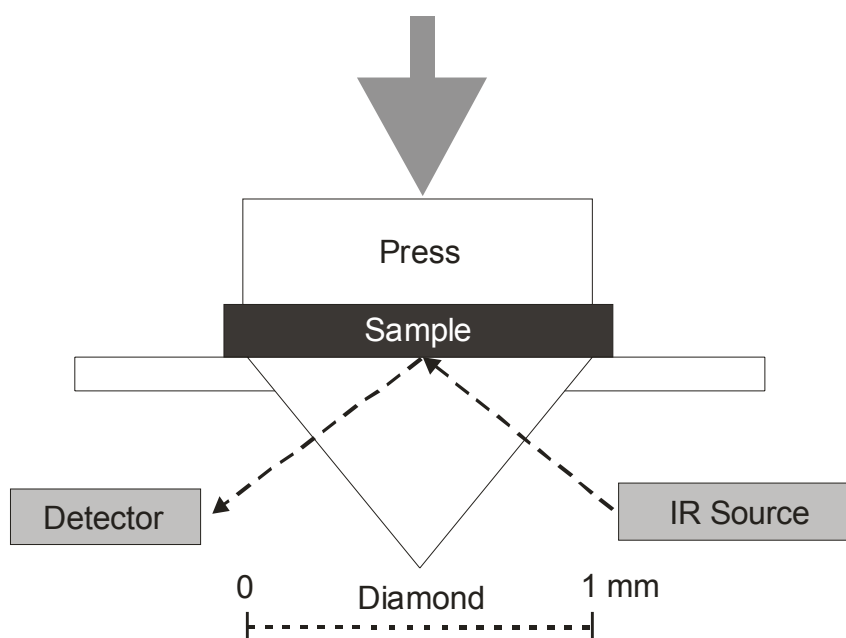


Fig. 4.5.1 - Scheme of the working principle of a ATR-IR.

ATR-IR was one of the methods used to shed light on the 3P reaction kinetics. Because the strength of the absorption is proportional to the concentration according to the Lambert-Beer law, the strength of the characteristic -NCO peak (belonging to the isocyanate) was being measured during the curing conditions to see the progress of the reaction (c.f. Fig. 4.5.2) [94]. One drop of the non cured samples was placed on the surface of the diamond. Several ATR-IR spectra were taken from time zero till the end of the curing process. Therefore the sample was kept 24h at room

temperature and 4h at 100°C, in order to simulate the curing conditions. Spectra were taken every 15 min during the first hour, afterwards every 30 min till the third hour and then every 60 min until the eighth hour. One last spectrum was taken when the twentieth curing hour at room temperature was reached. Further on, spectra were recorded every 30 min during the 4h of curing at 100°C. A Nicolet Impact 400D spectrometer device from Thermo Scientific (Karlsruhe, Germany) was used to carry out the measurements with an ATR-IR unit with diamond crystal from SensIR Technologies (originally Spectratech, Wiesbaden, Germany).

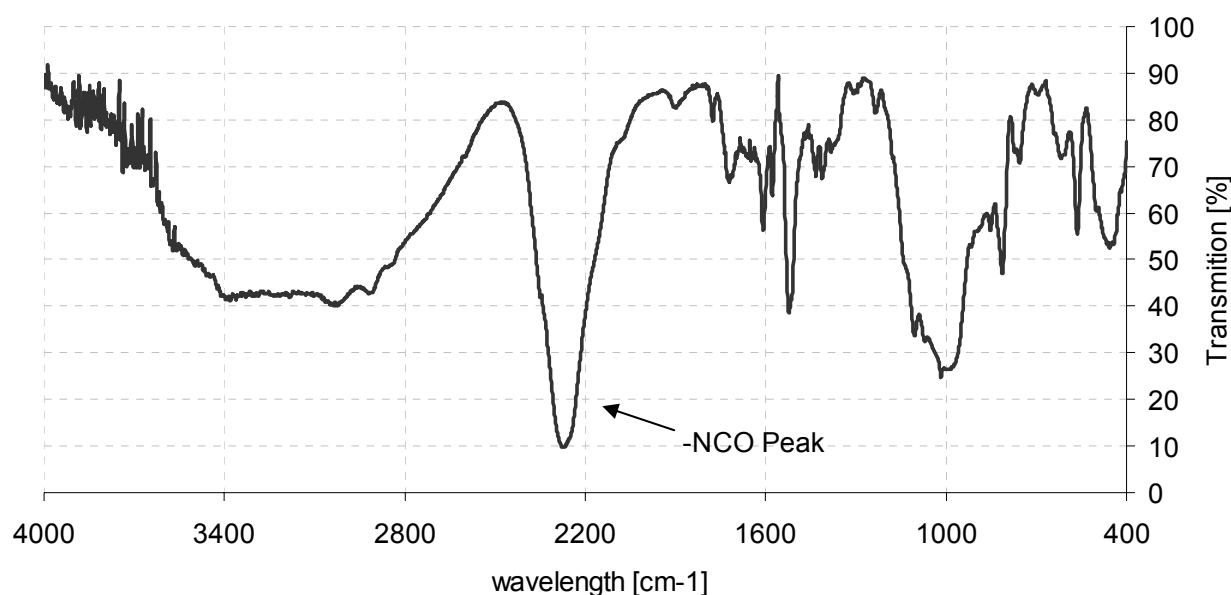


Fig. 4.5.2 - Typical FTIR transmission (%) vs. wavelength (cm^{-1}) diagram showing the characteristic -NCO peak ($2230\text{-}2280 \text{ cm}^{-1}$).

4.5.2 Differential Scanning Calorimetry

Differential scanning calorimetry (DSC) is a thermoanalytical technique in which the difference in the amount of heat required to increase the temperature of a sample and reference are measured as a function of temperature. The basic principle underlying this technique is that, when the sample undergoes a physical or chemical transformation, more (or less) heat needed to flow to it than into the reference to maintain both at the same temperature. Whether heat must flow to or deducted from the sample depends on whether the process is endothermic or exothermic. By observing the difference in heat flow between the sample and reference, differential scanning calorimeters are able to measure the amount of heat absorbed or released

during such transitions. DSC may also be used to observe more subtle phase changes, such as glass transitions [95].

A DSC device DSC821 Mettler Toledo (Giessen, Germany) was used to determine the glass transition temperature (T_g) of the cured systems. The related traces were taken in the range $T=25\dots+350^\circ\text{C}$ at a heating rate of $10^\circ\text{C}/\text{min}$ under nitrogen atmosphere (30 ml/min). Since the samples showed a strong endothermic peak, induced by the release of the water from the matrix, the samples were subjected to two heating cycles in order to reduce this effect. The first cycle was heating the sample from room temperature to 200°C , at a constant rate of 10°C and keeping this temperature for 1 min. With this procedure we ensure that most of the absorbed water is eliminated. Afterwards it was cooled back to room temperature before starting the second cycle from room temperature to 350°C .

DSC tests were also carried out in order to shed light on the system reaction kinetics. Therefore the uncured sample was placed in a Viton® sealed middle pressure pan and studied under curing conditions, 20h at room temperature and 4h at 100°C .

The conversion α_{ISO} at time t and temperature T was calculated by equation 4.12:

$$\alpha_{\text{ISO}} = \Delta H_t / \Delta H_{\text{tot}} \quad (\text{Eq. 4.12})$$

where the total heat reaction, ΔH_{tot} , was determined by the scan of an uncured sample in traditional dynamic mode. Therefore dynamic measurements were carried out in the temperature rang from 25 to 175°C with 5, 10 and $20^\circ\text{C}/\text{min}$ heat rate. To avoid the influence of endothermic effects on the curing kinetic the heat flows obtained for initial WG and TCP were subtracted from 3P thermograms. In order to simplify the kinetic determination it was supposed that ΔH_{tot} corresponded to 100% of reaction conversion [95-97].

4.5.3 Rheology

Rheology (from the Greek *rheos* = *to flow*) is the study of the deformation and flow of matter under the influence of an applied stress. Control of rheology is essential for the manufacture and handling of numerous materials and products, e.g. rubber, plastics, paints, inks, etc. Deformation is the relative displacement of points of a body

and it can be divided into two types: flow and elasticity. Flow is irreversible deformation; when the stress is removed, the material does not revert to its original form. This means that the work is converted to heat. Elasticity is reversible deformation; the deformed specimen recovers its original shape, and the applied work is largely recoverable. Viscoelastic materials show both flow and elasticity (c.f. Fig. 4.5.3).

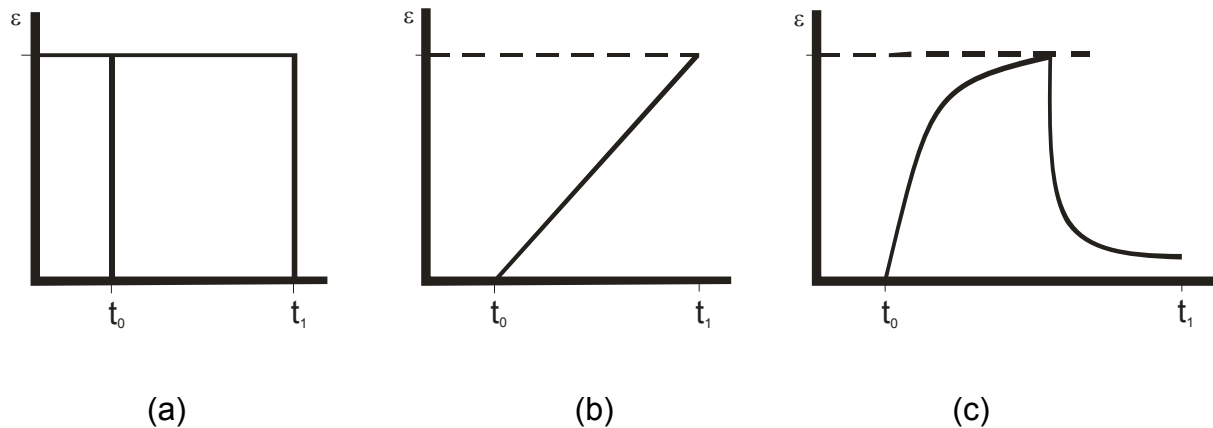


Fig. 4.5.3 – Response (strain) of an idealised material to a stress: (a) elastic, (b) viscous and (c) viscoelastic behaviour.

Similar to DMTA, in rheology the shear modulus G can be defined, which relates shear stress (τ) to shear strain (γ) $G = \tau/\gamma$. The shear modulus is a constant for homogeneous, isotropic and Hookean solids. It can be also represented by a complex variable, i.e., the complex dynamic modulus G^* , which is the ratio of the complex stress and the complex strain: $G = \tau^*/\gamma^*$. The dynamic modulus can also be resolved into two components: $G^* = G' + iG''$. The parameter G' is called the storage modulus and is in phase with the real components of γ^* and τ^* . It is a measure of elasticity and is associated with the energy stored in elastic deformation. The value of G' is high when a polymer is in its glassy state, but drops with increasing temperature as the polymer goes through the glass transition temperature and becomes soft and rubbery. If the polymer is crosslinked, the storage modulus does not drop so far after the glass transition. G'' is called the loss modulus. It arises from the out-of-phase components of γ^* and τ^* and it is associated with viscous energy dissipation, i.e., damping. The ratio between G''/G' gives another measure of damping, the

dissipation factor or loss tangent, $\tan \delta$, which is the ratio of energy dissipated to energy stored (Eq.4.13) [98-102].

$$\tan \delta = G''/G' \quad (4.13)$$

To get information on the rheological properties of the resins a plate/plate rheometer (ARES from Rheometric Scientific Inc., NJ, USA) was used (c.f. Fig 4.5.4). The samples were tested under strain controlled mode at a fixed strain of 1% and 1 rad/s at room temperature (diameter of the plates = 45 mm). Moreover the rheological studies of the uncured resins led us to obtain the gel point, T_{gel} , by observing the crossover point at $G'=G''$ (or $\tan\delta =1$). There the viscoelastic behaviour changes from a dominantly viscous, liquid-like ($G''>G'$) to a dominantly elastic, solid-like behaviour ($G'>G''$). This cross over point is also called the gel point, and it has been used in the rheology to denote a change from a more liquid-like to a solid-like behaviour [103-104].

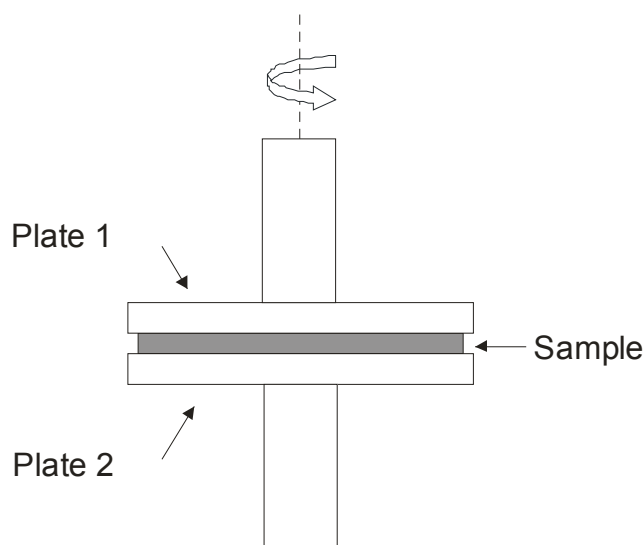


Fig. 4.5.4 – Scheme of the working principle of a plate-plate rheometer.

4.5.4 Thermogravimetric Analysis

Thermogravimetry is one of the oldest thermal analytical procedures and has been used extensively in the study of polymeric systems. The technique involves monitoring the weight loss of the sample in a chosen atmosphere as a function of temperature. It can be used to study any physical (such as evaporation) or chemical process (such as thermal degradation) that causes a material to lose volatile gases.

Thermogravimetric curves provide information about the decomposition mechanisms of various materials. In addition, the decomposition curves may be characteristic for each type of polymer and in some cases can be used even for identification purposes when coupled with additional analytical techniques. The onset of mass loss often defines the upper limit of thermal stability for the material. Though it must be underlined that extensive change in the polymer structure, may have already taken place before the point at which detectable changes in mass occur. The routes by which polymers degrade can be categorized according to six main mechanisms: main-chain scission, side group scission, elimination, depolymerization, cyclization and cross-linking [88, 105-107].

The thermogravimetric analysis of the 3P resin and its hybrids were performed with a TG50 device of Mettler Toledo (Giessen, Germany). The TGA experiments were conducted under nitrogen atmosphere in the temperature range $T = 25^{\circ}\text{C} \dots +600^{\circ}\text{C}$ with heating rate $20^{\circ}\text{C}/\text{min}$.

4.5.5 Flammability test

Flammability is a difficult property to measure in a meaningful way because small-scale laboratory test do not, in general, reflect burning behaviour in true fire conditions. A sample that does not burn well in a laboratory test may burn furiously in a burning room where temperatures are much higher and combustible gases have accumulated [21].

To test the flammability of the materials the UL 94, Tests for Flammability of Plastic Materials for Parts in Devices and Appliances, was used. This test covers several types of testing: The 94HB test describes the Horizontal Burn method; the 94V and 94VTM test used for Vertical Burn; the 94V test is for enclosures for products that are not easily moved or are attached to a conduit system; the 94HBF and 94HF are used for non-structural foam materials i.e., acoustical foam. For our purpose, 94V flammability test was chosen as it is a more stringent test than 94HB. In the 94V flammability test a specimen is supported in a vertical position and a flame is applied to the bottom of the specimen as shown in Fig 4.5.4. The flame is applied for ten seconds and then removed until flaming stops at which time the flame is reapplied for another ten seconds and then removed. Three specimens for each material were

tested. The samples were classified into three groups (94V-0, 94V-1 and 94V-2 – see bellow), depending on which requirements the samples meet.

94V-0: Specimens must not burn with flaming combustion for more than 10 seconds after either test flame application; total flaming combustion time must not exceed 50 seconds for each set of 5 specimens; specimens must not burn with flaming or glowing combustion up to the specimen holding clamp; specimens must not drip flaming particles that ignite the cotton; no specimen can have glowing combustion remain for longer than 30 seconds after removal of the test flame.

94V-1: Specimens must not burn with flaming combustion for more than 30 seconds after either test flame application; total flaming combustion time must not exceed 250 seconds for each set of 5 specimens; specimens must not burn with flaming or glowing combustion up to the specimen holding clamp; specimens must not drip flaming particles that ignite the cotton; no specimen can have glowing combustion remain for longer than 60 seconds after removal of the test flame.

94V-2: Specimens must not burn with flaming combustion for more than 30 seconds after either test flame application; total flaming combustion time must not exceed 250 seconds for each set of 5 specimens; specimens must not burn with flaming or glowing combustion up to the specimen holding clamp; specimens can drip flaming particles that ignite the cotton; no specimen can have glowing combustion remain for longer than 60 seconds after removal of the test flame [108-110].

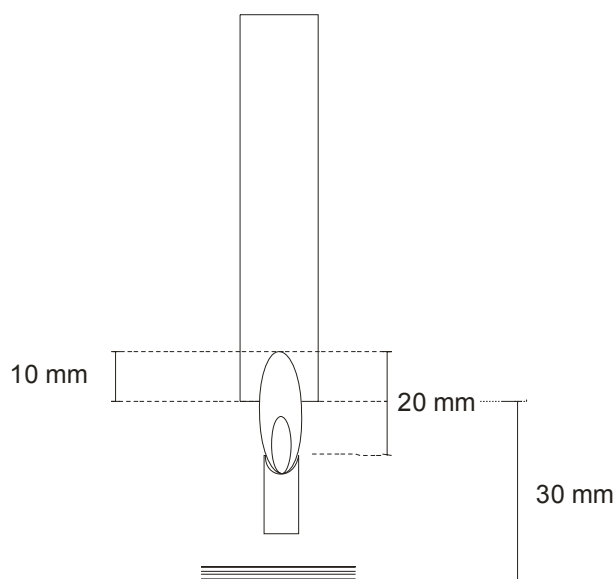


Fig. 4.5.4 – Scheme of the working principle of the UL-94V flammability test.

5. RESULTS AND DISCUSSION

5.1 3P Resins

In order to shed light on the effects caused on the morphology and mechanical properties; first 3P resins with diverse mixing and curing parameters were produced and studied. The same composition was kept for all 3P resins (42 wt.-% PMDI, 18 wt.-% phosphate and 40 wt.-% WG). The coding used to distinguish the different 3P resins is listed below in Table 5.1.1. However, for posterior comparisons with the 3P and 2P hybrid resins, a 3P reference was chosen and denoted as 3P. The latter was prepared as follows: dispersion of the WG in the PMDI (phosphate) by applying a rotation speed of 800rpm during 1 min with a cogged-wheel mixer, and curing for 24h at RT and postcuring for 4h at 100°C.

	Mixer type	Mix. speed	Mix. time	Curing
3P- p	Propeller	800rpm	1min	20h/RT - 4h/100°C
3P- c	Cogged-wheel	800rpm	1min	20h/RT - 4h/100°C
3P- 1	Cogged-wheel	800rpm	1min	20h/RT - 4h/100°C
3P- 2	Cogged-wheel	2000rpm	1min	20h/RT - 4h/100°C
3P- 3	Cogged-wheel	2000rpm	3min	20h/RT - 4h/100°C
3P- RT	Cogged-wheel	800rpm	1min	168h (7 days)/RT
3P- 80°C	Cogged-wheel	800rpm	1min	20h/RT - 4h/80°C
3P- 100°C*	Cogged-wheel	800rpm	1min	20h/RT - 4h/100°C
3P- 140°C	Cogged-wheel	800rpm	1min	20h/RT - 4h/140°C

Table 5.1.1 - Coding for the 3P resin systems produced under different mixing and curing conditions showing the type of mixer; speed and time used to disperse the WG in the PMDI (phosphate) and the following curing regimes. (Later on considered as reference 3P).*

5.1.1 Kinetics

The cure kinetics of the 3P hybrid systems was studied by ATR-IR. The progress of the reaction was monitored by following the intensity decrease of the characteristic absorbance band (-NCO) of the isocyanate (c.f. Fig 5.1.2). One can observe that during the first 4h of curing at RT ca 40% of the isocyanate reacted. Between the first 4h of reaction until the final 20h at RT, the system reacts more slowly since the bulky polymer chains formed hamper the progress of the reaction (c.f. Fig.5.1.3). This presumption is confirmed by rheology (c.f. Chapter 5.1.2). When subjecting the 3P

resins at the second curing temperature stage (100°C), the reaction reaches its maximum evidenced by the highly reduced –NCO band in the ATR-IR spectra (c.f. Fig. 5.1.2). At high temperatures the isocyanate which did not react at RT may as well undergo other reactions parallel to the urea formation; e.g. the trimerization to give isocyanurate; reaction with urea to yield biuret groups, the formation of urethane groups, the formation of carbodiimide and uretoneimine, or the formation of allophanate groups among others. This assumption is confirmed by the appearance of their characteristic absorbance bands at wavelengths (c.f. Fig 5.1): isocyanurate, 1420-1400 cm^{-1} ; biuret, 1630-1510 cm^{-1} ; urethane, $\sim 1540 \text{ cm}^{-1}$; allophanate, $\sim 1660 \text{ cm}^{-1}$; uretoneimine, 1680-1620 cm^{-1} [82]. However, the exact identification of such components was not possible because of the overlapping of their absorbance bands with other bands.

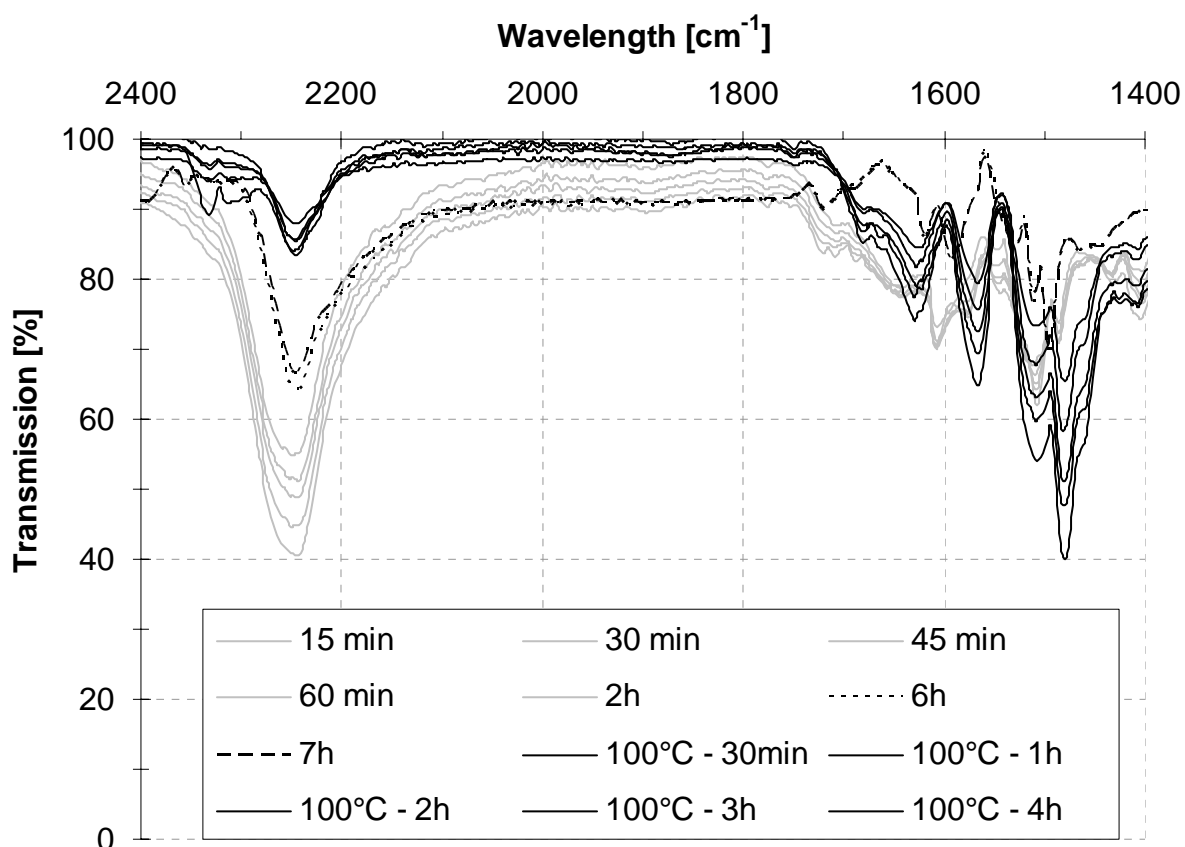


Fig.5.1.1. Transmission [%] vs. wavelength [cm^{-1}] for the characteristic bands of urea, 1600-1500 cm^{-1} , 1690-1620 cm^{-1} ; isocyanate, 2300-2200 cm^{-1} ; 1690-1620 cm^{-1} ; isocyanurate, 1400-1420 cm^{-1} ; biuret, 1630-1510 cm^{-1} ; urethane, $\sim 1540 \text{ cm}^{-1}$; allophanate, $\sim 1660 \text{ cm}^{-1}$; uretoneimine, 1680-1620 cm^{-1} during the curing process.

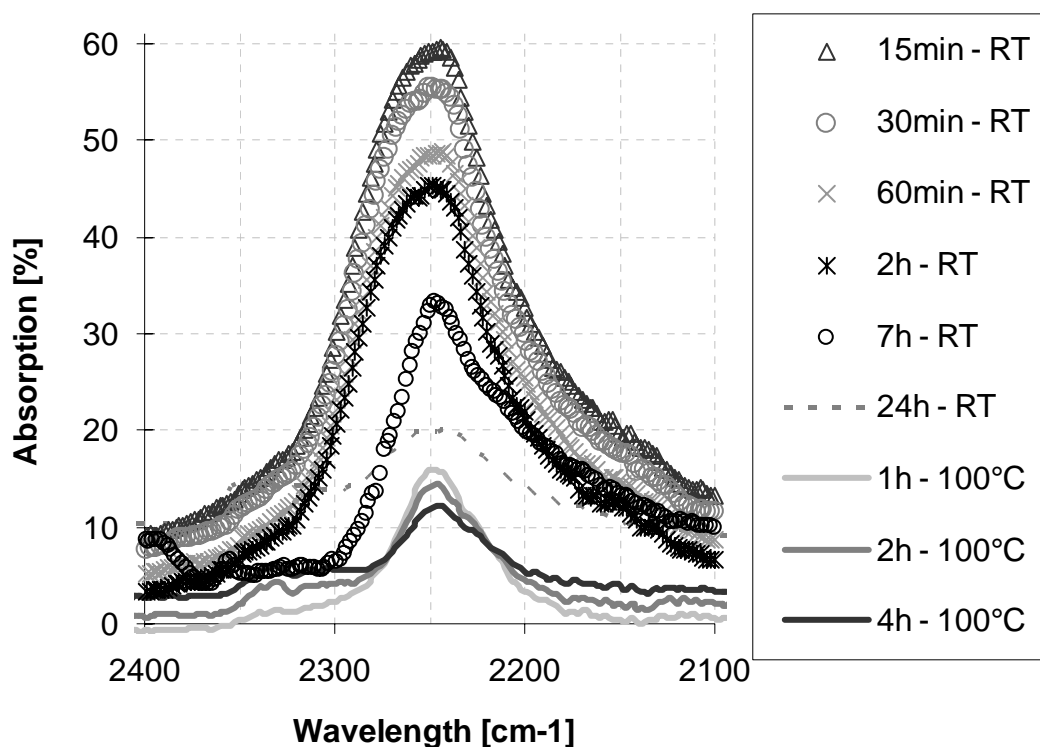


Fig.5.1.2. – Absorbance vs. wavelength of the ATR-IR spectra of the 3P resins at different stages of the curing process.

The maximum isocyanate conversion at the end of the curing process is ~90% (c.f. Fig.5.1.3). To calculate the maximum isocyanate conversion, the absorbance of the –NCO peak at a time t_i of the reaction ($A_0 - A_i$) was divided by the initial absorbance at t_0 , $(100 - A_0)$. As noted before, the high viscosity of the 3P resins at advanced stages of the curing process hinders the mobility of the polyurea chains and enables the non reacted isocyanate to form new polyurea linkages.

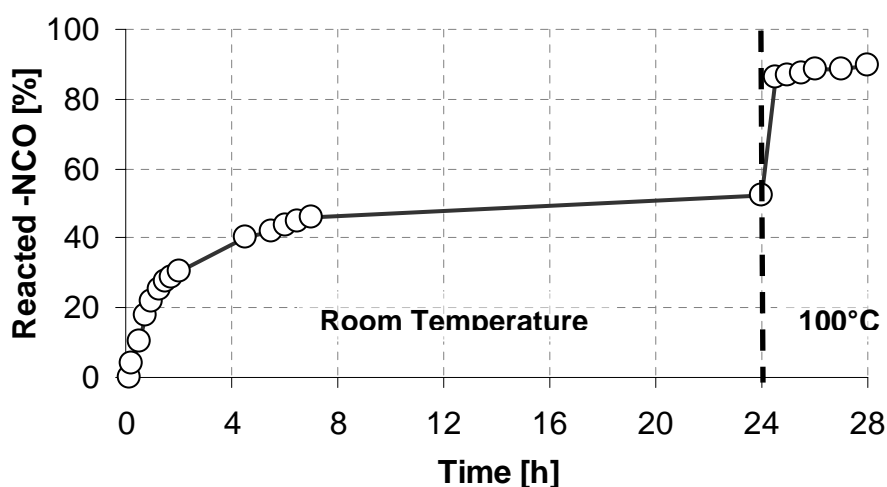


Fig.5.1.3. – Reaction progress during the curing process for the 3P resins.

In Fig.5.1.4 the obtained kinetic curves for different heating rates are presented. Since polyurea reaction is a step-growth polymerization, the reaction kinetics is generally modelled as an n^{th} -order reaction with Arrhenius temperature dependence [94]. The progress of the curves is similar to traditional second order reaction kinetics (S-shaped curve). Note that for lower conversions different reaction orders may hold, since deviations from linearity are observed in this region (two or more kinds of reactions may take part before reaching the “auto-acceleration” at $T > 90^{\circ}\text{C}$). This assumption could explain why no kinetic model concerned with reaction order was used in our work. As expected, for similar second order reactions, the auto-acceleration starts earlier when slower heating rates are used. At lower temperatures, the conversion is probably governed by the reaction between isocyanate and water and later on the reaction rate may be controlled by the reaction of isocyanate with the amine formed as well as by other possible by-side reactions.

The kinetic curve obtained from isothermal curing regime (c.f. Fig.5.1.5) differs completely from the one obtained by dynamic mode. The former resembles a first order reaction type at both, RT and 100°C . From the complicated kinetic curve at RT one could presume that more than one reaction takes place at the same time. In contrast to ATR-IR data a moderate increase in the reaction speed is observed for curing at RT. This may be related to the fact that ATR-IR measured only the progress of the isocyanate reaction by monitoring the extinction of its peak, though other reactions, which are not with -NCO conversion, may also take place. DSC measurements give us the total heat of the reaction, while ATR-IR informs us about the -NCO conversion kinetic. Nonetheless, the final conversion obtained from DSC agrees with that deduced from ATR-IR measurements.

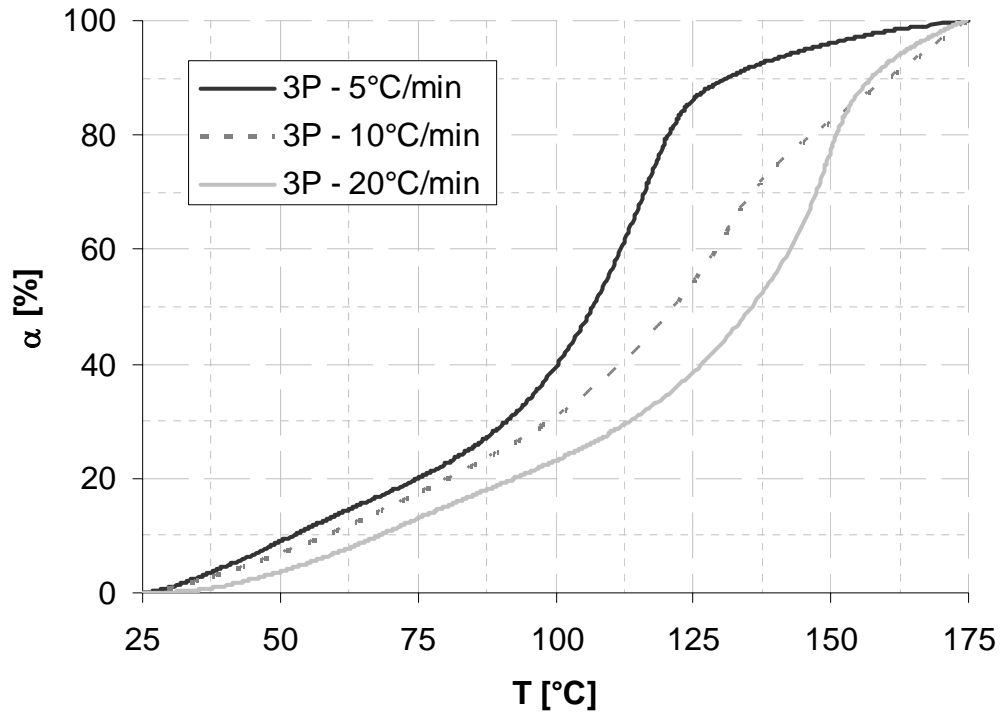


Fig.5.1.4. – Conversion [α] vs. time for the 3P resins at different heating rates.

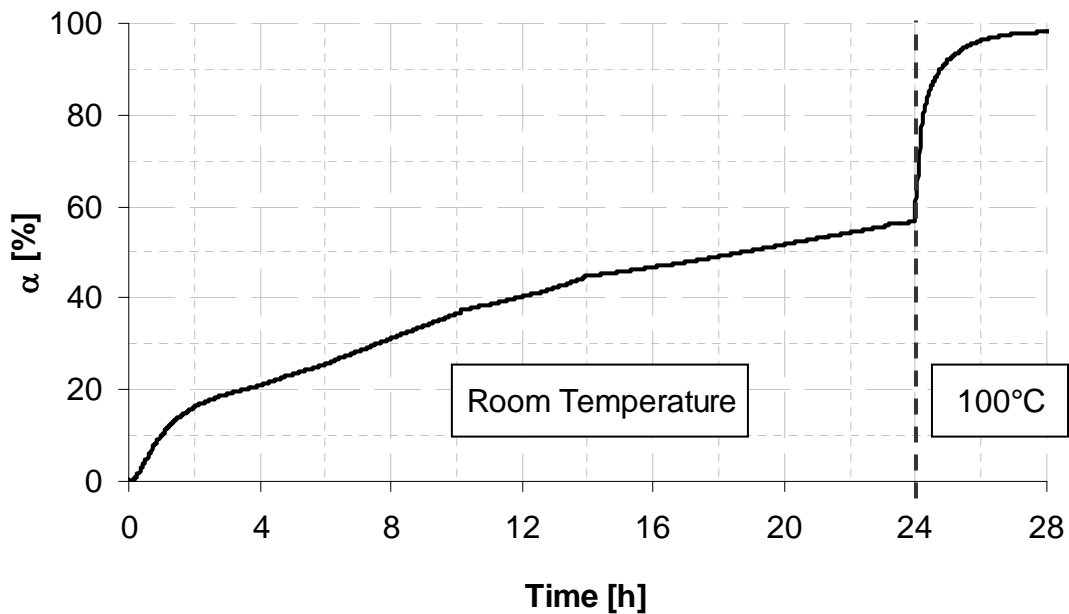
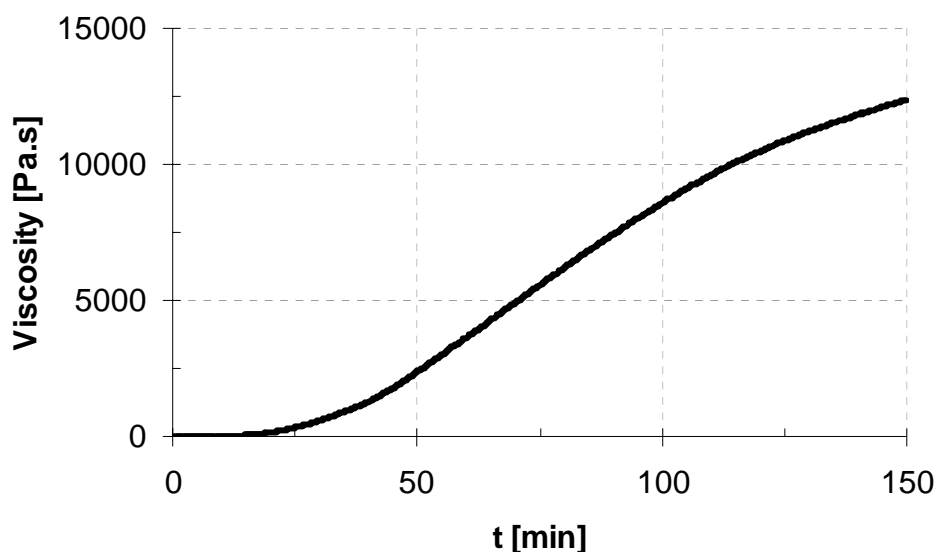


Fig.5.1.5. – Conversion [α] vs. time for the isothermal curing process of the 3P resins.

5.1.2 Rheology

The viscosity of the 3P resin system increases markedly during the first hour of curing at room temperature, as depicted in Fig 5.1.6. After the second hour of curing the viscosity value tripled and continued to increase, however the increment was not

as pronounced as at the beginning. It was observed that the mixing time and speed, as well as the mixer type, did have a negligible influence on the 3P viscosity.



5.1.6 – Viscosity [Pa.s] vs. time [min] for the reference 3P resin system.

5.1.3 Morphology

The characteristic morphology of the 3P resin system is revealed by the broken surface of CT samples (c.f. Fig. 5.1.7-a). The SEM pictures show the size distribution and characteristics of the polysilicate particles derived from the WG phase of the initial W(WG)/O(PMDI) emulsion. The particle size ranges from few micrometers up to 40 μ m. Recall that the WG droplets undergo a nonreversible hydrogel/xerogel transition (“hardening”) accompanied with a substantial contraction which causes the debonding of the polysilicate particles from the polyurea matrix [113]. This is the reason why the diameter of the particles is smaller than the corresponding holes (c.f. Fig 5.1.7 d). Further, the polysilicate particles are covered by needle crystals (Fig 5.1.7 b and c). The latter can be assigned to the formation of Na₂CO₃, which owes this kind of appearance and is formed during the silicification process (“hardening”).

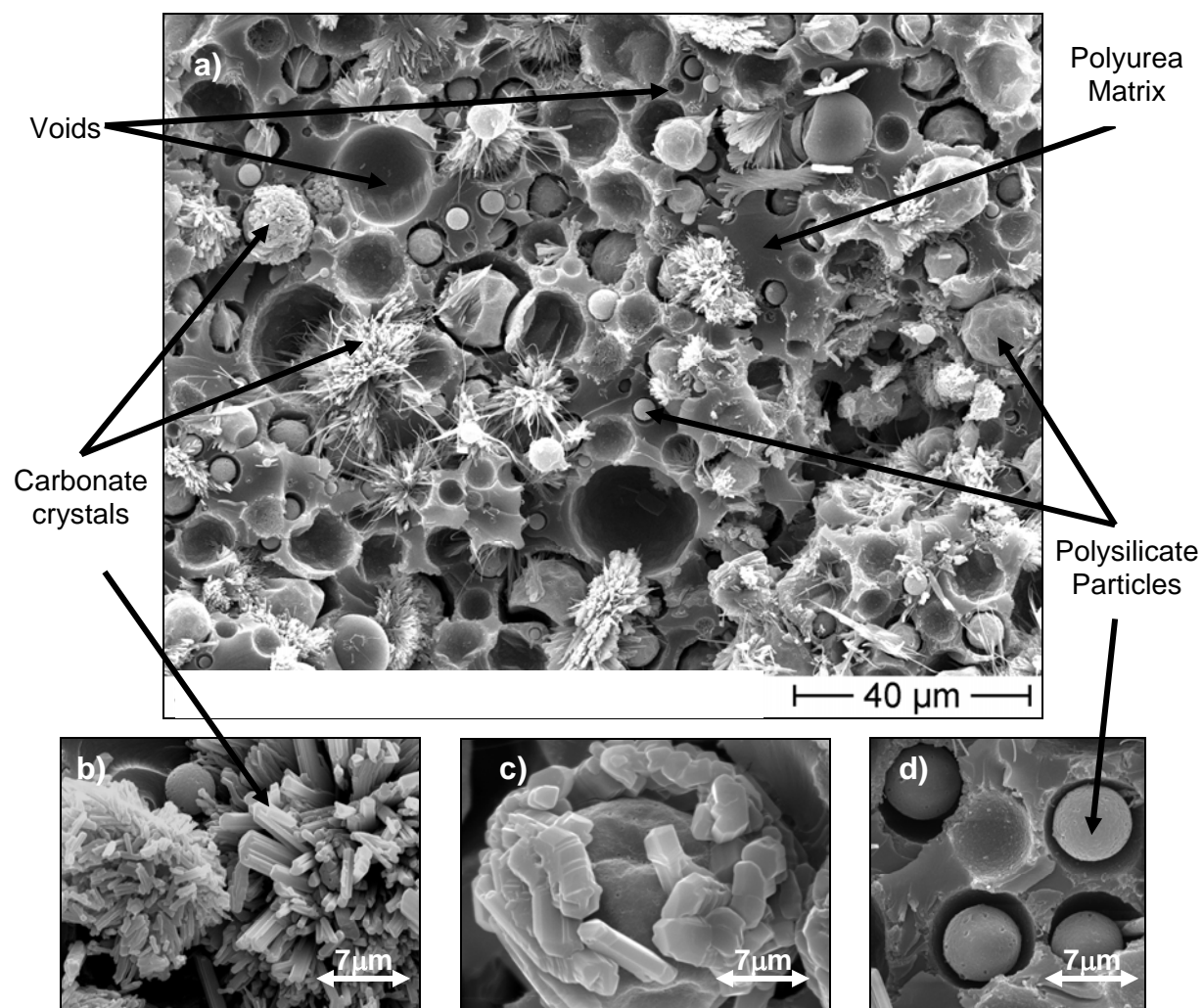


Fig. 5.1.7 - a) SEM picture of the broken surface of the reference 3P resin; b) detail of the needle like Na_2CO_3 crystals; c) Na_2CO_3 crystals covering a polysilicate particle; d) polysilicate particles detached from the matrix due to the hydrogel/xerogel transition .

Inspecting the SEM pictures taken from the broken surfaces of the 3P resins obtained under different mixing conditions (Fig. 5.1.8), one can clearly observe that the key factor controlling the morphology of the systems is the speed at which WG is dispersed in PMDI. This effect is well manifested when comparing the systems 3P-1, dispersed at 800rpm, and 3P-2, dispersed at 2000rpm. It is remarkable how the mean particle size of the polysilicate is reduced from 15.5 μm to 5.0 μm and its distribution becomes narrower (c.f. Table 5.1.2). Differences derived from the duration of the dispersion process are not so significant. However, longer dispersion times reduce somewhat the mean size and provide a narrower distribution of the polysilicate particles (c.f. Table 5.1.2).

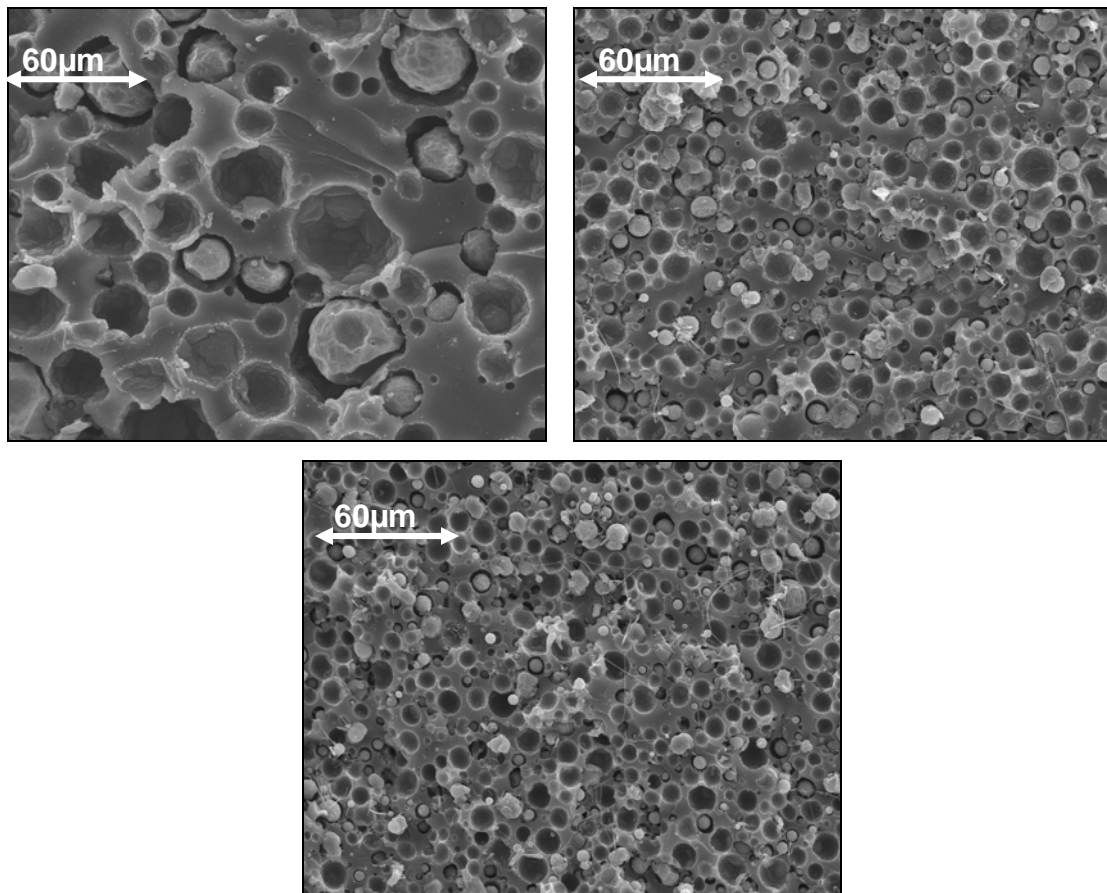


Fig. 5.1.8 – SEM images of the broken surfaces of the 3P resins; 3P-1 (top left); 3P-2 (top right); and 3P-3 (bottom). For coding cf. Table 5.1.1.

The effects of the mixer type on the morphology of the systems are patent when comparing the SEM images depicted in Fig 5.1.9. The use of a propeller mixer reduces the polysilicate particle size; however, when using a cogged-wheel mixer the particle size distribution is slightly narrowed (c.f. Table 5.3.1.2). The formation of the sodium carbonate crystals is not influenced by the mixer type. This is in line with the expectation as they form much later than the related emulsions.

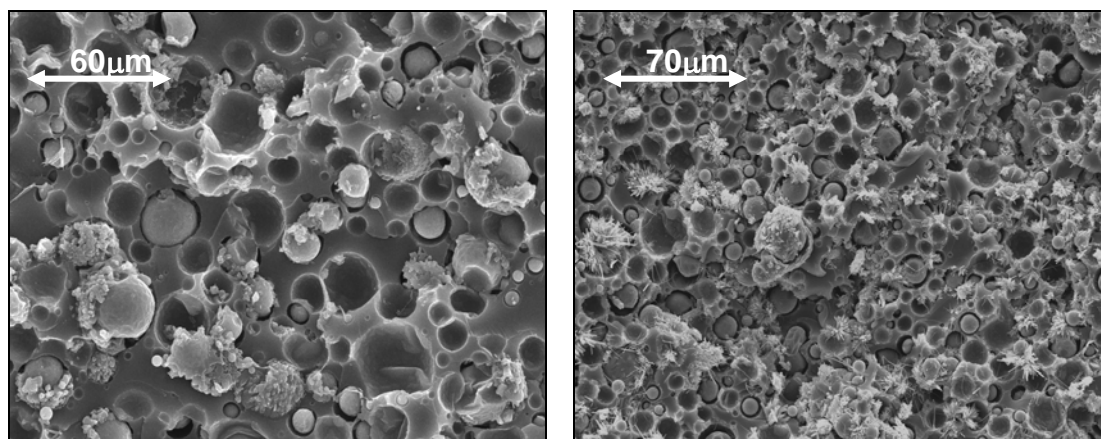
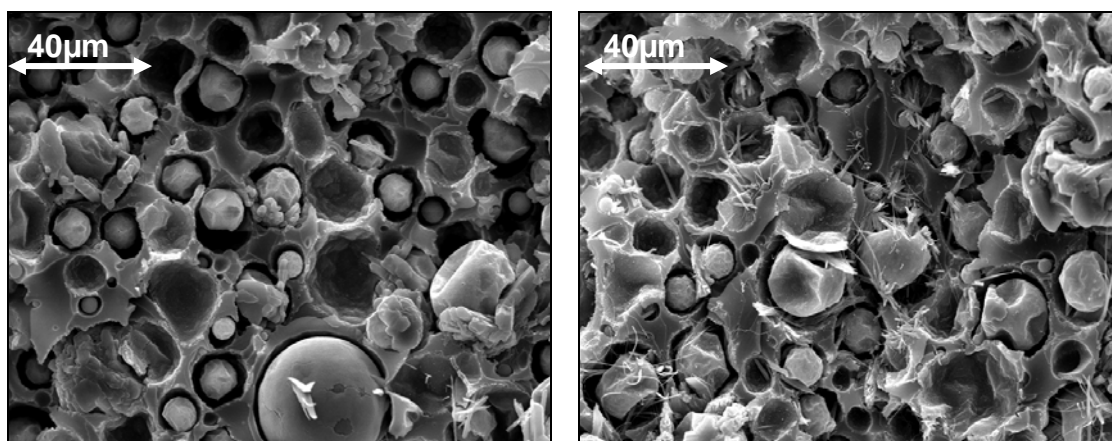


Fig. 5.1.9 - SEM pictures of the broken surfaces of the 3P resins prepared using a cogged-wheel mixer, 3P-c (left) and a propeller mixer, 3P-p (right).

Figure 5.1.10 shows the variation in the morphology resulting from different curing regimes. One can observe that the mean particle diameter is marginally affected by the different curing regimes though at higher temperatures the particle size is somewhat reduced. This may be caused by the fact that at higher temperatures the loss of water is greater and so the polysilicate particles undergo a more drastic contraction during the hydrogel/xerogel transition than at lower curing temperatures. Nevertheless, when comparing the polysilicate distribution of the systems, lower temperatures seem to render the particle distribution slightly narrower than higher curing temperatures (c.f. Table 5.1.2). Moreover, the Na_2CO_3 formation appears to be affected by the curing regime applied. Postcuring at 100°C and 80°C apparently favours the formation of carbonate crystals in needle form, while at RT and at 140°C , the amount of Na_2CO_3 crystals, covering the silicate particles, is reduced and they appear in form of block structures.



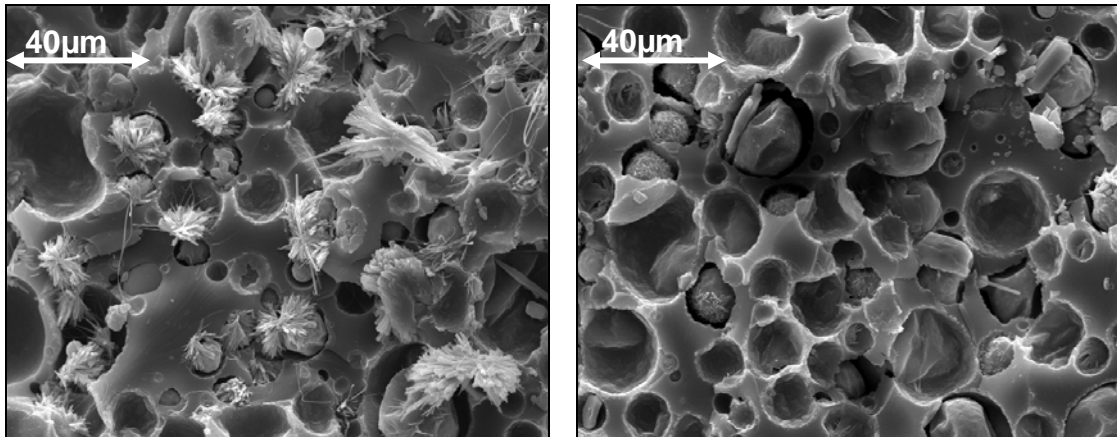


Fig. 5.1.10 - SEM images of the broken surfaces for the 3P resins with different curing regimes; 3P-RT (top left); 3P-80°C (top right); 3P-100°C (bottom left); and 3P-140°C (bottom right).

	d_n [μm]	d_w [μm]	d_w/d_n
3P- c	10.8	14.9	1.4
3P- p	7.7	10.9	1.4
3P- 1	15.5	22.4	1.5
3P- 2	5.0	7.1	1.4
3P- 3	4.2	5.7	1.4
3P- RT	11.2	14.8	1.3
3P- 80°C	12.0	15.5	1.3
3P- 100°C	10.8	14.9	1.4
3P- 140°C	10.4	14.2	1.4

Table 5.1.2 - Number- average (d_n) and weight-average (d_w) mean particle size of the polysilicate of the different 3P systems.

5.1.4. Mechanical Properties

The fracture toughness (K_C) and fracture energy (G_C) of the 3P systems are presented in Figure 5.1.11. One can see that both K_C and G_C values increase when using a cogged-wheel mixer during the dispersion process of the WG. It is remarkable that the substantial reduction of the particle size diameter induced by the use of a propeller mixer does revert in an improvement of the fracture properties. This may be explained considering the distribution of the polysilicate particles; system dispersed with cogged-wheel mixer, though having larger particle size, owe a narrower distribution than the system produced with a propeller mixer (c.f. Table

5.1.2). It is noteworthy that a finer and more uniformly dispersed silicate phase should be associated with improvements in the mechanical performance. This expectation is based on the fact that in such systems the stress concentration field induced by the particles is levelled off, which depresses premature failure of the specimens [69]. Systems cured at different temperatures show also different mechanical properties. The fracture energy is markedly reduced as the curing temperature is increased. Fracture toughness presents a similar behaviour; however, it decreases less abruptly. The improvement of the mechanical properties is also in concordance with finer polysilicate dispersions (c.f. Table 5.1.2). When taking into account the properties of the 3P systems obtained under different mixing conditions one can assume that the increase of dispersing velocity (2000 rpm), as well as its duration, is translated into an improvement of the K_C and G_C .

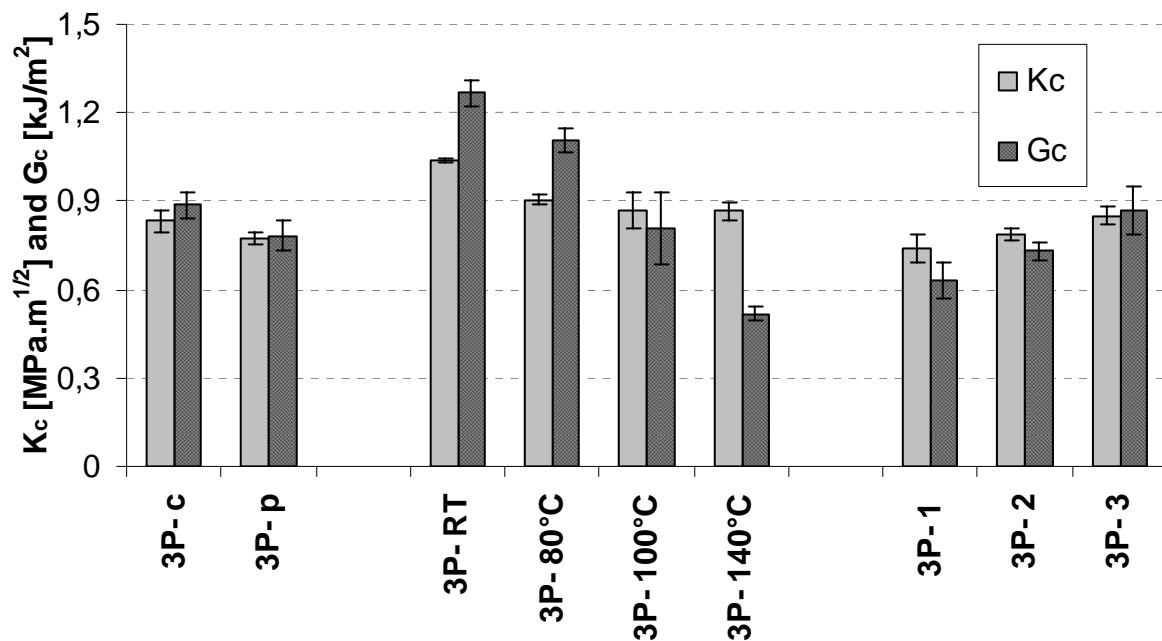


Fig. 5.1.11 –Fracture toughness (K_C) and fracture energy (G_C) for the 3P systems. For coding cf. table 5.1.1.

The flexural properties of the 3P systems are listed below in Table 5.1.3. One can observe that the use of different mixers to disperse the WG influenced the flexural properties, however not in a large extent. Systems obtained with a cogged-wheel-mixer possess higher values of flexural modulus E_f , flexural stress and strain than those obtained with a propeller mixer. Nevertheless, the 3P systems prepared under

different mixing conditions present also different flexural properties. Observing the data in Table 5.1.3 is notable that with increasing dispersion speed, the flexural modulus is enhanced, as well as the flexural strain and stress, however the increase of dispersion time affects negatively the flexural properties. Surprisingly the different curing regimes seem to have very little influence on the flexural properties of the systems, although, a slight improvement of the flexural properties can be observed with increasing curing temperatures until 100°C.

It is noteworthy that some of the results obtained underlay a considerably high scatter. This is due to inhomogeneities in the samples tested. In some cases the degassing process of the samples could not be completed due to the high viscosity of the resin and thus air was entrapped within. This generated in micro, and occasionally larger air bubbles in the sample.

Sample name	E_f [MPa]	s [MPa]	σ_{fm} [MPa]	s [MPa]	ε_M [%]	s [%]
3P- p	1165	16	39.5	1.0	4.3	0.3
3P- c	1207	124	44.7	2.8	5.0	0.5
3P- 1	1771	68	27.0	0.9	4.3	0.5
3P- 2	1629	69	62.7	3.0	5.4	0.6
3P- 3	1351	108	51.3	3.0	4.7	0.4
3P- RT	1095	120	33.9	1.8	4.7	1.4
3P- 80°C	1124	17	36.9	3.0	4.6	1.0
3P- 100°C	1207	124	44.7	2.8	5.0	0.5
3P- 140°C	1076	74	33.2	5.2	3.6	0.7

Table. 5.1.3 - Flexural modulus (E_f), strength (σ_{fm}), strain (ε_M) and standard deviation (s) for the 3P systems. For coding cf. table 5.1.1.

Depicted in Fig. 5.1.12 and Fig. 5.1.13 one can observe the variation of the storage modulus (E') and the mechanical loss factor $\tan \delta$ for the 3P systems obtained under different mixing and curing conditions. On Fig. 5.1.12, it is patent that the increasing mixing time and speed reduce the stiffness of the 3P systems, probably due to the retention of higher amounts of water in the matrix caused by the finer morphology of these systems. Note that these results are confirmed by the flexural tests (c.f. Table 5.1.3). One of the main characteristics of the 3P resin systems is the continuous increase of the $\tan \delta$ in the whole temperature range. This evidences the presence

of polymer segments with different flexibility, which allows this kind of systems to be used as damping materials (acoustic insulation, vibration damping, etc...) in a broad temperature range [114].

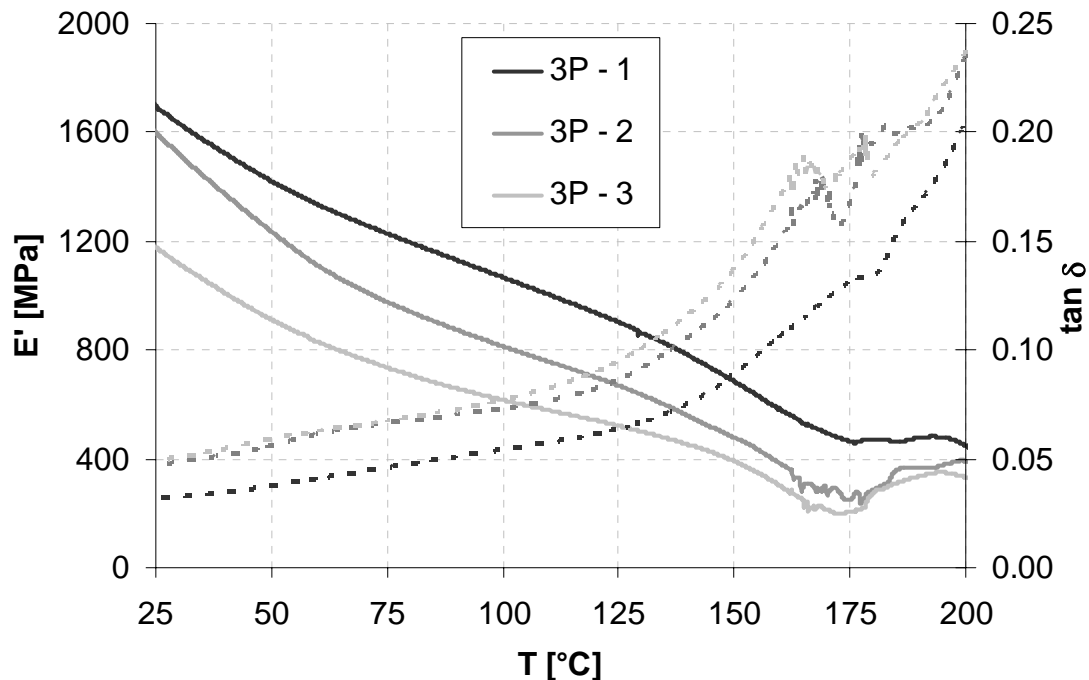


Fig. 5.1.12 – E' (continuous line) and $\tan \delta$ traces (broken line) vs. T for the 3P systems produced under different mixing conditions.

In Fig. 5.1.13 the viscoelastic properties of the 3P resins cured under different temperatures are depicted. One can observe that, in general, increasing curing temperature reduces the storage modulus (E') of the samples. This is not in complete accordance with the results obtained from the flexural tests. Nevertheless, it is the right point to recall that the results obtained from the flexural tests possessed high scatter. On the other hand, the $\tan \delta$ traces of the 3P systems cured at RT present two marked “shoulders”, one at $T \sim 50^\circ\text{C}$ and the other at $T \sim 110^\circ\text{C}$, which tend to disappear with increasing curing temperature. The glass transition temperature of the 3P resins may lie at temperatures over 200°C . Unfortunately, the premature failure events of the samples in form of bars at $T < 150^\circ\text{C}$ hampers their determination by DMTA.

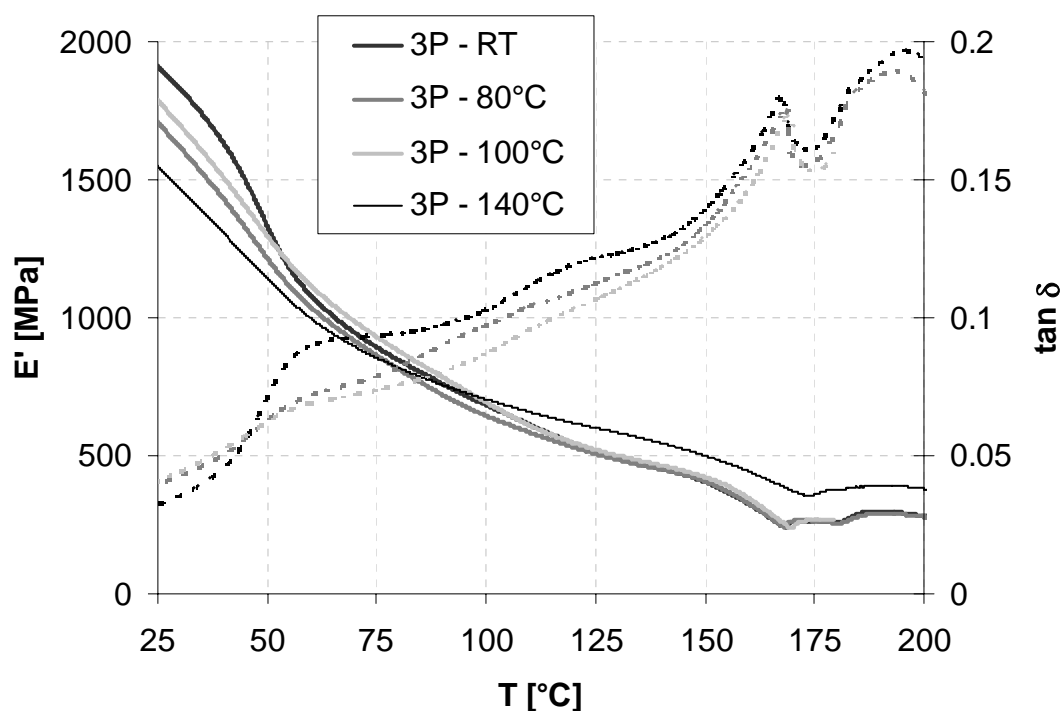


Fig. 5.1.13 – E' (continuous line) and $\tan \delta$ traces (broken line) vs. T for the 3P systems cured at different temperatures.

5.1.5. Thermal Properties

Characteristic TGA traces of 3P resin are depicted in Fig 5.1.14. In general, the degradation process of the 3P resin starts at temperatures ranging from 80°C-100°C, showing a maximum in the DTG at around ~150°C. This first mass loss corresponds in its majority to the evaporation of the water contained in the matrix. A second mass loss peak is detected at temperatures between 255°C-370°C, corresponding to the release of the hydrolysis products (for example, of the organic phosphate). Recall that tricresyl phosphate owes a boiling point of 240°C-265°C. At higher temperatures two mass loss peaks are found, which may belong to different degradation stages of the organic matrix. The different 3P systems present similar thermogravimetric behaviours. Mixing conditions such as dispersing velocity and duration or mixer type have very little influence. However, 3P systems cured under different temperatures show increasing $T_{5\%}$ (temperature at which 5% of their mass occurs) with increasing curing temperature. This may be linked to the fact that at higher curing temperatures the water contained in the matrix is released during the cure, and therefore the samples start to degrade later due to its lower water content.

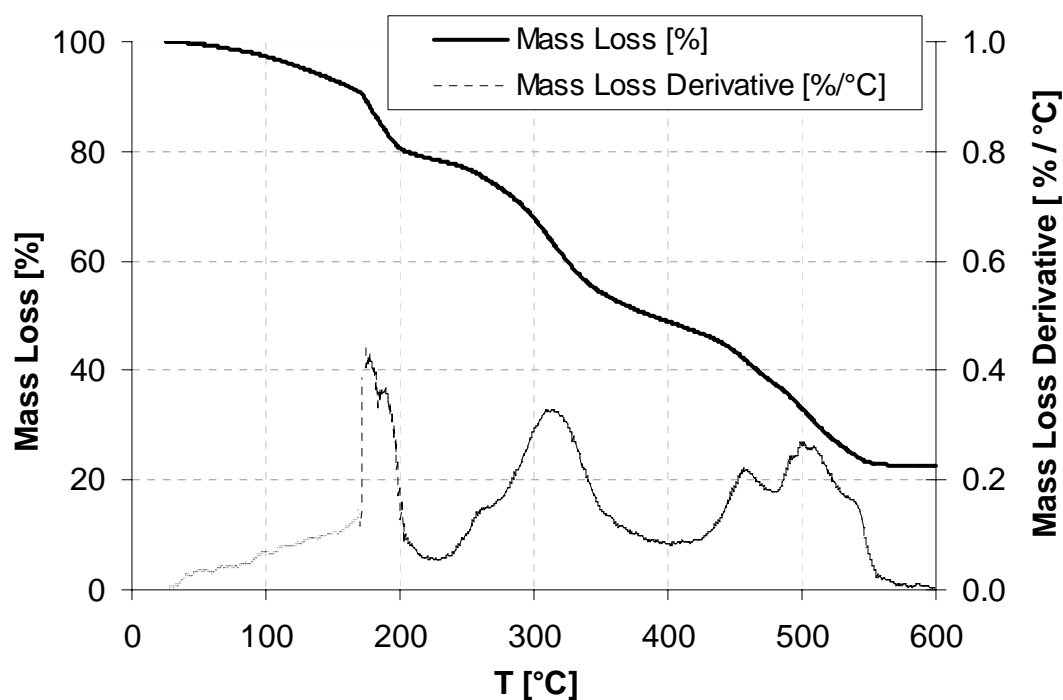


Fig.5.1.14. - Mass loss and mass loss derivative curves vs. T for the 3P reference resin.

DSC thermograms studied in the temperature range from 25°C to 200°C showed a strong endothermic peak induced mainly by the release of water contained in the matrix; therefore the samples were subjected to a second heating cycle in order to reduce this effect. The T_g of the 3P systems was determined using the DSC thermogram from the second heating cycle. The DSC thermogram of the 3P systems cured under different regimes (Fig 5.1.15) show that such systems possess a T_g which is superimposed to thermal evaporation degradation. In addition the DSC trace evidences the presence of a complex structure of the formed polymer. All the 3P systems cured at different temperatures present a similar behaviour with slightly different heat flux vs. temperature traces. The T_g temperatures found for the 3P systems are listed in Table 5.1.4. After the T_g (found between $T \sim 250^\circ\text{C}$ - 290°C) a marked exothermic effect is observable, this should be linked with thermal degradation. The T_g step is likely influenced by the evaporation of the organic phosphate contained in the matrix (occurring at approx. 280°C to 340°C). At $T > 300^\circ\text{C}$ the destruction of the organic matrix takes place accompanied by a strong heat release. These results reinforce the data obtained from the TG analysis. It is noteworthy to say that the T_g of the different systems, listed in Table 5.1.5, are shifted to higher temperatures along with increasing curing temperature. This may

be derived from the fact that at higher curing temperatures the crosslinking degree of the resins increases. Fig. 5.1.15 also shows the presence of a T_g like step at $T \sim 150^\circ\text{C}$ the reason of which is unknown.

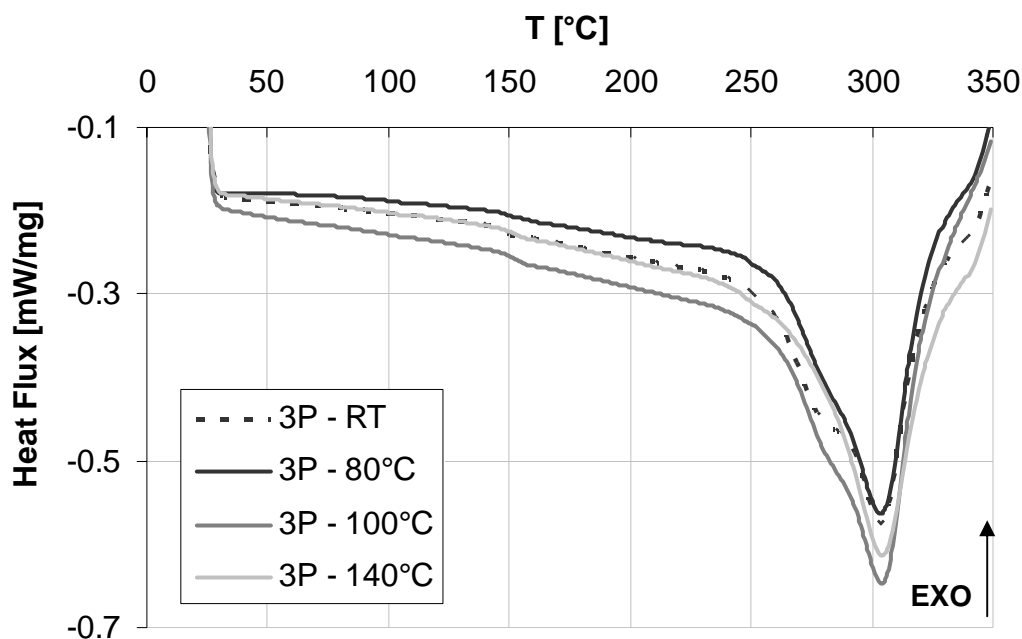


Fig. 5.1.15 – DSC curves for the 3P systems at different curing temperatures.

	3P- RT	3P- 80°C	3P- 100°C	3P- 140°C
T_g [°C]	256	257	272	289

Table 5.1.4 – Glass transition temperatures (T_g) for the 3P systems at different curing temperatures.

DSC thermogram for the 3P systems produced under different mixing conditions is shown in Fig. 5.1.16. These 3P systems owe a parallel behaviour to the 3P systems cured at different temperatures. One can also read the T_g from the related traces at $T \sim 240^\circ\text{C}$, (c.f. Table 5.1.5).

	3P- 1	3P- 2	3P- 3
T_g [°C]	251	213	209

Table 5.1.5 – Glass transition temperatures (T_g) for the 3P systems at different mixing conditions.

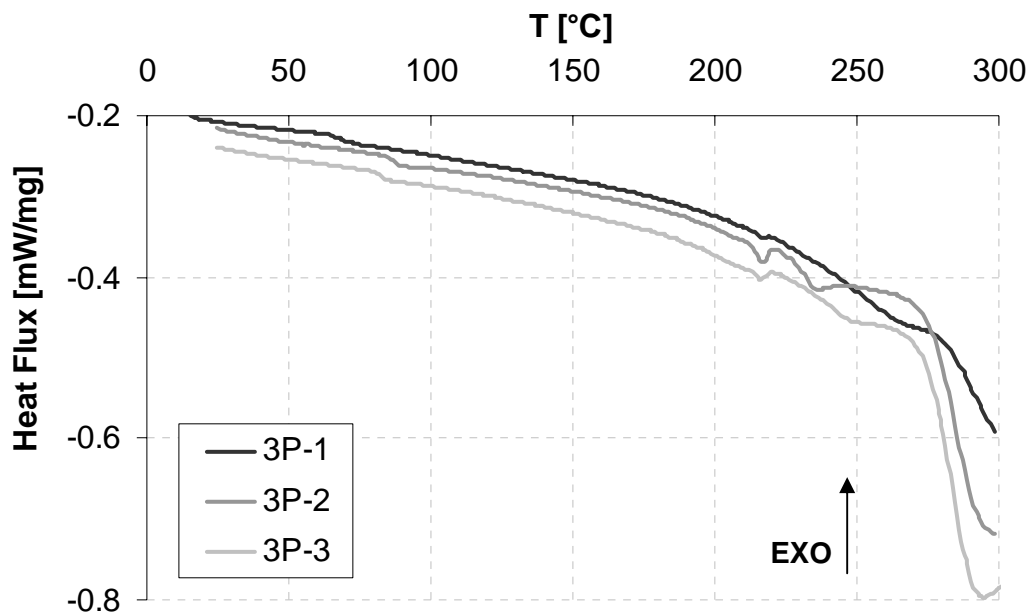


Fig. 5.1.16 – DSC curves for the 3P systems at different mixing conditions.

The flammability test for the 3P resins, which followed the 94UL standards for vertical burn (94V), showed that the specimens did not burn with flaming combustion after the flame application. The 3P resins did not burn with flaming or glowing combustion up to the specimen holding clamp. Moreover the 3P resins did not drip flaming particles that would ignite the cotton. The total flaming combustion time was zero; therefore the classification of the 3P resins according to the 94UL standards is V-0. The results obtained from the flammability test showed that 3P resins are good fire resistant materials. However, to prove that 3P resins are good fire insulators further studies should be conducted reproducing more accurately the fire conditions in a burning room where temperatures are much higher and combustible gases may be accumulated.

5.2. 3P / HYBRID RESINS

5.2.1. Vinylester resins

5.2.1.1. Rheology

The rheological studies conducted on the 3P/VE 50/50 wt.-% hybrid resin show the progressive increase of the viscosity with time (cf. Fig. 5.2.1.1). The viscosity of the 3P/VE 50/50 wt.-% hybrid systems increase exponentially in a very short lapse of time, whereas for the 3P reference systems, the viscosity increase is markedly slower. Due to this 3P/VE systems are extremely troublesome to process, since its pot life is less than 30 min.

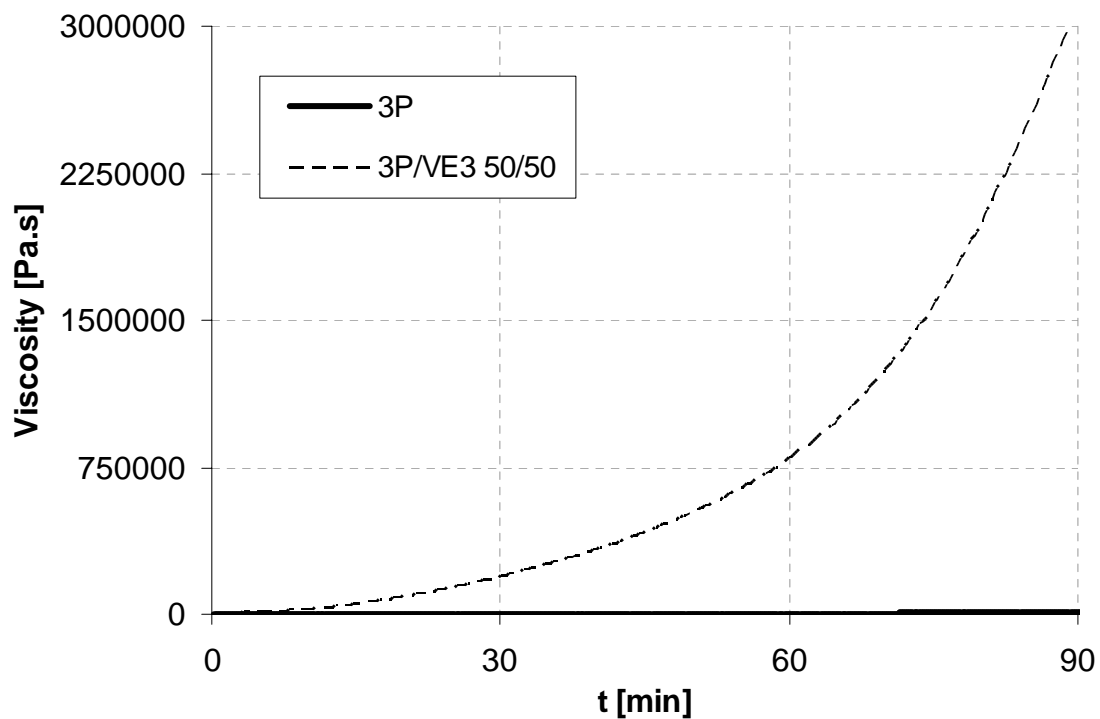


Fig.5.2.1.1 - Viscosity vs. time for the 3P/VE 50/50 hybrid resin and its reference 3P.

5.2.1.2. Morphology

The SEM pictures taken from the fracture surfaces of the 3P/VE hybrid resins at various composition ratios (Fig. 5.2.1.2) show the distribution of the polysilicate particles. Their number (d_n) and weight-average diameter (d_w) are given in Table 5.2.1.1. One can see that the silicate particles are present in a broad distribution (d_w/d_n) and show a rather high number and weight-average diameter for the reference 3P resin and 3P/VE 75/25 wt.-% hybrid resin. The distribution

becomes significantly narrower and the d_n and d_w are substantially reduced for the 3P/VE 50/50 wt.-% and 3P/VE 25/75 wt.-% hybrid systems. This indicates that the VE worked as an additional emulsifier for the initial W/O-type emulsion (i.e. WG dispersed in PMDI and phosphate) [7,70]. It is noteworthy to say that a finer and more uniformly dispersed silicate phase should be associated with improvements in the mechanical performance.

Sample name	d_n (μm)	d_w (μm)	d_w/d_n
3P	7.8	22.1	2.8
3P/VE - 25/75 wt.-%	8.6	21.5	2.5
3P/VE - 50/50 wt.-%	4.1	8.1	2.0
3P/VE - 75/25 wt.-%	2.6	7.0	2.7

Table 5.2.1.1 - Number (d_n) and weight-average diameter (d_w) of the polysilicate particles in the 3P/VE hybrid resins as a function of their composition.

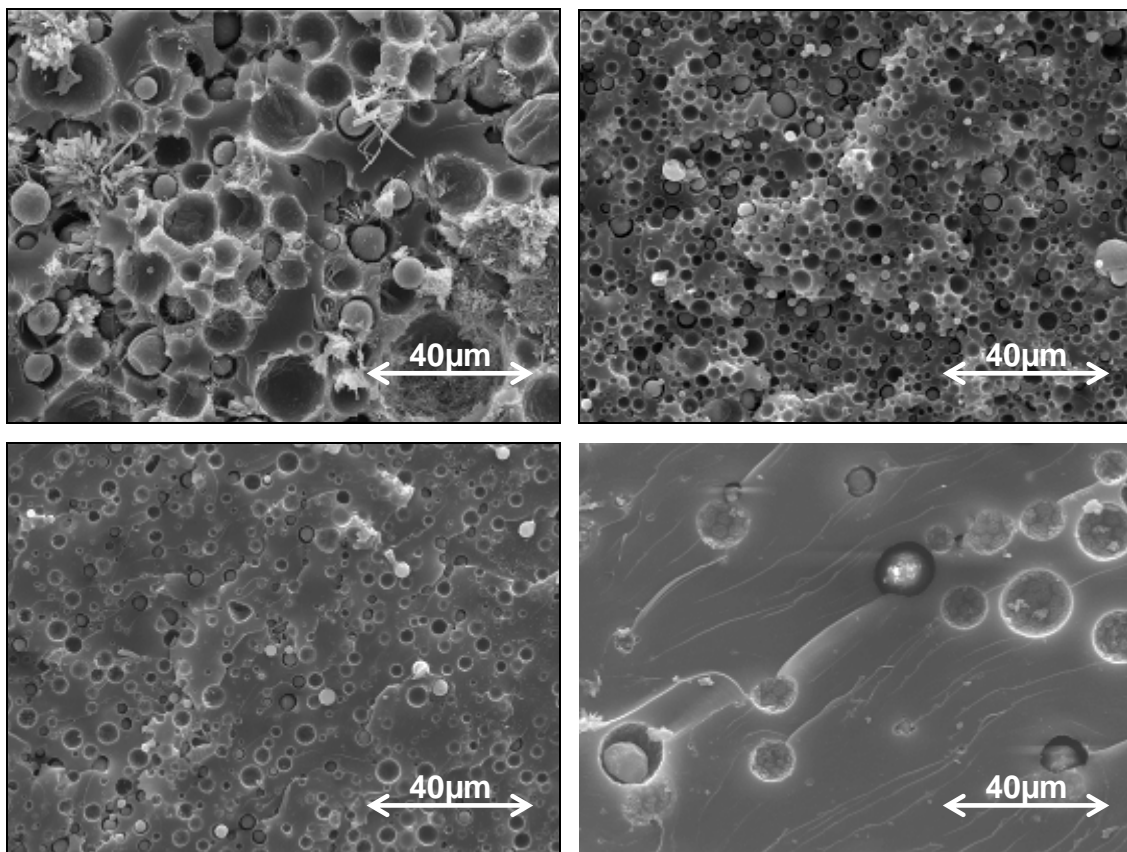


Fig. 5.2.1.2 - SEM pictures taken from the fracture surfaces of a 3P resin sample (top left); 3P/VE 75/25 wt.-% hybrid resin (top right); 3P/VE 50/50 wt.-% hybrid systems (bottom left); and 3P/VE 25/75 wt.-% hybrid systems (bottom right).

Inspecting the below depicted AFM pictures in Fig. 5.2.1.3, the differing structures of the two resins, viz. reference 3P and VE, are remarkable. The former possesses a fine structure while the latter owes a characteristic nodular structure (also called microgel). VE exhibits a two phase structure, since more or less spherical VE nodules are dispersed in a polystyrene-crosslinked-vinylester matrix. The presence of such two-phase dispersion was shown also by Mortaigne *et al.* who used laser ablation for the “physical etching” of VE [68,115]. When observing the 3P/VE 75/25 wt.-% and 3P/VE 50/50 wt.-% hybrids, one can see that their structure resemble to the one of 3P, on the other hand, as the VE content increases up to a 75 wt.-%, the structure of the corresponding 3P/VE hybrid becomes less finer and even nodules appear.

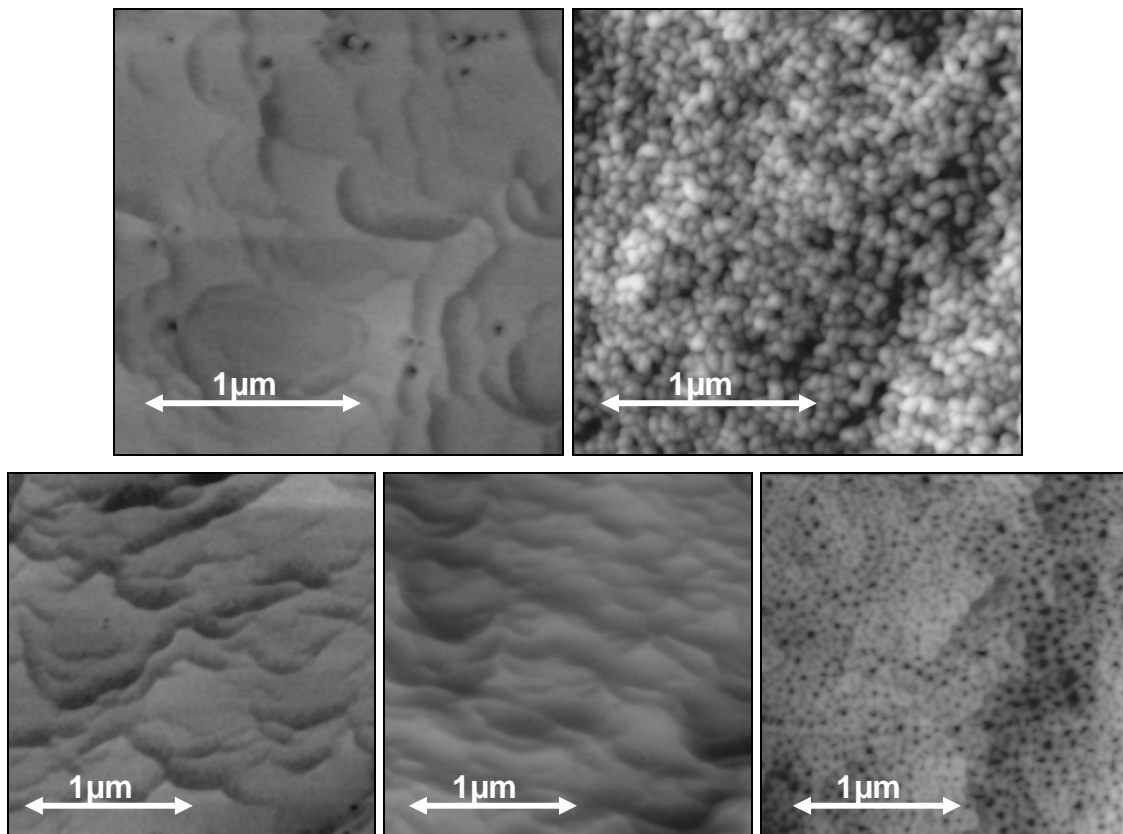


Fig. 5.2.1.3 – Amplitude-modulated AFM images taken from the ion-etched polished surfaces of the 3P (top left); VE (top right); 3P/VE 75/25 wt.-% (bottom left); 3P/VE 50/50 wt.-% (centre); and 3P/VE 25/75 wt.-% (bottom right).

5.2.1.3. Mechanical Properties

The effects of the compositional changes on the fracture toughness (K_C) and fracture energy (G_C) are depicted in Fig. 5.2.1.4. One can observe that the fracture toughness of most of the hybrids is improved when comparing it to the references 3P and VE. Note that G_C experiences a considerable increase when comparing it to the reference 3P and VE, as they present lower G_C values. Recall that the high K_C and G_C values are due to the complex crosslinking mechanisms which affect the morphology development. The resulting heterogeneous morphology is linked with relatively low stiffness as will be shown next in the DMTA traces.

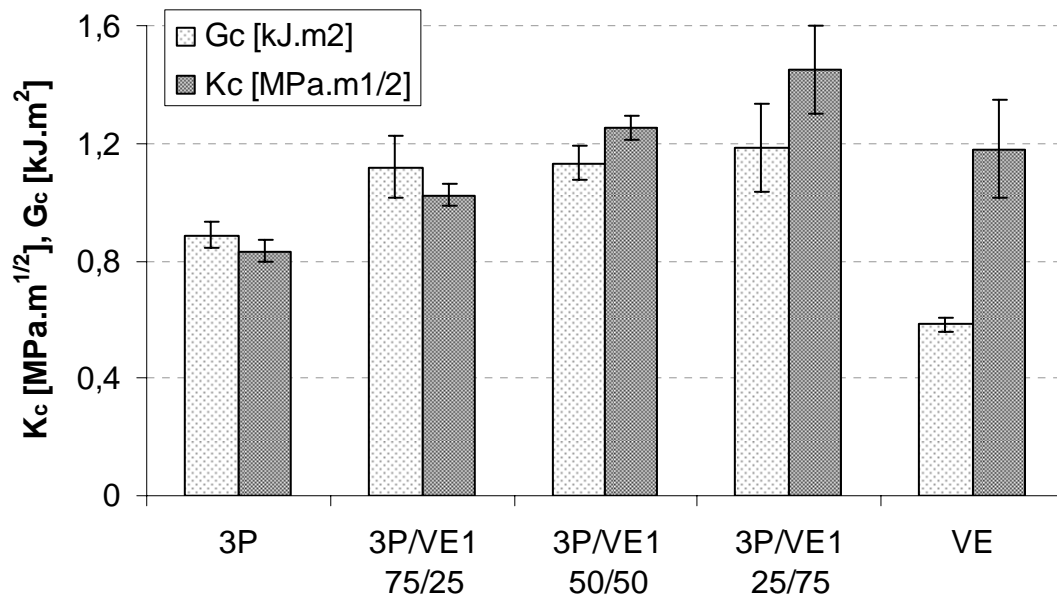


Fig. 5.2.1.4 - Effects of the compositional changes for the fracture toughness (K_C) and fracture energy (G_C).

The data obtained from the flexural tests depicted in Fig. 5.2.1.5 reveals that the flexural stiffness [E_f] of the specimens increases with increasing VE content showing a small deviation from the additivity. However, when comparing the flexural strength of the 3P/VE hybrids one can observe that the flexural strength goes through a minimum as a function of the 3P/VE ratio. Nonetheless, in the first approximation a linear relation between E_f and the composition ratio can be accepted.

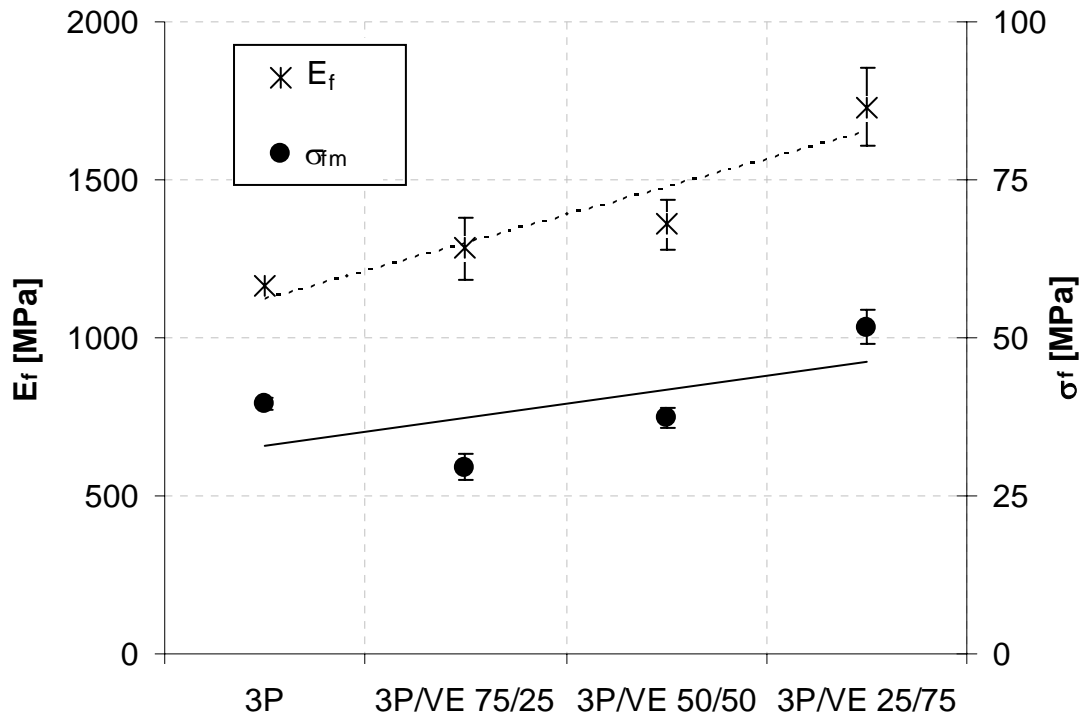


Fig. 5.2.1.5 - Changes in the flexural modulus and strength data as a function of the hybrid resin composition.

The DMTA results, presented in Fig. 5.2.1.6, in form of E' vs. T for the 3P, VE and their hybrid resins show that the stiffness (E') is increased considerably with the VE “hybridization” at least below a given threshold temperature. The E' values of the hybrids do not follow the trend with the compositional ratio in the whole temperature range (cf. Fig. 5.2.1.6). Observing the $\tan \delta$ vs. T traces, depicted in Fig. 5.2.1.7, one can recognize that the glass transition temperature (T_g), when assigned to the peak temperature of the $\tan \delta$, increases above a 3P/VE ratio of 75/25 wt.-%. It is worth of noting that the T_g of the neat 3P resin could not be determined due to premature failure of the tested specimen. Nevertheless, the related $\tan \delta$ vs. T traces suggest that it is at $T > 200^\circ\text{C}$. This is in accord with the results presented in Chapter 5.1. Note that the intensity of the $\tan \delta$ peak of the VE is reduced owing to the hybridization with 3P and also broadened at the same time.

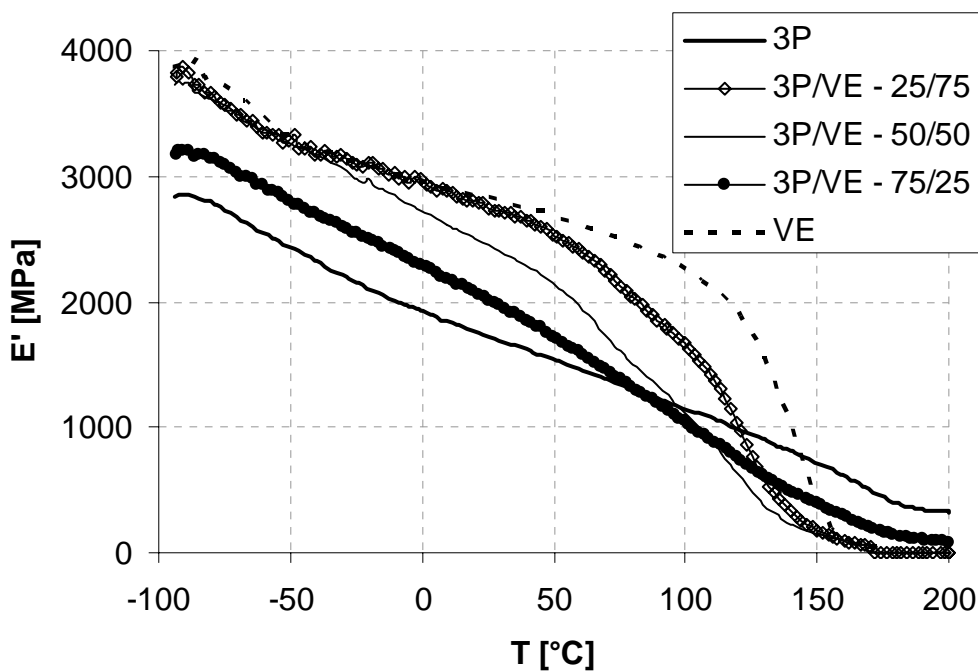


Fig. 5.2.1.6 - DMTA results displaying E' vs. T for the 3P, VE and their hybrid resins.

The DMTA behaviour of the hybrids suggest the formation of a heterogeneously crosslinked network. This may be a conetwork or a grafted interpenetrating one (g/IPN). As a g/IPN should be phase segregated while a conetwork not, attempts were made to shed light on this issue by AFM [30,70]. Recall that in Fig. 5.2.1.3 two differing structures for the two reference resins, viz. 3P and VE, were observed. The former possessed a fine structure while the latter owed a characteristic nodular structure (also called microgel). VE exhibited a two phase structure in AFM (spherical VE nodules dispersed in a polystyrene-crosslinked vinylester matrix) characteristic of g/IPN. On the other hand, 3P resins showed in AFM a featureless structure, which is typical for a conetwork. The 3P/VE hybrids presented transition structures between 3P reference and VE depending on their 3P/VE ratio. For 3P/VE ratios lower than 50/50, the structure based on the AFM pictures was mainly a conetwork, while for the 3P/VE 25/75, a phase segregation is observed. This is likely linked with the appearance of a g/IPN structure.

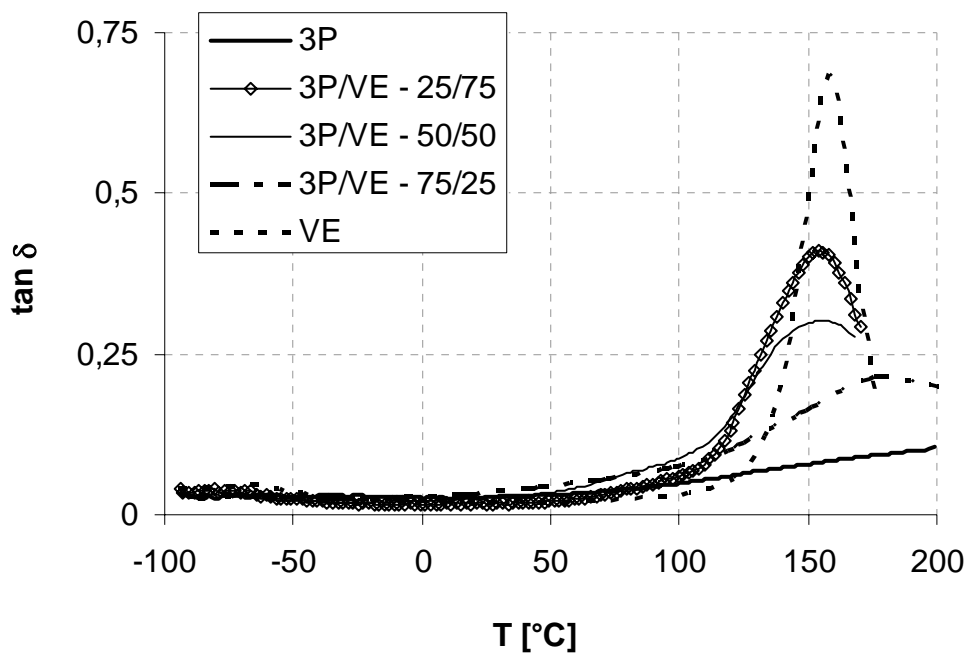


Fig. 5.2.1.7 - DMTA results displaying $\tan \delta$ vs. T for the 3P, VE and their hybrid resins.

5.2.1.4. Thermal properties

The TGA curves (mass loss vs. T) for the 3P, VE and its hybrids are shown in Fig. 5.2.1.8. Note that 3P resins start to degrade at rather low temperatures ($T \approx 200^\circ\text{C}$); a similar behaviour is observed for the 3P/VE 75/25 wt.-% hybrid, while other 3P/VE hybrids with increasing VE content are markedly stable at lower temperatures, emulating the thermal behaviour of VE. Comparing the results in Table 5.2.1.2 one can clearly see that the $T_{5\%}$, temperature in which the sample has already lost 5% of its weight, is significantly lower for the 3P and 3P/VE 75/25 wt.-% hybrid resins than for those richer in VE, including the VE itself. However, at higher temperatures the trend reverses. At $T > 400^\circ\text{C}$, 3P resins are more stable against thermal degradation than VE and its corresponding hybrids. 3P resins degrade progressively but slower than VE, which after a given temperature degrades abruptly almost without residue (cf. Table 5.2.1.2).

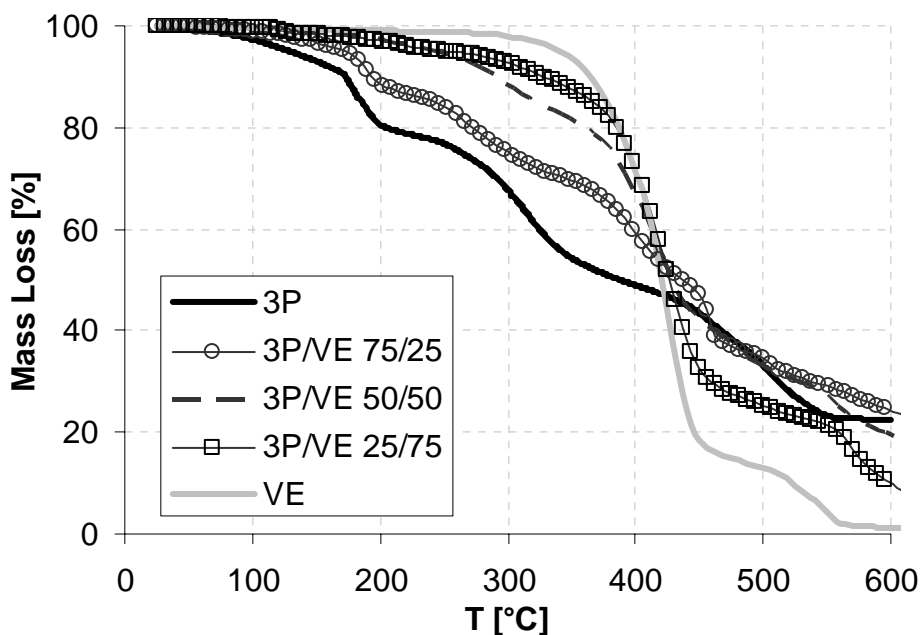


Fig. 5.2.1.8 - TGA curves (mass loss vs. T) for the 3P, VE and their hybrids.

Sample name	$T_{5\%}$ [°C]	Residue [%]
3P	196	23
3P/VE 75/25 wt.-%	171	22
3P/VE 50/50 wt.-%	247	17
3PVE 25/75 wt.-%	259	7
VE	342	1

Table 5.2.1.2 - $T_{5\%}$ [°C] and residue [%] for the 3P, VE and their hybrids.

In the DSC traces from the second heating cycle (Fig. 5.2.1.9) one can observe that the 3P/VE hybrids with different VE content show a similar behaviour to the reference 3P, however with some particularities. The endothermic effect caused principally by the evaporation of the organic phosphate (270°C-290°C) is less marked in the hybrid systems with higher VE ratio, since the phosphate content is lower in these systems. Moreover, the exothermic peak derived from the matrix degradation processes in the 3P/VE hybrids starts at higher temperatures than for the 3P reference resins. Note that the 3P/VE 25/75 wt.-% show an additional exothermic peak at $T \sim 275^\circ\text{C}$ which may be the result of post-polymerization processes of the VE resin.

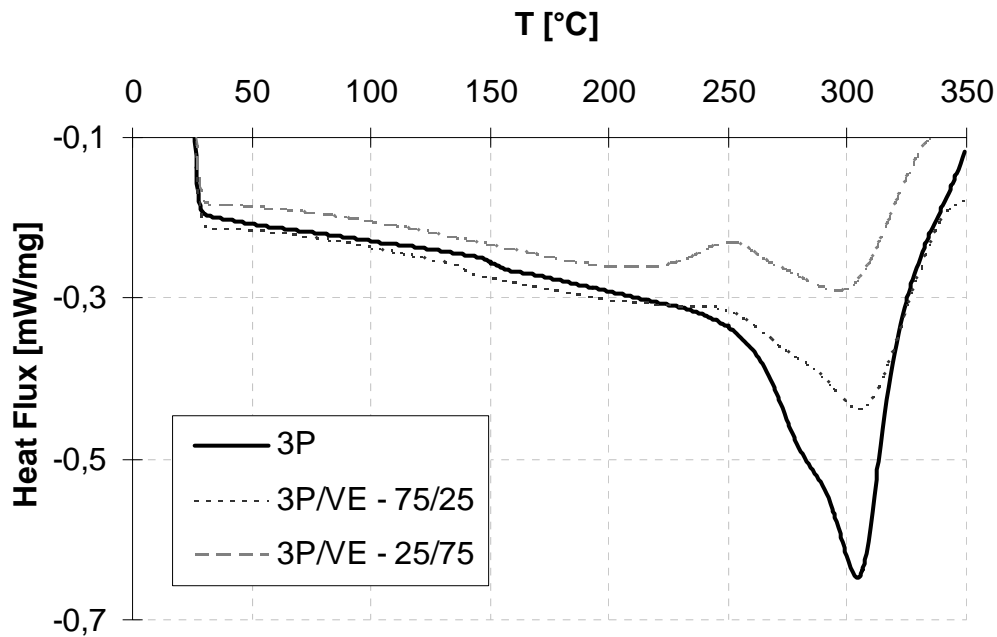


Fig. 5.2.1.9 - DSC curves vs. for the 3P/VE hybrids and the reference 3P resin.

The flammability of the 3P/VE hybrid resins differs from one another depending on the VE content. Hybrids owing the lowest VE content possess the same flammability grade as the 3P resins, that is V-0 or flame resistant. On the contrary, hybrids with higher VE content, 3P/VE 50/50 wt.-% and 3P/VE 25/75 wt.-%, were classified as V-2, the specimens burned up to two minutes after applying the flame and dropped flaming drips onto the cotton. Regarding the flammability of the novel 3P/VE resins one can assert that the hybridization with VE worsen the flame resistance properties of the reference 3P.

5.2.2. Epoxy resins

5.2.2.1. Rheology

The viscosity progression for the 3P/EP hybrid resins is depicted in Fig 5.2.2.1. One can clearly see that the EP resin acted as an additional emulsifier for the 3P resin systems, conferring a low viscosity even at times up to 150 min. This fact facilitates the posterior processing of the resin, since the viscosity of the reference resin 3P increases exponentially along with time. Moreover, one can observe that 3P/EP hybrids with higher EP content owe a reduced viscosity.

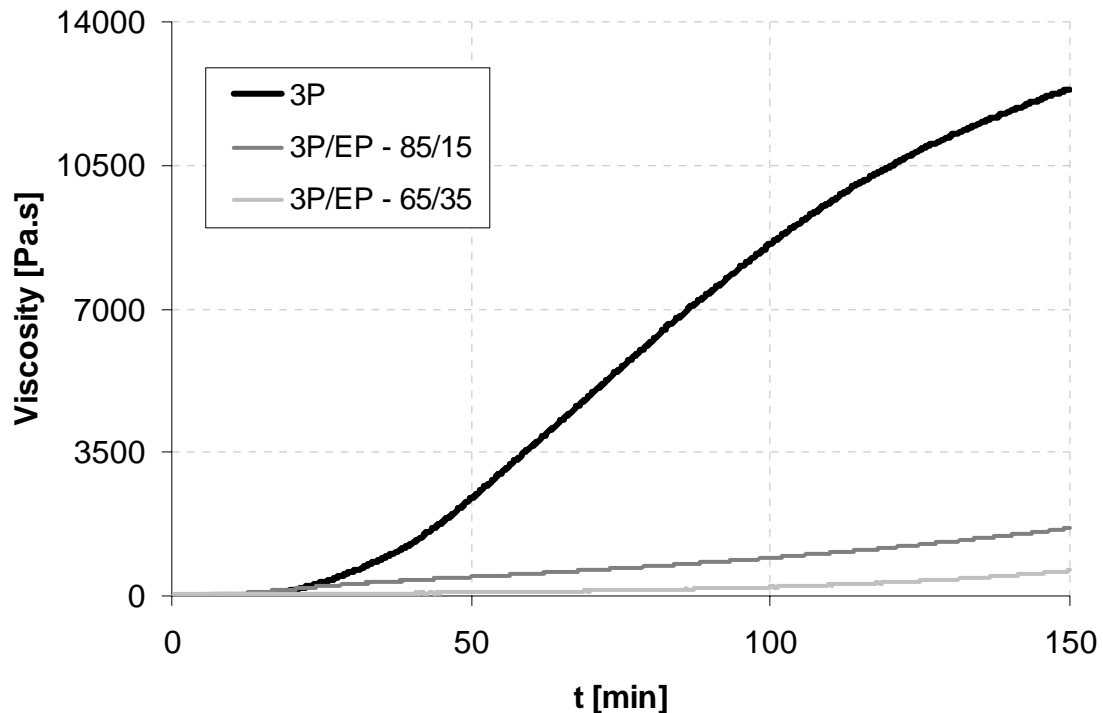


Fig.5.2.2.1- Viscosity vs. time traces of the hybrid resins 3P/EP 85/15 wt.-%, 3P/EP 65/35 wt.-% and the reference 3P resin.

5.2.2.2. Morphology

The SEM pictures of the broken surface of the 3P/EP resins are presented below in Fig.5.2.2.2. The change induced by the hybridization of 3P with EP resin, is obvious: the size of the polysilicate particles is radically reduced. Recall that the final dispersion of the reference 3P was accomplished at 800 rpm during 1 min; on the contrary for the 3P/EP systems the final dispersion took place at a mixing speed of 2000 rpm during 1 min. As observed before for the 3P reference systems, higher dispersing velocities induce the formation of smaller polysilicate particles. Therefore the morphology of the hybrids should be compared as well with the 3P system obtained under the same mixing conditions, designated by 3P-2. In Table 5.2.2.1 one can observe that, although an increase of the dispersing velocity reduces the particle size of the polysilicate to the half of it, the marked reduction of the mean particle diameter observed for the 3P/EP hybrid systems is originated mostly by the hybridization with EP resin.

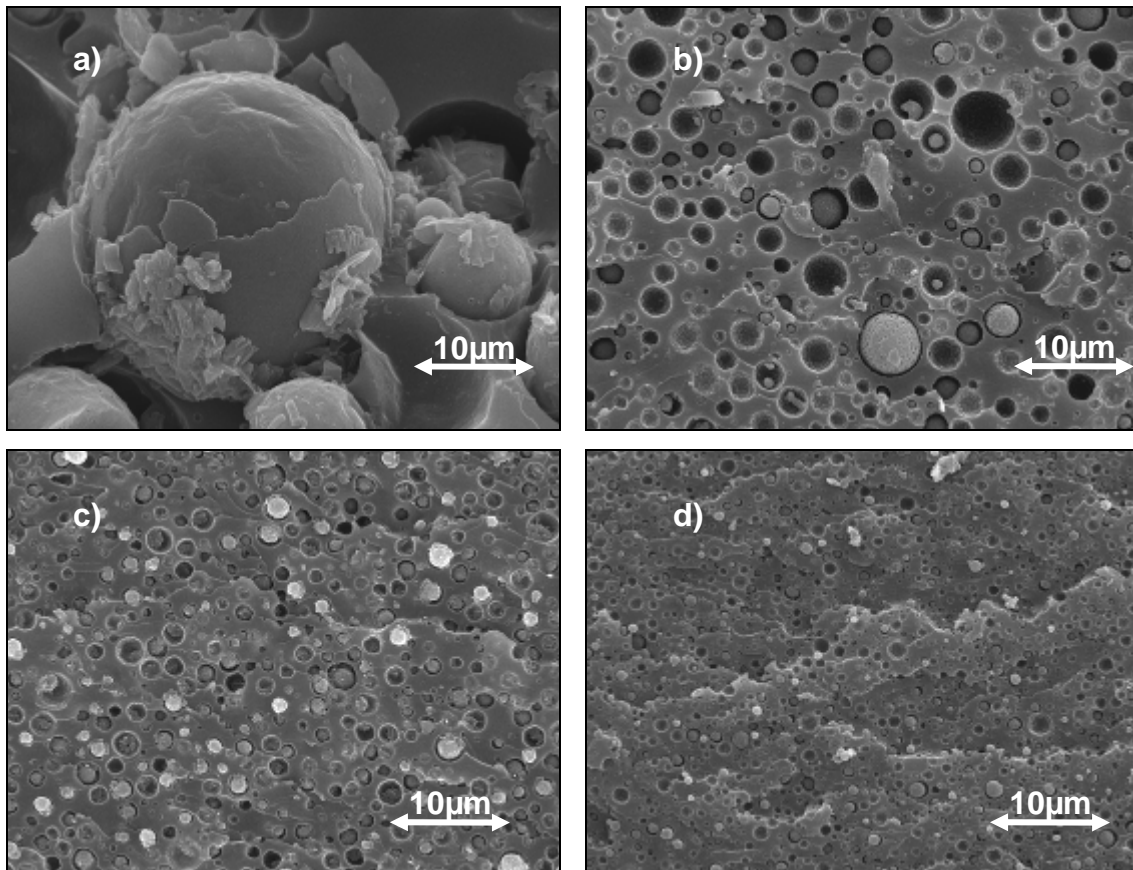


Fig.5.2.2.2- SEM pictures from the broken surfaces of the reference 3P resin (a); 3P/EP 85/15 wt.-% hybrid (b); 3P/EP 75/25 wt.-% hybrid (c); 3P/EP 65/35 wt.-% hybrid (d).

Sample name	d_n [μm]	d_w [μm]	d_w/d_n
3P	11.2	15.5	1.4
3P- 2	5.0	7.1	1.4
3P/EP 85/15 wt.-%	1.2	2.0	1.6
3P/EP 80/20 wt.-%	1.1	1.5	1.3
3P/EP 75/25 wt.-%	0.8	1.1	1.3
3P/EP 65/35 wt.-%	0.8	1.1	1.3

Table 5.2.2.1 - Number- average (d_n) and weight-average (d_w) mean particle size of the 3P/EP hybrid systems and their reference 3P resin.

In figure Fig.5.2.2.3 one can see that the mean particle size of the 3P/EP hybrid systems is centred at lower diameter values for the 3P/EP hybrids with higher EP content. Similarly, the distribution of the polysilicate phase narrows with increasing EP content.

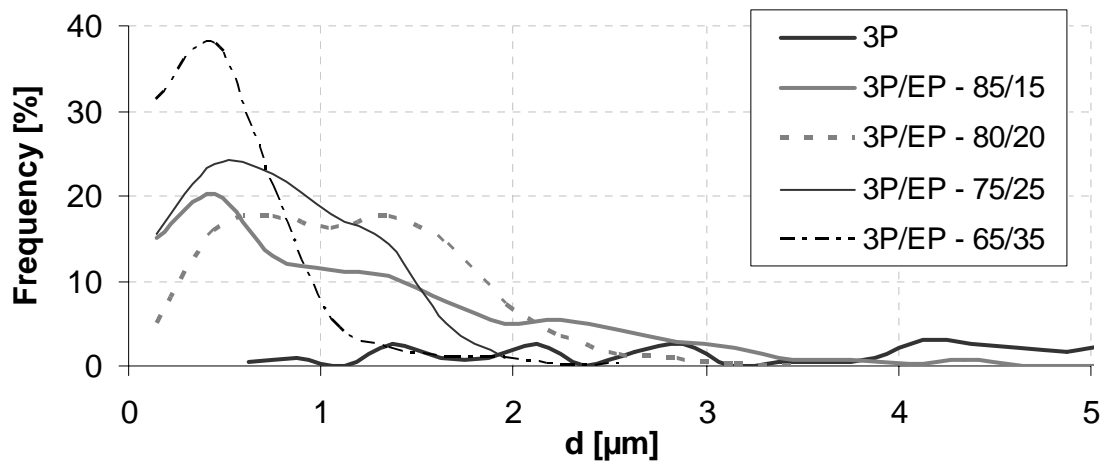


Fig.5.2.2.3 - Mean particle size diameter vs. frequency for the 3P/EP hybrid systems.

5.2.2.3. Mechanical Properties

The fracture mechanical properties displayed in Fig. 5.2.2.4 show that the novel 3P/EP hybrids possess enhanced fracture toughness (K_C) in comparison with the reference 3P resin. Moreover, K_C increases parallel to the EP content, with the exception of the 3P/EP 85/15 wt.-% hybrid system. Higher K_C values could be a result from the reduced particle size and the narrowing of the polysilicate dispersion of the systems. However, the hybridization with EP causes a negative effect on the fracture energy (G_C), which drops compared to that of the reference 3P.

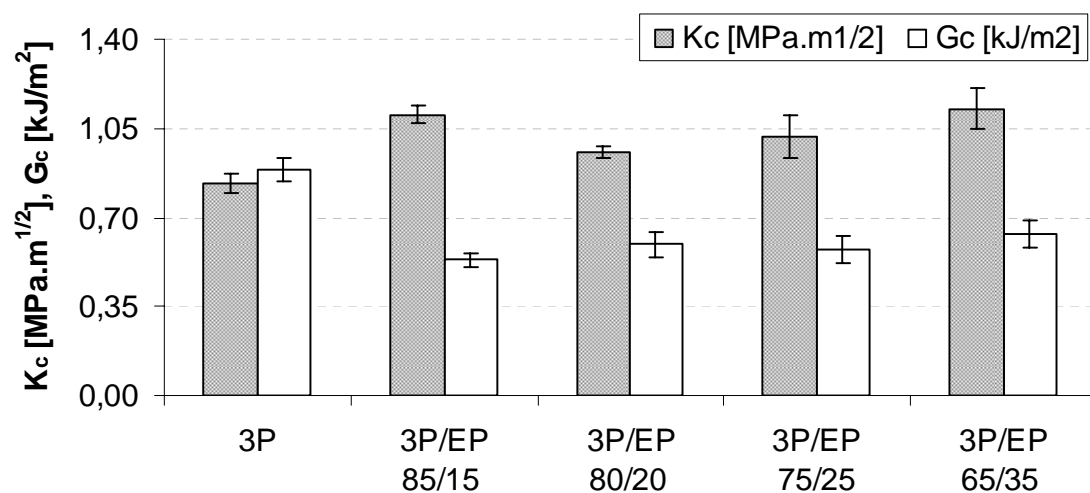


Fig.5.2.2.4 - Fracture toughness (K_C) and fracture energy (G_C) for the 3P/EP hybrids and their reference 3P resin.

The flexural tests carried out on the 3P/EP hybrid systems reveal, as expected, that the flexural modulus E_f of the novel hybrids increases with the EP content following the rule of additivity (Fig.5.2.2.5) in the composition range investigated. This tendency is not clearly defined for the flexural strength (σ_f), owing similar values for all the 3P/EP rates. However, in general the hybrid systems possess enhanced values of σ_f (c.f. Table 5.2.2.2).

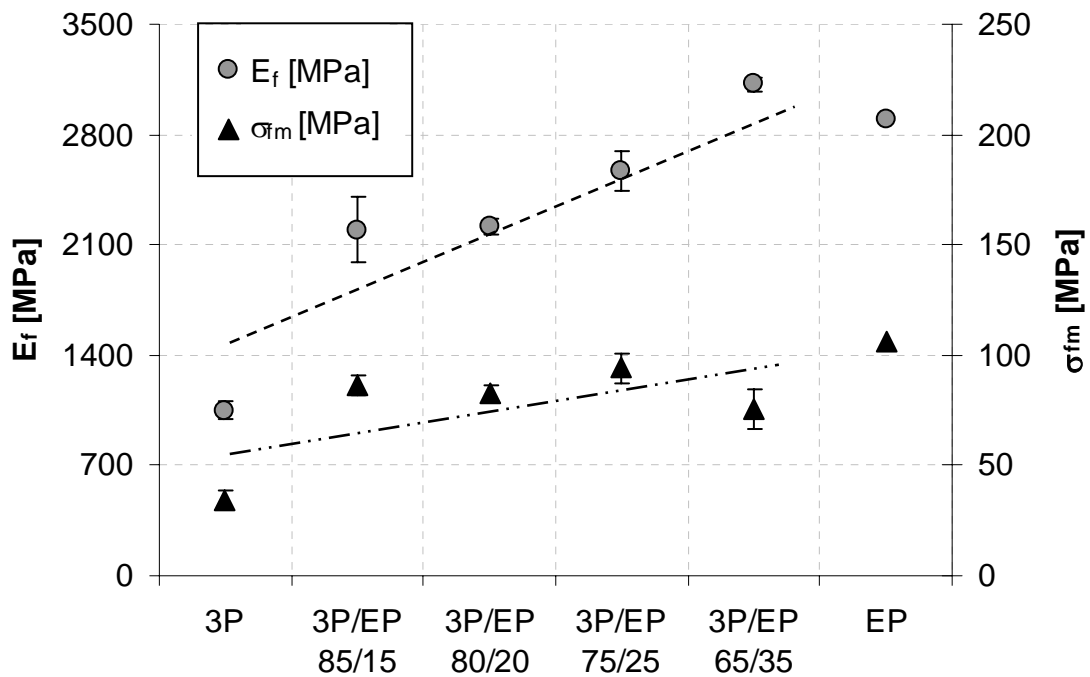


Fig.5.2.2.5- Flexural modulus (E_f) and flexural strength (σ_f) for the 3P/EP hybrid resins and their references 3P and EP.

Sample name	E_f [MPa]	s [MPa]	σ_{fm} [MPa]	s [MPa]	ε_M [%]	s [%]
3P	1047	56	34.6	3.9	4.4	0.9
3P/EP 85/15 wt.-%	2262	281	82.5	4.6	4.2	0.5
3P/EP 80/20 wt.-%	2254	122	80.7	15.8	4.4	1.9
3P/EP 75/25 wt.-%	2613	260	81.9	13.7	3.4	0.7
3P/EP 65/35 wt.-%	3118	45	75.6	9.3	2.5	0.4
EP	2900	-	106.0	-	4.0	-

Table 5.2.2.2- Flexural modulus (E_f), strength (σ_{fm}), strain (ε_m) and standard deviation (s) for the 3P/EP hybrid resins and their references 3P and EP.

The DMTA curves shown in figure 5.2.2.6 confirm the results obtained in the flexural tests. The higher the EP content, the higher the storage modulus (E') is. For temperatures ranging from 25°C to 135°C E' is markedly higher compared to the reference 3P - again with exception of the hybrid system with the lowest EP content. At temperatures around 150°C the specimens undergo premature failure, apart from the 3P/EP 65/35 wt.-% which shows a good thermal resistance at high temperatures.

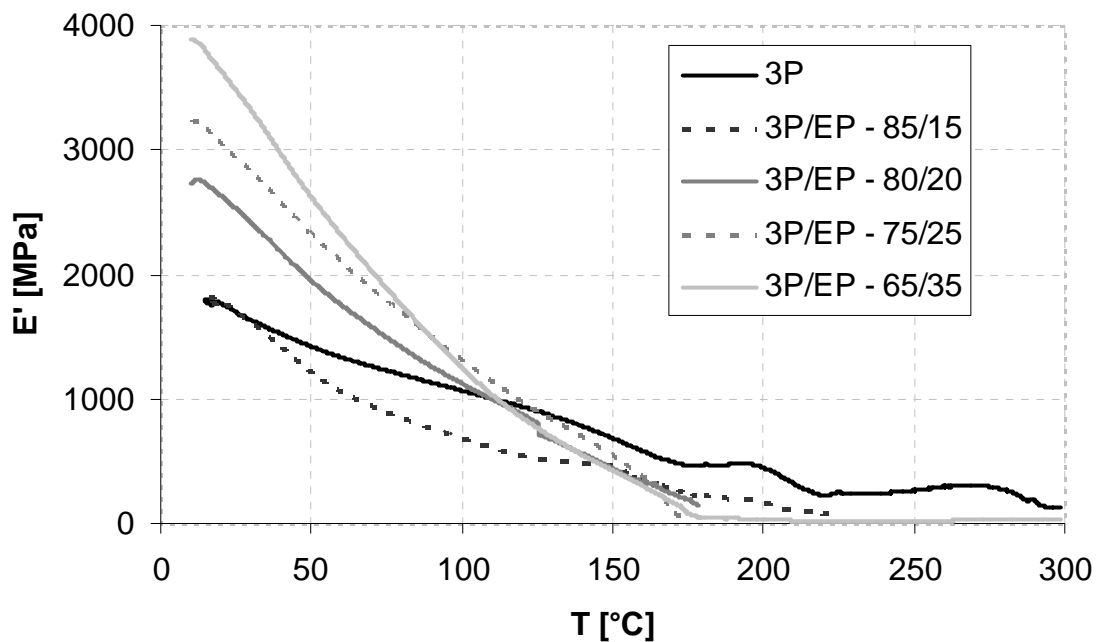


Fig.5.2.2.6 - DMTA results displaying E' vs. T for the 3P reference and its 3P/EP hybrids.

When taking into account the $\tan \delta$ vs. temperature traces the different behaviour of the novel hybrids in comparison to the reference 3P becomes obvious (Fig.5.2.2.7). While the 3P resins present a typical broad undefined peak at $T > 200^\circ\text{C}$, the 3P/EP hybrids exhibit minimum three peaks in the $\tan \delta$ traces of different intensity [116]. The first broad “shoulder” takes place at temperatures from 80°C to 120°C and it may correspond to the glass transition temperature of the epoxide homopolymers. This first “shoulder” is overlapped with a second peak (150°C-190°C), which is slightly more intense and may belong to the hybrid components formed between 3P and EP resin. The third $\tan \delta$ peak, which is well resolved, appears at temperatures from 250°C to

275°C and corresponds possibly to the glass transition temperature of the polyurea phase. Because of the premature failure of the specimens only the sub T_g relaxation peaks of the 3P/EP 80/20 hybrid system could be observed. However, posterior DSC tests confirm that the 3P/EP hybrid systems in all the 3P/EP ratio range possess these three relaxation transitions (c.f. Table 5.2.2.4).

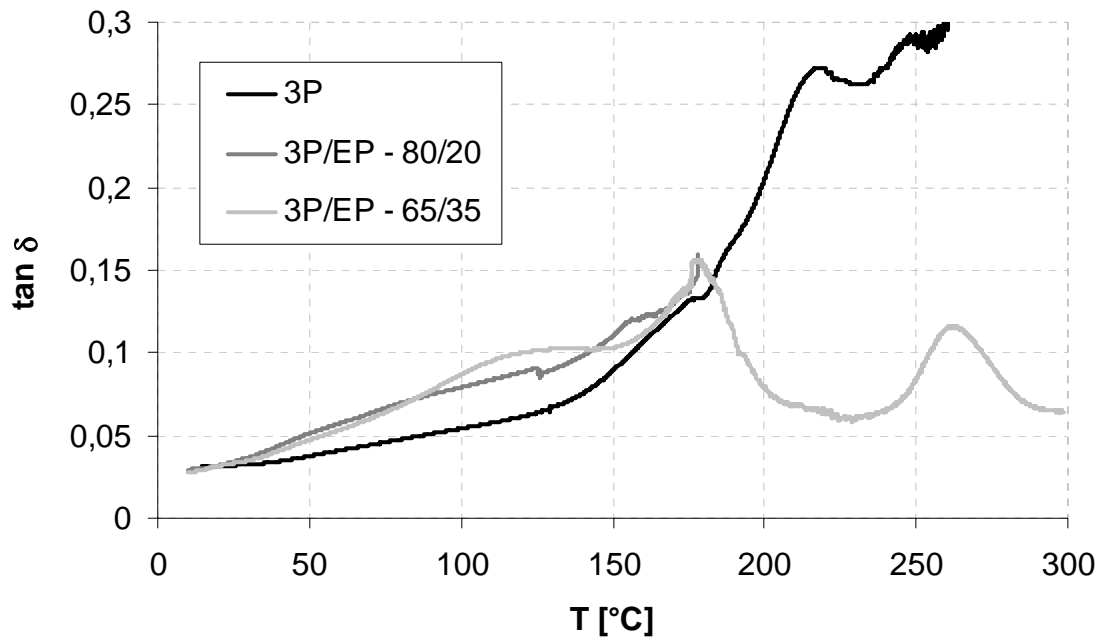


Fig.5.2.2.7 - DMTA results displaying $\tan \delta$ vs. T for the 3P and the 3P/EP hybrids.

5.2.2.4. Thermal properties

The thermal degradation of the 3P/EP hybrid resins, presented in Fig 5.2.2.8, show that the EP conferred to the hybrid systems an additional thermal stability at higher temperatures. The 3P/EP hybrid systems begin to experience a certain mass loss at $T < 250^\circ\text{C}$ while at the same temperature the reference 3P resin has already lost more than 20% its weight. One can observe that the 3P/EP systems are stable for a wide range of temperatures before suffering a drastic mass loss ($T \sim 350^\circ\text{C}$). On the contrary the reference 3P undergoes several degradation steps. In general, the higher the EP content of the hybrid systems the better is the resistance to thermal degradation. As listed in Table 5.2.2.3, one can see that the temperature at which the 5% of the mass is lost is higher for the hybrids with larger EP content. On the other hand, the final residue is slightly lower for these 3P/EP hybrids compared to the reference 3P.

Sample name	T _{5%} [°C]	Residue [%]
3P/EP 85/15 wt.-%	242	32
3P/EP 80/20 wt.-%	241	29
3P/EP 75/25 wt.-%	240	29
3P/EP 65/35 wt.-%	264	27

Table. 5.2.2.3 – T_{5%} [°C] and residue [%] for the 3P/EP hybrid resins.

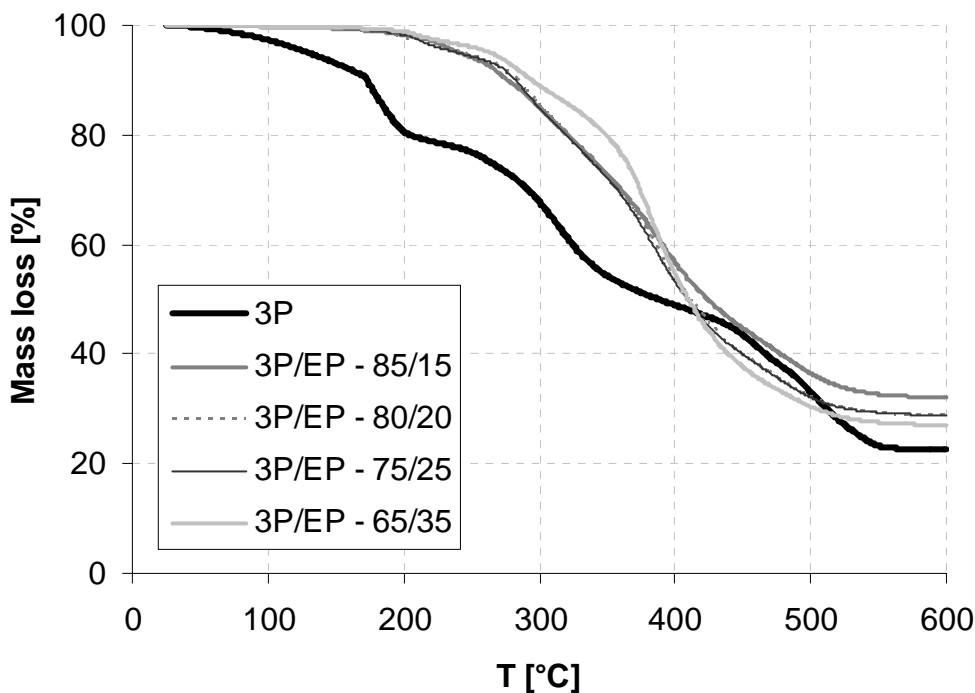


Fig. 5.2.2.8 - Mass loss vs. T for the 3P/EP hybrid resins and their reference 3P.

In figure 5.2.2.9 are presented those DSC traces, which were obtained from the second thermal scan. One can observe a strong endothermic peak at temperatures ranging from 250°C - 300°C belonging to the evaporation of the organic phosphate present in the matrix. As mentioned before, this is superimposed to the T_g transition. This peak is narrow and pronounced for the reference 3P resin; however, in the 3P/EP hybrids with increasing EP content the endothermic absorption broadens and decreases since higher EP ratios in the 3P/EP hybrid systems imply less phosphate content. Moreover at T>300°C an exothermic peak is observed corresponding to the destruction processes of the organic matrix. It is worth to remark that three different transitions were determined for the 3P/EP hybrid resin, which confirmed the results obtained by

the DMTA (c.f. Fig.5.2.2.7). The T_g of the 3P/EP epoxy hybrids shift to lower temperatures as the EP ratio in the 3P/EP hybrid systems increases (c.f. Table 5.2.2.4). The shift to lower temperatures could be related to an increase of the free volume due to a lower crosslinking density.

Sample name	Sub T_g [°C]	T_g [°C]
3P/EP 85/15 wt.-%	95/187	259
3P/EP 80/20 wt.-%	85/153	257
3P/EP 75/25 wt.-%	76/144	250
3P/EP 65/35 wt.-%	67/105	243

Table 5.2.2.4 – Transition temperatures (T_g) for the 3P/EP hybrid resins.

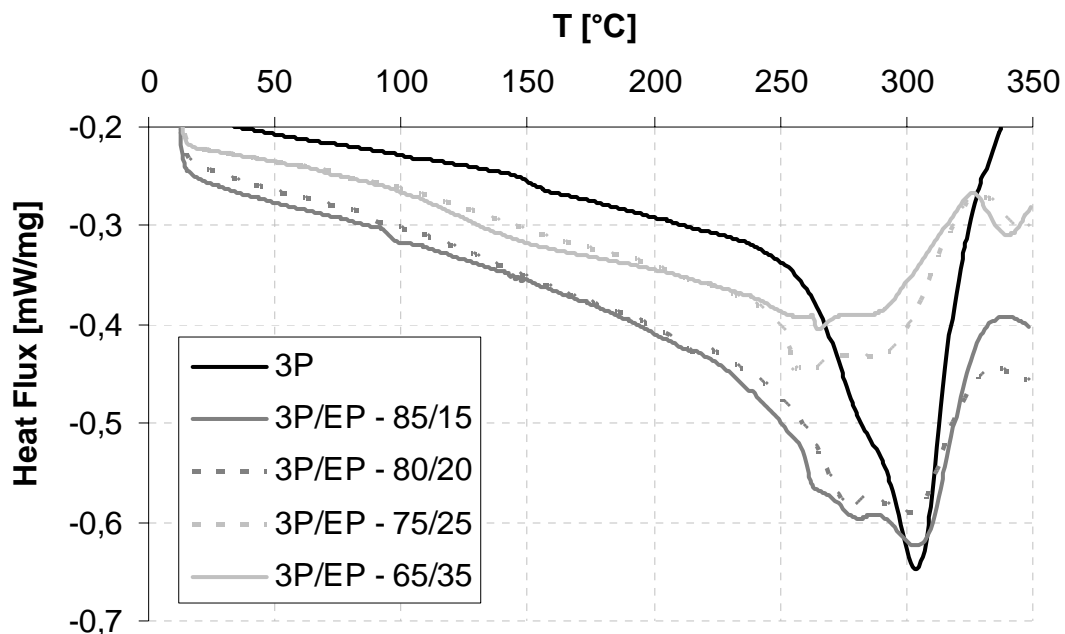


Table 5.2.2.9 – DSC curves for the 3P/EP hybrid resins and the reference 3P.

The flammability tests performed on the 3P/EP hybrid resins give a qualification of V-2 according to the UL 94 flammability test. The flammability of the hybrid resins is enhanced by the addition of epoxy resin. The specimens burned up to two minutes after applying the flame and dropped flaming drips. Therefore one can assume that the hybridization of the 3P resins with epoxy resin did not maintain the outstanding good fire resistance of the reference 3P resin.

5.2.3. Melamine formaldehyde resins

5.2.3.1. Rheology

The rheology tests performed on the 3P/MF hybrid resins showed that the hybridization of the 3P reference resins with MF reduced notably the viscosity. As presented below in the figure 5.2.3.1 one can observe that the decrease in viscosity for MF percentages of 1% is only effective at early times ($t < 75$ min) and afterwards the viscosity of the hybrid systems resemble those of the 3P reference resins. However, when increasing the MF content up to 10% the decrease in viscosity is remarkable. High MF contents reduce the viscosity to one third of the initial 3P viscosity. Therefore one can assume that MF worked as an additional reaction controlling agent for the 3P systems, prolonging the pot life of the systems and as a result favouring their posterior processing.

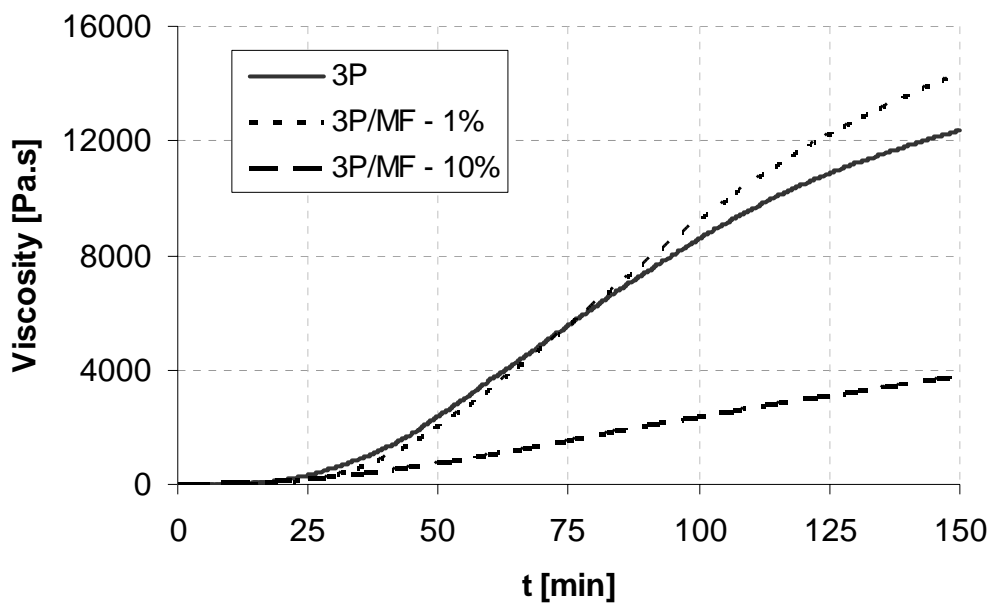


Fig. 5.2.3.1 - Viscosity vs. time traces of the hybrid resins 3P/MF-1%, 3P/MF- 10% and the reference 3P resin.

5.2.3.2. Morphology

The morphology of the 3P/MF hybrid systems, studied from the SEM pictures of the fracture surfaces (Fig. 5.2.3.3), reveal no apparently influence of the MF. Considering the morphology of the reference 3P and those of the 3P/MF hybrids, one can see that neither the particles size nor the distribution of the polysilicate particles altered by the hybridization of the initial 3P resin with MF.

However, when inspecting more accurately, one can observe that increasing MF contents reduce slightly the mean particle size diameter (c.f. Table 5.2.3.1). Depicted in figure 5.2.3.2 one can observe that the 3P/MF hybrids, as well as the reference resin 3P, possess similar broad particle distribution curves. It was found that the amount of MF of the hybrid resins had little influence on the polysilicate particle distribution c.f. Table 5.2.3.1).

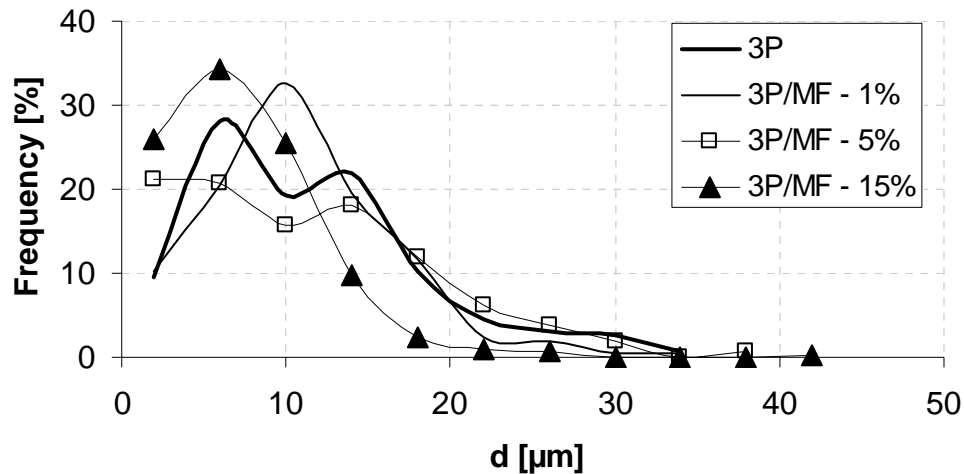


Fig. 5.2.3.2 – Particle size diameter vs. frequency for the 3P/MF hybrids and the reference 3P resin.

Sample name	d_n [μm]	d_w [μm]	d_w/d_n
3P	11.2	15.5	1.4
3P/MF - 0.5%	12.7	17.9	1.4
3P/MF - 1%	10.9	13.8	1.3
3P/MF - 2.5%	11.2	16.1	1.4
3P/MF - 5%	11.0	15.9	1.5
3P/MF - 10%	9.7	12.7	1.3
3P/MF - 15%	7.5	10.7	1.4

Table 5.2.3.1 – Number- average (d_n) and weight-average (d_w) mean particle size of the 3P/MF hybrid systems with increasing MF content and the reference 3P resin.

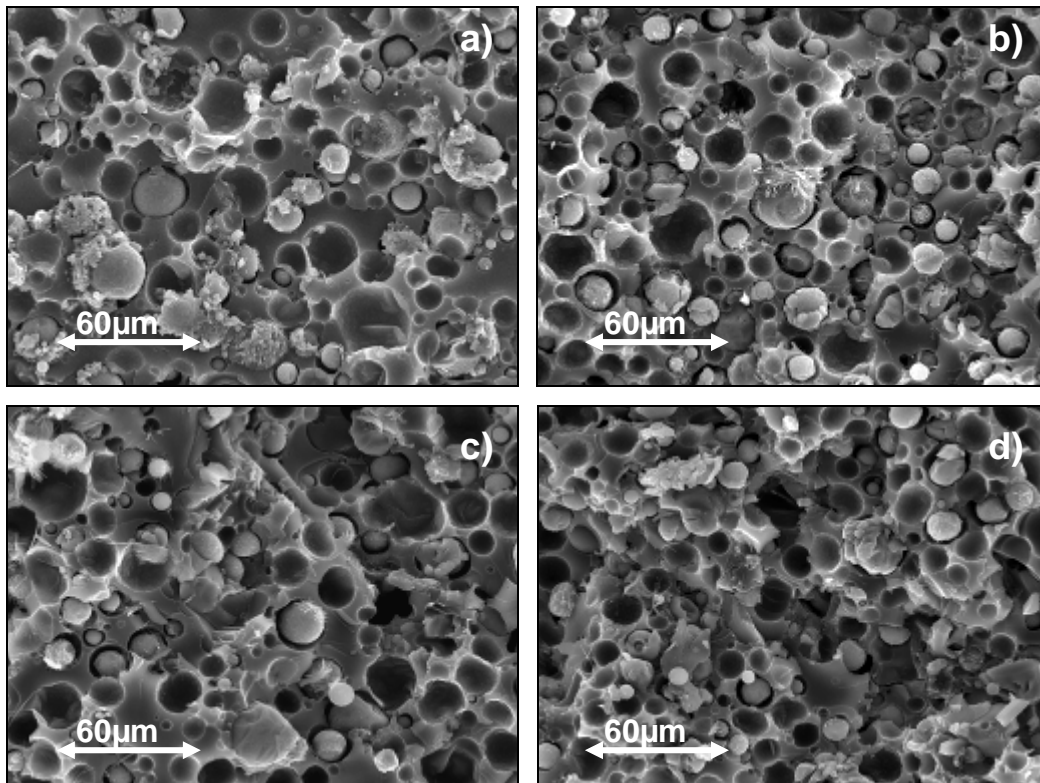


Fig. 5.2.3.3 – SEM pictures from the broken surfaces of the reference 3P resin (a); 3P/MF-1% hybrid resin (b); 3P/MF-5% hybrid resin (c); 3P/MF-10% hybrid resin (d).

5.2.3.3. Mechanical Properties

The fracture energy (G_C) and fracture toughness (K_C) for the 3P/MF hybrid resins are displayed below in Fig.5.2.3.4. The hybridization of the 3P resins with MF did have an effect on the fracture properties. Beholding the changes of the fracture properties for the hybrids with different MF content, one can see that the fracture energy of the hybrids is improved in relation to the reference. A G_C increase was found for all the hybrids up to an MF content threshold of 10 wt.-% MF, where G_C is slightly lower than the reference 3P. It is noteworthy that G_C decreases with the MF content of the hybrid resins. This could be related to the diminished polysilicate particle size (c.f. Table 5.2.3.1) with increasing MF content which affects the failure mode. On the other hand, K_C does not appear to be influenced by the hybridization with MF or by its amount. However, in general the fracture properties of the novel hybrid resins experienced a modest improvement.

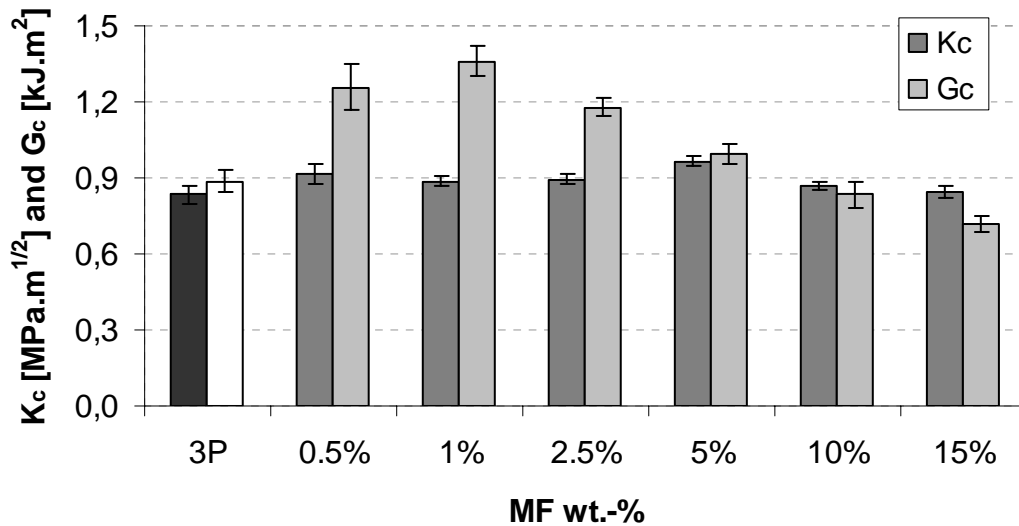


Fig. 5.2.3.4 - Fracture toughness (K_c) and fracture energy (G_c) for the 3P/MF hybrids and their reference 3P resin.

The flexural properties of the 3P/MF hybrid resins were positively influenced by the incorporation of MF (c.f. Fig. 5.2.3.5). Satisfactory results on the flexural properties were obtained from the hybridization of the 3P resins with MF. Increasing amounts of MF improve markedly the flexural modulus (E_f). In general, the increase of E_f is parallel to the increase in MF. Nonetheless, the flexural energy was improved in comparison with the reference 3P resin. Conversely the flexural strain decreased along with the increase of MF wt.-% (c.f. Table 5.2.3.2).

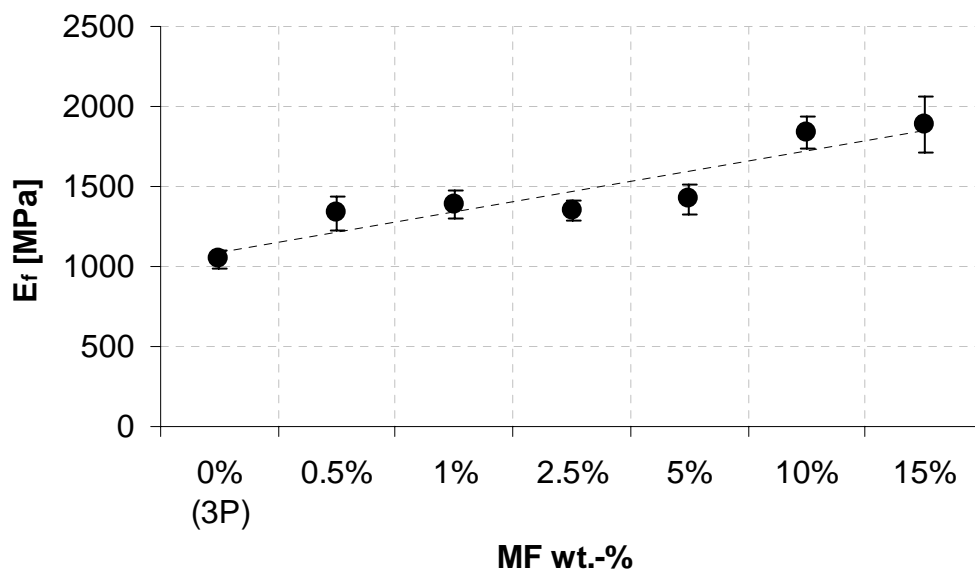


Fig. 5.2.3.5 - Changes in the flexural modulus as a function of the MF content.

Sample name	E_f [MPa]	s [MPa]	σ_{fm} [MPa]	S [MPa]	ε_M [%]	S [%]
3P	1047	56	34.6	3.9	4.4	0.9
3P/MF - 0.5%	1335	107	37.0	2.4	3.8	0.1
3P/MF - 1%	1383	87	37.4	1.8	3.5	0.2
3P/MF - 2.5%	1349	58	31.6	7.9	2.7	0.7
3P/MF - 5%	1424	94	34.6	4.7	2.9	0.4
3P/MF - 10%	1833	100	37.8	3.7	2.5	0.3
3P/MF - 15%	1891	173	35.9	2.9	2.4	1.0

Table 5.2.3.2 - Flexural modulus (E_f), strength (σ_{fm}), strain (ε_m) and standard deviation (s) for the 3P/MF hybrids and the reference 3P.

The DMTA tests results in form of E' vs. T traces (Fig.5.2.3.6) of the 3P and the 3P/MF hybrid resins confirm those obtained in the flexural tests. The storage modulus (E') is improved by the addition of MF in the systems, whereas, the E' modulus obtained for the reference 3P resin is somewhat higher at room temperature than the values obtained from the 3-point-bending (3PB) test. At temperatures around 150°C the 3P/MF specimens undergo a brusque discontinuity on the E' traces due to the premature failure at high temperatures. For the reference 3P resin failure takes place first at temperatures above 180°C.

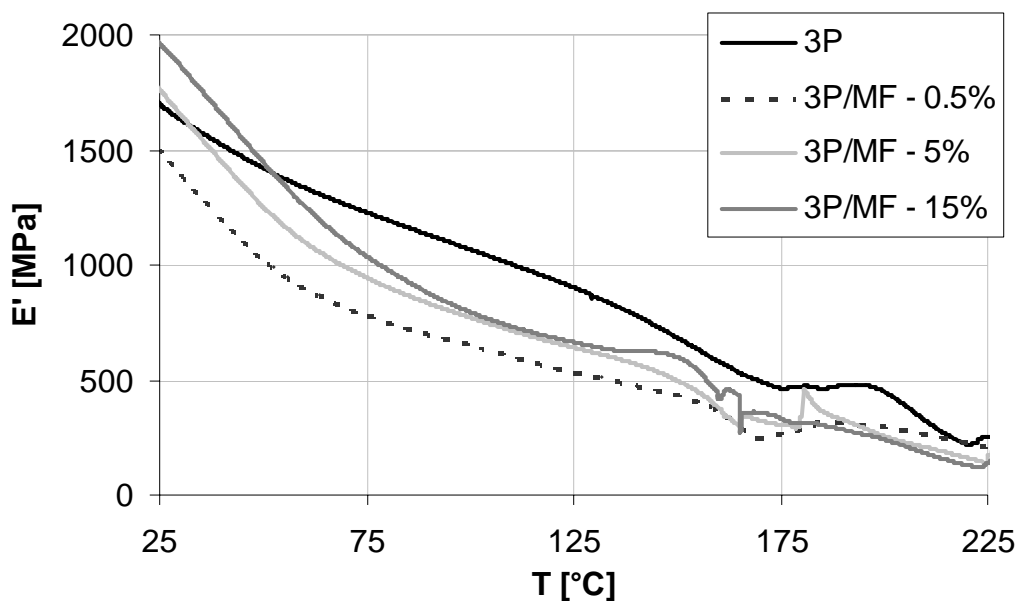


Fig. 5.2.3.6 - DMTA results displaying E' vs. T for the 3P reference and its hybrids 3P/MF.

Inspecting the $\tan \delta$ vs. T traces for the reference 3P and its 3P/MF hybrids depicted in Fig.5.2.3.7, one can observe that the 3P/MF hybrid resins present two broad "shoulders" in the $\tan \delta$ traces at temperatures from 50°C to 100°C and a second one from 130°C to 160°C. Further, a not well resolved α relaxation peak is also observed at temperatures from 180°C to 210°C, however the premature failure of the specimens at $T > 150^\circ\text{C}$ hampers its clear determination.

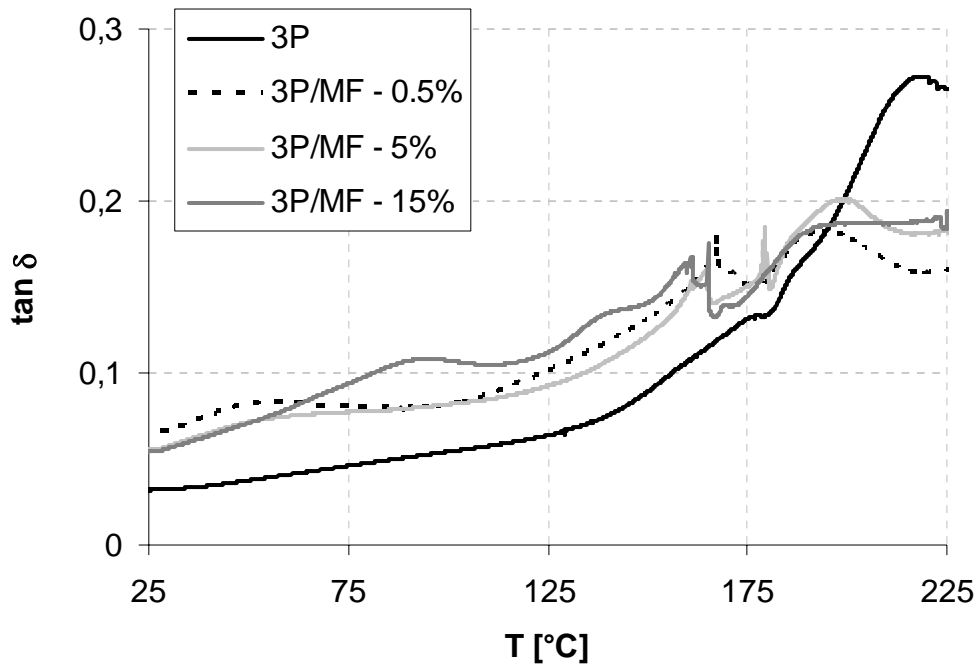


Fig.5.2.3.7 - DMTA results displaying $\tan \delta$ vs. T for the 3P and the 3P/MF hybrids.

5.2.3.4. Thermal properties

The thermal degradation behaviour of the 3P/MF hybrid resins, as well as their reference 3P, is shown in Fig. 5.2.3.8. When comparing the TG traces of the hybrids with that of the 3P reference, one can observe that the degradation steps for both resemble to one another, at least, from RT to 400°C. However, the degradation processes of the hybrids 3P/MF take place in general at higher temperatures. At temperatures above 400°C the reference 3P undergoes a considerable mass loss, while the 3P/MF hybrids continue to lose mass at a moderate rate [55].

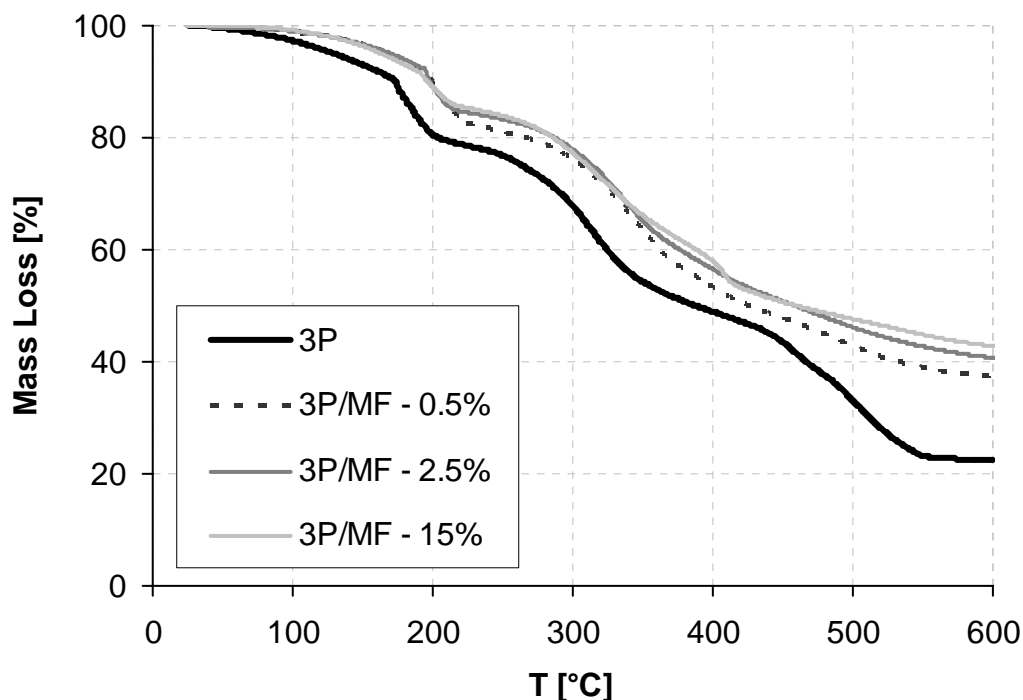


Fig. 5.2.3.8 - Mass loss vs. T for the 3P/MF hybrid resins and their reference 3P.

Observing more accurately the temperature at which the 5% of the mass is lost ($T_{5\%}$), one can clearly see that this ranges from 145°C to 180°C for the corresponding 3P/MF hybrids, while for the 3P reference the 5% of the mass is lost at the early temperature of 125°C (c.f. Table 5.2.3.3). Similarly, the residue remaining after the degradation process is significantly higher for the 3P/MF hybrids, increasing along with the MF content, than for the reference 3P, which is approximately a 23% of the initial specimen mass. To scan up we can assert that the hybridization of the 3P resins with MF had a positive influence in the thermal behaviour, obtaining hybrids capable of enduring higher temperatures.

MF wt.-%	0.5	1	2.5	5	10	15
$T_{5\%}$ [°C]	167	145	170	178	169	163
Residue [%]	37	39	41	43	43	43

Table 5.2.3.3 – $T_{5\%}$ [°C] and residue [%] for the 3P/MF hybrid resins with increasing MF content.

The DSC curves, presented below in Fig. 5.2.3.9, show an endothermic peak at temperatures ranging from 280°C to 310°C for the 3P/MF hybrids, as well as for

the 3P reference system. This, again superimposed to the T_{trans} , may be derived from the evaporation of the organic phosphate, which has a boiling point of 240°C-265°C. This endothermic effect is more marked for the reference 3P, and its intensity reduces successively with increasing MF content as the phosphate content in the 3P/MF hybrids is reduced. At $T > 300^\circ\text{C}$ an exothermic peak reflecting the destruction of the matrix can be observed.

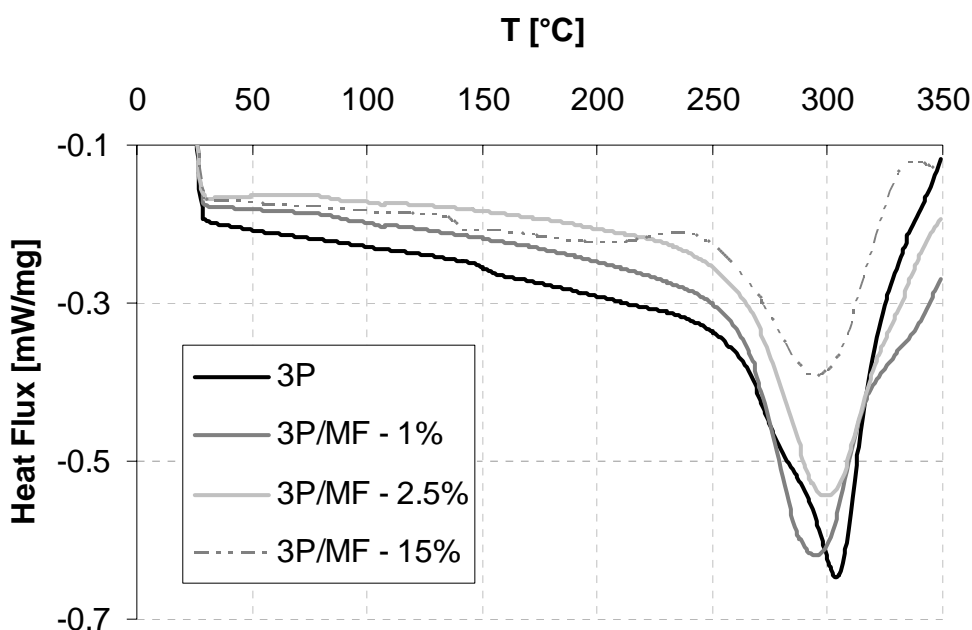


Fig. 5.2.3.9 – DSC curves for the 3P/MF hybrid resins and the reference 3P.

The T_{trans} determined from the DSC traces are listed in Table 5.2.3.4. Three transition temperatures could be detected. The first one observed at $T \sim 104^\circ\text{C}$ - 105°C shifts to higher temperatures along with increasing MF content. This may be linked to the crosslinked melamine formaldehyde homopolymer. A second transition was determined at $T \sim 139^\circ\text{C}$ and is shifted towards higher temperatures as the MF content decreases. Its onset may be assigned to the 3P/MF hybrid copolymers formed. Recall that this peak could not be detected for all the 3P/MF hybrids. These two transitions obtained may be responsible for the broad “shoulders” detected by DMTA. The third transition (T_g) at $T \sim 280^\circ\text{C}$ corresponds to the main glass transition of the 3P resins, as already observed. It is as well shifted to lower temperatures as the MF content increases. This may be due to one plasticizing effect induced, by the MF, in the 3P/MF systems.

Sample name	Sub T_g [°C]	T_g [°C]
3P/MF - 0.5%	104/140	283
3P/MF - 1%	105/ -	276
3P/MF - 2.5%	104/ -	279
3P/MF - 5%	105/139	280
3P/MF - 10%	105/139	272
3P/MF - 15%	105/138	272

Table 5.2.3.4 – Position of the transition peaks obtained from the DSC scan for the 3P/MF hybrid resins.

The flammability test for the 3P/MF hybrid resins, according to the 94UL standards for vertical burn (94V), give a classification of is V-0. The total flaming combustion time was zero, the specimens did not burn with flaming combustion after the flame application and they did not drip flaming particles that ignite the cotton. The results obtained from the flammability test showed that 3P/MF hybrid resins are good fire resistant materials.

5.3. 2P / HYBRID RESINS

5.3.1. Vinylester Resins

During the characterisation of the vinylester hybrid resins it turned out that the mechanical properties of the 2P/VE1/MF specimens were surprisingly poor. It was surmised that the properties of these hybrids can be improved by using vinylesters with higher amount of styrene. Therefore two further vinylester resins were considered in the related test series. The coding of the different vinylesters is as follows: VE1 (for the vinylester containing the lowest styrene content - 29 wt.-%), VE2 (medium styrene content - 33 wt.-%) and VE3 (highest styrene content 45 wt.-%).

5.3.1.1. Rheology

The rheological behaviour of the hybrid systems is depicted in Fig. 5.3.1.1, showing the viscosity vs. time traces for the 2P/VE/MF hybrids and reference 3P. As observed before for the 3P/MF hybrids, the viscosity of the 2P/VE/MF hybrids diminishes with increasing MF concentration. This effect confirms that MF acts as a good reaction controlling agent for the 3P systems at pot life times up to 60 min. Note that the hybrid 2P/MF/VE-1% shows a steeper course than the hybrid 2P/MF/VE-0.5% and similarly the 2P/MF/VE-10% hybrid showed a gentler slope than the 2P/MF/VE-15% hybrid. This phenomenon could be related to the fact that MF is added to the system in a powder form and at some MF wt.-% threshold the viscosity that the powder confers to the hybrid is higher than its emulsifying effect and likewise, for MF wt.-% lower than 0.5% the viscosity related to the addition of MF to the system has none or negligible effect. The 2P/VE/MF resins are, depending on their MF content, slightly more viscous than the 3P reference resins. However, their viscosity is far lower when comparing to the 3P/VE systems, which viscosity after 75 min reaches values up to 1500000 Pa.s.

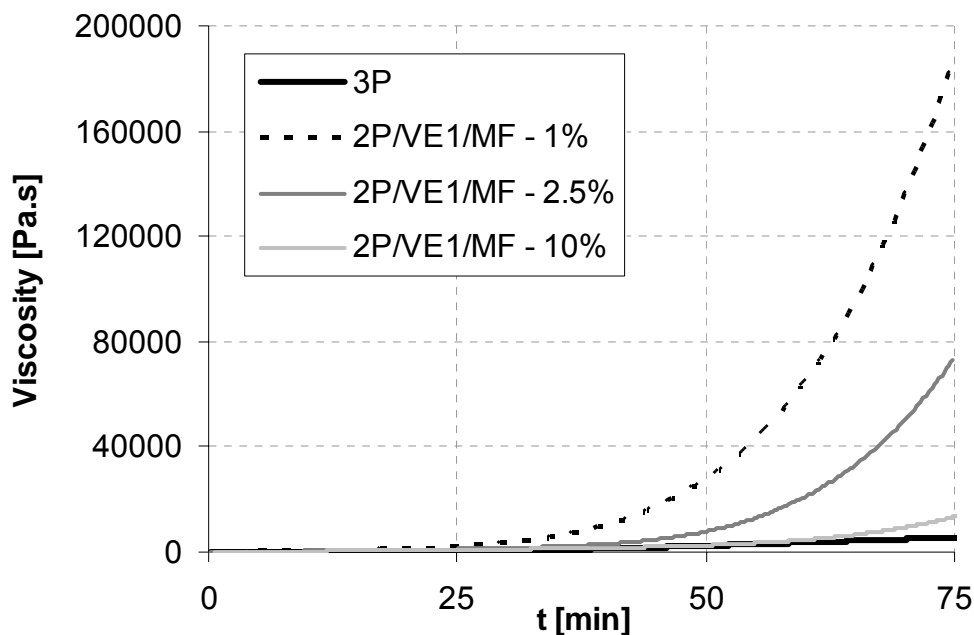


Fig. 5.3.1.1 - Viscosity vs. time traces of the hybrid resins 2P/VE1/MF (1%, 2.5% and 10% in MF) and the reference, 3P resin at RT.

5.3.1.2. Morphology

Inspecting the SEM pictures of the fracture surfaces of the 2P/VE/MF hybrids one clearly observe the differences caused by the VE varieties (Fig. 5.3.1.2). Specimens with equal MF concentration show significant differences in the polysilicate particle distribution as well in their mean diameter. The 2P/VE1/MF hybrids resemble to the 3P reference system, they possess larger particle size and a broader distribution in comparison to the 2P/VE2/MF and 2P/VE3/MF hybrids, which show a particle size ranging from less than $1\mu\text{m}$ to $10\mu\text{m}$. This is well reflected in Fig. 5.3.1.3. It appears that the higher the styrene content of the VE resin the better is its emulsifier action in the resulting system (cf. Table 5.3.1.1). Moreover VE seems to be also a suitable substituent for the phosphate emulsifier in the 3P systems, since it is a “reactive” emulsifier, i.e. it is chemically built in the final crosslinked structure. Recall that this occurs via the reaction between the secondary $-\text{OH}$ groups of the VE and $-\text{NCO}$ of the PMDI [113].

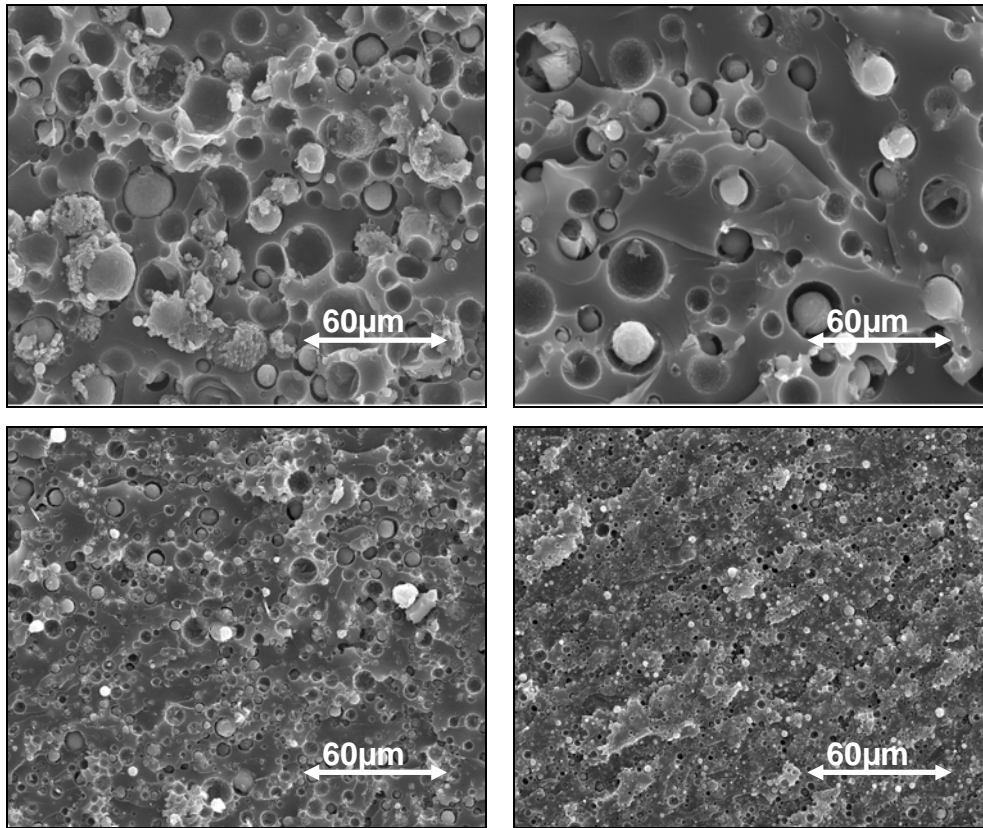


Fig. 5.3.1.2 - SEM pictures from the broken surfaces of the reference 3P resin (top left); 2P/VE1/MF-0.5% hybrid resin (top right); 2P/VE2/MF-0.5% hybrid resin (bottom left); 2P/VE3/MF-0.5% hybrid resin (bottom right).

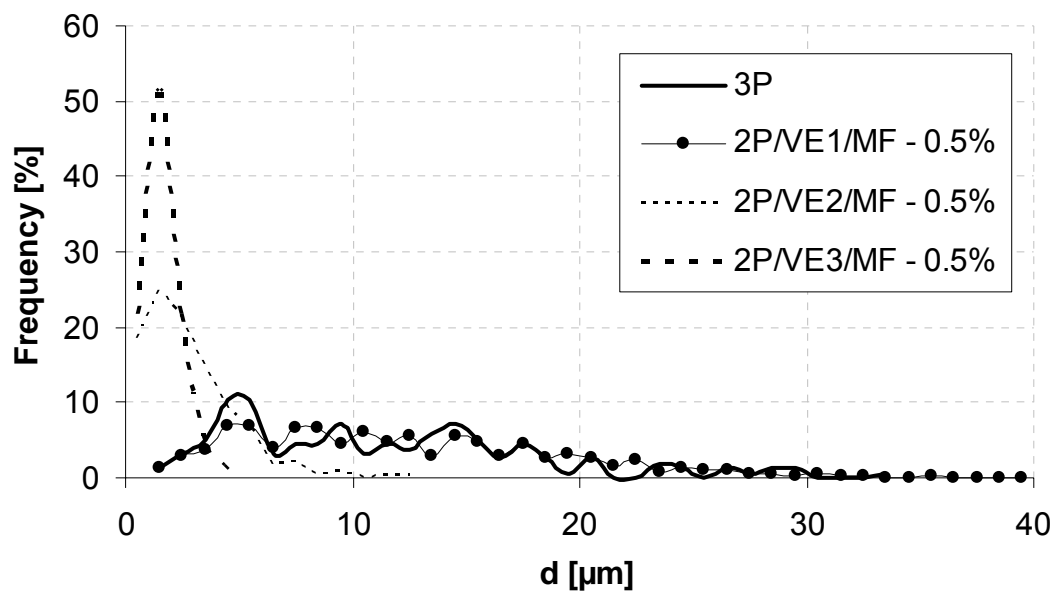


Fig. 5.3.1.3 - Particle size diameter vs. frequency for the 2P/VE/MF-0.5% hybrids of different vinylester and their 3P reference.

SEM pictures of the broken surfaces from systems produced with the same VE but with different amounts of MF are shown in Fig. 5.3.1.4. It is noticeable that with

increasing MF amount, the mean particle size of the polysilicates raises. Parallel to that the distribution of the silicates broadens with increasing MF content. However, there are some exceptions (cf. Table 5.3.1.1).

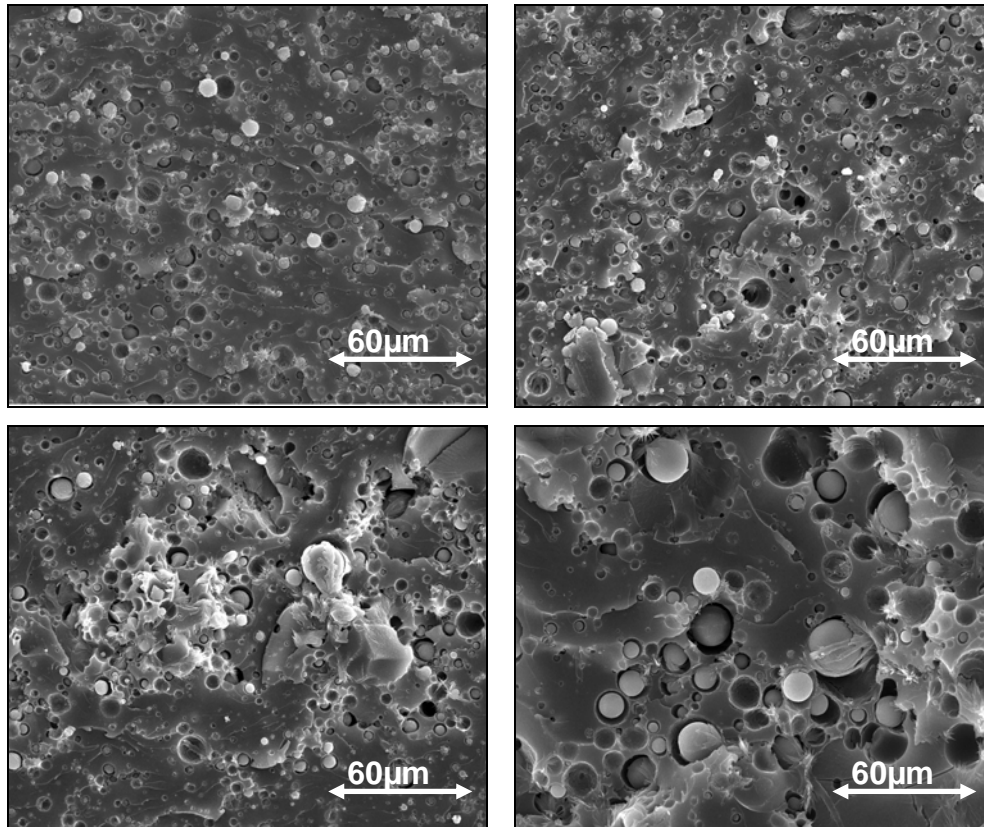


Fig. 5.3.1.4 - SEM pictures from the fracture surfaces of the 2P/VE2/MF-1% hybrid resin (top left); 2P/VE2/MF-5% hybrid resin (top right); 2P/VE2/MF-10% hybrid resin (bottom left); and 2P/VE2/MF-15% hybrid resin (bottom right).

MF wt.-%	2P/VE1/MF			2P/VE2/MF			2P/VE3/MF		
	d_n [μm]	d_w [μm]	d_w/d_n	d_n [μm]	d_w [μm]	d_w/d_n	d_n [μm]	d_w [μm]	d_w/d_n
0.5	12.2	16.0	1.3	2.7	4.1	1.5	1.6	2.0	1.3
1	29.1	46.9	1.6	2.6	3.8	1.5	1.4	2.0	1.4
2.5	20.5	32.5	1.6	2.7	4.1	1.5	1.2	1.6	1.4
5	12.1	16.7	1.4	2.4	4.2	1.7	1.2	1.6	1.3
10	21.4	36.9	1.7	3.5	4.9	1.4	1.4	1.9	1.3
15	21.3	37.9	1.8	4.8	9.1	1.9	2.0	2.7	1.3

Table 5.3.1.1 - Number- average (d_n) and weight-average (d_w) mean particle size of the polysilicate for the 2P/VE/MF hybrid systems.

Comparing the AFM pictures in Fig. 5.3.1.5 taken from 2P/VE1/MF, 3P and VE1 reference systems, it is well manifested that 2P/VE/MF hybrids and VE resins have a similar, though not equal structure. The nodules in VE resins are well resolved unlike to 2P/VE/MF. On the other hand, 3P resins possess a finer structure without nodules.

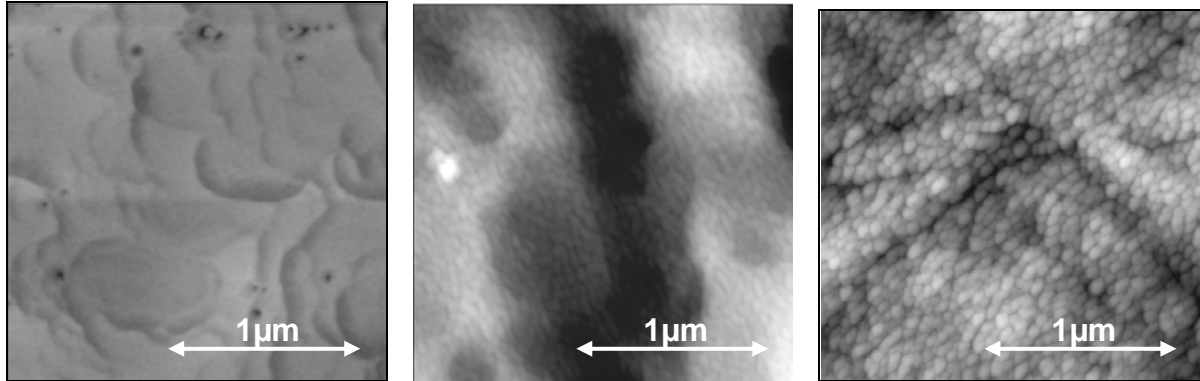


Fig. 5.3.1.5 - Amplitude-modulated AFM images taken from the ion-etched polished surfaces of the reference 3P (left); 2P/VE1/MF-10% hybrid resin (centre); and VE1 resin (right).

5.3.1.3. Mechanical Properties

The fracture toughness (K_C) and fracture energy (G_C) of the 2P/VE/MF hybrids, depicted in Fig. 5.3.1.6, depend markedly on the VE type used. The VE with higher styrene content show greater fracture toughness and energy values than the VE with lower styrene content. However, the G_C is far more affected than the K_C . So the presence of a polystyrene-rich VE improved the toughness of the 2P/VE/MF systems. On the other hand, one can observe that with increasing MF content, both, the fracture toughness and the fracture energy tend to decrease. When comparing the fracture mechanical data with the polysilicate dispersion values of Table 5.3.1.1, it is clearly seen, that the polysilicate dispersion is narrower for the hybrids containing less MF and for those with VE with higher styrene content. This meets the expectation, namely, hybrid systems with fine uniform dispersion of polysilicate are more resistant to fracture than those with coarse particles and broad dispersion.

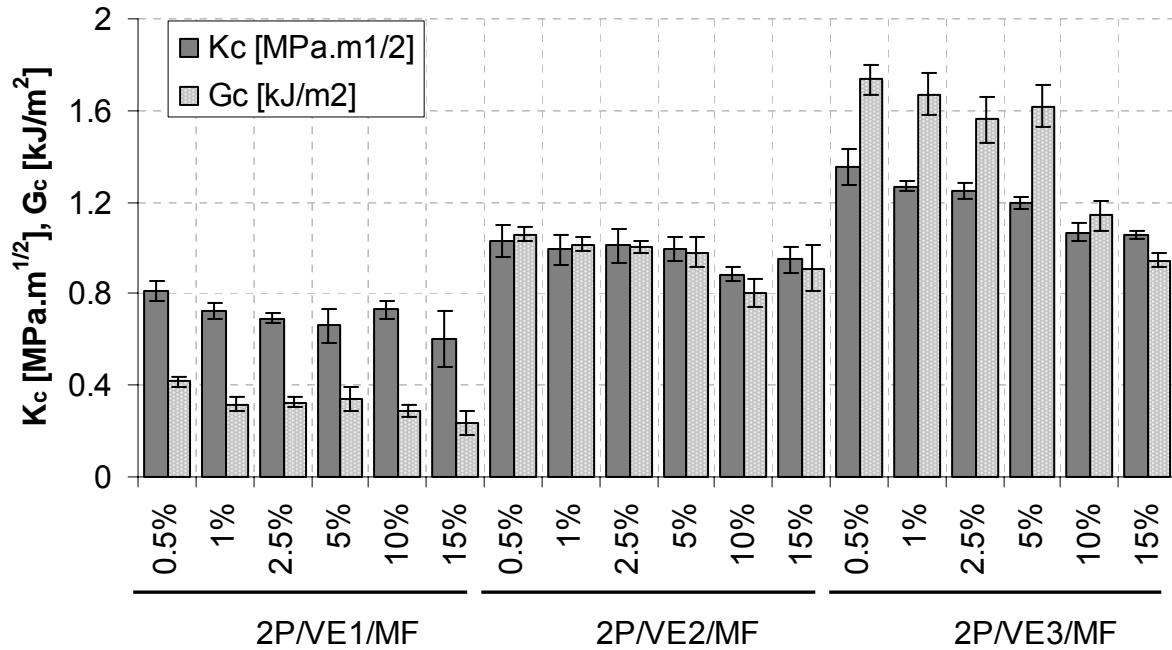


Fig. 5.3.1.6 - Fracture toughness (K_c) and fracture energy (G_c) for the 2P/VE1/MF, 2P/VE2/MF and 2P/VE3/MF hybrids.

The flexural properties of the 2P/VE/MF hybrids were not notably influenced by the VE type, e.g. in Table 5.3.1.2. One can recognize that the flexural modulus (E_f) increased with increasing MF content, except of the 2P/VE2/MF hybrids. On the other hand, both the maximum flexural strength (σ_{fm}) and strain (ε_m) decreased with increasing MF content of the hybrid resins. Attention should be paid to the fact that the stiffness and strength of the studied hybrids were markedly higher than those of the 3P resin but lower than those of the 3P/VE hybrids (c.f. Fig. 5.2.1.4).

	MF wt.-%	E_f [MPa]	S [MPa]	σ_{fm} [MPa]	S [MPa]	ε_M [%]	S [%]
2P/VE1/MF	0.5	2225	13	71.3	13.3	3.8	1.1
	1	2242	270	74.1	7.9	3.9	0.2
	2.5	2143	153	66.6	3.4	3.3	0.3
	5	2335	104	60.8	4.0	2.7	0.2
	10	2507	93	53.9	5.1	2.3	0.2
	15	2510	179	42.8	2.4	1.8	0.1
2P/VE2/MF	0.5	2166	160	63.1	5.2	3.2	0.3
	1	2093	184	59.7	7.8	3.1	0.5
	2.5	1971	185	57.6	4.7	3.2	0.3
	5	2052	166	47.2	8.5	2.3	0.4
	10	1934	192	42.3	1.2	2.1	0.2

	15	1987	95	36.8	5.3	1.8	0.3
2P/VE3/MF	0.5	1907	74	67.4	3.0	5.9	1.2
	1	2035	101	65.4	4.3	4.7	1.6
	2.5	2085	194	63.7	5.3	3.7	0.3
	5	2264	141	69.4	3.8	4.0	0.4
	10	2279	162	63.3	5.1	3.1	0.5
	15	2032	178	48.7	8.0	2.5	0.7

Table 5.3.1.2 - Flexural modulus (E_f), strength (σ_{fm}), strain (ε_m) and standard deviation (s) for the 2P/VE1/MF, 2P/VE2/MF and 2P/VE3/MF hybrids.

The presence of a heterogeneous co-network should be observable in the DMTA behaviour in form of a very broad glass transition peak (T_g). Figure 5.3.1.7 displays the storage modulus (E') and the mechanical loss factor ($\tan \delta$) as a function of temperature for the selected 2P/VE/MF systems with various VE types. The expected broad T_g relaxations, at $T \sim 150^\circ\text{C}$ for the 2P/VE1/MF hybrid systems and at $T \sim 135^\circ\text{C}$ for the hybrid systems 2P/VE2/MF and 2P/VE3/MF, are well discernible in Fig. 5.3.1.7. One can see that the hybridization with MF (incorporation of stiff melamine units) enhances the stiffness of the corresponding hybrids, in comparison with the reference 3P. Moreover, the stiffness is also improved as the MF content increases and as well as enhanced by the use of styrene-poor VE (c.f. Table 5.3.1.3). These results are in concordance with the data obtained from the flexural tests (c.f. Table 5.3.1.2). The slight shift in the T_g peak position towards lower temperatures with MF content can be traced to the complex chemistry involving both simultaneous and consecutive reactions (c.f. Fig. 5.3.1.7). On the other hand, the 2P/VE/MF hybrids owe, in general, lower T_g than the corresponding phosphate containing hybrids 3P/VE 50/50 ($T_g \sim 156^\circ\text{C}$). This is a surprising result since the phosphate acts as a plasticiser in the final crosslinked resins and therefore its presence should reduce the T_g . Presumably, the incorporation of MF in the 2P/VE/MF hybrid systems modified their crosslinking, since increasing amounts of MF shifted the T_g to lower temperatures.

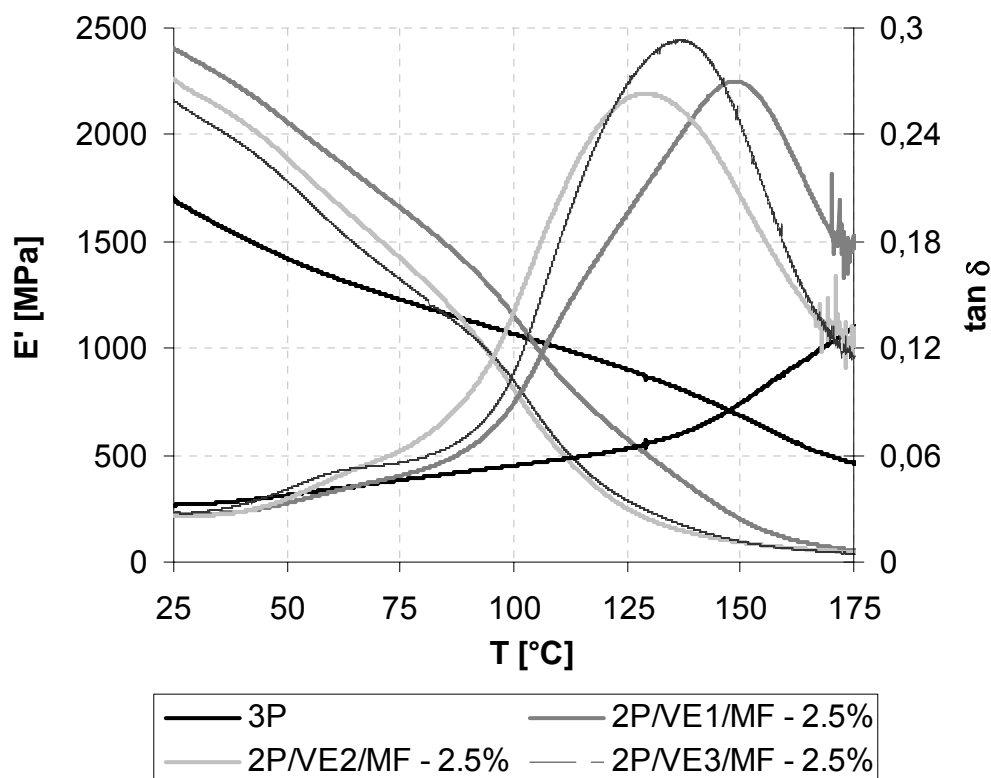


Fig 5.3.1.7 - E' and $\tan \delta$ vs. T for the 2P/VE/MF hybrids with equal MF wt.-% but different styrene containing VE and their reference 3P.

MF wt.-%	2P/VE1/MF		2P/VE2/MF		2P/VE3/MF	
	T_g [°C]	E' [MPa]	T_g [°C]	E' [MPa]	T_g [°C]	E' [MPa]
0.5	150	2132	130	2539	149	2072
1	152	2494	131	2157	133	2077
2.5	149	2403	129	2258	135	2157
5	148	2433	132	2275	132	2194
10	145	2646	133	2273	140	2326
15	148	3352	136	2508	140	2264

Table 5.3.1.3 - Glass transition temperature (T_g) and storage modulus (E') at 25°C for the 2P/VE1/MF, 2P/VE2/MF and 2P/VE3/MF hybrids.

5.3.1.4. Thermal Properties

The TGA curves, depicted in Fig. 5.3.1.8, show the effects of different VEs on the thermal degradation of 2P/VE/MF hybrids. The thermal resistance of the 2P/VE/MF hybrids raised parallel with the styrene content of the VE. It is noticeable that the hybrid resins with VE1 (lower styrene content) start to degrade approximately 30°C before than the 2P/VE2/MF and 2P/VE3/MF hybrids and result in lower residues, as

well (c.f. Table 5.3.1.4). Nevertheless, the 2P/VE/MF hybrids show a mixed thermal behaviour between their reference materials, viz. VE and 3P. At lower temperatures their thermal resistance is greater, resembling to the behaviour of the VE resins, rather than the 3P resins, which start to degrade at temperatures around 200°C. However, at higher temperatures the hybrids do not degrade as dramatically as the VE. It has to be underlined that, the substitution of the phosphate by MF resin affected positively the thermal resistance of the hybrids, in the whole range of temperature. This fact becomes clear when comparing the TGA traces of 3P/VE and 2P/VE/MF traces (Fig. 5.3.1.8). In terms of MF content, the amount of MF in the hybrid resins exerted no remarkable effect on the thermal response of the related hybrids.

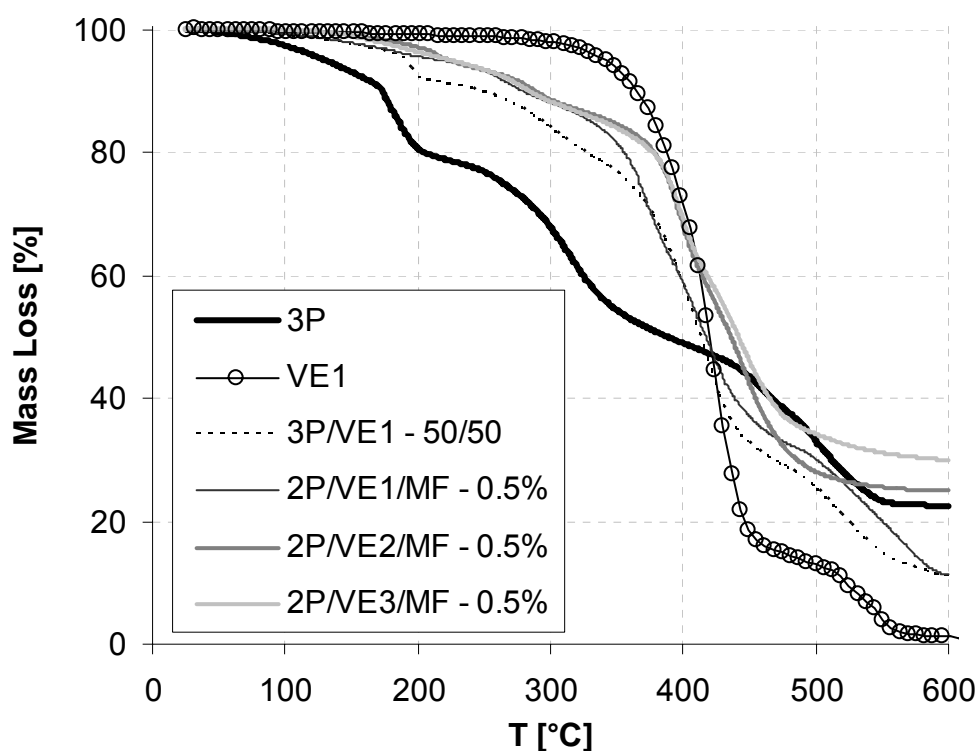


Fig. 5.3.1.8 – TGA curves vs. T for the 2P/VE/MF hybrids with different VE types and for their references VE, 3P and 3P/VE 50/50.

MF wt.-%	2P/VE1/MF		2P/VE2/MF		2P/VE3/MF	
	$T_{5\%}$ [°C]	Residue [%]	$T_{5\%}$ [°C]	Residue [%]	$T_{5\%}$ [°C]	Residue [%]
0.5	204	19	239	30	239	25
1	186	18	228	28	241	28
2.5	196	19	238	25	210	30

	2P/VE1/MF		2P/VE2/MF		2P/VE3/MF	
5	216	11	223	25	224	30
10	170	16	224	26	232	28
15	168	8	218	26	228	24

Table 5.3.1.4 – $T_{5\%}$ [°C] and residue at $T=600^{\circ}\text{C}$ [%] for the 2P/VE/MF hybrid resins with different VE types and increasing MF content.

The DSC curves from the second heating cycle, represented in Fig.5.3.1.9, show the behaviour of 2P/VE/MF hybrid systems with equal MF content but with different VEs (recall that the styrene content of the VEs is, $\text{VE1} < \text{VE2} < \text{VE3}$). Their thermal behaviour resembles more the one of the 3P/VE hybrid resins than to the 3P reference resin (c.f. Fig. 5.2.1.9). The 2P/VE/MF hybrid systems show an exothermic peak at $T \sim 280^{\circ}\text{C}$, also present in the 3P/VE resins, which probably reflects postcuring processes. Furthermore, in the DSC traces of the 2P/VE/MF hybrid resins one can observe the extinction of the characteristic endothermic peak derived mainly from the evaporation of the phosphate contained in the 3P resin and its 3P hybrids and not present in the 2P hybrids.

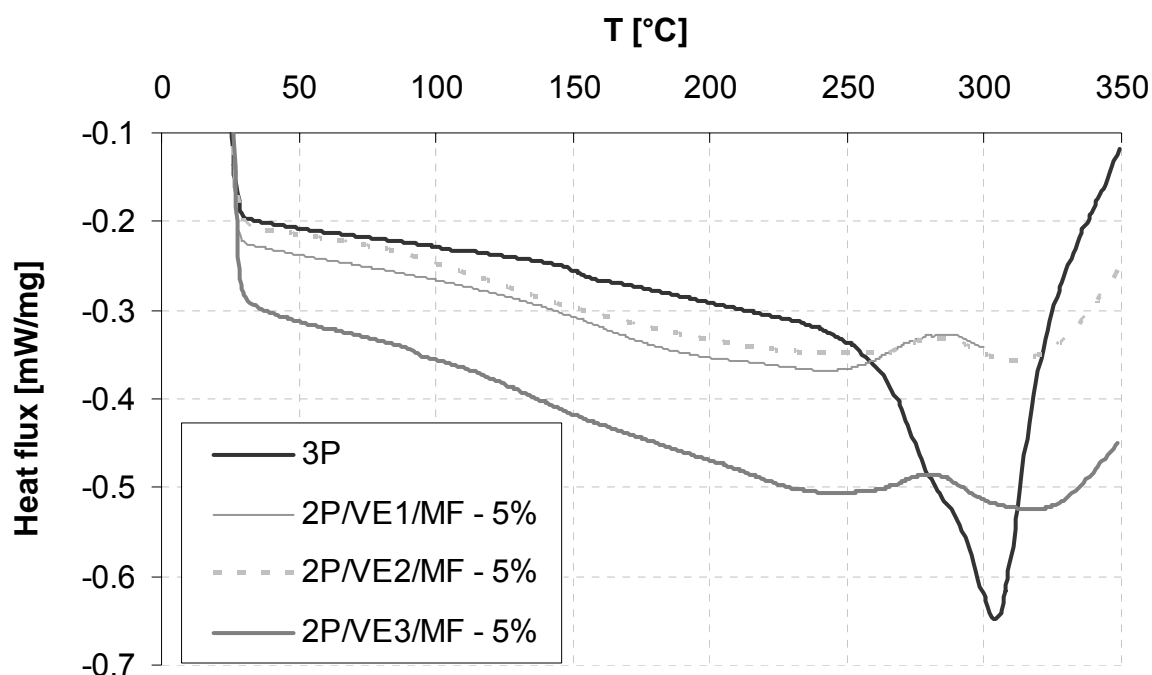


Fig.5.3.1.9 – DSC curves vs. T for the 2P/VE/MF hybrid resins with different VE and their reference 3P.

When taking into account the same VE type but varying the MF content of the 2P/VE/MF hybrids (Fig. 5.3.1.10), one can see that the hybrid systems with lower MF

content (0.5 wt.-% MF and 1 wt.-% MF) present the exothermic peak at lower temperatures followed by a broad endothermic peak. The transition temperatures obtained for the different 2P/VE/MF hybrid systems are listed in table 5.3.1.5. Increasing amount of MF shifts the T_{trans} transition at the highest temperature, as already seen for the 3P/MF hybrids. For the 2P/VE3/MF systems three different transitions could be determined from the DSC curves. The first transition could be assigned to the styrene homopolymer phase (recall that VE3 was the VE richer in styrene) while the third one may be the main transition of the polyurea phase. On the other hand, the second transition observed in the 2P/VE3/MF hybrids could be caused by the 2P/VE/MF copolymer phase. Note that due to the overlapping of endothermic and exothermic peaks it is difficult to trace the related transitions.

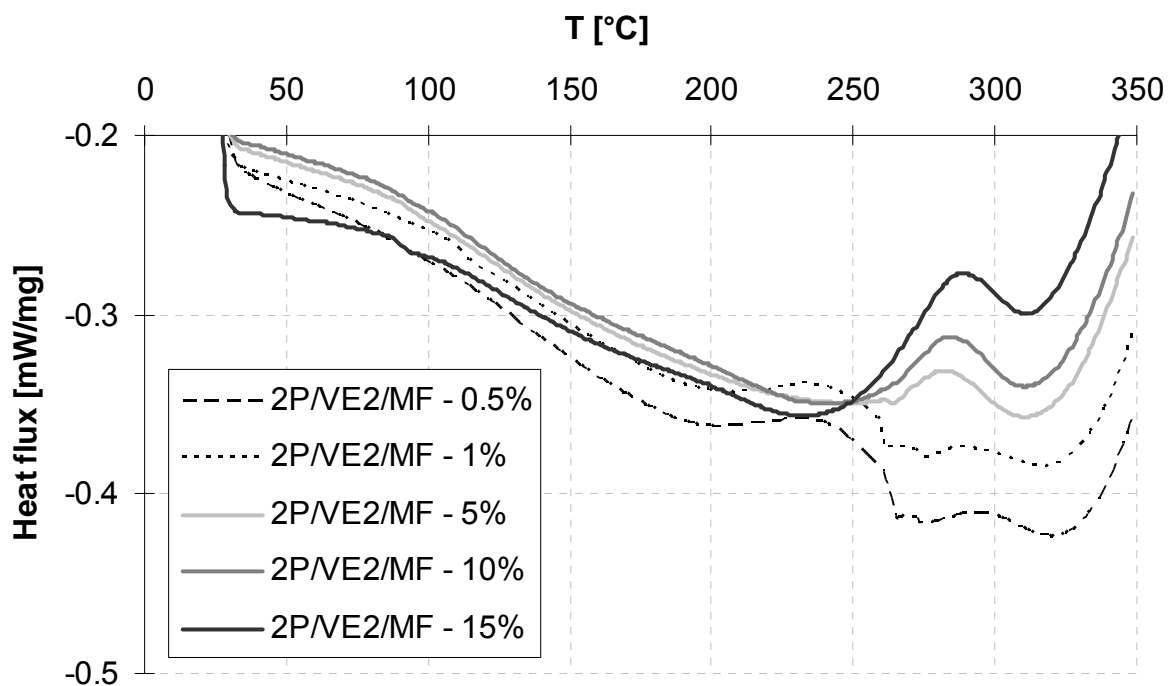


Fig.5.3.1.11 – DSC curves vs. T for the 2P/MF hybrid resins with different MF amounts.

MF wt.-%	2P/VE1/MF	2P/VE2/MF		2P/VE3/MF	
	Sub T_g [°C]	Sub T_g [°C]	T_g [°C]	Sub T_g [°C]	T_g [°C]
0.5	133	86	263	90 / 230	266
1	135	-	260	95 / 227	261
2.5	132	-	262	93 / 227	257
5	138	-	263	90 / 227	262

10	128	86	259	93 / 221	257
15	126	87	258	94 / 221	259

Table 5.3.1.5 – Sub T_g and T_g obtained from the DSC scans of the 2P/VE/MF hybrid resins with different VE types and increasing MF content. Note that the T_g of the 2P/VE1/MF hybrids could not be determined due to overlapping with the postcuring exothermic peak.

According to the UL 94 flammability test performed, the 2P/VE/MF samples are classified as V-1. The specimens burned with flaming combustion less than 30 seconds after each test flame application; the total flaming combustion time did not exceed 250 seconds and the specimens either did not burn with flaming or glowing combustion up to the specimen holding clamp, nor dripped flaming particles that ignited the cotton. None of the specimens had glowing combustion remain for longer than 60 seconds after removal of the test flame. These results confirm MF as a good flame retardant, since systems with the same 3P/VE ratio (3P/VE - 50/50) were classified as V-2. However, the flame resistance is not as good as the one of the 3P reference systems.

5.3.2. Epoxy resins

5.3.2.1. Rheology

The effects on the viscosity when hybridizing the 3P resin with epoxy are well patent in Fig 5.3.2.1. The epoxy resin (EP) confers to the system a reduced viscosity for times up to 75 min, which facilitates the posterior processing of the resulting hybrid resin. Increasing percentage of EP does not decrease significantly the viscosity. It is remarkable to say that the substitution of the organic phosphate does not affect negatively the rheological properties; even the contrary occurs as the viscosity is somewhat lower for 2P/EP than for 3P.

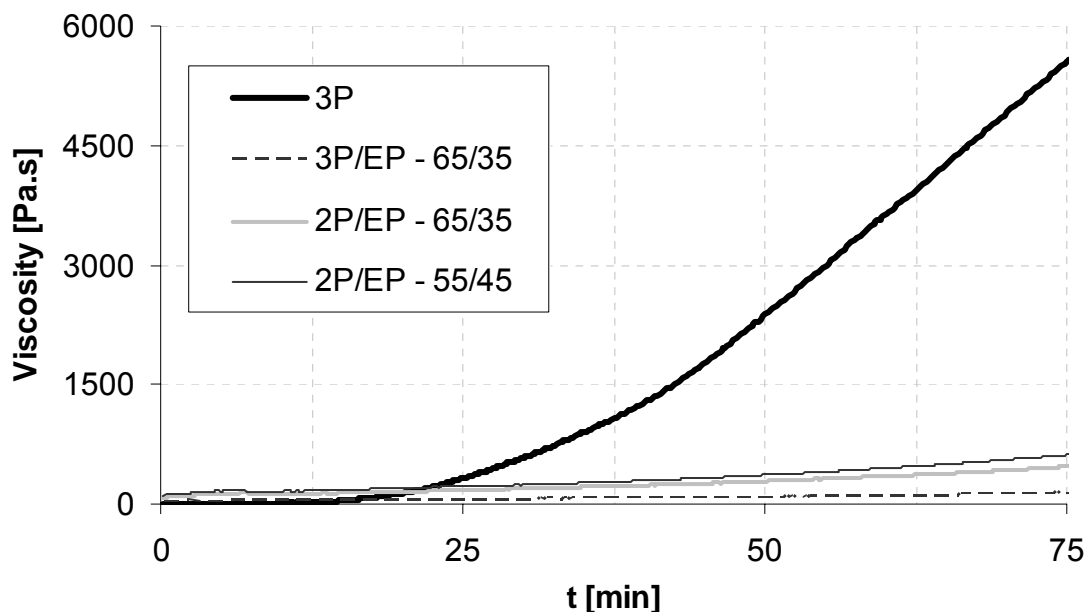


Fig.5.3.2.1- Viscosity vs. time traces of the hybrid resins 3P/EP-65/35 wt.-%, 2P/EP-65/35 wt.-%, 2P/EP-55/45 wt.-% and the reference 3P resin.

5.3.2.2. Morphology

Observing the SEM pictures obtained from the fracture surface of the hybrid samples (Fig. 5.3.2.2), one can clearly see the outstanding change on morphology caused by the hybridization with EP. When comparing with the reference 3P (Fig.5.3.2.2 - a) it is clear that the silicate particle diameter is drastically reduced from micrometre range to tens of nanometre. Recall that the final dispersion of the WG in the 2P/EP systems was accomplished at 2000 rpm within 1 min, while for the 3P reference systems was at 800 rpm, during one minute as well. As observed before, higher mixing velocities reduce the mean particle size of the polysilicate phase. Therefore the morphology of the 2P/EP hybrids should be compared with that 3P system which was produced under the same mixing conditions, viz. 3P-2 (c.f. Table 5.3.2.4). Although the 3P-2 resin has a smaller polysilicate particle size than the 3P reference, it is yet patent that the marked reduction of the particle diameter of the 2P/EP hybrid resins is mostly due to the hybridisation with EP resin. It is also interesting to remark that the broken surface of the 2P/EP hybrid resins show a kind of layers in form of “terraces”, while the 3P resins broken surface present a rather uniform surface. Moreover, the formation of needle Na_2CO_3 crystals is somewhat diminished.

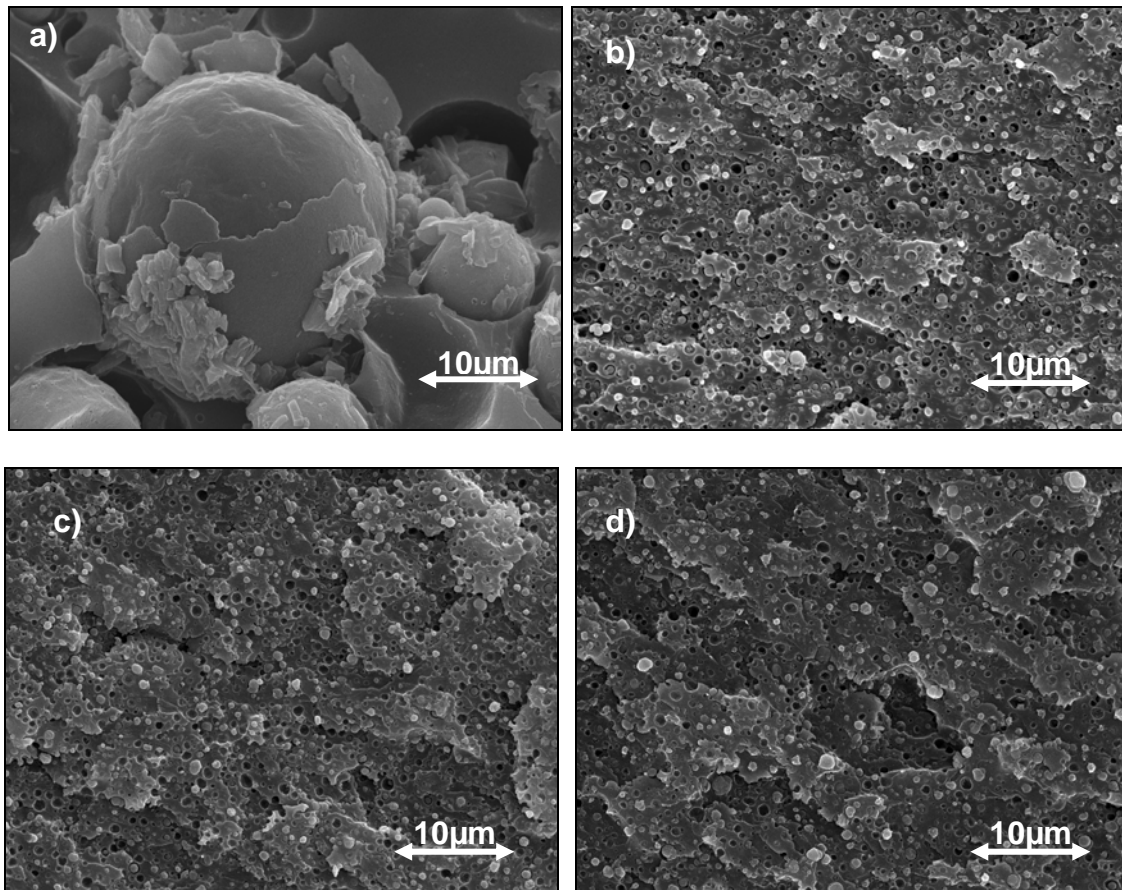


Fig.5.3.2.2- SEM pictures from the broken surfaces of the reference 3P resin (a); 2P/EP-65/35 wt.-% hybrid resin (b); 2P/EP-60/40 wt.-% hybrid resin (c); 2P/EP-55/45 wt.-% hybrid resin (d).

Inspecting the polysilicate particle distribution depicted in Fig.5.3.2.3 one can observe that although all the 2P/EP hybrids possess a narrow distribution, centred at small diameter values, the higher the EP content the narrower is the distribution of the polysilicate particles. This fact is also evidenced in Table 5.3.2.1. Compared to the 3P reference, the mean particle diameter of the polysilicate is reduced approximately twenty times, and further, the distribution is significantly narrowed. If one compares the 3P system obtained by dispersing the WG at 2000 rpm (3P-2) the emulsifying effect that of EP resin also well manifests: the mean particle diameter is, in this case, ten times smaller and the distribution is also narrower than the 3P system produced in equal dispersing conditions. Note that the substitution of the phosphate by EP did also induce a positive effect on the particle diameter (reduced) and on its distribution (narrowed; c.f. Table 5.3.2.1 for the hybrid systems 3P/EP-65/35 wt.-% and 2P/EP-65/35 wt.-%).

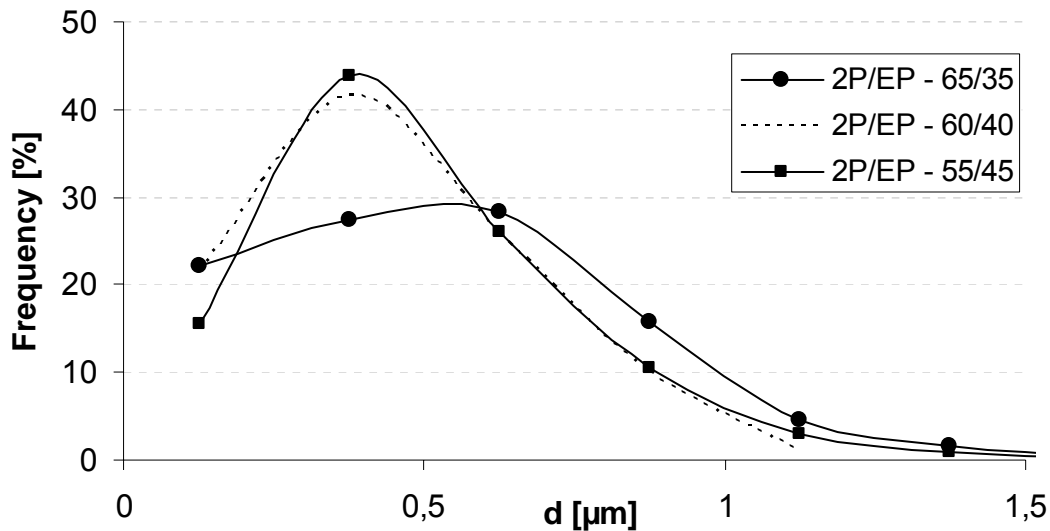


Fig.5.3.2.3- Relative frequency vs. mean particle size diameter for the 2P/EP hybrid systems.

	d_n [μm]	d_w [μm]	d_w/d_n
3P	11.2	15.5	1.4
3P - 2	5.0	7.1	1.4
3P/EP - 65/35 wt.-%	0.8	1.1	1.3
2P/EP - 65/35 wt.-%	0.6	0.7	1.2
2P/EP - 60/40 wt.-%	0.5	0.5	1.0
2P/EP - 55/45 wt.-%	0.5	0.6	1.1

Table 5.3.2.1 - Number- average (d_n) and weight-average (d_w) mean particle size of the 2P/EP hybrid systems and their reference 3P resin.

5.3.2.3. Mechanical Properties

With regard to the fracture mechanical properties displayed in Fig. 5.3.2.4, a significant increase of the fracture toughness (K_{Ic}) can be noticed for the 2P/EP hybrids. However, the change in K_{Ic} does not follow a clear tendency with the EP resin content. On the other hand, the fracture energy, G_c , is markedly reduced, when comparing to the reference 3P resin. Moreover, G_c shows a decreasing tendency with increasing EP content.

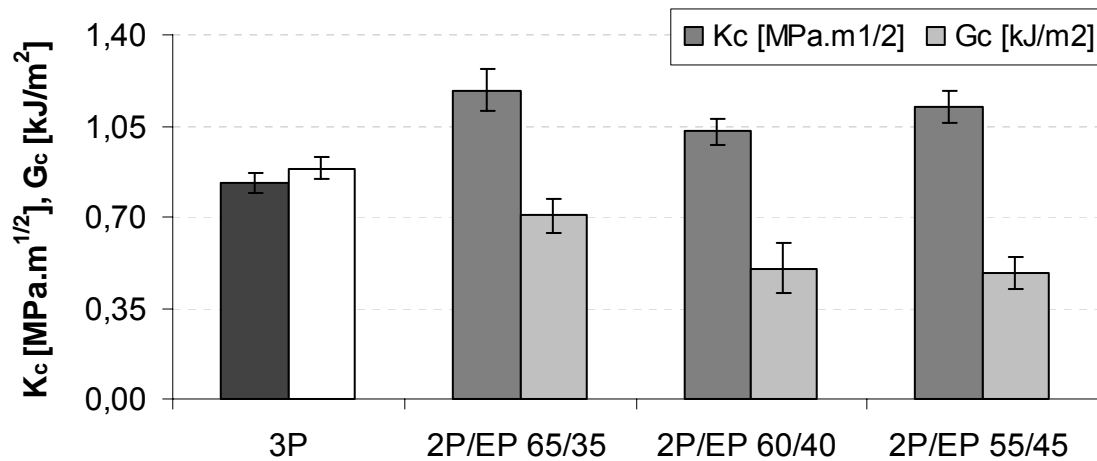


Fig.5.3.2.4 - Fracture toughness (K_c) and fracture energy (G_c) for the 2P/EP hybrids and their reference 3P resin.

The flexural properties of the 2P/EP hybrid resins are depicted in figure 5.3.2.5. The flexural modulus (E_f) presents a clear growing tendency with increasing EP content, following the rule of addition in the studied composition range. However, the flexural modulus does not reach the values of the pure EP resin. On the contrary, the flexural strength (σ_f) does show significant changes as a function of the composition. Nonetheless, one can assume that the flexural properties of the 3P resins are in general enhanced when hybridizing with EP (c.f. Table 5.3.2.2).

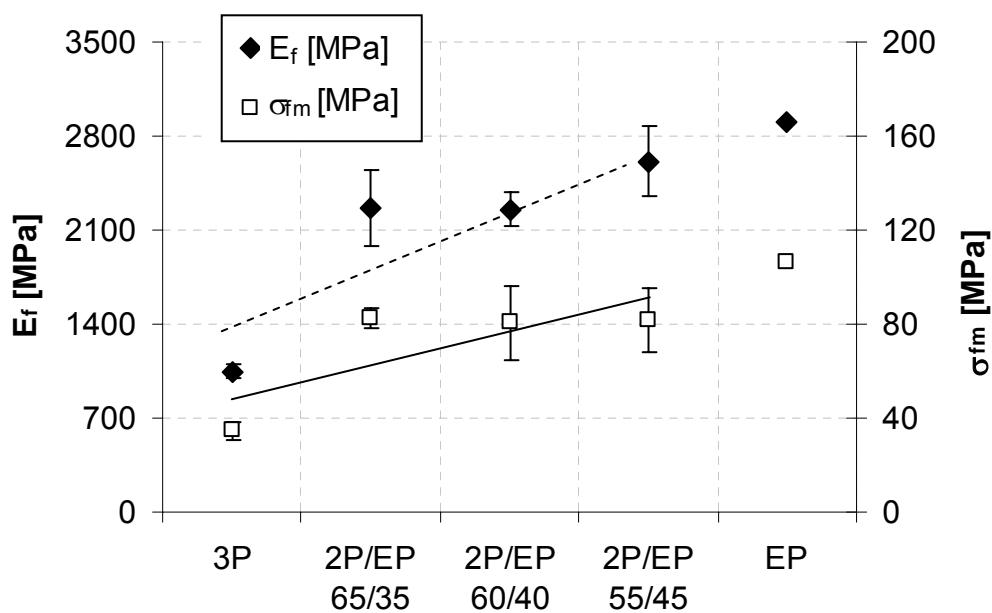


Fig.5.3.2.5- Flexural modulus (E_f) and flexural strength (σ_{fm}) for the 2P/EP hybrid resins and their references 3P and EP.

	E_f [MPa]	s [MPa]	σ_{fm} [MPa]	s [MPa]	ε_M [%]	s [%]
3P	1047	56	34.6	3.9	4.4	0.9
2P/EP 65/35 wt.-%	2262	281	82.5	4.6	4.2	0.5
2P/EP 60/40 wt.-%	2254	122	80.7	15.8	4.4	1.9
2P/EP 55/45 wt.-%	2613	260	81.9	13.7	3.4	0.7
EP (DER331)	2900	-	106.0	-	4.0	-

Table 5.3.2.2- Flexural modulus (E_f), strength (σ_{fm}), strain (ε_m) and standard deviation for the 2P/EP hybrid resins and their references 3P and EP.

The 2P/EP hybrid systems show alike viscoelastic behaviour to the 3P/EP hybrid systems. The DMTA traces, displayed in Fig. 5.3.2.6, confirm the tendency observed before by the flexural tests: the 2P/EP hybrids possess higher storage modulus (E') as the EP content increases. The storage modulus of the hybrid systems drops along with the temperature increase, until reaching values close to zero at $T \sim 180^\circ\text{C}$. Differently from the 3P/EP systems, the 2P/EP hybrid resins owe an improved resistance to high temperatures. It is noteworthy to say that the storage modulus of the 2P/EP hybrids is notably higher than for the 3P/EP hybrids (c.f. Fig. 5.2.2.6). This fact could be related to the absence of the phosphate causing plastification.

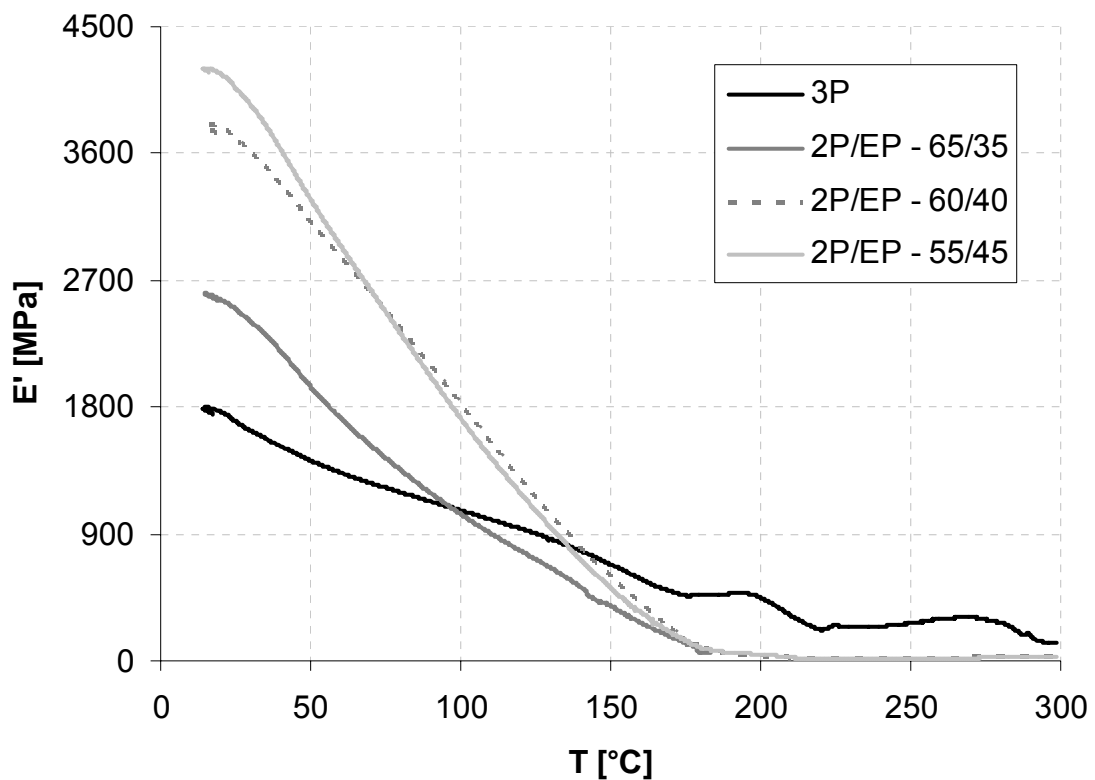


Fig.5.3.2.6- DMTA results displaying E' vs. T for the 3P reference and its 2P/EP hybrids.

Considering the $\tan \delta$ vs. T traces in Figure 5.3.2.7, one can observe an increase in the damping factor $\tan \delta$ at $T \sim 180^\circ\text{C}$. This relaxation peak is overlapped with a second peak of lesser intensity at $T \sim 230^\circ\text{C}$. Moreover, a third peak in the $\tan \delta$ curve is noticeable at $T \sim 260^\circ\text{C}$. These results, obtained also for the 3P/EP hybrid systems, were confirmed by performing the DSC test. It is the right point to remark that, the EP content did not affect significantly the course of the damping factor as a function of T . On the other hand, the 2P/EP hybrid resins show different viscoelastic behaviour than the reference 3P resin. Changes induced due to the absence of the organic phosphate are also patent in the 2P/EP hybrid systems; the broad shoulder and the $\tan \delta$ maximum at 175°C observable for the 3P/EP hybrid resins disappear to give a single peak in the 2P/EP hybrid systems. This could be the result from an enhanced compatibility between the epoxide homopolymer and the polyurea phases, which is not influenced by the organic phosphate [117].

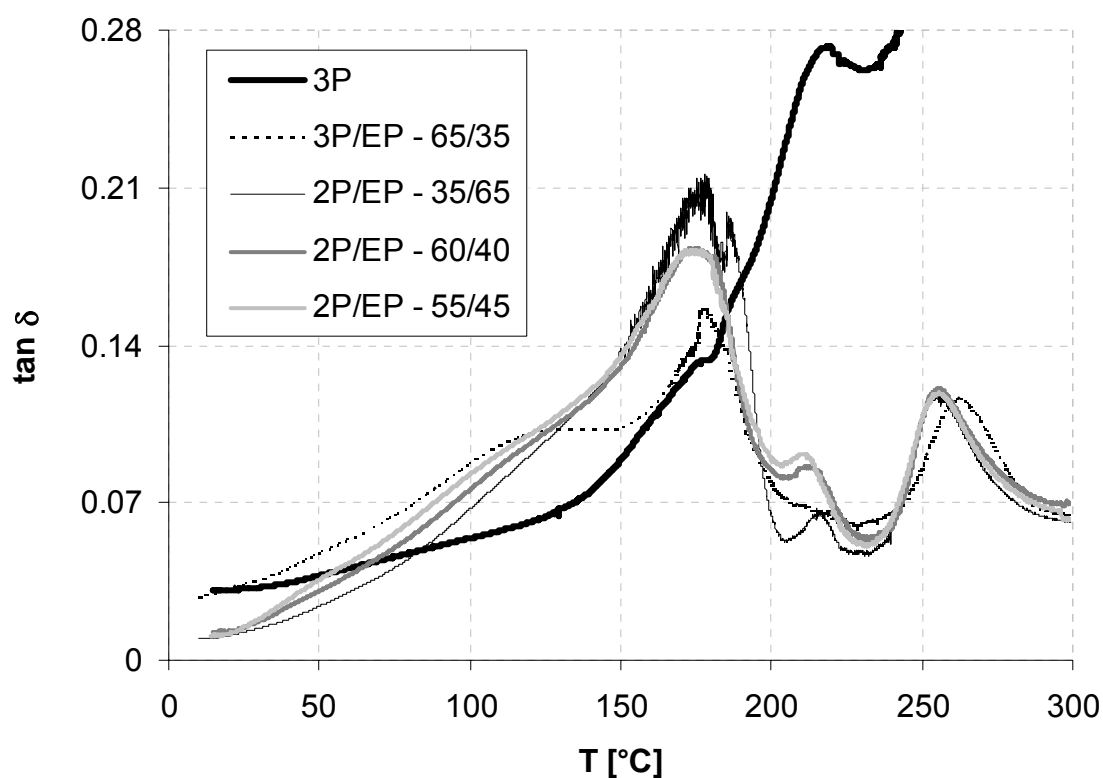


Fig.5.3.2.7 - DMTA results displaying $\tan \delta$ vs. T for the 3P and the 2P/EP hybrids.

5.3.2.4. Thermal properties

The thermal degradation of the 2P/EP hybrid resins is depicted in Fig. 5.3.2.8, one can observe that the 2P/EP hybrids owe a very similar thermal behaviour independently of the EP content. The first mass loss process is observed at

T~200°C, corresponding to the water evaporation contained in the matrix and hydrolysis products, followed by a drastic second mass loss at T~390°C due to the organic matrix destruction. When comparing the TGA response of 2P/EP systems those of the phosphate containing 3P/EP (c.f. Fig. 5.3.2.8), it becomes clear that the systems without phosphate withstand to higher temperatures than those with phosphate. However, the residue at the end of the process, as well as the temperature at which the specimen loses its 5% of the mass ($T_{5\%}$) are very similar for both systems (c.f. Tables 5.3.2.3). On the other hand, when comparing the novel 2P/EP hybrid systems to the reference 3P, one can clearly see that the hybridisation with EP resulted in enhanced thermal stability.

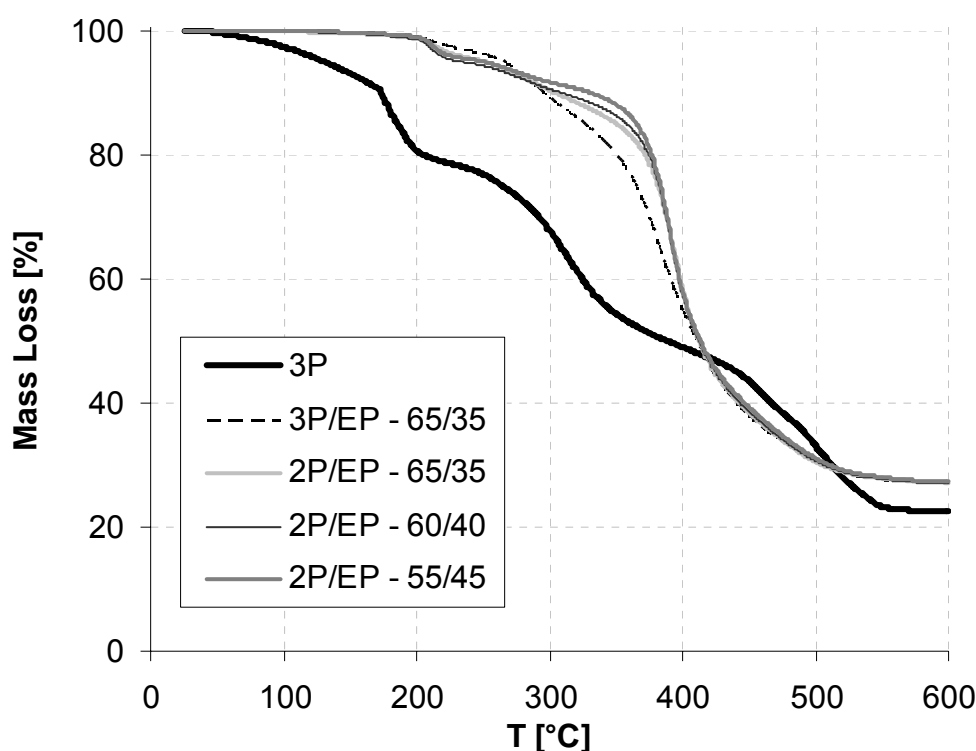


Fig. 5.3.2.8 - Mass loss vs. T for the 2P/EP hybrid resins and their reference 3P.

	$T_{5\%}$ [°C]	Residue [%]
3P/EP - 65/35 wt.-%	264	27
2P/EP - 65/35 wt.-%	250	27
2P/EP - 60/40 wt.-%	232	27
2P/EP - 55/45 wt.-%	249	27

Table. 5.3.2.3 – $T_{5\%}$ [°C] and residue [%] for the 2P/EP hybrid resins.

The DSC curves depicted in Fig. 5.3.2.9 show, as expected from the DMTA data, three transition temperatures. The transition temperature of the hybrids decreases

with increasing EP content (c.f. Table 5.3.2.4). A characteristic attribute of the 2P/EP systems is that they do not possess the intense endothermic peak characteristic of the systems with phosphate (3P and 3P/EP). This is an important fact that accentuates the influence of the organic phosphate emulsifier on the crosslinking and destruction processes that take place at high temperatures.

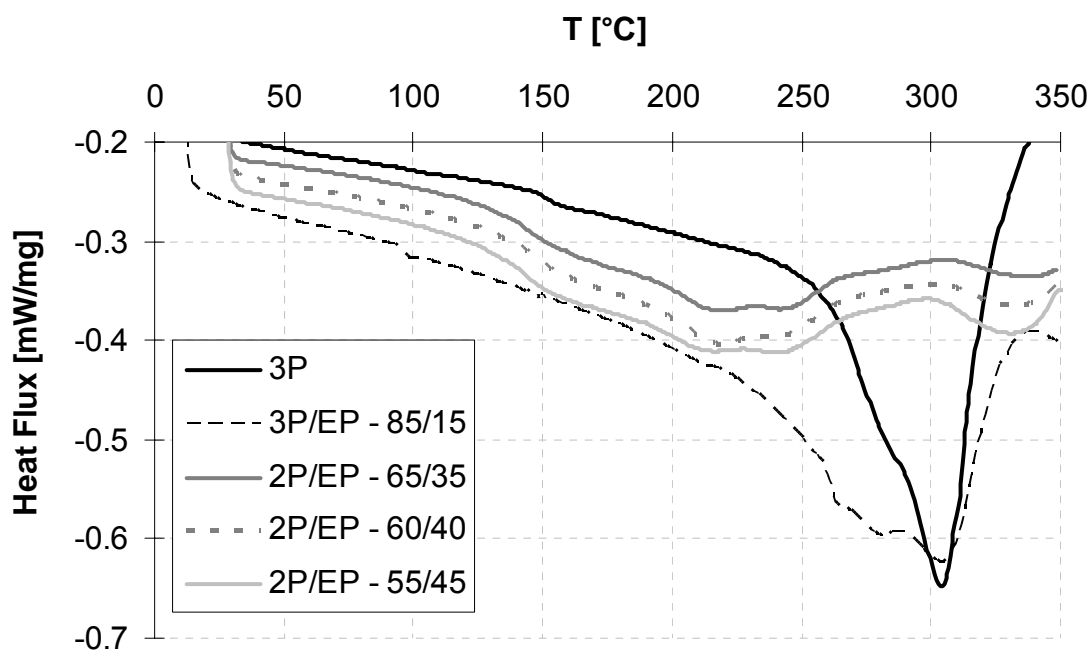


Fig. 5.3.2.9 – DSC curves for the 2P/EP hybrid resins and the reference 3P.

Sample name	Sub T_g [°C]	Sub T_g [°C]	T_g [°C]
2P/EP - 65/35 wt.-%	84	121	209
2P/EP - 60/40 wt.-%	79	107	202
2P/EP - 55/45 wt.-%	65	104	200

Table 5.3.2.4 – Transition temperatures (T_{trans}) for the 2P/EP hybrid resins.

The flammability tests performed on the 2P/EP hybrid resins give a qualification of V-1 according to the UL 94 flammability test. The specimens burned about thirty seconds in average after applying the flame but did not drop any flaming drip. The flammability of the hybrid resins is enhanced by the addition of epoxy resin compared to the excellent flame resistance of the reference 3P resin. However, when comparing to the 3P/EP systems, its flammability is reduced in absence of the organic phosphate.

5.3.3. Melamine Formaldehyde Resins

5.3.3.1. Rheology

The 2P/MF studied systems reveal that increasing MF amount reduces the viscosity of the related systems (Fig.5.3.3.2). However, MF is a modest reaction controlling agent compared to the organic phosphate. The viscosity of the 2P/MF systems is much higher compared to the one of the 3P reference, which makes the posterior processing of the 2P/MF systems slightly troublesome. Recall that at $t = 60$ min the viscosity of the 2P/MF hybrid resins is about 40 times higher than for the same hybrid system containing phosphate. Despite that, MF confirms itself to be a suitable substituent of the phosphate, as observed before for the hybrids 2P/VE/MF. Nonetheless, 2P/VE/MF hybrids due to the additional emulsifying effect of the vinyl ester exhibited lower viscosity values at early times.

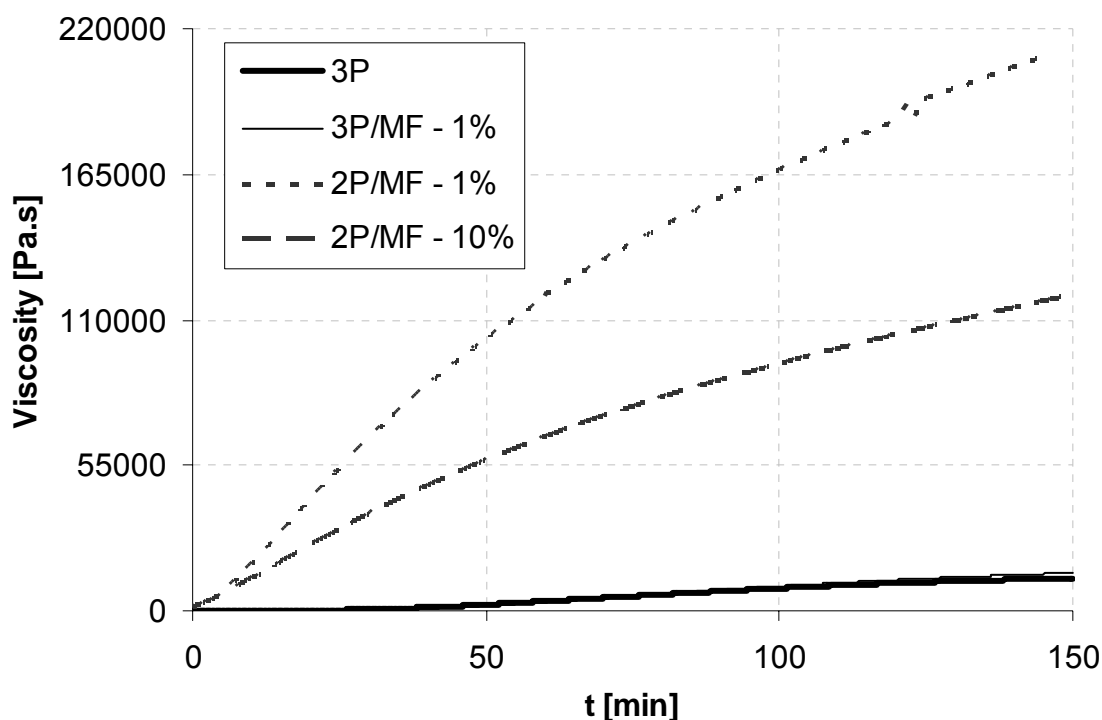


Fig.5.3.3.1 - Viscosity vs. time for the 3P/MF-1%, 2P/MF-1% and 2P/MF-10% hybrid resins and its reference 3P.

5.3.3.2. Morphology

The SEM pictures obtained from the broken surface of the 2P/MF systems are presented in figure 5.3.3.2. The substitution of the phosphate by the MF reduced substantially the particle size of the polysilicate in comparison with the reference 3P

resins. This is evident when observing the distribution curves in figure 5.3.3.3 which are narrower and centred at lower diameter values for the 2P/MF hybrid resins. The reference 3P resin had an average particle size diameter of $10\mu\text{m}$, while for the 2P/MF hybrid systems this was reduced to its half, however, with some exceptions (c.f. Table 5.3.3.1). Moreover, the substitution of the phosphate by MF did not broaden the polysilicate distribution. Nevertheless, smaller particle size diameters are obtained when combining the 2P systems, without phosphate, with MF and VE (mean particle size: $\sim 2\mu\text{m}$).

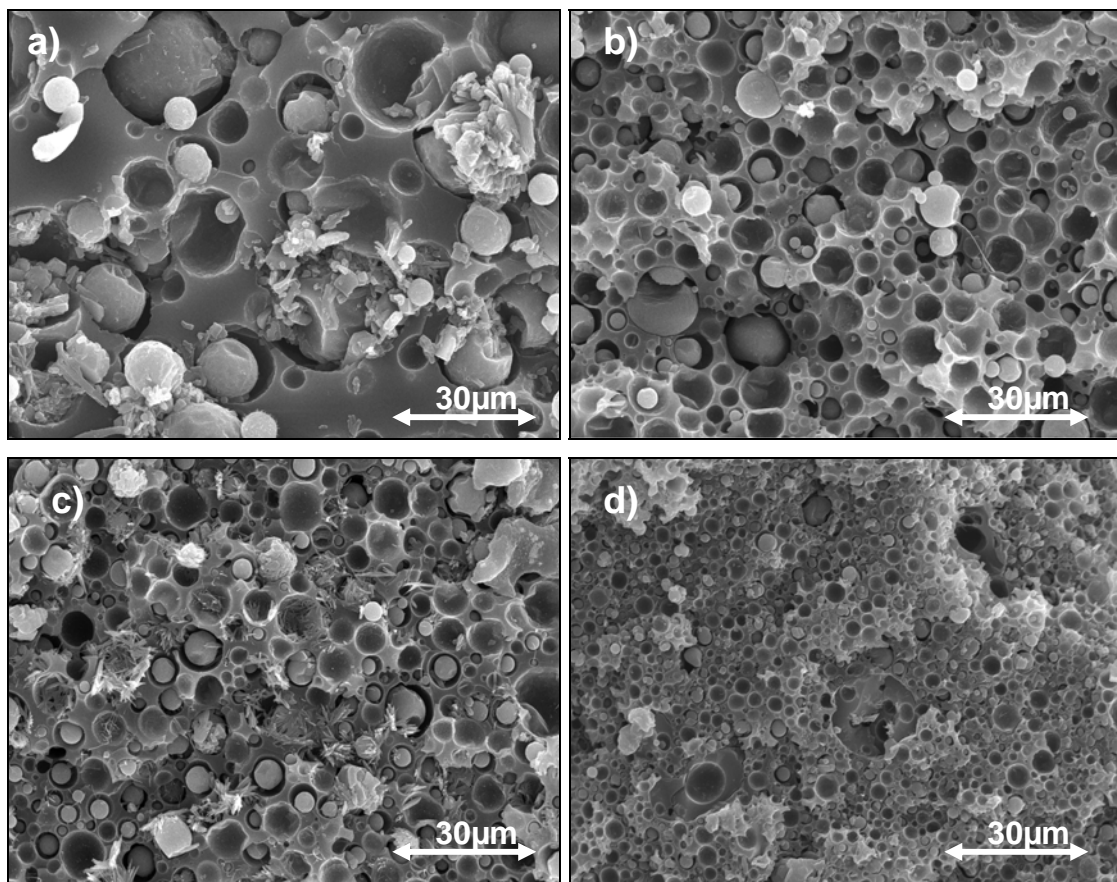


Fig.5.3.3.2 - SEM pictures taken from the fracture surfaces of the 3P resin sample (a); 2P/MF-1% hybrid resin (b); 2P/MF-5% hybrid systems (c); 2P/MF-10% hybrid systems (d).

Attention should be paid to the fact that the system 2P/MF-10% owes a very small particle size and a narrower distribution compared to the other hybrids. This is well reflected in figure 5.3.3.2.d as well as in figure 5.3.3.3. In the latter figure a narrow distribution peak is obtained in contrast to the broad distribution peaks of the other 2P/MF hybrids and their reference 3P resin.

MF wt.-%	0.5	1	2.5	5	1	15
d_n [μm]	3.9	4.0	4.7	3.9	2.6	6.2
d_w [μm]	5.5	5.6	7.2	5.3	2.7	8.8
d_w/d_n	1.4	1.4	1.5	1.3	1.1	1.4

Table 5.3.3.1 - Number (d_n) and weight-average diameter (d_w) of the polysilicate particles in the 2P/MF hybrid resins.

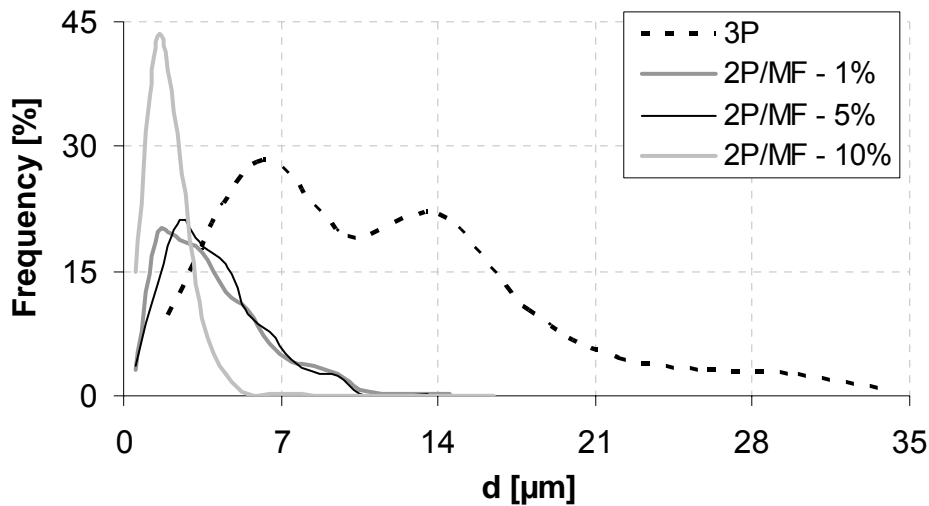


Fig. 5.3.3.3 – Relative frequency vs. particle size diameter for the 2P/MF-1%, 2P/MF-5% and 2P/MF-10% hybrids and their 3P reference.

The AFM pictures reveal that the hybrid systems 2P/MF possess rougher and globular like structure in comparison to the 3P reference systems. Despite of this, they do not show a finely defined nodular structure as the 2P/VE/MF hybrid systems do (c.f. Fig 5.3.3.4).

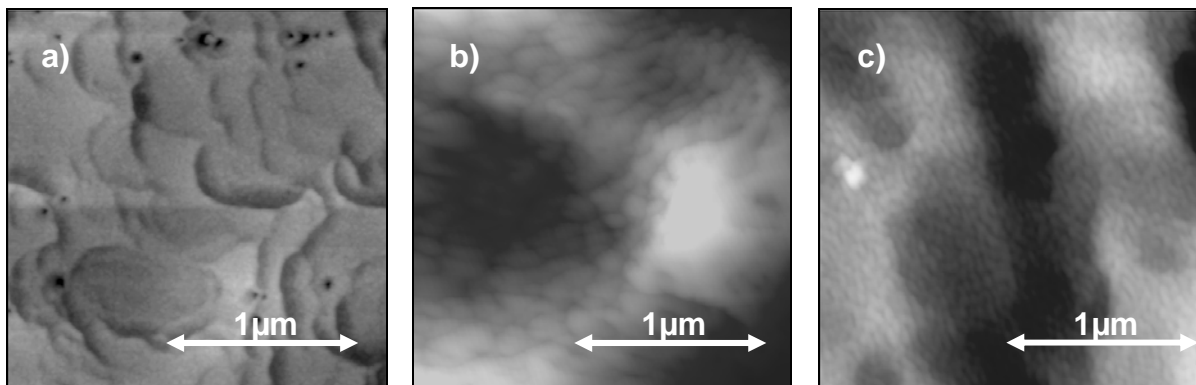


Fig. 5.3.3.4 - Amplitude-modulated AFM images taken from the ion-etched polished surfaces of the reference 3P (a); 2P/MF-10% hybrid resin (b); and 2P/VE/MF-10% hybrid resin (c).

5.3.3.3. Mechanical Properties

The results of the fracture tests carried out on the 2P/MF hybrid resins are depicted in figure 5.3.3.5. According to the results obtained, the substitution of the phosphate by the MF (in smaller amount) improved the fracture energy (G_c) of the hybrids only for MF contents lower than 2.5 wt.-%. With increasing MF amount in the hybrid systems G_c decreased. On the other hand, fracture toughness (K_c) was only slightly influenced by the amount of MF introduced. It is the right place to remark that, the system 2P/MF-10% gave comparable K_c and G_c results with the 3P reference.

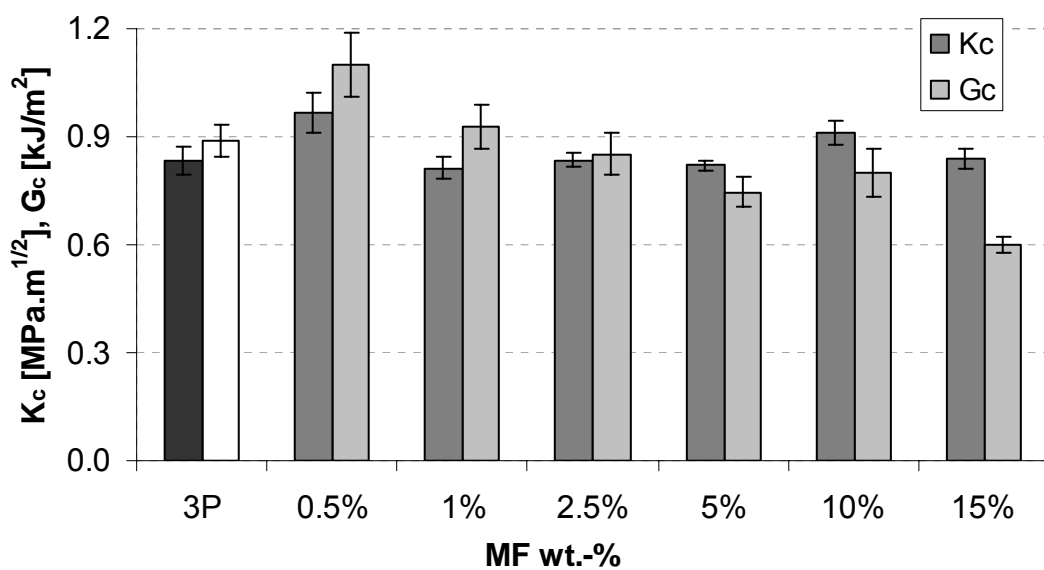


Fig.5.3.3.5 - Effects of the compositional changes on the fracture toughness (K_c) and fracture energy (G_c) of 2P/MF samples and the reference 3P.

The flexural properties of the 2P/MF hybrids presented in table 5.3.3.2 reflect how the replacement of the phosphate by MF improves the stiffness of the systems in comparison to the 3P reference resin. The flexural modulus E_f and strength (σ_{fm}) increase with increasing MF content, however, at expenses of the flexural strain (ε_M). This is comprehensible since larger amounts of MF confer higher rigidity to the samples and therefore they undergo smaller deformation at a given loading.

Sample name	E_f [MPa]	s [MPa]	σ_{fm} [MPa]	s [MPa]	ε_M [%]	s [%]
3P	1047	56	34.6	3.9	4.4	0.9
2P/MF - 0.5	1463	147	40.5	1.4	4.2	0.1
2P/MF - 1	1375	95	37.4	1.9	3.5	0.3

2P/MF - 2.5	1661	133	40.3	2.5	3.1	0.4
2P/MF - 5	1618	174	44.2	3.9	3.3	0.2
2P/MF - 10	2029	147	47.9	2.3	2.9	0.2
2P/MF - 15	2085	113	51.8	5.3	2.9	0.3

Table 5.3.3.2 - Flexural modulus (E_f), strength (σ_{fm}) and strain (ϵ_m) for the 2P/MF hybrid resins and their reference 3P.

The DMTA traces, depicted in Fig.5.3.3.6, in form of E' vs. T for the 3P and the 2P/MF hybrid resins corroborate the results obtained in the flexural tests. The stiffness (E') increases following the increase of MF in the systems and is higher than for the 3P resins. One can recognise an abrupt discontinuity in the E' traces at T around 180°C for the 2P/MF systems as well as for the 3P reference resin due to the starting failure of the specimens at high temperatures.

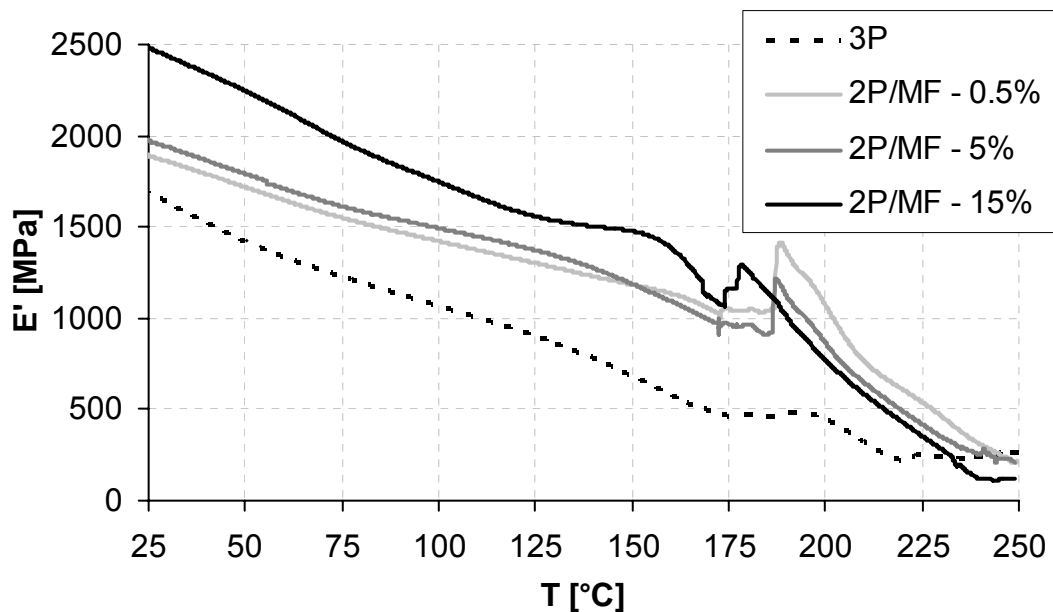


Fig.5.3.3.6 - DMTA results displaying E' vs. T for the 3P reference and the 2P/MF hybrids.

Observing the $\tan \delta$ vs. T traces, depicted in Fig. 5.3.3.7, one can not clearly discern the glass transition temperature (T_g), when assigned to the peak temperature of the $\tan \delta$. However, despite of the premature failure, the 2P/MF-0.5% and 2P/MF-5% hybrid resins show a reasonably definite peak at temperatures ranging from 200°C to 250°C and a second broad and less resolved peak of low intensity centred at $T \sim 175^\circ\text{C}$. For the other hybrids, containing larger amounts of MF, the $\tan \delta$ maximum

is not well resolved. Nevertheless one could assume that the related peak is located at temperatures above 250°C.

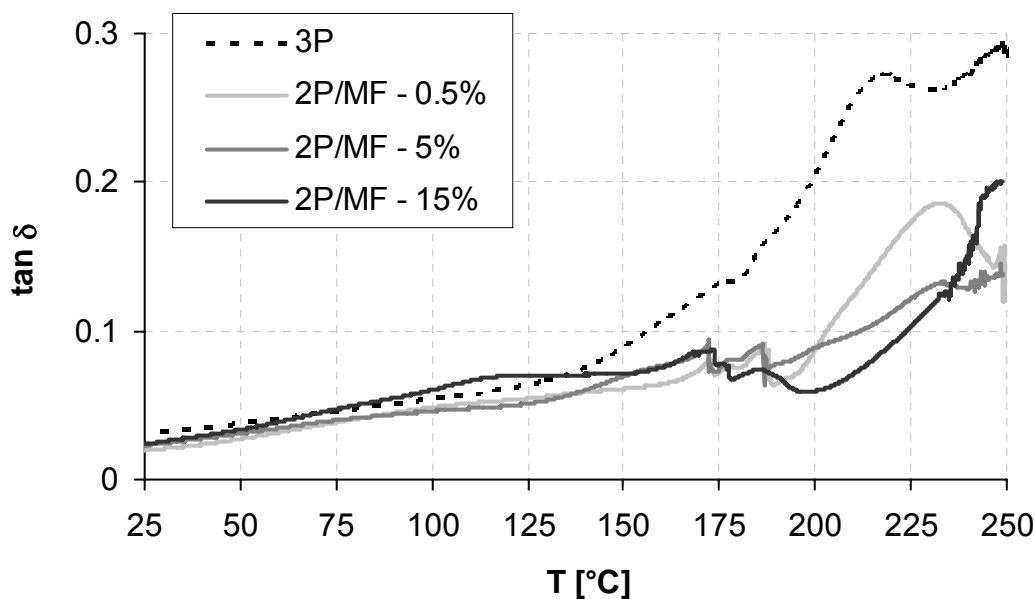


Fig.5.3.3.7 - DMTA results displaying $\tan \delta$ vs. T for the 3P and the 2P/MF hybrids.

5.3.3.4. Thermal Properties

TGA curves depicted in figure 5.3.3.8 show the thermal behaviour of the 2P/MF hybrids with different MF content. The response of the diverse hybrids seems not to be influenced by the MF content, since they do not differ one from another in a great manner, yet the 2P/MF-10% system presents a markedly different behaviour (c.f. Table 5.3.3.3). The 2P/MF hybrid systems are stable at temperatures below 200°C, as seen before in the DMTA analysis, before they suffer a brusque loss of mass. Nonetheless, the continuous mass loss is not as severe as for the reference 3P, which at temperatures above 300°C exhibits a second remarkable mass loss. Therefore, the substitution of the phosphate by MF appears to influence positively the thermal resistance of the novel hybrids.

MF wt.-%	0.5	1	2.5	5	10	15
$T_{5\%}$ [°C]	160	143	147	159	126	171
Residue [%]	32	34	34	34	20	34

Fig. 5.3.3.3 – $T_{5\%}$ [°C] and residue [%] for the 2P/MF hybrid resins with increasing MF content.

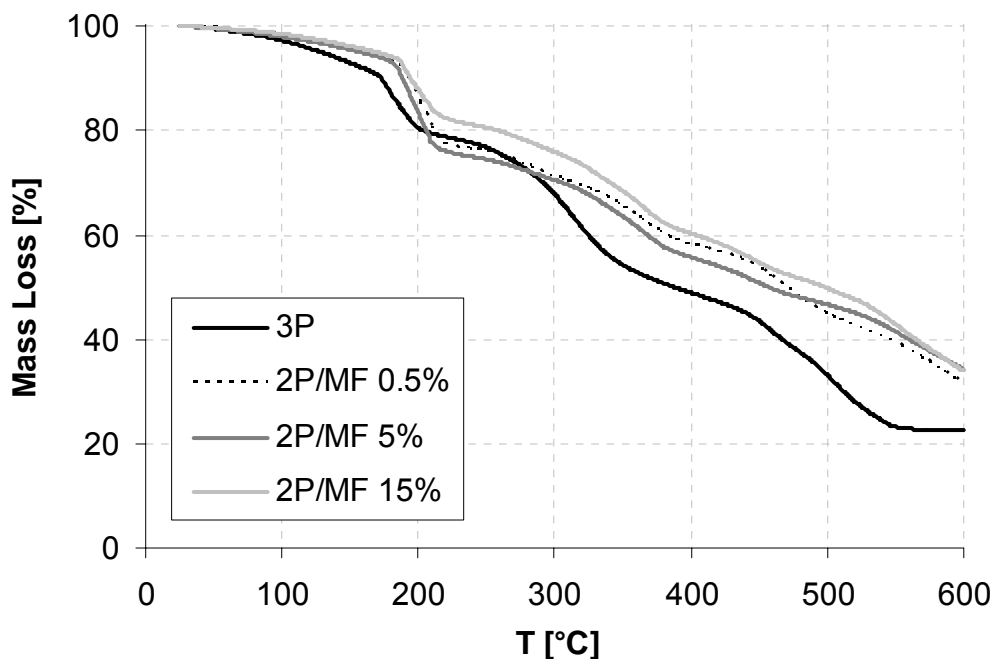


Fig. 5.3.3.8 – TGA curves for the 2P/MF hybrid resins with different MF amounts and their reference 3P.

The DSC curves obtained from the first and second heating cycles for the 2P/MF hybrid resins are depicted in Fig.5.3.3.9. The curves from both first and second heating scans reveal two strong endothermic peaks for the 2P/MF hybrid resins. The first one is found at $T \sim 175^{\circ}\text{C} - 225^{\circ}\text{C}$. This peak is very prominent in the first scan while in the second heating scan it disappears for the hybrids with less than 1 wt.-% of MF. For other 2P/MF hybrids the intensity of this peak is considerably reduced. Recall that this endothermic peak was observed also in the first heating cycle of the 3P/MF hybrids and it disappeared in the second scan for all the 3P/MF hybrids (c.f. Fig 5.2.3.9). On the other hand, this peak was not found in the 3P reference resins. When comparing with the data obtained by TGA, one can observe that in these range of temperatures the 2P/MF hybrid resins experience a sudden mass loss. This, and the fact that the 2P/MF hybrids do not present a strong endothermic peak in the first scan at $T \geq 100^{\circ}\text{C}$ (typical for the 3P resins assigned to the evaporation of water contained in the matrix), could be derived from a strong water release retained by MF. A second strong endothermic peak for the 2P/MF hybrids appears at $T \sim 265^{\circ}\text{C} - 295^{\circ}\text{C}$, in the region where the organic phosphate evaporates. The reason of this heat absorption is not yet known, since the 2P/MF hybrid resins do not contain phosphate.

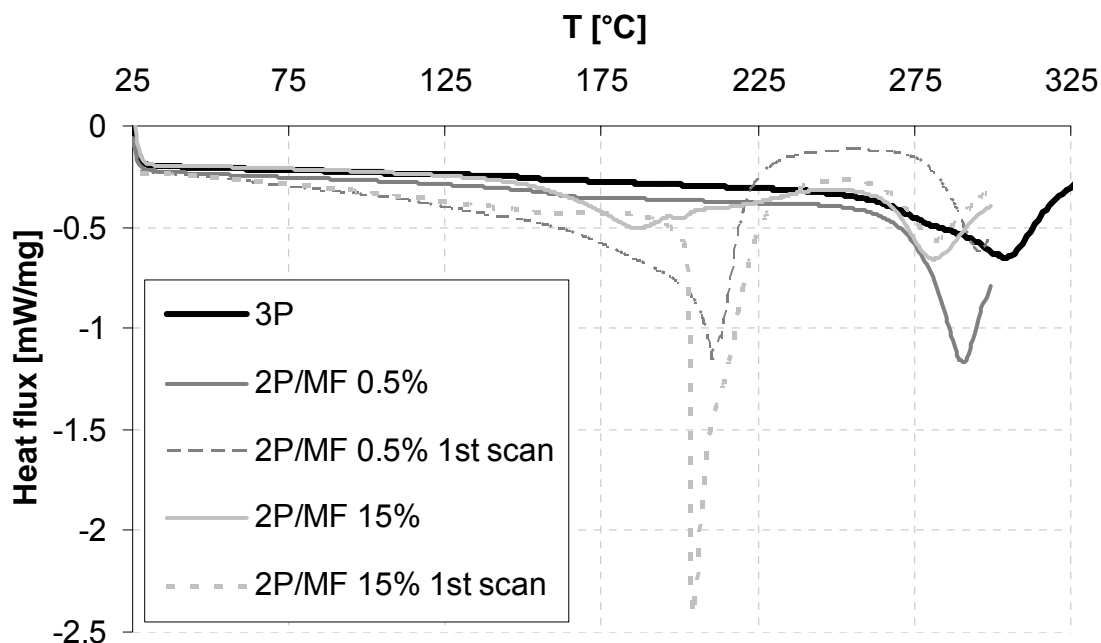


Fig. 5.3.3.9 – DSC curves vs. T for the 2P/MF hybrid resins with different MF amounts and their reference 3P.

DSC analysis (c.f. Table 5.3.3.4) shows two transition temperatures which are in accordance with the DMTA data. The first one is detected at temperatures ranging between 170°C-180°C and may correspond to the 2P/MF copolymers. The transition temperatures obtained for the 2P/MF hybrids shift to lower values with increasing MF content. This suggests that the MF either affected the crosslinking density of the final polymer and/or had some plasticising effect. The T_g determined at temperatures ranging from 272°C to 283°C may correspond to the main transition temperature of the polyurea phase.

Sample name	Sub T_g [°C]	T_g [°C]
2P/MF - 0.5%	179	283
2P/MF - 1%	180	280
2P/MF - 2.5%	178	279
2P/MF - 5%	196	278
2P/MF - 10%	173	275
2P/MF - 15%	171	272

Table 5.3.3.4 – T_{trans} obtained from the DSC second scan for the 2P/MF hybrid resins.

The flammability tests, conducted on the 2P/MF hybrid resins, showed that the specimens did not burn with flaming combustion after the flame application as well as they did not burn with flaming or glowing combustion up to the specimen holding clamp. Moreover the 2P/MF resins did not drip flaming particles that ignite the cotton. The total flaming combustion time was zero or one second for some specimens; therefore the classification of the 2P/MF resins according to the 94UL standards is V-0. The results obtained from the flammability test showed that 2P/MF resins are good fire resistant materials and that the substitution of the phosphate (which is an active flame retardant additive) by MF resin is straight forward also in terms of fire resistance.

6. SUMMARY AND OUTLOOK

Polyurea hybrid resins with in-situ produced silicate filler from water glass, named 3P resins, were synthesized and characterized. The improvement in their properties, not only mechanical but also thermal and fire resistance properties, was accomplished by means of resin hybridization. Three different resins (VE, EP and MF) were chosen according to their promising properties to fulfil the hybridization strategy. Major target of the latter was to reduce the phosphate emulsifier or even eliminate it by suitable “additives” whereby maintaining or even improving the property profile of the state-of-art 3P resins. Consequently, various 3P hybrid resins were prepared and characterized. Further, non-phosphated hybrids 2P were also synthesized and characterized. This development follows the European Community Regulation on chemicals and their safe use REACH, which calls for the progressive substitution of the most dangerous chemicals. Next the results obtained from present work, are briefly summarized.

3P resins

The morphological, mechanical and thermal properties of novel 3P resins were characterized. During their production the mixing parameters (mixer type, mixing time and mixing speed) as well as the curing and postcuring conditions have been varied.

It was found that the viscosity of the non-cured 3P resins was not affected by any of the above listed parameters. On the other hand, the mixing parameters had a crucial effect on the morphology of the systems. By increasing the speed of the final dispersion from 800rpm to 2000rpm (cogged-wheel mixer) the particle size of the inorganic phase was reduced to one third and the distribution of the polysilicate particles became finer. Moreover, when dispersing the WG for 3min instead of 1min, the particle size was reduced and the distribution of the polysilicate particles was even more narrow and homogeneous. In respect to the mixer type, it was established the use of a propeller mixer reduced the particle size of the polysilicate but the distribution was much broader than using a cogged-wheel mixer. The different curing temperatures applied to the systems did have a marginal effect on the particle size and distribution, as expected.

Regarding the fracture mechanical test results obtained, the highest values of K_{Ic} and G_c were obtained for the samples cured at RT. With increasing postcuring temperatures (from RT to 140°C) the fracture energy, G_c , was reduced to the half and fracture toughness K_{Ic} slightly decreased. However, the curing temperature exerted a marginal effect on the flexural modulus, strength and strain. Furthermore, it was observed that improved fracture mechanical properties can be obtained by increasing the mixing time and speed during the final dispersion process of WG in the phosphate containing polyisocyanate. The flexural modulus of the systems obtained at high mixing speed and time was enhanced but at expenses of the flexural strength and strain. The use of a cogged-wheel mixer enhanced moderately both the flexural and fracture mechanical properties.

The thermal stability of the 3P systems was not affected by the mixing parameters (mixer type, mixing time and mixing speed) and the curing temperatures set did not markedly affect the thermal stability of the samples. The flammability test carried out showed that the 3P-systems have outstanding flame resistant.

3P/hybrid resins

The hybridisation of the 3P resins influenced the viscosity of the hybrid samples differently. It was proved that the hybridization with VE increased in a great extent the viscosity of the corresponding hybrids, reduced the pot life and yielded high exothermic reactions. On the other hand, 3P/EP and 3P/MF hybrid resins exhibited even lower viscosities than the 3P reference resin. Hybrid resins with increasing amount of EP and MF showed lower viscosities than the corresponding hybrids at higher 3P content. Therefore satisfying results were obtained from the hybridization of 3P resins with MF and EP, respectively, since longer pot life were achieved and as a result, the posterior processing of the samples was simplified.

Hybridization of the 3P resins with VE, EP and MF, respectively, resulted in considerable morphological changes. In the case of the 3P/EP hybrid resins, the particle diameter of the polysilicate formed was approx. 1µm. This means a reduction of one tenth in respect to the original polysilicate particle diameter of the 3P resins (~10µm). The particle size decreased as the EP content in the 3P/EP hybrids increased and parallel to that the particle size distribution was narrowed. Similarly,

the 3P/VE hybrids showed reduced particle size diameters as the VE content increased in the 3P/VE hybrid resins. However, this reduction was not as prominent as for the 3P/EP hybrids and moreover, the distribution of the polysilicate particles in the 3P/EP hybrids was coarser than in the 3P reference system. On the contrary, the hybridisation of the 3P resins with MF did not improve either the distribution or reduced significantly the particle size of the inorganic phase.

The fracture mechanical parameters were improved by the hybridisation of the 3P resins. The fracture toughness (K_{IC}) was moderately enhanced in all novel 3P hybrids, being doubled in the particular case of the 3P/VE 25/75 wt.-%. Considering the fracture energy (G_c), 3P/VE and 3P/MF hybrids presented higher values than the reference 3P. Surprisingly, 3P/EP hybrids showed lower G_c values than the 3P resins. Recall that these hybrids owed an extraordinary reduced particles size and narrow dispersion. Regarding the flexural properties, clear improvements were achieved by the hybridisation of the 3P resins. In particular, 3P/EP hybrid resins presented outstanding flexural moduli, which in some cases almost tripled the values of the 3P reference resin. A notable improvement in the flexural strength was found, only for the 3P/EP hybrid systems.

In general, the thermal stability of the 3P resins was improved by means of hybridisation. 3P/VE hybrid resins showed an excellent resistance to degradation at low temperatures ($T < 400^\circ\text{C}$). However, at $T > 400^\circ\text{C}$ 3P/VE hybrids suffered an abrupt mass loss. This effect is more prominent in the hybrids containing higher ratios of VE, since their thermal behaviour resembles to that of VE (c.f. Fig. 5.2.1.9). In contrast, the 3P/MF hybrids presented an improved resistance to high temperatures, undergoing, however, a moderate mass loss and a significant degradation at lower temperatures. The thermal degradation of 3P/EP hybrid resins is in between the 3P/VE and 3P/MF systems. Such hybrids withstand temperatures up to 300°C with a modest mass loss before progressively degrade with increasing temperatures. Similarly to the 3P/VE hybrids, the thermal resistance of the 3P/EP hybrids at low temperatures is significantly improved with increasing EP content. However, their degradation is faster at higher temperatures than the reference 3P.

The transition temperatures (T_g) of the 3P/VE hybrids lay between the T_g of the VE and the T_g of the 3P depending on their actual 3P/VE ratio. For the 3P/EP hybrids, the T_g was shifted to lower temperatures with increasing EP ratio. On the other hand, 3P/MF hybrids presented a broad transition temperature which was shifted slightly to lower temperatures compared to the T_g of the 3P. The varying amount of MF, present in the 3P/MF hybrids, did not clearly affect the T_g .

The hybridisation of the 3P resins did not result, in most of the cases, in improved fire resistance. Combining 3P resins with VE and EP reduced the outstanding resistance to flame of the reference 3P resin and yielded more “flammable” hybrid resins. On the other hand, the hybridisation with MF maintained the excellent fire resistance properties of the 3P resins.

2P/hybrid resins

The elimination of the environment pollutant phosphate emulsifier in the 3P reference resins and in the related 3P hybrids changed in a great extent the properties of the resulting 2P systems. One of the most pronounced changes was found in the marked increase of the viscosity of the samples, which was to expect, since the phosphate acted as emulsifier and plasticiser in the 3P systems. It was found for the 2P/VE/MF hybrids, that their viscosity is low at $t < 30\text{min}$ before growing exponentially with time. The elimination of the phosphate in the 3P/MF hybrid resins to obtain the 2P/MF hybrid resins, lead to extremely viscous systems, hampering the posterior processing. As experienced before for the phosphate containing hybrids, increasing amounts of MF reduced the viscosity of the systems.

Surprising results on the morphology of the 2P hybrids were obtained when eliminating the phosphate emulsifier. It was found that particle size distribution of the inorganic phase was more homogeneous and narrower in the 2P/VE/MF and 2P/EP hybrid resins and was not altered for the 2P/MF in comparison to the respective phosphate containing hybrids. Furthermore, for the 2P/VE/MF hybrid systems, the particle size was reduced to one third in comparison to the 3P/VE hybrid resins and to one eighth when comparing to the reference 3P. Considerable particle reduction was also achieved in the 2P/MF hybrids. A reduction of one third of the polysilicate particles was noticed compared to the 3P/MF resins which had, on average, a similar

diameter as the 3P reference resin. A moderate reduction of the polysilicate mean diameter was also observed for the 2P/EP systems. These results were unexpected since the phosphate emulsifier was alone responsible for controlling and stabilizing the W/O emulsion and slowing down the reaction of the polyurea formation in the 3P. Recall that the silicate particle size is controlled by that one of the initial W/O emulsion. A suitable emulsifier should cause the size reduction of silicate particles in the crosslinked resin. Accordingly, we can state that the VE, EP and MF resins had an active emulsifying effect in the W/O emulsions of the hybrid systems, which was even more pronounced in those hybrids which did not contain phosphate as emulsifier.

The fracture mechanical properties were distinctively modified by the elimination of the phosphate. In the 2P/VE/MF hybrids, K_c did not suffer any significant change while the G_c increased. Compared to the 3P reference resins, both K_c and G_c were enhanced. Similar results were obtained for the 2P/EP hybrid resins: the fracture toughness and energy increased in comparison to the 3P/EP systems. However, their values were still lower than for the 3P resins. On the other hand, the absence of phosphate in the 2P/MF hybrid systems worsened their fracture mechanical properties. The flexural tests conducted on the 2P hybrids showed an increase of the flexural modulus and strength compared to the 3P hybrid systems. The absence of the phosphate, did not affect negatively the flexural properties. The flexural modulus and strength were enhanced in comparison to the respective phosphated hybrids.

The absence of the phosphate in the 2P hybrids affected slightly their thermal stability. The 2P/VE/MF hybrids presented an improved stability to temperatures lower than 400°C, however, between 475°C-525°C the degradation was faster than in the corresponding 3P/VE. The amount of MF contained in the 2P/VE/MF hybrid resins did not have a clear influence. The 2P/EP hybrids showed a better withstand to thermal degradation in the whole temperature range than the corresponding 3P/EP hybrids. The 3P/EP ratio was a key parameter concerning the thermal stability of the related systems. On the contrary, 2P/MF hybrids showed a more marked degradation at low temperatures than the corresponding 3P/MF hybrids. Nevertheless, for all 2P hybrid systems, the thermal stability was satisfactorily improved when compared to the reference 3P.

The observed glass transition temperatures of the 2P/VE/MF hybrids were shifted to lower temperatures when compared to those of the corresponding 3P/VE hybrid systems. For the 2P/EP hybrid systems a significant shift of the T_g to higher temperatures was found along with increasing EP content. When comparing the 2P/EP with the 3P/EP hybrid systems, the glass transition temperature of the former was shifted to higher temperatures due to the absence of the plasticising effect of the phosphate. Such a shift was also observed for the 2P/MF hybrid resins when comparing the respective T_g s of the 3P/MF hybrid systems. For the 2P/MF hybrid systems a slight shift of the T_g towards lower temperatures with increasing MF was observed.

The flammability of the 2P/VE/MF hybrid resins was considerably reduced. The substitution of the phosphate by a small amount of by MF (both being flame retardants), reduced significantly the flammability of these hybrid systems. On the other hand, the absence of phosphate in the 2P/EP and 2P/MF hybrids did not improve the initial flammability. To conclude the summary a brief list of the most outstanding results obtained by hybridising the 3P resins are presented below:

- The pot life and the posterior processing was prolonged and simplified by a significant reduction of the viscosity in the 3P/EP and 2P/EP hybrid systems as well as for the 3P/MF hybrid systems with high MF content (c.f. Fig. 6.1).

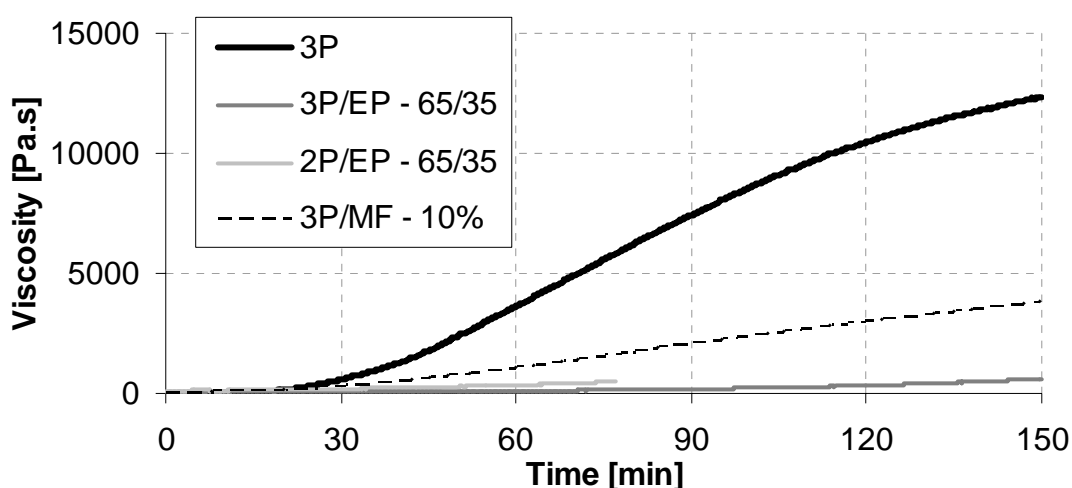


Fig 6.1 – Viscosity vs. time traces of the hybrid resins 3P/EP, 2P/EP, 3P/MF and the reference 3P resin.

→ In general the all novel hybrids (3P and 2P) presented enhanced fracture mechanical and flexural properties when compared to the reference 3P. However, the VE hybrids (3P/VE and 2P/VE/MF) showed the most significant improvement of the fracture mechanical properties (c.f. Table 6.1). On the other hand, outstanding flexural properties were obtained for the EP hybrids (3P/EP and 2P/EP) as well as for the non phosphated 2P/VE/MF hybrids.

Sample name	K_c [MPa.m ^{1/2}]	G_c [kJ/m ²]
3P	0.8	0.9
3P/VE1 25/75	1.5	1.2
3P/VE1 50/50	1.3	1.1
3P/VE1 75/25	1.0	1.1
2P/VE3/MF - 0,5%	1.4	1.7
2P/VE3/MF - 1%	1.3	1.7
2P/VE3/MF - 2,5%	1.3	1.6
2P/VE3/MF - 5%	1.2	1.6
2P/VE3/MF - 10%	1.1	1.1
2P/VE3/MF - 15%	1.1	0.9

Table 6.1 - Fracture toughness (K_c) and fracture energy (G_c) for the 3P/VE1 and 2P/VE3/MF hybrid systems and their reference 3P resin.

→ Regarding the morphology, the 3P/EP, 2P/EP and 2P/EP (c.f. Table 6.2) systems possessed a pronounced mean particle size (d_n) reduction (from five to twenty times smaller than the original 3P resins mean particle size) accompanied with a finer distribution of the polysilicate particles (d_w/d_n).

	d_n [μm]	d_w [μm]	d_w/d_n
3P	11.2	15.5	1.4
2P/VE3/MF - 0.5%	1.6	2.0	1.3
2P/VE3/MF - 5%	1.2	1.6	1.3
2P/VE3/MF - 10%	1.4	1.9	1.3
2P/VE3/MF - 15%	2.0	2.7	1.3
2P/EP - 65/35	0.6	0.7	1.2
2P/EP - 55/45	0.5	0.6	1.1
3P/EP - 85/15	1.2	2.0	1.6
3P/EP - 65/35	0.8	1.1	1.3

Table 6.2 - Number- average (d_n) and weight-average (d_w) mean particle size for the 3P/EP, 2P/EP and 2P/VE3/MF hybrid systems and their reference 3P resin.

→ The thermal stability at $T < 400^\circ\text{C}$ was markedly higher for the VE and EP hybrid systems. On the contrary at $T > 400^\circ\text{C}$ the MF hybrid systems showed and enhanced resistance to thermal degradation (c.f. Fig. 6.2).

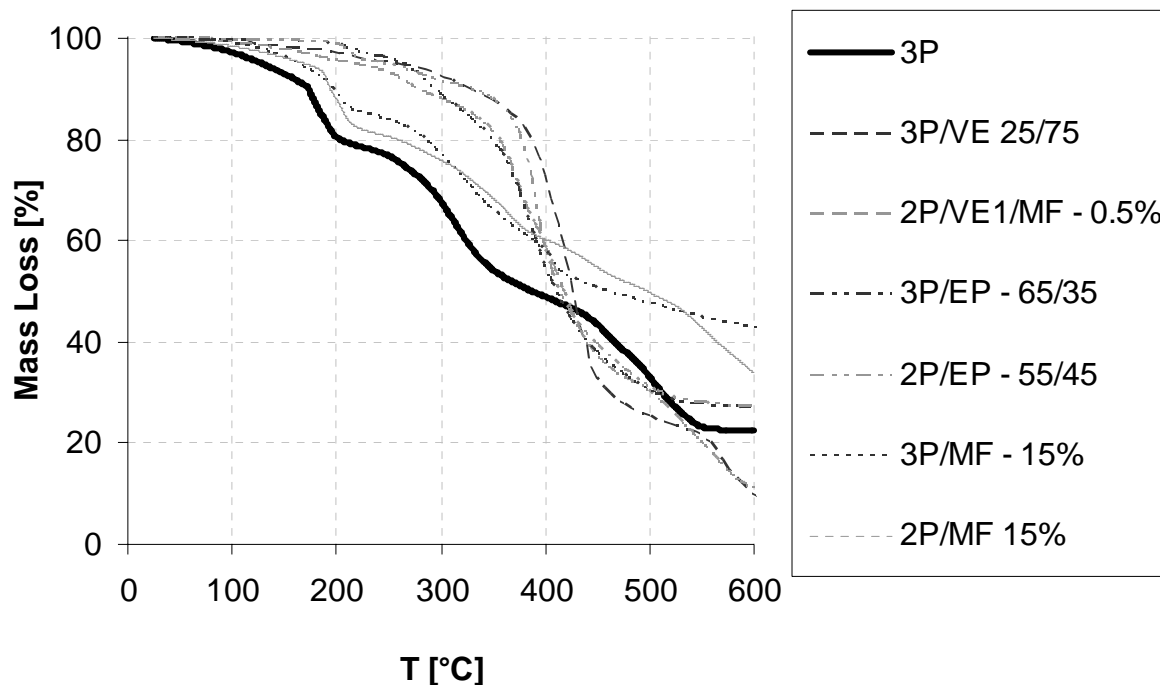


Fig 6.2 – Mass loss vs. T for the different 3P and 2P hybrid systems and their reference 3P.

→ The hybridization with MF (3P/MF and 2P/MF) conferred to the 3P systems and additional resistance to flame. On the other hand the hybridization with VE and EP enhanced this flammability of the novel hybrid resins.

In a future continuation of our work efforts will be made to clarify the reaction kinetics of the 3P and 2P hybrid resins, as well as a better understanding of the reaction processes which take place during the formation of the polyurea with in presence of WG. Moreover, the absorption and desorption of water and its effects on the hybrid system characteristics (morphology, fracture mechanical properties, flexural properties, thermal stability, etc.) are merits of study. In addition suitable resins should be found and checked whether or not their incorporation yields improved properties.

7. APPENDIX

Water Absorption

All organic polymeric materials absorb moisture to some extent resulting in swelling, dissolving, leaching, plasticizing and/or hydrolyzing, events which can cause discoloration, embrittlement, loss of mechanical and electrical properties, lower resistance to heat and weathering and stress cracking [118].

To calculate the amount of water absorbed by the materials when immersed in water for a stipulated period of time, rectangular specimens were cut from each sample with dimensions $w \leq 100d$, where w is the specimen length and d is the specimen width, measured in mm. Three parallel specimens were tested and the results were presented as an average of the tested specimens. The samples were dried in an oven at 50°C for 24h, cooled in a desiccator and immediately weighted to $\pm 0,001g$. In order to measure the water absorption of the materials, all samples were immersed in distilled water for 24h $\pm 1h$ at room temperature as described in ASTM D 570-99 (ASTM 1999) procedure. Excess water on the surface of the samples was removed prior to weighting. The sample weight increase was measured in periods of time of 24h, 48h, 96h, 192h, etc until constant weight was reached with $\pm 0,001g$ accuracy. The percentage increase in weight during immersion was calculated as follows (Eq. 7.1):

$$\text{Increase weight \%} = \frac{\text{Wet weight} - \text{Initial weight}}{\text{Initial weight}} \times 100 \quad (7.1)$$

Water absorption results:

The water absorption of the 3P and 2P hybrid resins, as well as their reference 3P resin is presented in Fig. 7.1-3. After almost 20 weeks of being submerged in distilled water, the water uptake of the hybrid systems did not reach equilibrium. However, their absorption tends slowly to reach a constant value.

The hybridization of the 3P resins with VE reduced clearly the water absorption of the resulting hybrids (c.f. Fig. 7.1). The most significant results were obtained for the 3P/VE hybrids. The higher the VE content of the hybrid the lower is the absorption of water, excepting the 3P/VE - 50/50 system which presents a considerable resistance to absorb water. On the other hand, the elimination of the phosphate emulsifier affects negatively the properties of the 2P/VE/MF novel hybrids, which present an increased water uptake. Recall that the ratio 2P/MF-VE of the 2P/VE/MF hybrid resins was kept 1:1, therefore such hybrids are comparable to the 3P/VE - 50/50. As it will be discussed next, the incorporation of MF does not show to have a decisive role on the water uptake (c.f. discussion 3P/MF hybrids).

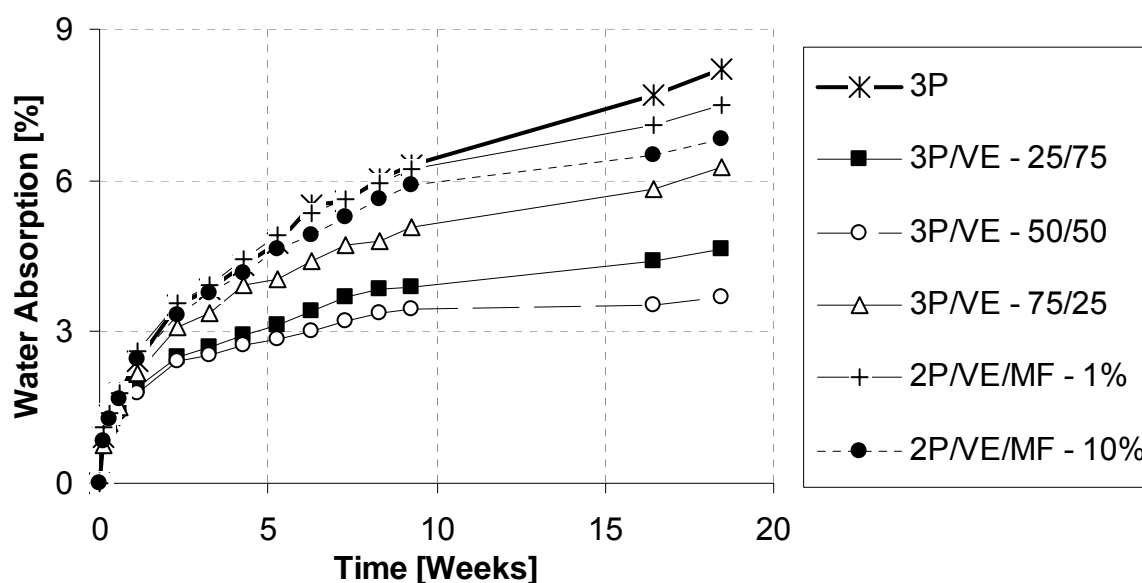


Fig. 7.1 – Water absorption vs. time for the 3P/VE, 2P/VE/MF hybrids and their reference 3P.

Inspecting the absorption of the 3P/EP and 2P/EP hybrids (c.f. Fig 7.2) we can observe, that similarly to the VE hybrids, the hybridisation with EP, reduced considerably their absorption of water. This is obvious when comparing the 3P/EP hybrids with different 3P/EP ratio. Hybrids with higher 3P content tend to absorb more water than the hybrids with increasing EP content. Once more, the elimination of the organic phosphate influenced negatively the properties of the hybrids. Hybrids with the same 3P/EP ratio but without phosphate absorb 1,5% more water (c.f. Fig 7.2). However, the water uptake of the 3P/EP and 2P/EP hybrids is lower than for the 3P reference resin.

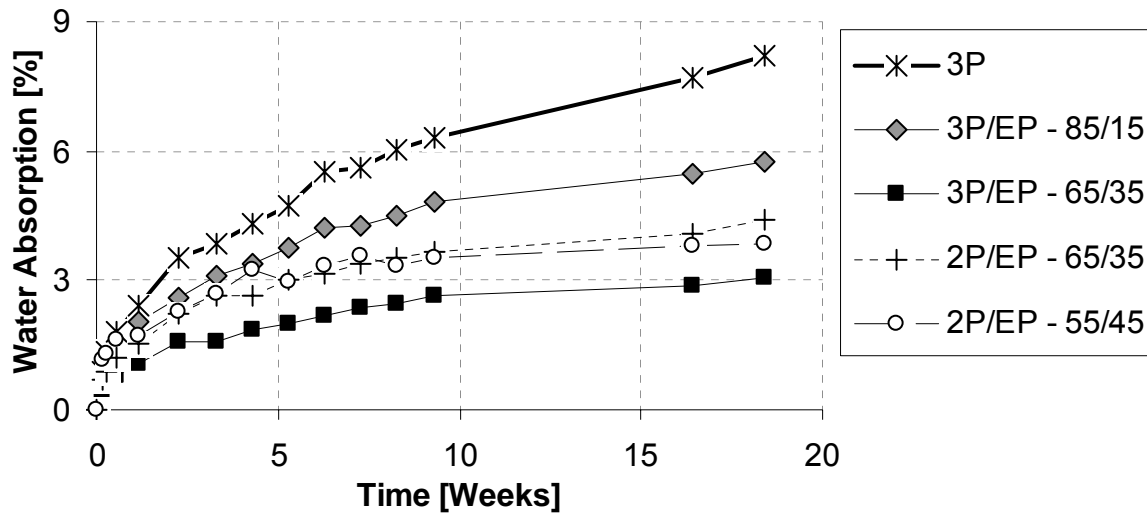


Fig. 7.2 - Water absorption vs. time for the 3P/EP, 2P/EP hybrids and their reference 3P.

Fig.7.3 shows the water uptake of the 3P/MF and 2P/MF hybrids. One can observe that the incorporation of MF did not affect in a great extent the absorption of water. However, the tendency shows that higher MF amounts reduce the water uptake of the resins. On the other hand, a prominent water uptake is detected for the 2P/MF hybrids containing no phosphate. This spectacular increment of weight is caused in part, as already discussed, by the elimination of phosphate. Further on, the 2P/MF hybrids possessed a very high viscosity from the beginning of their synthesis, which made their posterior processing (degassing) troublesome. This leads to resins with microporous morphology, which caused an increase in water absorption.

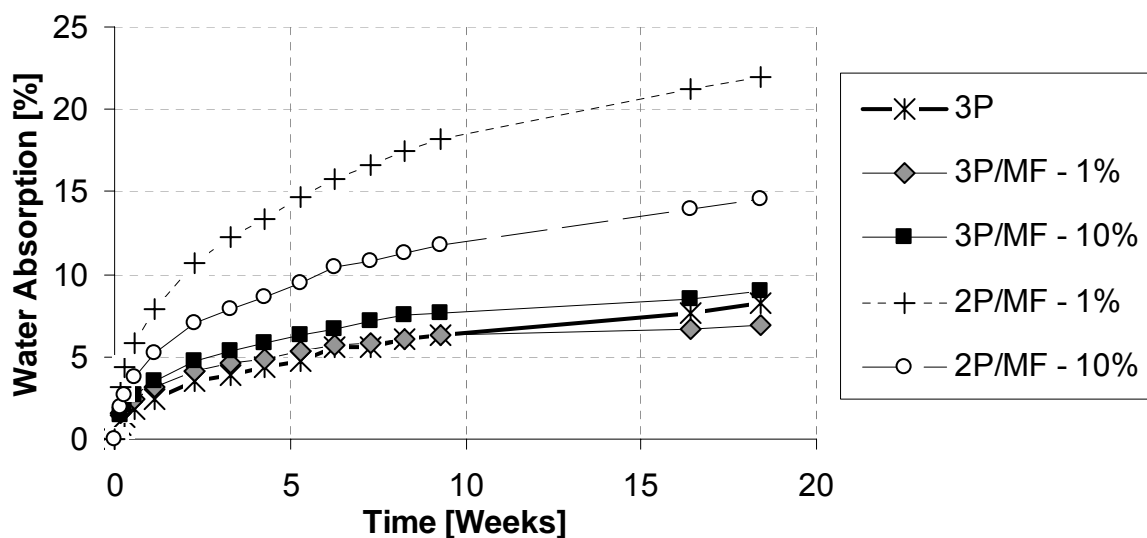


Fig. 7.3 - Water absorption vs. time for the 3P/MF, 2P/MF hybrids and their reference 3P.

8. LITERATURE

- [1] Haas K. H.; Rose, K.: Hybrid Inorganic/Organic Polymers with Nanoscale Building Blocks: Precursors, Processing, Properties and Applications. *Reviews Advanced Material Science*, Vol.5 (2003), pp. 47-52.
- [2] Laughlin, J. B.; Sarquis, J. L.; Jones, V. M; Cox, J. A.: Using Sol-Gel Chemistry to Synthesize a Material with Properties Suited for Chemical Sensing. *Journal of Chemical Education*, Vol. 77 No. 1 (Jan. 2000).
- [3] Fletcher, P.D.I.: The Partitioning of Solutes between water-in-Oil Microemulsions and Conjugate Aqueous Phases. *Journal Chemical Society, Faraday Trans. 1*, Vol. 82 (1986), pp. 2651-2664.
- [4] Gaishun , V. E.; Kosenok, Y. A.; Kovalenko; D. L.; Semchenko, A. V.: Sol-Gel Methods for Materials Processing - Sol-Gel Process Preparation of Functional Silica Materials and Their Application. Ed. Springer, Netherlands (2008).
- [5] KICKELBICK, G.: Hybrid Materials. Synthesis, Characterization, and Applications. Wiley-VCH Verlag, Weinheim (2007).
- [6] Ghosh, S.K.: Functional Coatings. Wiley-VCH Verlag, Weinheim (2006).
- [7] Karger-Kocsis, J.; Erdélyi, S.; Nagy, G.: Polyurea/Vinylester Hybrid Thermoset Resins with In Situ Produced Silicate Filler: Preparation and Static Mechanical Properties. *Journal of Applied Polymer Science*, Vol. 103 (2007), pp. 853-859.
- [8] Binks, B. P.: Modern Aspects of Emulsion Science. Royal Society of Chemistry (1998).
- [9] Stock, N.: Emulsionen. http://www.uni-kiel.de/anorg/bensch/lehre/Dokumente/versuch_k3_emulsionen.pdf. Assessed on 03.11.2008.

- [10] Deng, Q.; Moore, R. B.; Mauritz, K. A.: Nafion[®]/(SiO₂, ORMOSIL, and dimethylsiloxane) hybrids via in situ sol-gel reactions: characterization of fundamental properties. *Journal of Applied Polymer Science*. Vol. 68 (1998), pp. 474-763.
- [11] Inoue, S.; Morita, K.; Asai, K.; Okamoto, H.: Preparation and Properties of Elastic Polyimide-Silica Composites using Silanol Sol from Water Glass. *Journal of Applied Polymer Science*, Vol. 92 (2004), pp. 2211-2219.
- [12] Ozawa, K.; Solans, C.; Kunieda, H.: Spontaneous Formation of Highly Concentrated Oil-in-Water Emulsions. *Journal of Colloid and Interface Science*, Vol. 188 (1997), pp. 275-281.
- [13] Stoye, D.: *Paints, Coating and Solvents*. Wiley-VCH Verlag, Weinheim (1993).
- [14] Zhang, G.; Dass, A.; Rawashdeh, A. M.; Thomas, J.; Council, J. A.; Sotiriou-Leventis, C.; Fabrizio, E. F.; Ilhan, F.; Vassilaras, P.; Scheiman, D. A.; McCorkle, L.; Palczer, A.; Johnston, J. C.; Meador, M. A.; Leventis, N.: Isocyanate-crosslinked silica aerogel monoliths: preparation and characterization. *Journal of Non-Crystalline Solids*, Vol. 350 (2004), pp. 152-164.
- [15] Jesionowski, T.: *Silica Nanofillers: Preparation and Characterization*. *Macromolecular Symposia*, Vol. 194 (2003), pp. 247-252.
- [16] Ramírez, J.R.: Mapeo estructural de sílica xerogel utilizando espectroscopía infraroja. *Revista mexicana de física*, Vol. 48 (2), pp. 142-149.
- [17] Department of Materials Science and Engineering, CTH: Dynamic Mechanical Thermal Analysis (DMTA). Course: Polymeric Materials Advanced Course.
- [18] Polyurethanes. <http://sunilbhangale.tripod.com/pu.html>. Assessed on 03.11.2008.

- [19] Gurke, T.: New Advances in Polymeric MDI Variants. Huntsman Polyurethanes. EUROCOAT 2002, Barcelona, Spain (Jun. 2002).
- [20] Ege, S.: Química orgánica - Estructura y reactividad. Ed. Reverte, Vol 1-2 (2000).
- [21] Stevens, M.P.: Polymer Chemistry. An Introduction. Oxford University Press. New York - Oxford (1990).
- [22] Nicholson, J.W.: The Chemistry of Polymers. The Royal Society of Chemistry (2nd Ed.). London, (1997).
- [23] Zhenga, J.; Ozisika, R.; Siegela, R. W.: Disruption of self-assembly and altered mechanical behaviour in polyurethane/zinc oxide nanocomposites. Polymer, Vol. 46 (2005), pp. 10873-10882.
- [24] Norio Nishil Nishil, N.; Tsunemi, M.; Nakamura, K.; Tokura, S.: Polymerization reaction with diphenylphosphoryl azide. Preparation of polyamides, polyureas and polyurethanes. Makromolekulare Chemie., Vol. 192 (1991), pp. 1811-1820.
- [25] Hau, N.;, Atanabe, M.; Iwakura, Y.: Synthesis of Aromatic Polyurea-Carbonates from Diisocyanate- Carbonates. Journal of Polymer Sciences: Polymer Chemistry Edition, Vol. 19 (1981), pp. 1279-1282.
- [26] Mallakpour, S.; Rafiee, Z.: Synthesis of Photoactive Polyureas Derived from 4-(4-Dimethylaminophenyl)- 1,2,4-triazolidine-3,5-dione and Diisocyanates. Polymer Bulletin, Vol. 56 (2006), pp. 293-303.
- [27] Miyamoto, M.; Takashima, Y.; Kimura, Y.: Preparation of Novel Thermally Stable Polyurea by the Cationic Ring -Opening Isomerization Polymerization of Polycyclic Pseudourea. Macromolecules, Vol. 31 (1998), pp. 6822-6827.

- [28] Rao, B.S.; Madec, P.J.; Marechal, E.: Synthesis of vinyl ester resins. Evidence of secondary reactions by ^{13}C NMR. *Polymer Bulletin*, Vol. 16 (1986), pp. 153-157.
- [29] Zaske, O. C.; Goodman, S. H.: Unsaturated Polyester and Vinyl Ester Resins. *Handbook of Thermoset Plastics*. 2nd Ed. (1999).
- [30] Karger-Kocsis, J.; Fröhlich, J.; Gryshchuk, O.; Kautz, H.; Frey, H.; Mülhaupt, R.: Synthesis of reactive hyperbranched and star-like polyethers and their use for toughening of vinylester–urethane hybrid resins. *Polymer*, Vol. 45 (2004), pp. 1185-1195.
- [31] Karger-Kocsis, J.; Gryshchuk, O.: Toughness Behaviour of Vinylester/Epoxy Thermosets with Interpenetrating Network Structure. *Macromolecular Symposia*, Vol. 217 (2004), pp. 317-328.
- [32] Chian, K.S.; Yi, S.: Synthesis and Characterization of an Isocyanurate-Oxazolidone Polymer: Effect of Stoichiometry. *Journal of Applied Polymer Science*, Vol. 82 (2001), pp. 879-888.
- [33] Mikheev, V.V.; Ivanova, R.R.: Synthesis of Epoxy-Oxazolidone Oligomers. *Russian Journal of Applied Chemistry*, Vol. 77 (2004), N°. 6, pp. 972-975.
- [34] Stefani, P.M.; Moschiar, S.M.; Aranguren, M.I.: Epoxy-Urethane copolymers: Relation between Morphology and Properties. *Journal of Applied Polymer Science*, Vol. 82 (2001), pp. 2544-2552.
- [35] Stefani, P.M.; Moschiar, S.M.; Aranguren, M.I.: Curing Kinetics of Epoxy-Urethane Copolymers. *Journal of Applied Polymer Science*, Vol.79 (2001), pp. 1771-1779.
- [36] Eldin, S.H.; Renner, A.: Cyanoacetamide Accelerators for the Epoxide /Isocyanate Reaction. *Journal of Applied Polymer Science*, Vol. 41 (1990), pp. 1505-1516.

- [37] Parodi, F.: Fast-Curing and High-Performance Isocyanate-Epoxy FPR Resin Systems for Structural Composites and Heavy-Duty Electrical/Electromechanical Applications. www.fpchem.com.
- [38] Senger, J. S.; Yilgor, I.; McGrath, J. E.; Patsiga, R. A.: Isocyanate-Epoxy Reactions in Bulk and Solution. *Journal of Applied Polymer Science*, Vol. 38 (1989), pp. 373-382.
- [39] Ho, T.; Wang, C.: Synthesis of Aralkyl Novolac Epoxy Resins and Their Modification with Polysiloxane Thermoplastic Polyurethane for Semiconductor Encapsulation. *Journal of Applied Polymer Science*, Vol. 74(1999), pp. 1905-1916.
- [40] Potter, W. G.: The Chemistry and Uses of Epoxide Resins. *Oxford Journals. Occupational Medicine*, Vol. 13, 1, (1963), pp. 42-47.
- [41] Deka, M.; Saikia, C.N.: Chemical modification of wood with thermosetting resin: effect on dimensional stability and Strength property. *Bioresource Technology*, Vol. 73 (2000), pp. 179-181.
- [42] Bauer, D.R.: Degradation of Organic Coatings. I. Hydrolysis of Melamine Formaldehyde/Acrylic Copolymer films. *Journal of Applied Polymer Science*, Vol. 27 (1982), pp. 3651-3662.
- [43] Schindlbauer, H.; Anderer, J.: Eine einfache Charakterisierung von Melamin-Formaldehyd-Kondensaten mit Hilfe von NMR-Messungen *Fresenius Zeitschrift für Analytische Chemie*, Vol. 301(1980), pp. 210-214.
- [44] Scheepers, M. L.; Gelan, J.M.; Carleer, R.A.; Adriaensens, P.J.; Vanderzande, D.J.: Investigation of melamine-formaldehyde cure by Fourier transform Raman spectroscopy. *Vibrational Spectroscopy*, Vol. 6 (1993), pp. 55-69.

- [45] Konar, B.B.: A Kinetic and Rheometric Investigation of Hexamethylol Melamine Derivative on the Cure of Natural Rubber Compounds. *Journal of Applied Polymer Science*, Vol. 63 (1997), pp. 233-237.
- [46] Mahler, J.; Rafler, G.: Modified melamine resins for optical applications. *Optical Materials*, Vol. 12 (1999), pp. 363-368.
- [47] Kumar, A.: Polymerization of Melamine and Formaldehyde in Homogeneous Continuous- Flow Stirred-Tank Reactors Using Functional Group Approach: Part B: Molecular Weight Distribution. *Journal of Applied Polymer Science*, Vol. 34 (1987), pp.1383-1397.
- [48] Brawn, D.; Egradic, V.: Strukturaufklärung der Methylolmelamine. *Die Angewandte Makromolekulrcrre Chemie*, Vol. 34 (1973), pp. 35-53.
- [49] Wilson, R. C.; Pfohl, W. F.: Study of cross-linking reactions of melamine-formaldehyde resin with hydroxyl functional polyester by generalized 2-D infrared spectroscopy. *Vibrational Spectroscopy*, Vol. 23(2000), pp. 13-22.
- [50] Yuan, L.; Liang, G.; Xie, J.; He, S.: Synthesis and characterization of microencapsulated dicyclopentadiene with melamine–formaldehyde resins. *Colloid and Polymer Science*, Vol. 285 (2007), pp. 781-791.
- [51] Shieh, J.; Wang, C.: Synthesis of novel flame retardant epoxy hardeners and properties of cured products. *Polymer*, Vol. 42 (2001), pp. 7617-7625.
- [52] Costa, L.; Camino, G.: Thermal Behaviour of Melamine. *Journal of Thermal Analysis*, Vol. 34 (1988), pp. 423-429.
- [53] Devallencourt, C.; Saiter, J.M.; Fafet, A.; Ubrich, E.: Thermogravimetry/Fourier transform infrared coupling investigations to study the thermal stability of melamine formaldehyde resin. *Thermochimica Acta*, Vol. 259 (1995) , pp. 143-151.

- [54] Anderson, D.G.; Netzel, D. A.; Tessari, D. J.: The Synthesis and Characterization of Monomeric Etherified Methylolated Melamines Using Gel Permeation Chromatography and Proton Magnetic Resonance Spectroscopy. *Journal of Applied Polymer Science*, Vol. 14 (1970), pp. 3021-3032.
- [55] Blank, W.J.; He, Z.A.; Hessel, E. T.; Abramshe, R. A.: Melamine Formaldehyde Networks with improved Chemical Resistance. King Industries, Inc. www.wernerblank.com.
- [56] McGarraghy, M.; Hegarty, A. F.: The Alcoholysis Reaction of Isocyanates Giving Urethanes: Evidence for a Multimolecular Mechanism. *Journal of Organic Chemistry*, Vol. 63 (1998), pp. 6878-6885.
- [57] ASTM D 3912 Chemical 12 Month Exposure - Huntsman Technical Bulletin - Chemical Resistance Testing Chemical Resistance Training for Polyurea Spray Elastomers Chemical resistance.
- [58] Czél, G.; Czigány, T.: Development and Analysis of Filament Wound New Composite Pipes Made of Glass Fibre Reinforced 3P Resin. *Macromolecular Symposia*, Vol. 239, 1, (Jun. 2006), pp. 232-244.
- [59] <http://www.polyurea.com/spps/ahpg.cfm?spgid=89>. Assessed on 03.11.2008.
- [60] Northcroft, I. W.: Innovative Materials and Methods for Ground Support, Consolidation and Water Sealing for the Mining Industry. The South African Institute of Mining and Metallurgy (SAIMM) - Operator's Conference, 11-12 September 2006.
- [61] Primeaux II, D. J.: History, Chemistry & Basic Formulating Techniques. A Presentation by Primeaux Associates LLC. 2004, Primeaux Associates LLC.
- [62] Polyurea Elastomers. Hercules Vertriebsgesel. GmbH. www.hercules.co.at.

- [63] Highly reactive, two component fire resistant urea-silicate injection resin for strata consolidation - MEYCO® MP 364 Flex BASF Construction Chemicals Europe Ltd.
- [64] Broekaert, M.: Polyurea spray coatings. Huntsman International LLC (2002).
- [65] Orbán, S.; Vilimi, L.: Aromatic Isocyanates and their Derivates: Market Situation Application and Development Trends. Müanyag és Gumi. www.muanyagesgumi.hu.
- [66] UL 94 flammability testing. <http://www.ul.com/plastics/flame.html>.
- [67] 3P-Plus-Shortliner. <http://www.jt-elektronik.de/English/products/renovation/3plusplushortliner/index.html>
- [68] Karger-Kocsis, J.; Gryshchuk, O.; Schmitt, S.: Vinylester/epoxy-based thermosets of interpenetrating network structure: Anatomic force microscopic study. *Journal of Material Science*, Vol. 38 (2003), pp. 413-420.
- [69] Kiefer, J.; Heidrick, J.L.; Hilborn, J.G.: Macroporous thermosets by chemically induced phase separation. *Advanced in Polymer Science*, Vol.147 (1999), pp.161-247, Springer-Verlag Berlin-Heidelberg.
- [70] Grishchuk, S.; Castellà, N.; Karger-Kocsis, J.: Hybrid resins from polyisocyanate/vinylester/waterglass systems: Structure and Properties. *European Polymer Journal*, Vol. 43 (2007), pp. 1245-1257.
- [71] Available Resins. <http://www.polymertechnology.com/>
- [72] Brydson, J.A.: *Plastics Materials*, 7th Ed. Butterworth-Heinemann, London (1999).
- [73] REACH – European Community Regulation. http://ec.europa.eu/environment/chemicals/reach/reach_intro.htm

-
- [74] Hafner, B.: Scanning Electron Microscopy Primer. Characterization Facility, University of Minnesota -Twin Cities (2007).
- [75] Atomic Force Microscopy - A Guide to Understanding and Using the AFM. Galloway Group - Texas State University Manuals. <http://www.txstate.edu>
- [76] Smith, A.: Atomic force microscopy. Microbiology Today, Vol. 26 (May 1999).
- [77] Biological Instrumentation and Measurement Laboratory - Atomic Force Microscope. Massachusetts Institute of Technology (MIT) - Open Course Ware - <http://ocw.mit.edu/>
- [78] History of Atomic Force Microscopy.
http://www.lot-oriel.com/site/pages_il_en/int/int/int.php
- [79] Blanchard, C. G.: Atomic Force Microscopy. The Chemical Educator, 1, Vol. 1, N° 5 (1996), Springer-Verlag New York, Inc.
- [80] Pisarski, H.: Fracture toughness testing.
<http://www.twi.co.uk/content/kscsw011.html>
- [81] Gehlen, P.C.; Hoagland, R.G.; Popelar, C.H.: A method of extracting dynamic fracture toughness from CT tests. International Journal of Fracture, Vol. 15, N° 1, (Feb. 1979).
- [82] Ceriolo, L.; Di Tommaso, A.: Fracture Mechanics of Brittle Materials: A Historical Point of View. 2nd Int. PhD Symposium in Civil Engineering 1998 Budapest.
- [83] Biegefestigkeit.
<http://www1.unileoben.ac.at/~buero41/Download/Datenblaetter/BiegefestigkeitA4.pdf>

- [84] Harper, C. A.: Modern Plastic Handbook, (Chapter 11 – Plastic Testing). McGraw-Hill Professional, New York (2000).
- [85] Luckenbach, T. A.: DMTA: Dynamic Mechanical Thermal Analysis. Rheometrics, Inc. - Piscataway, NJ, 08854, U.S.A (1990).
- [86] Menges, G.: Werkstoffkunde der Kunststoffe. Carl Hanser Verlag (1979).
- [87] Domke, W.: Werkstoffkunde und Werkstoffprüfung. Cornelsen Verlag Schwann-Girardet GmbH & Co. KG, Düsseldorf (1987).
- [88] Bilyeu, B.; Brostow, W.; Menard, K. P.: Compuestos Epóxicos Termoestables y sus Aplicaciones. II Análisis Térmico. Journal of Materials Education, Ed. en Español. Vol. 22 (4-6), pp. 1009-131.
- [89] Dougan, C. E.; Stephens, J. E.; Mahoney, J.; Hansen, G.: E* - Dynamic Modulus: Test Protocol - Problems and Solutions. Report Number: CT-SPR-0003084-F-03-3, University of Connecticut.
- [90] Sherman Hsu, C.-P.: Handbook of Instrumental Techniques for Analytical Chemistry. Chapter 15 - Infrared Spectroscopy - Frank Settle Ed.
- [91] Günzler, H.; Böck, H.: IR-Spektroskopie – Eine Einführung. VCH (1993).
- [92] Harrick, N.J.: Internal Reflection Spectroscopy. John Wiley & Sons Inc, (1967).
- [93] FT-IR Spectroscopy - Attenuated Total Reflectance (ATR). Perkin Elmer Life and Analytical Sciences. www.perkinelmer.com
- [94] Wang, K. J.; Hsu, T. J.; James Lee, L.: Rheokinetic Changes during Polyurea Reactions in Solution. Journal of Applied Polymer Science, Vol. 41 (1990), pp. 1055-1072.

- [95] Bhadeshia, H. K. D. H.: Differential Scanning Calorimetry. University of Cambridge, Materials Science & Metallurgy.
- [96] Li, S.; Vuorimaa, E.; Lemmetyinen, H.: Application of Isothermal and Model-Free Isoconversional Modes in DSC Measurement for the Curing Process of the PU System. *Journal of Applied Polymer Science*, Vol. 81 (2001), pp. 1474-1480.
- [97] Ng, H.; Manas-Zloczower, I.: A Nonisothermal Differential Scanning Calorimetry Study of the Curing Kinetics of an Insaturated Polyester System. *Polymer Engineering and Science*, Vol. 29, N° 16, (Aug. 1989).
- [98] Bylund, G.: Dairy Processing Handbook. Tetra Pack Processing Systems AB, Lund, Sweden (1995). Chapter 3 - Rheology, pp. 37-44.
- [99] Steffe, J. F.: Rheological methods in food process engineering. Freeman Press.
- [100] Encyclopedia of Polymer Science and Technology. Rheological Measurements, Vol. 11, pp. 473-536. John Wiley & Sons, Inc.
- [101] Cogswell, F. N.: Polymer Melt Rheology - A Guide for Industrial Practice. Woodhead Publishing Ltd (1981).
- [102] Winter, H. H.: Can the Gel Point of a Cross-linking Polymer Be Detected by the G' - G'' Crossover? *Polymer Engineering and Science*, Vol. 27 (Dec. 1987), No. 22.
- [103] Mishra, S. P.; Krishnamoorthy, K.; Sahoo, R.; Kumar, A.: Organic-inorganic hybrid polymers containing 3,4-ethylenedioxythiophene and chalcogens in the main chain. *Journal of Materials Chemistry*, Vol. 16 (2006), pp. 3297-3304.

- [104] Vernon, D.; Plischke, M.: Viscoelasticity near the gel point: A molecular dynamics study. *Physical Review E*, Vol. 64, 031505.
- [105] Era, V.A.: Thermal Analysis of Thermosetting Resins. *Journal of Thermal Analysis*, Vol. 25 (1982), pp. 79-87.
- [106] *Encyclopedia of Polymer Science and Technology. Thermal Analysis of Polymers*, Vol.1, pp. 1-85 (2005) John Wiley & Sons, Inc.
- [107] Price, D. M.; Hourston, D. J.; Dumont, F.: *Encyclopaedia of Analytical Chemistry. Thermogravimetry of Polymers*. pp. 8094–8105 - John Wiley & Sons Ltd, Chichester, 2000.
- [108] Beyer, G.: Flame Retardancy of Nanocomposites - from Research to Technical Products. *Journal of Fire Sciences*, Vol. 25 (1) (Jan. 2007), pp. 65-78.
- [109] UL Flame Rating - UL 94
http://www.ides.com/property_descriptions/UL94.asp
- [110] Mamunya, Y.P.; Iurzhenko, M.V.; Lebedev, E.V.; Ischenko, S.S.; Boiteux, G.; Seytre, G.: Dielectric and thermal–mechanical properties of hybrid organic-inorganic polymer systems based on isocyanate-containing oligomers. *Journal of Non-Crystalline Solids*, Vol. 353 (2007), pp. 4288-4292.
- [111] Karger-Kocsis, J.; Castellà, N.; Grishchuk, S.: Hybrid resins from polyisocyanate, vinyl ester, melamine formaldehyde and water glass: structure and properties. *Plastics, Rubber and Composites*, Vol. 37 N° 5/6 (2008).
- [112] Lakes, R. S.: High Damping Composite Materials: Effect of Structural Hierarchy. *Journal of Composite Materials*, Vol. 36, N° 03 (2002).

-
- [113] Racich, J. L.; Koutsky, J. A.: Nodular Structure in Epoxy Resins. *Journal of Applied Polymer Science*, Vol. 20 (1976), pp. 2111-2129.
- [114] Cervenya, S.; Ghilarducci, A.; Salva, H.; Marzocca, A.J.: Glass-transition and secondary relaxation in SBR-1502 from dynamic mechanical data. *Polymer*, Vol. 41 (2000), pp. 2227-2230.
- [115] Unsworth, J.; Li, Y.: Thermal Degradation of Epoxy/ Silica Composites Monitored via Dynamic Mechanical Thermal Analysis. *Journal of Applied Polymer Science*, Vol. 46 (1992), pp. 1375-1379.
- [116] Mamunya, Y.P.; Shtompel, V.I.; Lebedev, E.V.; Pissis, P.; Kanapitsas, A.; Boiteux, G.: Structure and water sorption of polyurethane nanocomposites based on organic and inorganic components. *European Polymer Journal*, Vol. 40 (2004), N°10, pp. 2323-2331.

LIST OF PUBLICATIONS

Journals

1. Grishchuk, S.; Castellà, N.; Karger-Kocsis J.: Hybrid Resins from Polyisocyanate/Vinyl Ester/Water Glass Systems: Structure and Properties. *European Polymer Journal*, Vol.43, N° 4 (2007), pp. 1245-1257.
2. Castellà, N.; Grishchuk, S.; Karger-Kocsis J.: Thermoset Polyurea Resins with in Situ Produced Silicate Filler from Water Glass: Effects of Water Dispersible Alumina Nanoparticles. *Plastics, Rubber and Composites*, Vol.36, N° 3 (2007), pp.122-127.
3. Grishchuk, S.; Karger-Kocsis J.; Castellà, N.; Gryshchuk, O.; Shevchenko, V.: Hybrid Poly (silicate)/Poly (Vinyl Ester-Urethan-Urea) Systems. I. Mechanical Properties and Morphology (Гибридные полисиликат / полиэпоксиакрилат-уретан-мочевинные системы. I. Механические свойства и морфология). *Questions of Chemistry and Chemical Technology (Вопросы химии и химической технологии)*, 2007, N°3. – pp. 67-74 (in Russian).
4. Grishchuk, S.; Karger-Kocsis J.; Castellà, N.; Gryshchuk, O.; Shevchenko, V.: Hybrid Poly (silicate)/Poly (Vinyl Ester-Urethan-Urea) Systems. II. Morphology by Atomic Force Microscopy (Гибридные полисиликат / полиэпоксиакрилат-уретан-мочевинные системы. II. Морфология методом атомной силовой микроскопии). Submitted to *Polymer Journal*, (Полимерный журнал). December, 2007 – (in Russian).
5. Karger-Kocsis J.; Castellà, N.; Grishchuk, S.: Hybrid Resins from Polyisocyanate, Vinyl Ester, Melamine-Formaldehyde and Water Glass: Structure and Properties. *Plastics, Rubber and Composites*, September, 2007 (3rd China-Europe)
6. Corobea, M.-C.; Donescu, D.; Grishchuk, S.; Castellà, N.; Apostolov, A. A.; Karger-Kocsis, J.: Organophilic Layered Silicate Modified Vinylester-Urethane

Hybrid Resins: Structure and Properties. Submitted to Polymer and Polymer Composites, February, 2008.

Conference and Symposium Proceedings

Castellà N., Grishchuk S., Karger-kocsis J.: Thermoset polyurea resins and hybrid resins from polyisocyanate/vinyl ester hybrid resins in water glass systems: Structure and properties. The international conference on structural analysis of advanced materials ICSAM 2007. Patras (Greece), 2-6 September 2007, Poster 4-6.

Castellà N., Grishchuk S., Karger-kocsis J.: Thermoset polyurea hybrid resins: Structure, properties. VI Open Ukrainian conference of young scientists on macromolecular compounds. Kyiv (Ukraine) September 30 - October 3 2008, Poster 113.

CURRICULUM VITAE

PERSONAL INFORMATION:

Name: Núria Castellà Maymó

Birth Date: 13.12.1982

Birth Place: Badalona (Spain)

Nationality: Spanish



EDUCATION:

2000-2006 **Graduated in Chemistry at the Universitat de Barcelona (UB).**

Speciality: Organic chemistry.

10/2005 - 02/2006 **Socrates-Erasmus European Programme TU Kaiserslautern.**

Five month stage as trainee.

<http://www.chemie.uni-kl.de/fachrichtungen/oc/kubik/>

PROFESSIONAL EXPERIENCE / INTERNSHIPS:

2001-2004 **Sociedad Española de Desarrollos Químicos, Barcelona**

Laboratory assistant during the University summer break periods.

<http://www.sedq.es/>

03/2006 - 08/2006 **Institut für Verbundwerkstoffe GmbH, Kaiserslautern.**

Five month practical training in the material science department thanks to a Leonardo da Vinci Scholarship.

10/2006 - **Institut für Verbundwerkstoffe GmbH, Kaiserslautern.**

Research associate in the material science division.

<http://www.ivw.uni-kl.de>

